AWARD NUMBER: W81XWH-13-1-0370

TITLE: **Pterostilbene, a Potent Analog of Resveratrol, a Therapeutic Agent in Prostate Cancer: Epigenetic Mechanisms of Action**

PRINCIPAL INVESTIGATOR: **Anait S Levenson**

CONTRACTING ORGANIZATION: University of Mississippi Medical Center
Jackson, MS 39216

REPORT DATE: October 2015

TYPE OF REPORT: Annual

PREPARED FOR: U.S. Army Medical Research and Materiel Command
Fort Detrick, Maryland 21702-5012

DISTRIBUTION STATEMENT: Approved for Public Release;
Distribution Unlimited

The views, opinions and/or findings contained in this report are those of the author(s) and should not be construed as an official Department of the Army position, policy or decision unless so designated by other documentation.

REPORT DOCUMENTATION PAGE

Form Approved
OMB No. 0704-0188

Public reporting burden for this collection of information is estimated to average 1 hour per response, including the time for reviewing instructions, searching existing data sources, gathering and maintaining the data needed, and completing and reviewing this collection of information. Send comments regarding this burden estimate or any other aspect of this collection of information, including suggestions for reducing this burden to Department of Defense, Washington Headquarters Services, Directorate for Information Operations and Reports (0704-0188), 1215 Jefferson Davis Highway, Suite 1204, Arlington, VA 22202-4302. Respondents should be aware that notwithstanding any other provision of law, no person shall be subject to any penalty for failing to comply with a collection of information if it does not display a currently valid OMB control number. **PLEASE DO NOT RETURN YOUR FORM TO THE ABOVE ADDRESS.**

1. REPORT DATE October 2015	**2. REPORT TYPE** Annual	**3. DATES COVERED** 30Sep 2014 - 29Sep 2015
4. TITLE AND SUBTITLE **Pterostilbene, a Potent Analog of Resveratrol, a Therapeutic Agent in Prostate Cancer: Epigenetic Mechanisms of Action**		**5a. CONTRACT NUMBER** W81XWh-13-1-0370 **5b. GRANT NUMBER** GRANT11202829 **5c. PROGRAM ELEMENT NUMBER**
6. AUTHOR(S) Anait S Levenson E-Mail: alevenson@umc.edu		**5d. PROJECT NUMBER** **5e. TASK NUMBER** **5f. WORK UNIT NUMBER**
7. PERFORMING ORGANIZATION NAME(S) AND ADDRESS(ES) University of Mississippi Medical Center 2500 North State Street Jackson, MS 39216-4500		**8. PERFORMING ORGANIZATION REPORT NUMBER**
9. SPONSORING / MONITORING AGENCY NAME(S) AND ADDRESS(ES) U.S. Army Medical Research and Materiel Command Fort Detrick, Maryland 21702-5012		**10. SPONSOR/MONITOR'S ACRONYM(S)** **11. SPONSOR/MONITOR'S REPORT NUMBER(S)**

12. DISTRIBUTION / AVAILABILITY STATEMENT

Approved for Public Release; Distribution Unlimited

13. SUPPLEMENTARY NOTES

14. ABSTRACT

The goal of this project is to elucidate MTA1-mediated anticancer efficacy of pterostilbene (PTER). For this, PC3M prostate cancer cells which express high levels of MTA1 were transduced with lentiviral MTA1shRNA and cells were characterized in functional assays. Cell were also tagged with luciferase to be utilized in vivo for monitoring tumor growth in live animals. We also examined the effects of PTER on PTEN expression in DU145 cells *in vitro* and in DU145-senografts. ChIP experiments showed that MTA1 can directly bind VEGF promoter. We completed experiments with *Pten*-null mice, in which we demonstrated MTA1-mediated anticancer effects of PTER. Treatment efficacy was determined by examining disease severity and pathology (H&E)and IHC, tissue and serum accumulation of pterostilbene by GC-MS, changes in molecular targets by qRT-PCR and western blots. We showed that high levels of MTA1 in Pten-loss prostate cooperate with key oncogenes, including c-Myc and Akt among others, to promote prostate cancer progression. In addition, loss-of-function studies using human prostate cancer cells indicated direct involvement of MTA1 in inducing inflammation and EMT. Importantly, pharmacological inhibition of MTA1 by pterostilbene resulted in decreased proliferation and angiogenesis and increased apoptosis reducing tumor development and progression in prostate-specific Pten-null mice by 52 %

15. SUBJECT TERMS

Advanced prostate cancer; MTA1, epigenetics, pterostilbene, MTA1-PTEN; orthotopic xenografts, metastasis, prostate-specific Pten knockout

16. SECURITY CLASSIFICATION OF:			**17. LIMITATION OF ABSTRACT**	**18. NUMBER OF PAGES**	**19a. NAME OF RESPONSIBLE PERSON**
a. REPORT	**b. ABSTRACT**	**c. THIS PAGE**			USAMRMC
Unclassified	Unclassified	Unclassified	UU	137	**19b. TELEPHONE NUMBER** *(include area code)*

Standard Form 298 (Rev. 8-98)
Prescribed by ANSI Std. Z39.18

Table of Contents

Page

1. Introduction……. 4

2. Keywords……. 4

3. Overall Project Summary……... 4

4. Key Research Accomplishments…… 21

5. Conclusion…… 21

6. Publications, Abstracts, and Presentations…….…..……. 22

7. Inventions, Patents and Licenses…… 24

8. Reportable Outcomes..…… 24

9. Other Achievements…… 25

10. References…… 25

11. Appendices……. 25

1. **INTRODUCTION:** The goal of this project is to demonstrate anticancer efficacy of pterostilbene (PTER) in prostate cancer.

   It is well established that diet is one of the risks of developing prostate cancer. It is also known that epigenetic alterations are a major driving force for onset and development of cancer. The non-toxic natural epigenetic regulators, i.e. dietary compounds, can be utilized for prevention of epigenetic age-related alterations leading to prostate cancer. These bioactive agents can also serve as chemical sensitizers in combination strategies with already approved drugs to achieve beneficial additive or synergistic effects. Our research interest is an epigenetic reader, metastasis-associated protein 1 (MTA1) which is a part of nucleosome remodeling and deacetylation (NuRD) co-repressor complex. MTA1 plays critical role in progression and metastasis of prostate cancer through different mechanisms including deacetylation of tumor suppressors and direct regulation of target genes network. We found that natural compound pterostilbene downregulates MTA1 and MTA1-guided signaling in prostate cancer. We will determine exact mechanisms of pterostilbene efficacy in vitro and using comprehensive pre-clinical studies with orthotopic xenografts and knockout mouse models. Our data will provide a strong platform for developing targeted and combinatorial therapies in advanced metastatic prostate cancer.

2. **KEYWORDS:** prostate cancer; MTA1/NuRD; epigenetics; posttranslational modifications, acetylation/deacetylation; pterostilbene (PTER); MTA1-PTEN; MTA1-p-Akt; MTA1-target genes; MTA1-guided signaling; orthotopic xenografts; metastasis; prostate-specific *Pten* knockout mice, novel therapeutic strategy, combinatorial approach, luciferase imaging

3. OVERALL PROJECT SUMMARY

The goal of this project is to dissect MTA1-mediated anticancer and antimetastatic properties of natural analog of resveratrol, pterostilbene, in prostate cancer. The major tasks are: 1) establishment of MTA1 knockdown PC3M prostate cancer cell lines; 2) examination of MTA1 downstream signaling and changes in response to pterostilbene treatment; 3) examination of the role of MTA1 in PTER-mediated anticancer effects in vitro; 4) examination of the role of MTA1 in PTER-mediated anticancer effects in prostate cancer xenografts, and 5) evaluation of the therapeutic efficacy of pterostilbene and combination modalities in prostate-specific *Pten* knockout mice.

Task 1 (a): establishment of MTA1 knockdown PC3M and PC3M-luc prostate cancer cells.

PC3M cells were maintained and expanded in RPMI 1640 containing 10% fetal bovine serum (FBS) and 1% antibiotics, at $37^{0,}$ 5% CO_2. We first generated PC3M-luciferase (luc) cells by transducing the cells with the lentiviral luciferase construct (a gift from Dr. Graeser, Department of Medical Oncology, Freiburg, Germany). We selected sable clones using G418 (neomycin, Sigma-Aldrich, IN) for high luciferase expression. Several bright clones were repeatedly selected again and pooled together for cells with high luciferase expression to be used *in vivo*.

PC3M parental and PC3M-luc cells were transduced with the three GIPZ MTA1 lentiviral shRNAs, GIPZ GAPDH lentiviral shRNA as positive control and GIPZ Non-silencing lentiviral shRNA as negative control. The GIPZ lentiviral shRNA system (GE Heathcare Dharmacon) contains puromycin resistant gene for selection of transduced cells and TurboGFP for monitoring the selection under the

fluorescence microscope. For preparation of the viral particles, we used the pCMV-ΔR8.91 packaging plasmid and the pMD.G envelope plasmid (Addgene). Cells were transduced using RPMI medium (Life Technologies) which contained 4 µg/ml polybrene (Sigma-Aldrich) with lentiviral particles at multiplicity of infection (MOI) = 8. On day 2 post-transduction, selection was initiated with 200 µg/ml puromycin (Sigma-Aldrich) and GFP-positive clones were selected and propagated.

We next validated MTA1 stable silencing in PC3M and PC3M-luc cells. Total RNA was isolated and qRT-PCR was performed. For this, total RNA was isolated using RNeasy kit (Qiagen). RT-PCR was performed on the CFX96 Touch Real Time PCR Detection System (Bio-Rad) using protocol for the SuperScript III platinum two-step qPCR kit with SYBR green (Life Technologies) with the following primers (Integrated DNA Technologies): MTA1 sense: 5'-AGCTACGAGCAGCACAACGGGGT-3', MTA1 antisense: 5'-CACGCTTGGTTTCCGAGGAT-3', β-actin sense: 5'-CGTGGGCCGCCCTAGGCACCA-3', β-actin antisense: 5'-TTGGCTTAGGGTTCAGGGGGG-3'. Calculations were performed using double-delta Ct method. Results showed that the best MTA1 mRNA knockdown was achieved with shMTA1#3 (Fig. 1A). For immunoblot analysis, lysates were prepared in the RIPA buffer containing protease and phosphatase inhibitor cocktail (ThermoFisher Scientific). Samples containing 70 µg of protein were loaded in 10-12% SDS-PAGE and transferred onto polyvinylidene difluoride (PVDF) membranes. Membranes were incubated in 5% nonfat dry milk/TBST blocking buffer for 1hr at room temperature, followed by an overnight incubation at 4^0C in the presence of corresponding primary antibodies, anti-MTA1 (1:1000; Cell Signaling Technologies) and anti β-actin (1:2500; Santa Cruz Biotechnology). Membranes were then washed with TBST and incubated in the presence of HRP-conjugated secondary antibodies. Signal detection was carried out using SuperSignal West Dura chemiluminescent substrate (ThermoFisher Scientific). Results showed that best knockdown was achieved with shMTA1#3 in both cell lines.

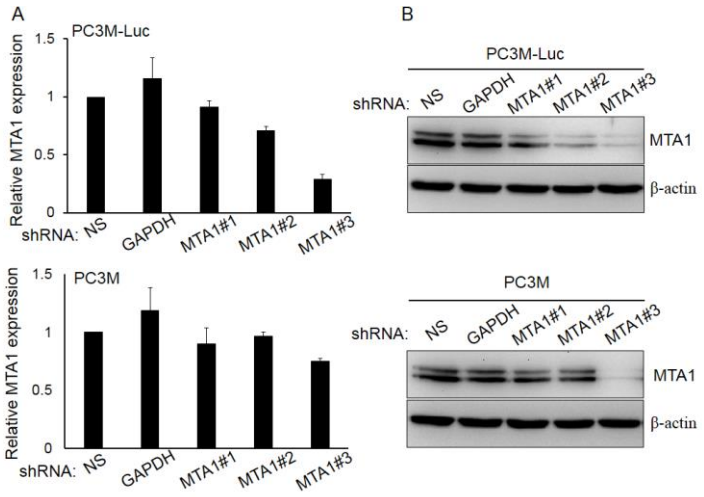

Fig. 1. Validation of stable MTA1 silencing in PC3M and PC3M-luc cells. **A**. Total RNA was isolated and qRT-PCR was performed. Expression levels of MTA1 mRNA are displayed as relative expression over β-actin mRNA with cells transduced with NS shRNA setting at 1.0. **B**. Western analysis of MTA1 protein expression using whole lysates from stably transduced PC3M and PC3M-luc cells. Anti-MTA1 and anti-β-actin antibodies were used. Signals were visualized using enhanced chemiluminescence.

For *in vitro* imaging, cells tagged with luc were serially diluted in a black, clear bottom 96-well plate (Costar, Corning, NY). D-luciferin (150 µg/well) was added to the wells, the plate was incubated at 37^0 C, 5% CO_2 for 10 min after which images were taken (Fig. 2).

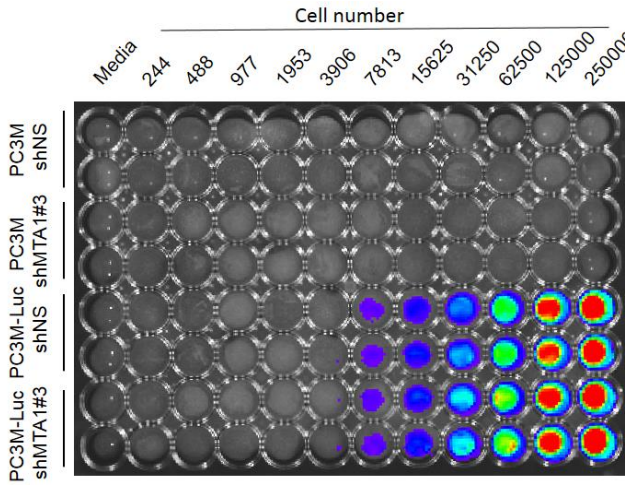

Fig. 2. *In vitro* validation of luciferase expression in PC3M-luc cells. Luc-positive cells were tested to confirm specificity and sensitivity. PC3M-luc-shNS and PC3M-luc-shMTA1 cells showed the same luciferase activity and are ready for in vivo utilization. Negative controls: PC3M-shNS and PC3M-shMTA1 and media only.

Task 1(b): Functional characterization of PC3M and PC3M-luc MTA1 knockdown cells

Cell proliferation: PC3M-shNS and PC3M-shMTA1#3 as well as PC3M-luc-shNS and PC3M-luc-shMTA1#3 cells were plated at $3{,}5x10^3$ cells/well of a 6-well plate in regular RPMI-1640 media with 10% FBS. Media was replaced every other day with fresh media. Cell number was counted using a microscope and cell-counter every day and plotted as shown in Fig. 3. Cell proliferation assay using MTT was also performed with formazin measurements at days 2- 6. Viable cells are plotted (Fig. 4). The differences in cell growth between cells expressing MTA1 and silenced for MTA1 was not significant.

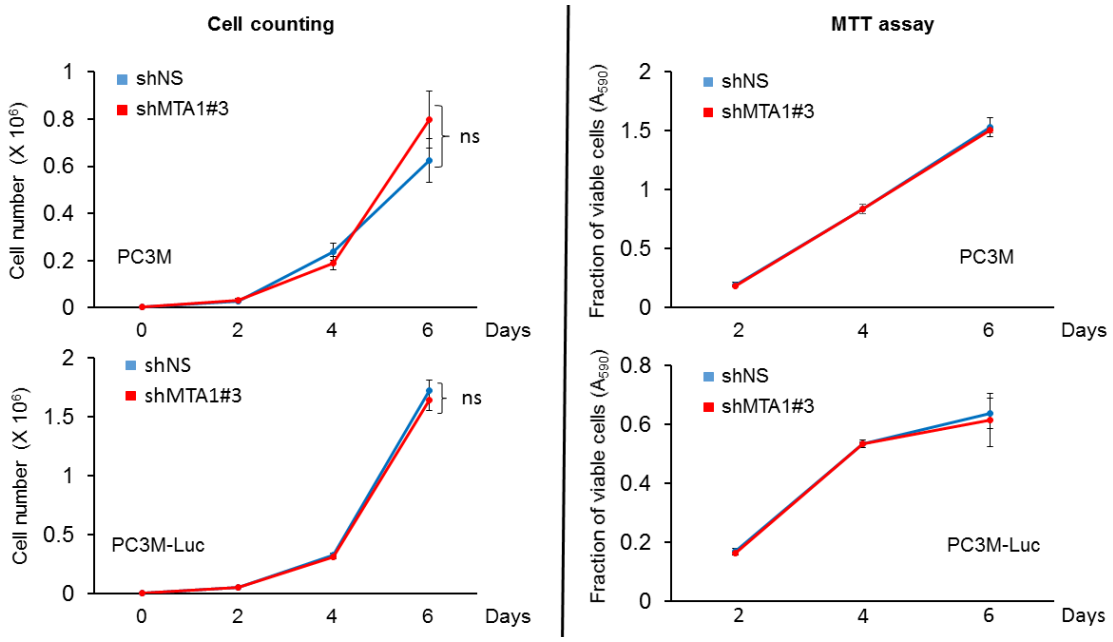

Fig. 3. (*left*). The effect of MTA1 knockdown on cell proliferation. PC3M-shNS and PC3M-shMTA1#3 and Luc-tagged cells were seeded in a 6-well plate. One well for each cell line was harvested every 2 days and the cells were counted on a hemocytometer under the microscope. **Fig. 4**. (*right)* cell were seeded in a 96-well plate. 20 µl of MTT reagent was added to three wells for each cell line every 2 days. MTT solvent (150 µl) was added to dissolve the formazan crystals and the plate was read at 590 nm. Viable cells are plotted as fraction of untreated cells (Ctrl) which is set as 1. Data represent the mean ± SE of three independent experiments...

Colony formation assay was performed as described before (1). Two agar layers were made (1.2% and 0.7%) and cells (PC3M-shNS &PC3M-shMTA1 and PC3M-luc-shNS & PC3M-luc-shMTA1) were inoculated on top of the layers. The media was replaced with a fresh media every other day during the 2-weeks observation time. After 2 weeks of incubation at 37^0 C, when colonies were freely visible (> 50 cells/colony), cell were fixed with formaldehyde and stained with 0.01% of crystal violet solution overnight at 4^0C. Colonies were analyzed at 4x magnification using Olympus CKX41 microscope with U-CMAD3 camera. The images were acquired using the Infinity Analyze software. ImageTool software was used for counting the number of colonies in five-to-seven fields in each dish. The experiments were done in triplicates (Fig. 5). We will repeat these experiments again to verify the differences between the two clones in colony formation ability, which will tell us about the role of MTA1 in metastatic capacity of prostate cancer cells.

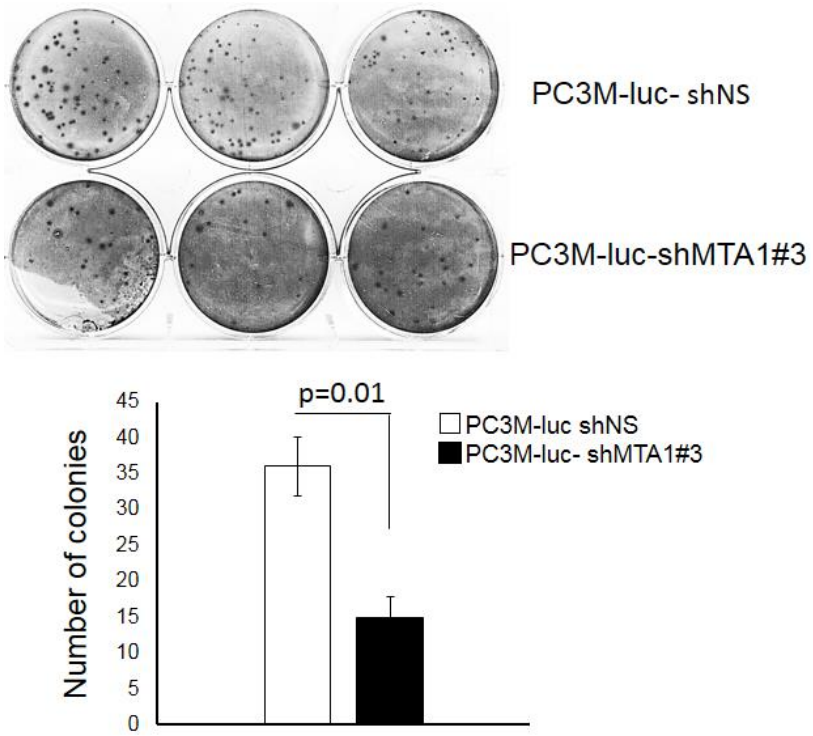

Fig. 5. The effect of MTA1 knockdown on cancer cell colony formation. The growth of PC3M-luc-shNS (Control) and PC3M-luc-shMTA1#3 cells was determined after 2 weeks incubation. Representative images are shown. The number of colonies with diameter ≥3 mm were counted under 4x magnification. Results are shown as means ± SE of three independent experiments. P values were calculated using one-tailed Student's *t* test. p=0.01 compared with cell expressing MTA1.

Invasion assay was performed using Corning Transwell Permeable Support Coated with Cultrex Basement Membrane Extract for Cell Invasion Assay. PC3M parental or PC3M-Luc cells harboring either Non-silencing (NS) or MTA1 shRNA were cultured to about 90% confluence in 6 cm dishes, then rinsed with DPBS and starved in serum free media (No serum in 4 ml RPMI) for 24 hours. 100 µl to each insert and 500 µl to each receiver well of serum free media was added to rehydrate the inserts and incubated at 37 °C in a CO2 incubator for at least 1 hour. The cells, serum starved for 24 hours, were harvested and counted. Excess media from the rehydrated inserts and the receiver cells was removed and 5 x103 cells in 500 µl of serum free media were added to the insert. 500 µl of the complete media (10% serum in RPMI) was added to the receiver wells and the assembled chamber was incubated at 37^0C in a CO_2 incubator for 24 hours.

The insert and the receiver wells were then aspirated and the cells sticking to the membrane inside of the insert were removed. The cells sticking to the membrane outside of the insert were rinsed with DPBS and stained with 0.8% crystal violet made in methanol for 30 minutes. The membrane was then destained with several rinses of water and imaged under a bright field microscope to count the number of cells. The ratio of number of cells invaded to the number of cells seeded gives us the percent invasion.

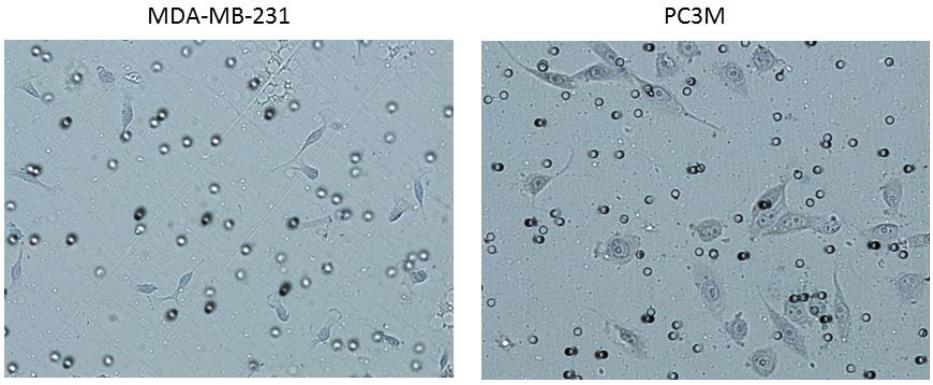

Fig. 6. The effect of MTA1 knockdown on cell invasion. These experiments are still in progress. We used MDA1-MB-231 invasive breast cancer cells and PC3M invasive prostate cancer cells to trouble-shoot some methodological problems we are accounting and to optimize the protocol.

Wound healing assay/Scratch assay. PC3M parental or PC3M-Luc cells harboring either Non-silencing (NS) or MTA1 shRNA were cultured to about 90% confluence in 6 well dishes, then rinsed

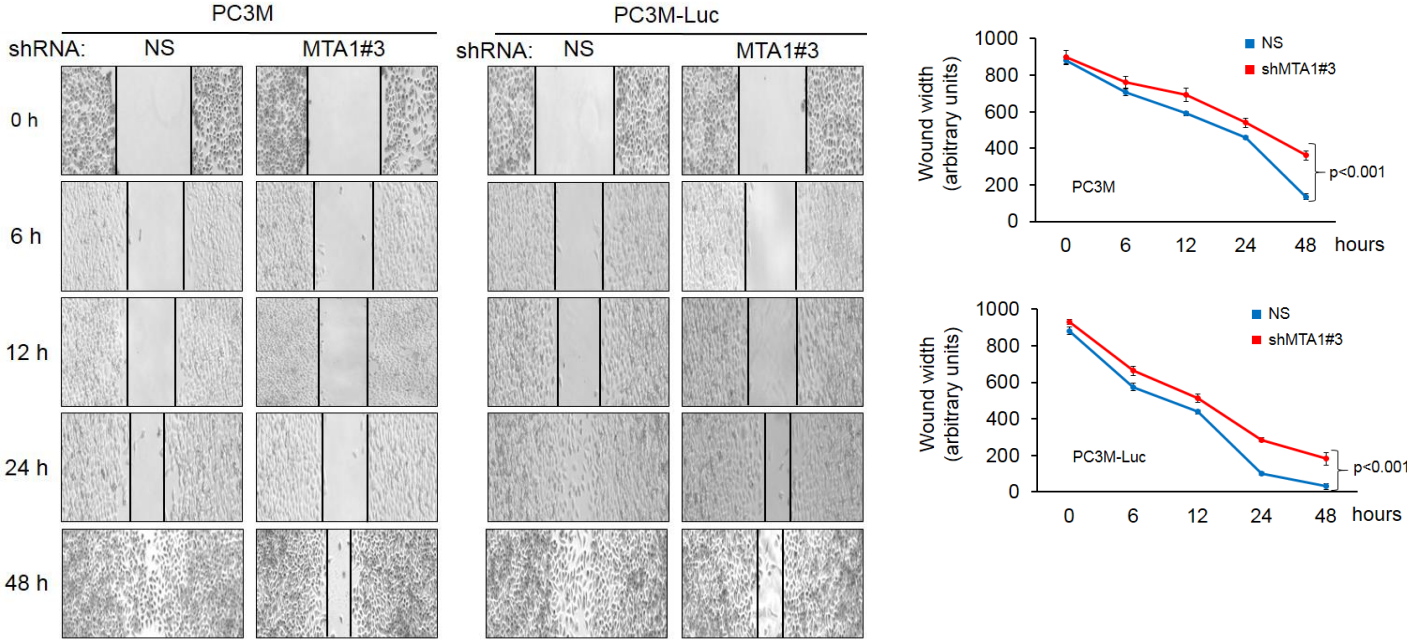

Fig. 7. The effect of MTA1 knockdown on cell migration. Cell migration was monitored at the indicated time points. Wound width is calculated using the ImageJ software. Each point was derived by calculating 6 images. P values are calculated using Student's *t* test.

with DPBS and starved in low serum media (0.1% serum in 2 ml RPMI) overnight. A line with a

marker was drawn on the bottom of the dish. Using a sterile 200 µl pipet tip, three separate wounds were scratched through the cells moving perpendicular to the line drawn with the marker. The cells were then rinsed with DPBS and replenished with the low serum media. The wound area was then imaged under a phase contrast microscope at 4x above and below the marker line to help orient the measurements and the imaging was repeated at 6, 12, 24 and 48 hours.

We are planning to start *in vivo* characterization of PC3M-luc-shMTA1 cells by injecting them into nude male mice to monitor tumor growth with cells expressing MTA1 (PC3M-luc-NS) and not (PC3M-luc-shMTA1#3). These experiments will elucidate the role of MTA1 in the progression of prostate cancer and possibly development of metastasis.

Task 2. Examination of MTA1 downstream signaling in cells treated with pterostilbene.

In our previous studies we have shown p53 and PTEN deacetylation by MTA1 leading to inhibition of apoptosis and activation of survival pathways in prostate cancer and that resveratrol/pterostilbene are able to reverse that effects by inhibiting MTA1/HDACs (2-4). Further, we found that pterostilbene increased expression of PTEN in both "normal" and cancer cells slightly more effective than resveratrol (Fig. 8). In DU145 cells, pterostilbene increased levels of PTEN at both mRNA and protein level (Fig. 9). RNA was isolated using miRNeasy Mini kit (Qiagen). Real-time PCR was perform using Specific PrimeTime human PTEN primers: forward 5'-GAACTTGTCTTCCCGTCGT-3' and reverse 5'-AATGTTCAGTGGCGGAACT-3' (Integrated DNA Technologies).

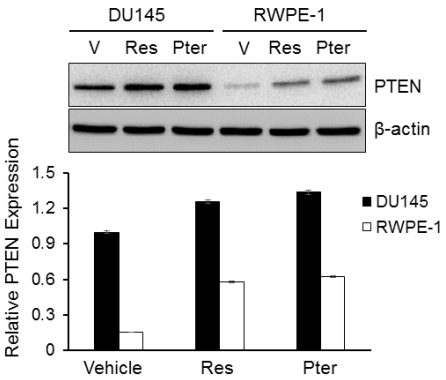

Fig. 8. Resveratrol (Res) and pterostilbene (Pter) induce expression of PTEN protein in RWPE-1 "normal" prostate epithelial cells and in DU145 prostate cancer cells. Cells were treated with Res and Pter at 50µM, protein was isolated and western blot was performed as described above and ref). PTEN antibody (1:1000, Cell signaling). β-actin was a loading control.

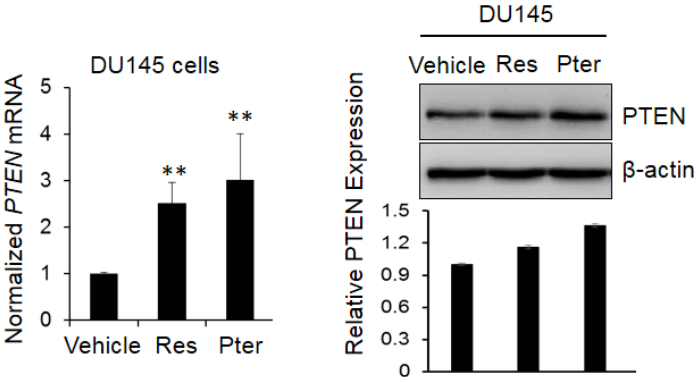

Fig. 9. Pterostilbene induces PTEN on transcriptional level. Cells were treated with Res and Pter (50µM) and total RNA and protein was isolated for qRT-PCR (left) and immunoblotting (right). Fold change in expression of mRNA was calculated by the 2 –ΔΔCt method. **$p < 0.01$ vs control vehicle. Induction of PTEN protein level was not statistically significant.

We next examined the effects of Res and Pter on DU145 cell proliferation using MTT assay. Cells were grown in phenol-red free plus 5% charcoal stripped serum media containing various concentrations (1-100µM) of agents. MTT was performed with formazan measurements at day 8.

DU145 cells were transduced with luciferase primarily for monitoring cell growth in vivo. Prior

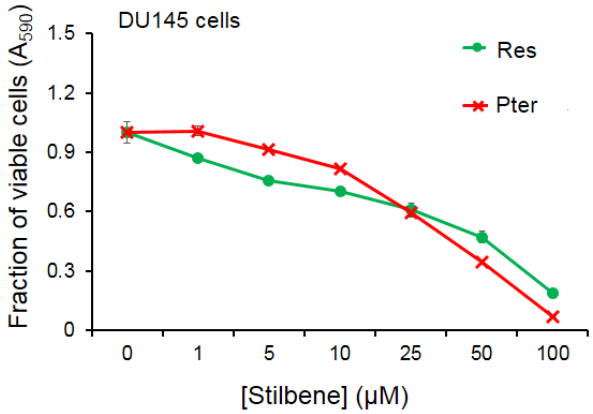

Fig. 10. Comparison of Res and Pter treatment on DU145 cell viability *in vitro.* Viable cells are plotted as fraction of untreated cells (0) which is set as 1. Data represent the mean ± SEM from three independent experiments. IC_{50} was calculated for Res (28.2) and Pter (11.1) by the linear interpolation method using MS Excel software.

injection into mice, we checked luciferase expression and specificity in vitro (see description above, p.) (Fig. 11)

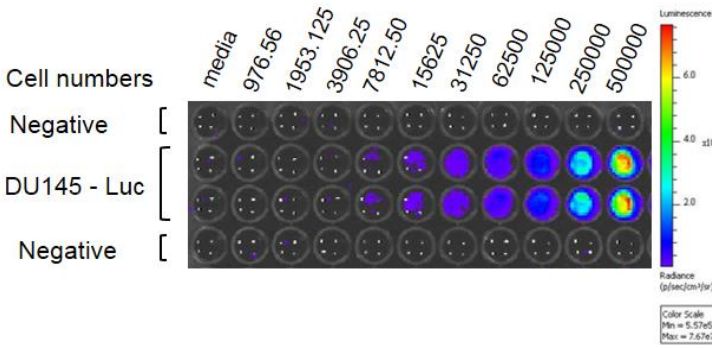

Fig. 11. *In vitro* validation of luciferase expression in DU145-luc cells. Luc-positive cells were tested to confirm specificity and sensitivity. DU145-luc cells showed luciferase activity. Negative controls: DU145 parental and media only.

Task 4. Examine PTER-mediated anticancer effects in vivo using orthotopic xenografts. We used DU-145-luc cells to investigate the effect of pterostilbene on tumor growth in prostate cancer xenografts. Cells were injected subcutaneously (s.c.) into Fox n1 nu/nu male mice purchased from Harlan Lab. Housing and care of all animals were in accordance with the guidelines established by the UMMC AICUC and ACURO (DoD Programs). Upon arrival all animals were given a phytoestrogen-free AIN76A diet (Research Diets) ad libitum. Cells were injected s.c. on the dorsal right flank of mice. Starting from day 4, bioluminescencence (BL) was measured and based on the total flux signal intensities, mice were randomized into two groups (8 mice/each): vehicle (10% DMSO) and Pter treated (50 mg/kg bw). Intraperitoneal injections (i.p) were performed daily, 5 days a week, for 39 days.

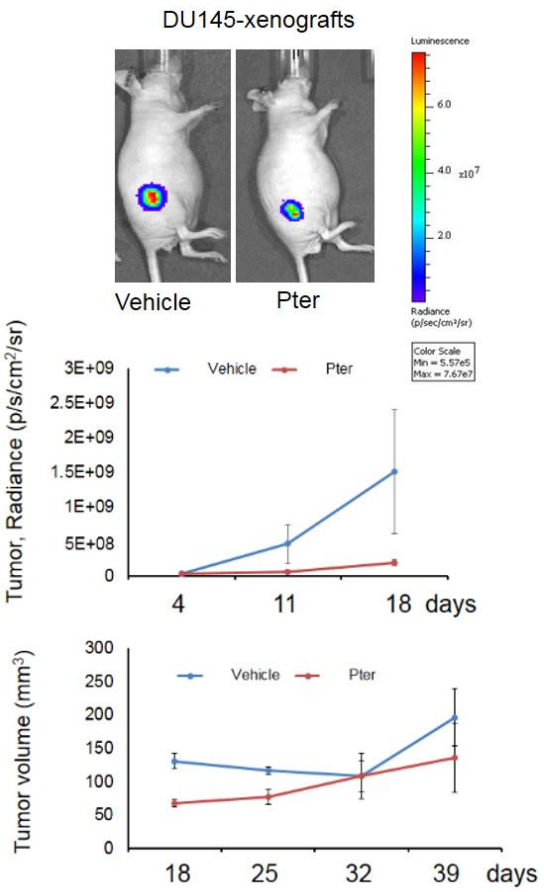

Fig. 12. Pterostilbene inhibits the tumor growth in prostate cancer xenografts. Bioluminescence (BL) images of representative mice from each group (n=8/group) at day 39 are shown. Quantitative analysis of BL signals from day 4 after cancer cell injections until day 18 is shown. Light emission data in Total Flux (photons/sec) are plotted. C. Pterostilbene treatment reduced tumor volumes. Tumor growth was monitored using digital caliper once a week starting at day 18 (see text and ref. 4).

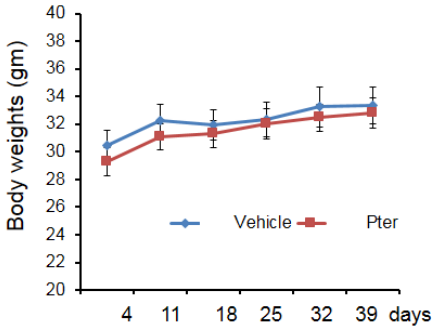

Fig. 13. Body weight analysis of nude mice with tumors in vehicle and pterostilbene treated groups. Mice were weighed once per week for 6 weeks. There were no significant differences in the body weights of mice among all groups (p=0.61).

Tumor growth was monitored weekly by BL imaging and caliper measurements, which complimented each other, until day 39 when mice were sacrificed and tumors and sera collected for analysis (Fig. 12). Tumor measurements by BL imaging in the first 18 days revealed tumor inhibition by pterostilbene. After day 18 we noticed inconsistent BL measurements due to limitations of photon emission detection of large s.c. tumors that consist of necrotic areas and infiltrating host cells. On the other hand, caliper-based measurements were feasible only after day 18, after which they were more reliable than BL measurements and demonstrated significant differences between control and treated tumors by day 39 (Fig.12). Pterostilbene treatment did not affect body weights of mice (Fig. 13).We also demonstrated that pterostilbene induced PTEN protein expression and apoptosis (cleaved caspase-3 and M30) and inhibited tumor cell proliferation (Ki-67) in the tumor tissues (Fig. 14) The study further linked these findings with miR-17 family of oncomirs-mediated effects of pterostilbene (4) (out of scope of the proposal).

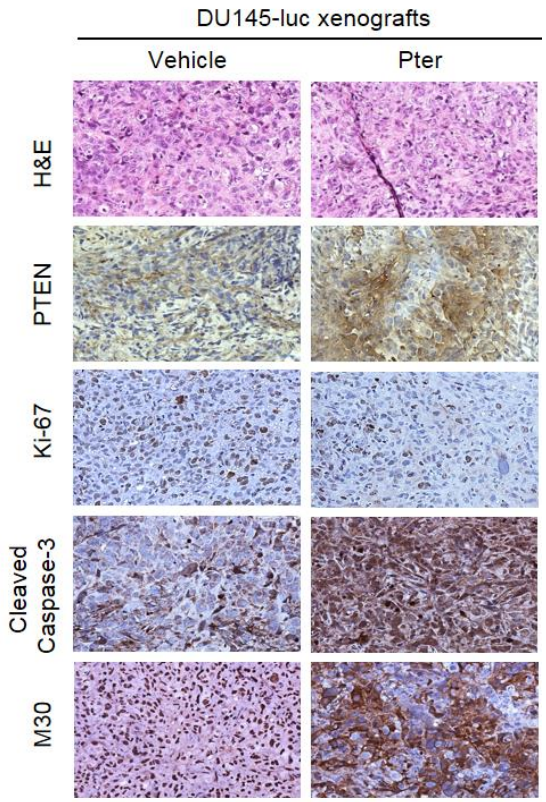

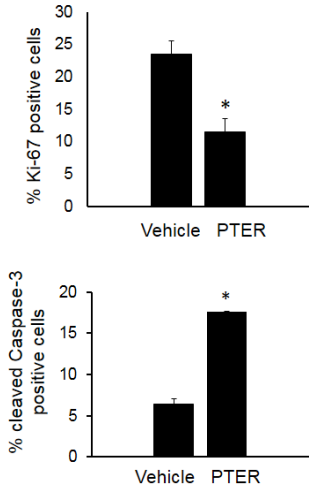

Fig. 14. Pterostilbene induces PTEN expression and apoptosis and inhibits cell proliferation in prostate cancer xenografts. Representative H&E and IHC images of PTEN, ki-67 (proliferation) and cleaved caspase-3 and M30 (apoptosis) staining of DU145 xenografts upon pterostilbene (Pter) treatment (magnification x100). B. Percent quantitation of Ki-67 and cleaved caspase-3 staining is shown (n =3 per group).Data represent the mean±SEM more than 15 fields of counting. *p < 0.05 (two-sample two-tailed Student's t test).

Task 2, 3: Elucidating MTA1 downstream signaling

Our published data indicate a link between overexpression of MTA1 and increased angiogenesis in

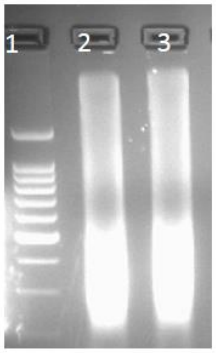

1: 100 bp DNA ladder
2, 3: sheared PC3M chromatin

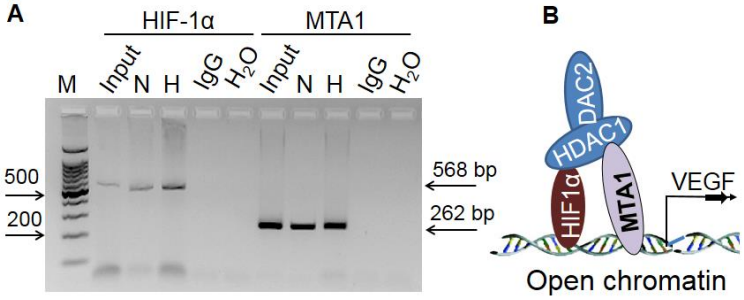

Fig. 15. MTA1 directly binds to VEGF. Left, sheared chromatin. **A**. ChIP analysis showing novel binding site for MTA1 on VEGF promoter. Two different pair of primers for detecting VEGF promoter were used. **B**. Schematic depiction of putative MTA1 molecular mechanisms.

vitro and *in vivo* (5,6). We showed that MTA1-knockdown makes PC3 cells less angiogenic in endothelial migration assay and leads to considerable decrease levels of VEGF in the conditioned media. We also demonstrated that, *in vivo*, MTA1-deficient tumor xenografts (s.c. and orthotopic) are less vascularized, have smaller-size vessels and show reduced VEGF levels compared to their MTA1-positive counterparts (5). In a separate experiment, using orthotopic PCa xenografts we detected significantly lower CD31 IHC staining in MTA1-knockdown compared to MTA1-expressing prostate

tumors (6). Since we repeatedly found the tight link between MTA1 and angiogenesis, we hypothesized that HIF-1α might represent one of the MTA1-piggy-back proteins for VEGF regulation by MTA1. Interestingly, however, our initial ChIP experiments showed hypoxia-increased MTA1 binding to the VEGF promoter, albeit with different primers than HIF-1α, suggesting different but direct binding sites for MTA1 and HIF-1α (Fig. 15). Briefly, we crosslinked protein complex with chromatin by formaldehyde, sonicate cell lysates and perform immunoblotting and IP. We analyzed fractionated (~600 bp) chromatin-bound protein complex for MTA1. Immunoprecipitation of DNA-associated HIF1-α was performed using HIF1-α and MTA1 antibodies. For PCR, the sense 5'-GCTCTGCCAGACTCCACAGT and antisense 5'-GGCTACGTGGAAGGCAAGTA and the sense 5'-CAGGTCAGAAACCAGCCAG and antisense 5"-CGTGATGATTCAAACCTACC primers for hypoxia-responsive element (HRE) in the VEGF promoter were used. PCR products were calculated and analyzed using Opticon Monitor software. These experiments were performed under normoxic (20% O_2) and hypoxic (2% O_2) conditions.

We used MTA1 knockdown LNCaP and DU145 cells to investigated MTA1 regulation of molecules identified as putative MTA1 targets by MTA1 ChIP-Seq analysis (out of scope of this proposal). We

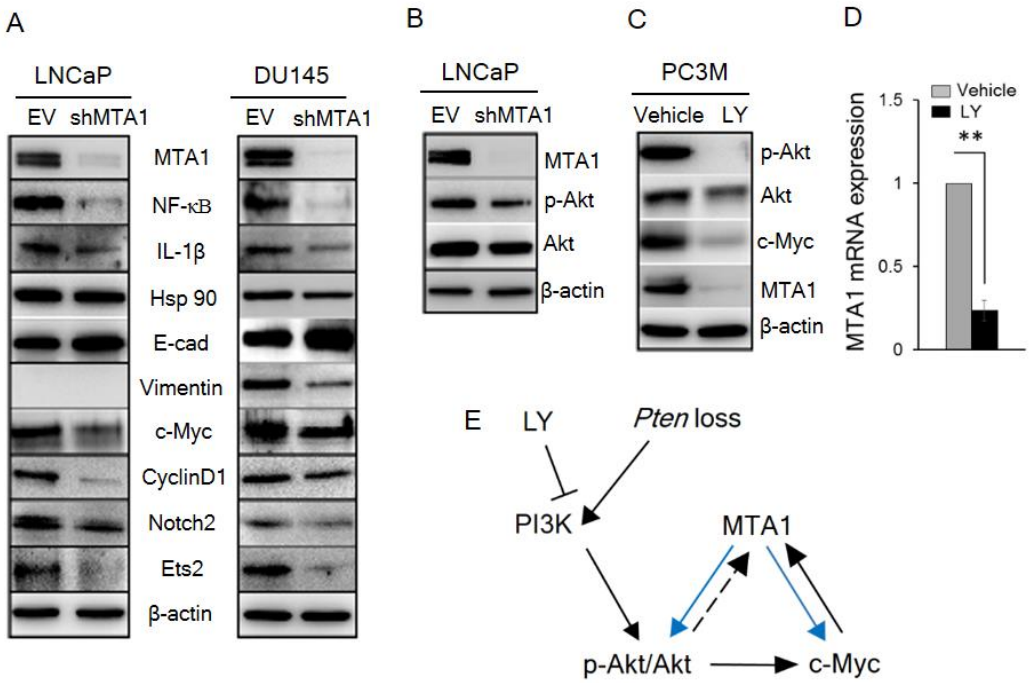

Fig. 16. MTA1 directly regulates key molecular drivers of tumor promotion. **A,** Immunoblots of MTA1, NF-κB (p65), IL-1β, Hsp90, E-cadherin (E-cad), Vimentin, c-Myc, Cyclin D1, Notch2, and Ets2 in LNCaP (left) and DU145 (right) cells expressing (EV) and silenced for MTA1 (shMTA1). **B**, Immunoblot of MTA1, p-Akt and Akt in LNCaP EV and shMTA1 cells. **C**, Immunoblot of p-Akt, Akt, c-Myc and MTA1 and **D**, qRT-PCR of MTA1 mRNA levels in PC3M cells treated with vehicle (DMSO) and LY (LY294002). **E**, Proposed mechanism involved in Pten loss-induced upregulation of MTA1, exhibiting the MTA1-Akt and MTA1-c-Myc feed-forward signaling loops (blue arrows), putative Akt-MTA1 link (dotted arrow). β-actin was used as a loading control. qRT-PCR data represent the mean ± SEM (n = 3), *$p < 0.05$; **$p < 0.01$ (two-tailed, two-sample t-test).

found a reduction in NF-κB (p65), IL-1β, and Vimentin and upregulation of E-cadherin protein levels in MTA1 knockdown (shMTA1) cells (Fig. 16A), suggesting direct involvement of MTA1 in inflammation and epithelial-to-mesenchymal transition (EMT) in PCa. Likewise, we detected a reduction in the levels of c-Myc, CyclinD1, Notch2, Ets2, and Hsp90 protein levels in shMTA1 cells (Fig. 16A), suggesting a role for MTA1 upstream to the critical oncogenes c-Myc, Notch2 and Ets2. Since Akt1 was among the MTA1 target promoters in the MTA1 ChIP-Seq analysis (not shown), we

hypothesized possible direct association between MTA1 and Akt. Indeed, MTA1 depletion in Pten-deficient LNCaP cells led to partial inactivation of Akt, at least in part, through downregulation of Akt protein levels (Fig. 16B). Besides, inhibition of the Akt pathway by phosphatidylinositol 3-kinase (PI3K) inhibitor LY294002 led to reduced MTA1 protein and mRNA in PC3M cells (Fig. 16C,D). Akt pathway is known to promote the stability of c-Myc protein, an identified transcriptional activator of MTA1. We found that inhibition of Akt pathway led to a reduction in c-Myc protein levels (Fig. 16C) but not mRNA. On the other hand, the downregulaton of MTA1 by LY294002 was at protein and mRNA levels (Fig. 16C,D) suggesting that the Akt pathway positively regulates MTA1 at the transcriptional level by promoting the stability of c-Myc protein (Fig. 16E). Together, these results suggest a direct positive crosstalk between MTA1 and Akt pathway independent of PTEN and a novel MTA1-c-Myc axis in prostate cancer. (Manuscript submitted).

Task 5. Evaluate the therapeutic efficacy of pterostilbene and combination modalities in prostate-specific PTEN knockout mice

Animal housing, care and treatments were in accordance with approved protocol by IACUC (UMMC) and ACURO (DoD). During the study, animals were monitored daily for their general health. As we indicated in our previous report, C57BL/6J mouse homozygous for the "floxed" allele of Pten gene ($Pten^{f/f}$) was purchased from Jackson Laboratories and bred with Pb-Cre4 male from the B6.Cg genetic background (NCI mouse repository) that specifically express Cre recombinase in the prostate epithelium. After series of breeding strategies and genotyping (Fig. 17), we collected more than 60 $Pten^{f/f}$ male mice for our intervention experiments.

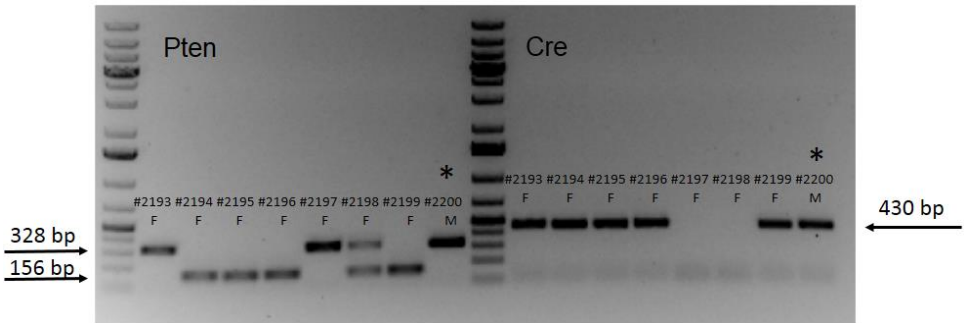

Fig. 17. An example of genotyping of prostate-specific Pten-null mice. $Pten^{+/f}$ female was bred with $Pten^{+/f}$, Cre4 male. Eight pops were born (seven females and one male). Tail-genomic DNA was isolated and amplified by PCR using the following primers: PTEN geno olMR9554F:5′-CAA GCA CTC TGC GAA CTG AG-3′; PTEN geno olMR9555R:5′-AAG TTT TTG AAG GCA AGA TGC-3′ with wt band of 156 bp and mutant band of 328 bp; and Cre F: 5′-TCG CGA TTA TCT TCT ATA TCT TCA G-3′; Cre R: 5′-GCT CGA CCA GTT TAG TTA CCC-3′ with a band of 393 bp. Results: one male is $Pten^{f/f}$, Cre4 (*) and two females that are Cre-negative can be used for breeding ($Pten^{f/f}$ and $Pten^{+/f}$). Although #2193 female is $Pten^{f/f}$, it cannot be used for breeding b/c of Cre-positivity.

For an intervention study we procured a total of 64 $Pten^{f/f}$ male mice maintained on AIN76A diet and employed by simple randomization with slightly larger allocation probability for treatment group. Mice were treated five days per week, i.p with either 10% DMSO (vehicle control, n =31) or 10 mg/kg bw of pterostilbene (n = 33). The animals were started on treatment immediately after weaning for either 3 (6 week-old), 7 (10 week-old), 12 (15 week-old), 17 (20 week-old), 22 (25 week-old) or 30 weeks (33 week-old). As an overall control, an additional group of littermates with Cre- negative $Pten^{f/f}$ genotype, which possess normal prostates were also put on AIN 76A diet. Necropsy was performed at respective time points (3-30 weeks of treatment) for $Pten^{f/f}$ mice. The $Pten^{f/f}$ (*Pten*-null) mice mimic stage-defined progression of human PCa and we found an age-dependent increase in MTA1 expression along with expected increased levels of p-Akt as compared to their normal counterparts, accompanied by changes in AR levels (Fig. 18A), suggesting a strong correlation with

the progression of PCa. This notion has been supported by our previous studies of human specimens, in which MTA1 overexpression was correlated with PCa progression, aggressiveness and metastasis (7, 8). Immunohistochemical (IHC) analysis of the Pten-null prostates showed high MTA1 expression in the multilayers of luminal epithelial cells and in the reactive stroma (Fig. 18B). Since several factors and cytokines, including NF-κB (p65), IL-1β, and Hsp90 have been implicated either in MTA1 regulatory network or induction of reactive stroma or both, we found that concomitant with MTA1, the expression of these proteins was increased with continued tumor development (Fig. 18A), suggesting a pro-inflammatory role for MTA1 in both the tumor and reactive stroma. Moreover, the expression of E-cadherin (an epithelial marker) was downregulated along with upregulation of Vimentin (a mesenchymal marker) (Fig. 18A), indicating the involvement of MTA1 in epithelial-to-mesenchymal transition (EMT) of PCa cells.

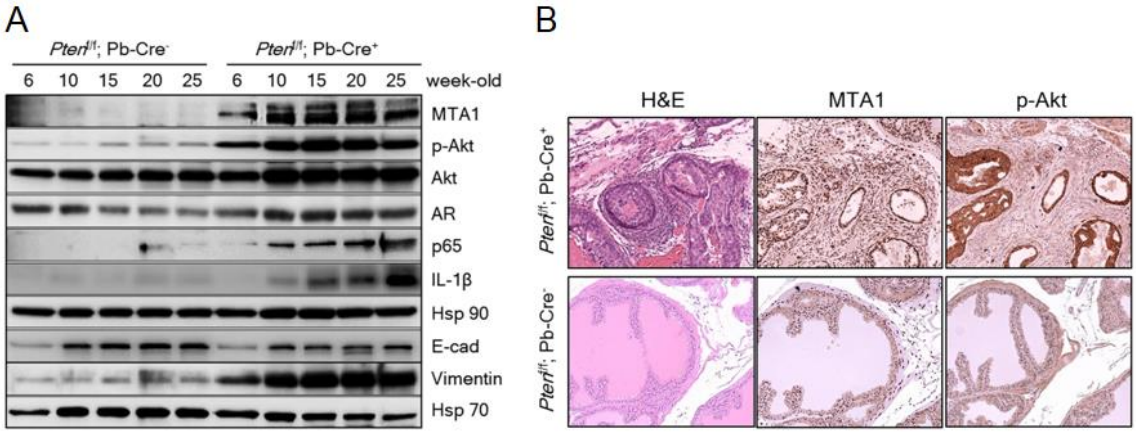

Fig. 18. **A**. Immunoblots of MTA1, p-Akt, Akt, AR, NF-κB (p65), IL-1β, Hsp90, E-cadherin (E-cad) and Vimentin in the prostate tissues from Pten$^{f/f}$ mice compared to NP controls, isolated at the indicated ages (time points). Hsp70 was used as a loading control. **B**. Comparison of H&E, MTA1, and p-Akt staining in the prostate tissues from 10-week-old Pten$^{f/f}$ mice and NP controls. Scale bars, 100 μm.

We compared tumor tissues between control and pterostilbene treated mice and found that pterostilbene treatment blocks progression to adenocarcinoma by lowing MTA1, pAkt, AR, IL-1β, HSP90 and increasing levels of E-cadherin in the prostate tissue of Pten-null mice (Fig. 19A). By 10 weeks of age, 67% of the Pten$^{f/f}$ mice contained regions of pre-invasive adenocarcinoma with enlarged, hardened prostates, which progressed to invasive adenocarcinoma by 25-33 weeks of age in all the mice examined but shrank upon pterostilbene treatment as evident by gross anatomy and *ex vivo* images of dissected prostatic lobes and UGS weights (Fig. 19B, C). Overall, 64% of the vehicle-treated mice exhibited pre-invasive or invasive adenocarcinoma whereas daily 10 mg/kg pterostilbene treatment reduced the incidence of adenocarcinomas to 12% and halted the progression at PIN stage (Fig. 19D) (Manuscript submitted).

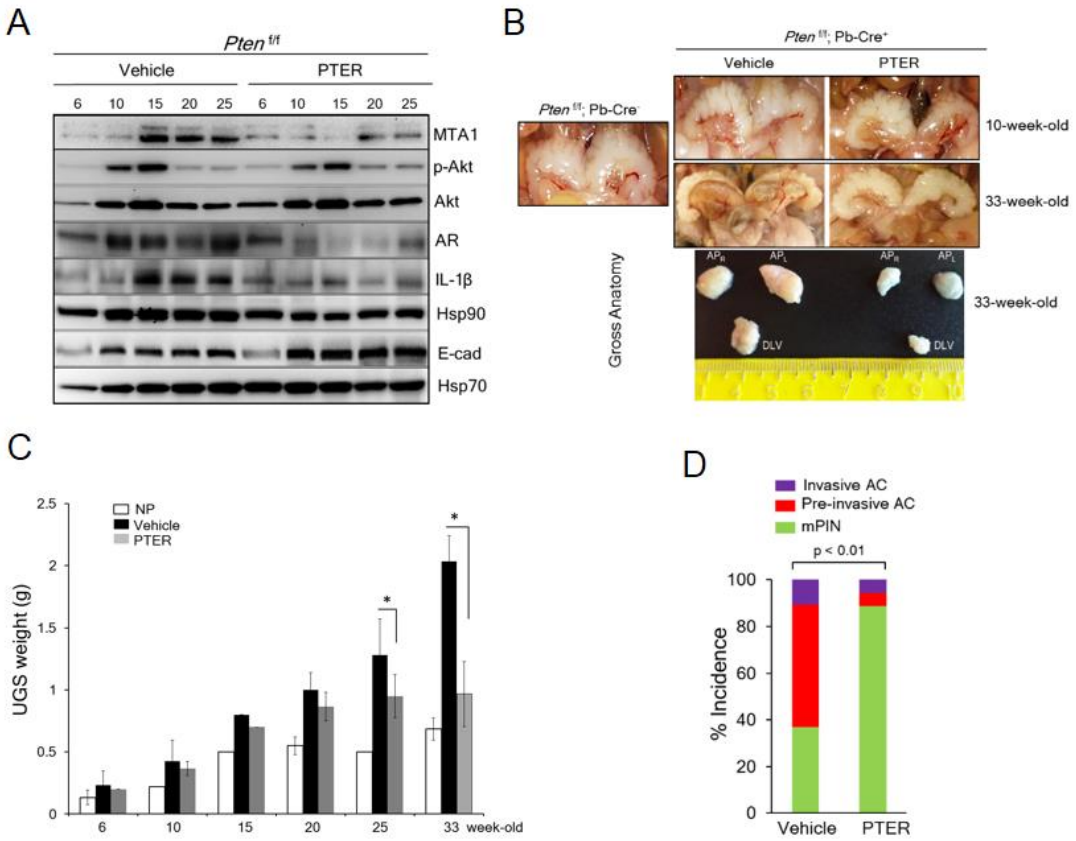

Fig. 19. A. Immunoblots of MTA1, p-Akt, Akt, AR, IL-1β, Hsp90 and E-cadherin (E-cad) in the prostates of vehicle and PTER treated Ptenf/f mice, isolated at indicated ages. **B**. Gross anatomy of the representative UGS from 10-week-old (top) and 33-week-old (middle) $Pten^{f/f}$ mice treated with vehicle (DMSO) and 10 mg/kg bw PTER. Representative images of dissected prostate lobes of $Pten^{f/f}$ mice (bottom). **C.** Comparison of UGS weights of vehicle or PTER treated $Pten^{f/f}$ mice, isolated at the indicated ages (n = 3/group). *$p < 0.05$ (two-tailed, two-sample t-test). **D**. Incidence of mPIN, pre-invasive and invasive adenocarcinoma (AC) in $Pten^{f/f}$ mice treated with vehicle (n = 19) and PTER (n = 18). $p < 0.01$ (Fisher's exact test).

As seen in Fig. 20 vehicle-treated mice developed enlarged prostates characterized by disorganized glandular structures, which contained regions of cribriform carcinoma with signs of microinvasion, i.e., loss of the basal membrane (SMA) and CK8-positive luminal cells that escaped into reactive stroma. In contrast, PTER-treated mice mostly showed characteristics of PIN, which retained a basal layer of SMA-positive cells and CK8-positive luminal cells along with only residual hypercellularity. Immunohistochemical analyses of tissues showed a substantial decrease in MTA1 levels in response to pterostilbene treatment at all ages. Importantly, pterostilbene intervention inhibited MTA associated maintenance of already highly activated Akt pathway. In addition, pterostilbene once again showed downregulation of AR levels (Fig. 21).

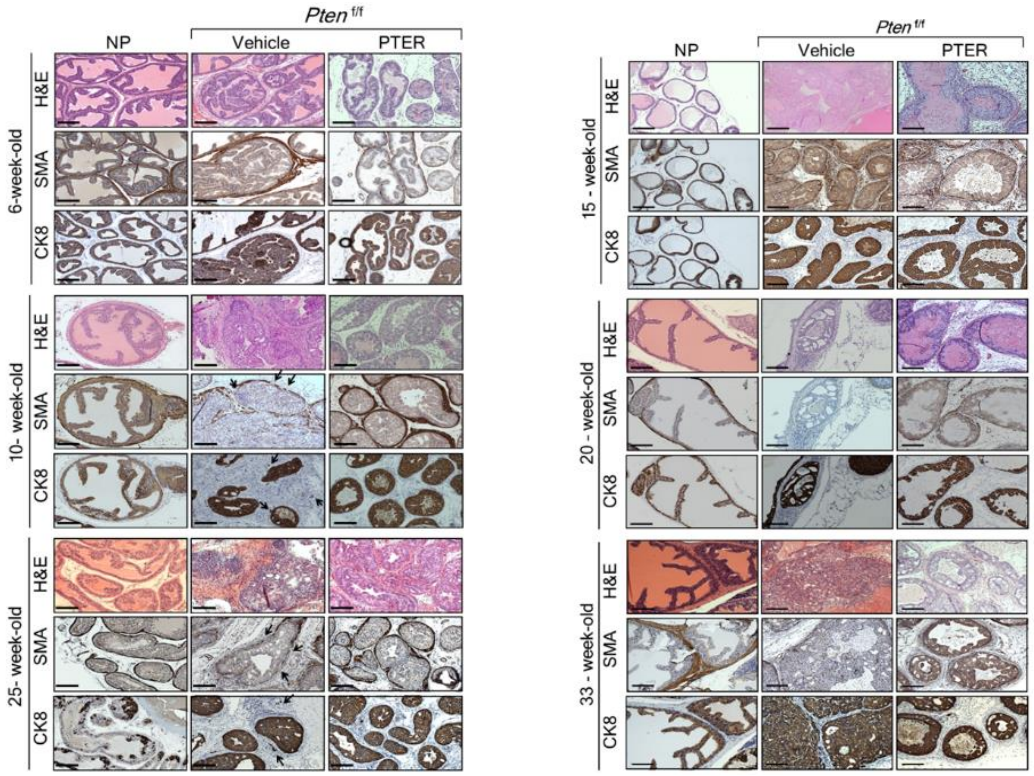

Fig. 20. Histopathology of representative Pten$^{f/f}$ mice at 6, 10, 15, 20, 25, and 33-weeks age. Comparison of H&E (top) and IHC for SMA (middle) and CK8 (bottom) in prostate tissues from Cre-negative mice with normal prostate (NP) and Pten$^{f/f}$ mice treated with vehicle and PTER. Scale bars, 100 µm

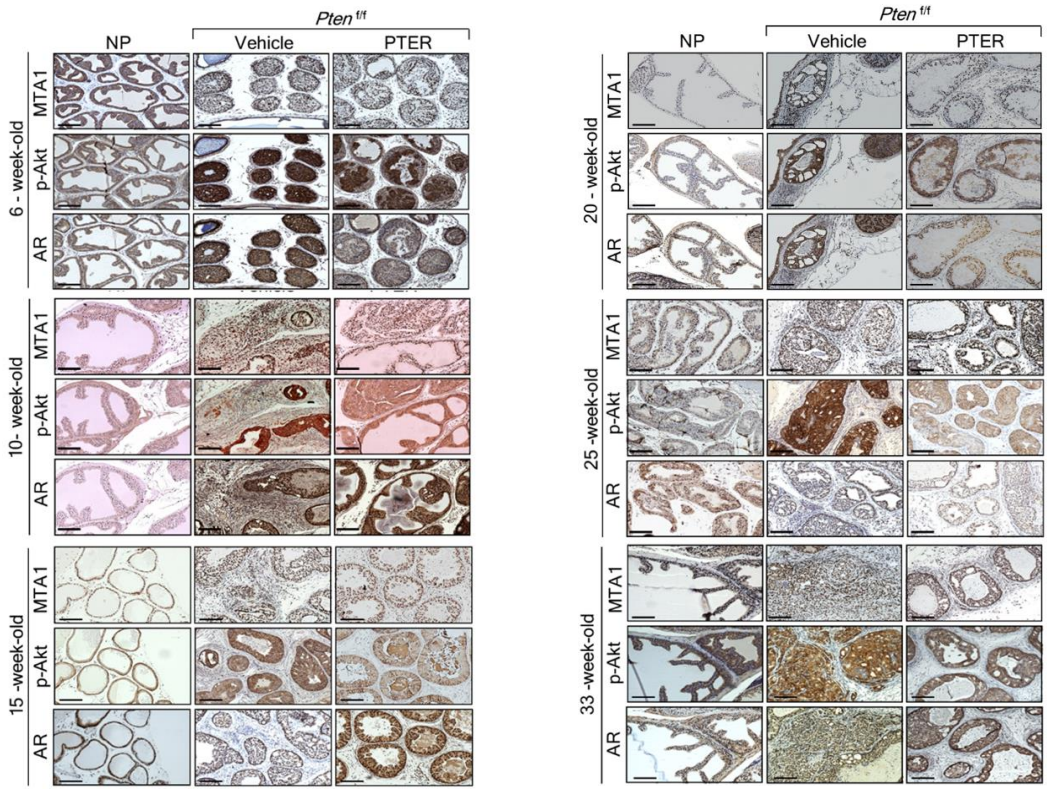

Fig. 21. IHC analyses of representative Pten$^{f/f}$ mice at 6-, 10-, 15-, 20-, 25-, and 33-weeks of age. Comparison for MTA1 (top), p-Akt (middle) and AR (bottom) from prostate tissues of Cre-negative (NP) and Pten$^{f/f}$ vehicle and PTER treated mice, respectively. Scale bars, 100 µm

To further investigate the lobe-specific differential impact of pterostilbene treatment, we performed immunoblot analysis using right anterior (AP_R), left anterior (AP_L) and dorso-latero-ventral (DLV) prostatic tissues. MTA1 was highly expressed in all lobes of $Pten^{f/f}$ prostates with various intensities, the highest being detected in AP_L (Fig. 22). The increase in MTA1 levels was inhibited on an average by 50% in all prostatic lobes of mice treated with pterostilbene (Fig. 22B). Pterostilbene had less consistent p-Akt-inhibitory effects in different lobes; yet, remarkably the effect was mostly evident in the AP_L prostatic lobe, in which MTA1 inhibition by pterostilbene was most significant. It is quite possible that one of the mechanisms of pterostilbene inhibition of the Akt pathway in these mice is through MTA1. Finally, AR levels were also markedly reduced in the prostates from the pterostilbene-treated group compared to control mice (Fig. 22B).

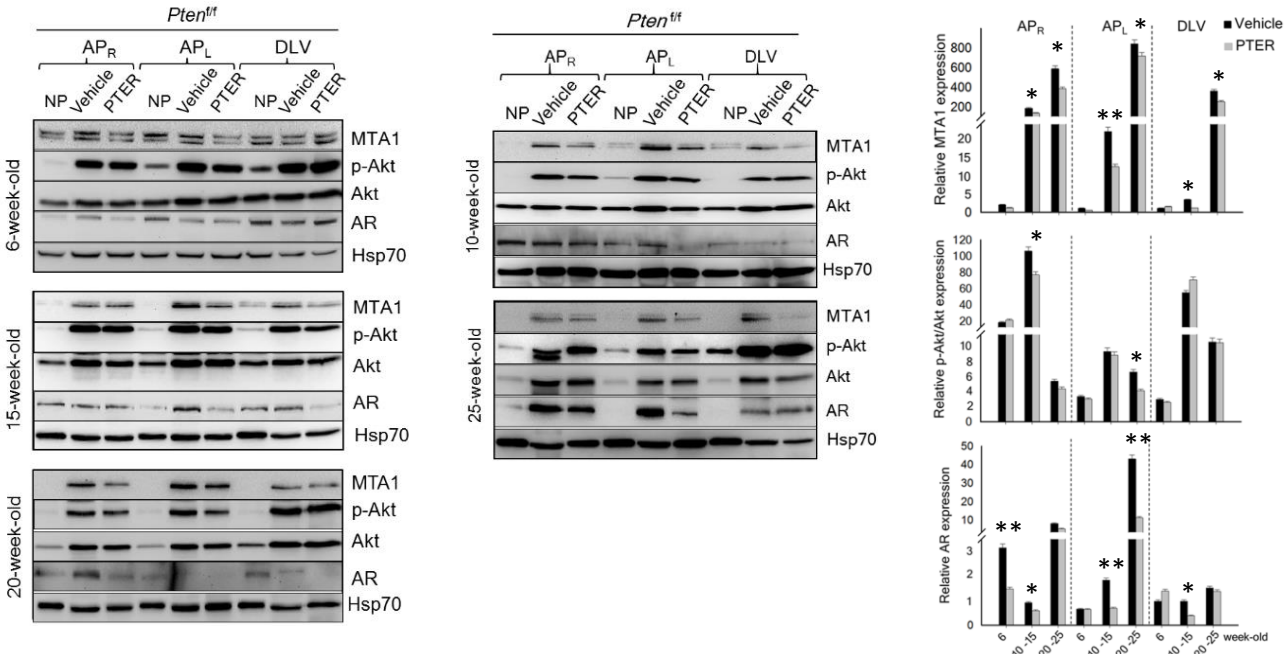

Fig. 22. **A**. Representative immunoblots of MTA1, p-Akt, Akt, AR in lysates from prostate lobes isolated from 6, 10-, 15-, 20, and 25-week-old Cre-negative (NP) and $Pten^{f/f}$ vehicle and PTER treated mice. Hsp70 was used as a loading control. **B**. Quantitation of MTA1, p-Akt/Akt and AR expression in prostate lobes of $Pten^{f/f}$ mice at different ages from three independent experiments. Values are mean ± SEM. **$p<0.01$, *$p<0.05$ (two-tailed, two-sample t-test).

Pterostilbene treatment induced apoptosis in prostate tissues of $Pten^{f/f}$ mice. Analyses of cleaved caspase-3 showed marked and an age-dependent increase, indicative of prolonged treatment benefits (Fig. 23).

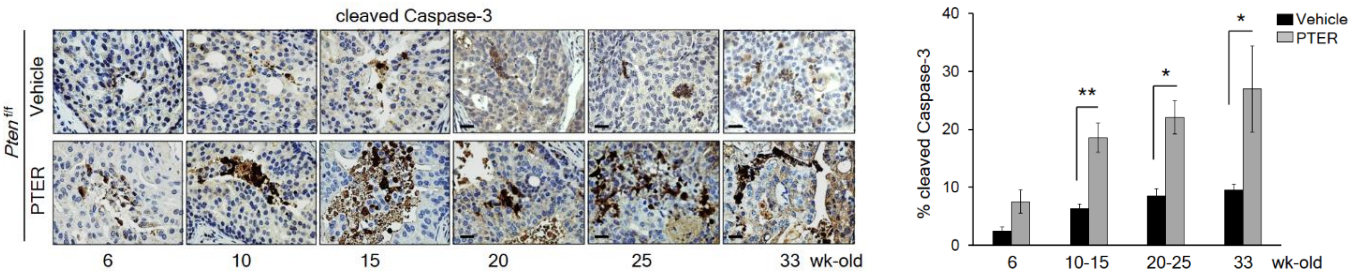

Fig. 23. Pterostilbene significantly induces MTA1-targeted apoptosis. A. Representative images and B, quantitation of cleaved caspase-3 staining at the indicated ages of vehicle and PTER treated Ptenf/f mice (n =5/group). Scale bars, 10 µm. Data are mean ± SEM from three independent experiments. *p < 0.05; **p < 0.01; (two-tailed, two-sample t-test).

Finally, consistent with our previous reports on the link between MTA1 and angiogenesis (5,6) pterostilbene treatment led to decreased angiogenesis, as evident by CD31 and VEGF-C immunostaining (Fig. 24).

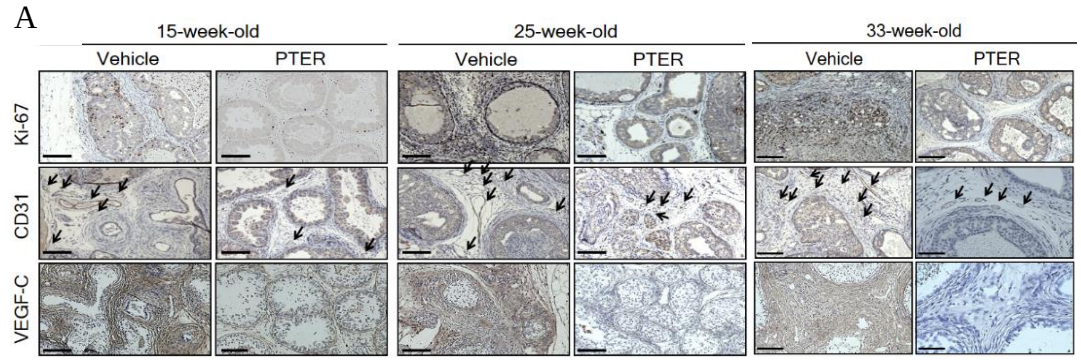

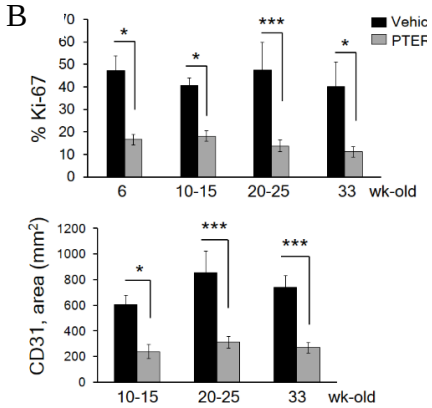

Fig. 24. Pterostilbene significantly inhibits MTA1-dependent cell proliferation and angiogenesis. **A**. Representative Ki-67 (top), CD31 (middle) and VEGF-C (bottom) staining and **B**, quantitation of Ki-67 (top) and CD31 (bottom) of the prostates from $Pten^{f/f}$ mice treated with vehicle and PTER, at indicated ages (n = 5/group). Arrows indicate vessels. Scale bars, 100 µm.

To check for metastasis, lymph nodes were isolated after injecting the mice subcutaneously at the foot pad (25µl/ foot pad) with Evans Blue dye and euthanizing after 30 minutes. The Evans Blue dye labels the popliteal LN, which drains centrally to the iliac and renal LNs along the midline. We did not find any lymph node metastasis even in mice aged over one year, by examining in total 34 renal and iliac lymph nodes of control or treated mice (Fig. 25).

To ascertain the clinical significance of our findings, we investigated the correlation between MTA1 and PTEN in human PCa by analyzing the expression of MTA1 and PTEN mRNA in the GSE41967 dataset from the Gene Expression Omnibus (GEO) database. We observed a significant inverse correlation between MTA1 and PTEN which became stronger with severity of the disease as evidenced by the increased Gleason scores (Fig.26A). Moreover, we found a significant positive correlation between MTA1 and AKT1 and no correlation between MTA1 and AR (Fig. 26B, C).

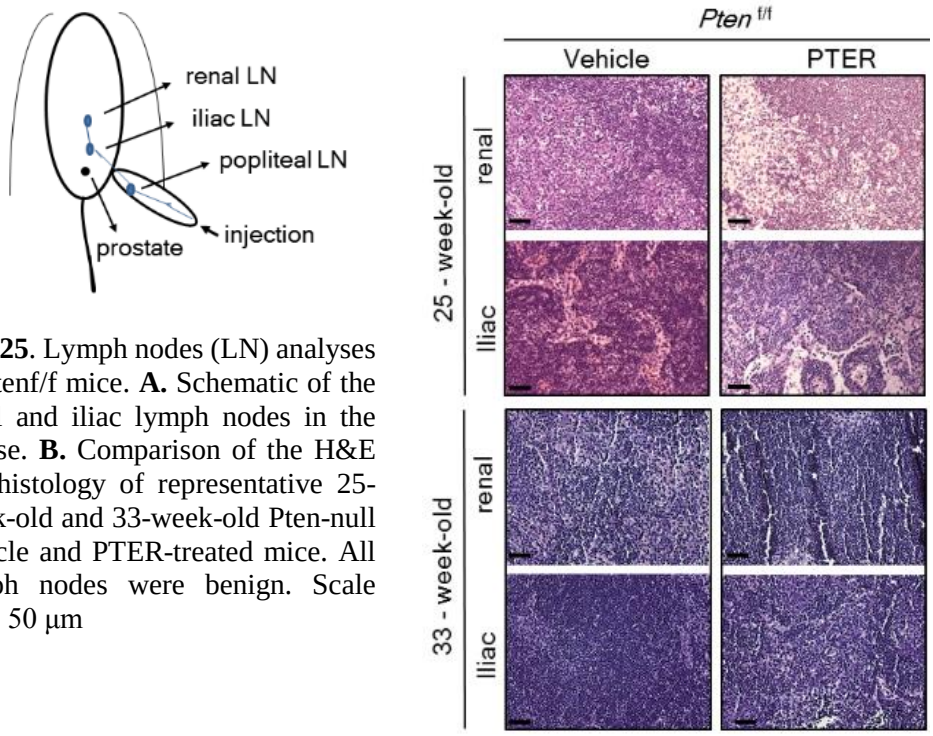

Fig. 25. Lymph nodes (LN) analyses of Ptenf/f mice. **A.** Schematic of the renal and iliac lymph nodes in the mouse. **B.** Comparison of the H&E LN histology of representative 25-week-old and 33-week-old Pten-null vehicle and PTER-treated mice. All lymph nodes were benign. Scale bars, 50 μm

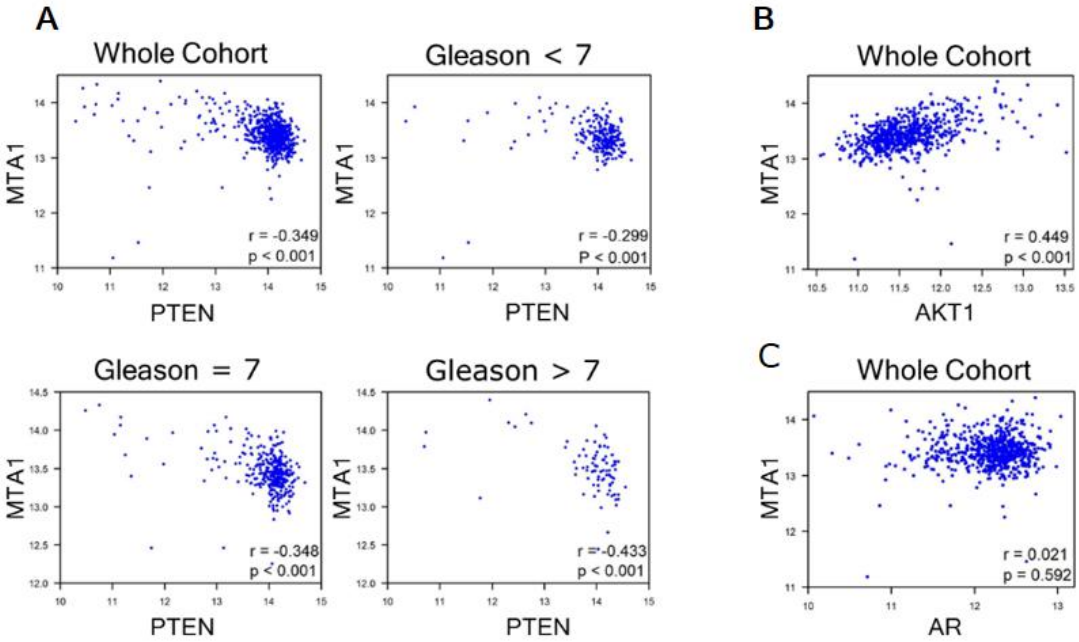

Fig. 26. GEO analyses for correlation of MTA1 with PTEN, AKT1 and AR. GSE41967 study of human prostate tissues (n=639) was used. **A.** Scatter plot depicting robust negative correlation between MTA1 and PTEN (r = -0.349, whole cohort), which becomes stronger with increased Gleason score (r = -0.299, Gleason < 7; r = -0.348, Gleason = 7; r = -0.433, Gleason > 7, p < 0.001); **B.** Positive MTA1 correlation with AKT1 expression (r = 0.499, whole cohort, p < 0.001); **C**. No correlation between MTA1 and AR (r =0.021, whole cohort, p = 0.592). p- values were calculated using two-tailed one-sample z-test for a correlation coefficient.

To determine whether pterostilbene reaches the target tissue, we analyzed pterostilbene concentrations in prostate tissues, as well as in the serum, from Pten$^{+/f}$ and Pten$^{f/f}$ mice. We found accumulation of pterostilbene in the prostates from both mouse models, with apparent greater accumulation when administered i.p. (Table 1), suggesting that high lipophilicity, membrane permeability and metabolic stability of pterostilbene secure its potent biological activity *in vivo*.

Table 1. Pterostilbene levels in serum and prostate tissues

Mouse model	Route	Dose	Age at sacrifice	PTER (mean ±SEM)	
				Serum (ng/ml)	Tissue (ng/g FW)
Pten $^{+/f}$	diet	100 mg/kg diet	8-12 mo	8.16 ± 0.11 (n = 26)	7.97 ± 1.15 (n = 17)
Pten $^{f/f}$	i.p	10 mg/kg bw	6-33 wks	11.79 ± 1.75 (n = 25)	30.14 ± 4.72 (n = 7)

Serum and prostate tissues were collected at sacrifice. Pterostilbene (PTER) levels were measured and quantified by GC-MS. Tissues were pooled together from at least three mice at each time point, and PTER was measured when detectable. The values represent mean ± SEM of two repeated measurements of combined tissues within each group. $p < 0.05$ for comparison in serum, $p < 0.01$ for comparison in tissue, two-sided Welch's t -test. FW, fresh weight; bw, body weight; wks, weeks; mo, months; n, number of mice

4. KEY RESEARCH ACCOMPLISHMENTS:

- In addition to already established LNCaP and DU145 cells, we established PC3M luciferase (PC3M-luc) and PC3M MTA1 knockdown cells (PC3M-luc-shMTA1). We characterized these cells *in vitro* (mRNA, protein, proliferation, invasion, colony formation, wound healing assays) and initiated *in vivo* studied to elucidate the role of MTA1 in prostate cancer progression and metastasis.
- We found additional pathways by which pterostilbene restores PTEN expression, namely, miRNA-mediated pathways.
- We performed MTA1 ChIP-Seq analysis of prostate tissues from transgenic mice and identified potential MTA1 target genes that are involved in prostate cancer development, progression and metastasis
- Continuous comprehensive ChiP-Seq data analysis reveals signaling partners for MTA1, which may play role in advanced metastatic prostate cancer (NFκB, IL-1β, Akt,c-Myc, CyclinD1, Notch2, Est2, HIF1-α, VEGF-C and others)
- Direct regulation of some of these genes by MTA1 was demonstrated by utilizing MTA1 knockdown cells
- The preliminary results of ChIP analysis showed novel direct MTA1-binding site on VEGF promoter
- We accumulated prostate-specific *Pten* null mice for intervention experiments
- We showed that high levels of MTA1 expression in *Pten*-null prostate cooperate with key oncogenes, including c-Myc and Akt among others, to promote PCa progression. In addition, loss-of-function studies using human PCa cells indicated direct involvement of MTA1 in inducing inflammation and promoting epithelial-to-mesenchymal transition (EMT) and survival pathways

- We demonstrated that pterostilbene has MTA1-mediated antitumor effects *in vivo.* Our experiments in *Pten* null mice clearly showed that pterostilbene treatment blocked the development of adenocarcinoma reducing tumor development and progression by 52%, at least in part, by inhibiting MTA1 and MTA1-associated signaling
- We analyzed pterostilbene levels in serum and prostate tissues and found that pterostilbene reaches its target tissues.
- Combination strategy PTEN plus SAHA experiments are ongoing

5. CONCLUSIONS:

Our completed research demonstrated the role of MTA1 and MTA1-guided molecules in prostate cancer progression. Furthermore, we identified novel putative MTA1-associated circuitry involved in *Pten* loss-driven prostate tumorigenesis and cancer progression. We found that MTA1 plays critical role in advancing prostate cancer by positively regulating oncogenic and angiogenesis-involved molecules such as Ets2, c-Myc, Cyclin D1, HIF-1α, VEGF and others. Importantly, our *in vitro* and *in vivo* studies demonstrated that pterostilbene exerts its anticancer activity, at least in part, through inhibition of MTA1 and MTA1-guided onset, development and progression of prostate cancer. Our findings in pre-clinical autochthonous mouse models have high translational relevance since they offer a perspective on the use of pterostilbene as an intervention strategy for patients at high risk for developing aggressive prostate cancer (i.e with Pten deficiency) and for patients with early-stage prostate cancer, who are recommended for "active surveillance" but offered no treatment. Our pre-clinical study on anti-cancer efficacy of a natural dietary compound, pterostilbene, provides a strong platform for its development as natural product drug and for initiation of much-needed clinical trials.

6. PUBLICATIONS, ABSTRACTS, AND PRESENTATIONS

Lay Press:

- Graduate Report, Spring 2015. The University of Mississippi Medical Center. Curing Cancer: Cancer Institute, HBCU students partner for summer research, June 2015, pp27-28 https://www.umc.edu/uploadedFiles/UMCedu/Resources/Grad_spring_2015_WEB.pdf

- Community Report , September 2015. https://www.umc.edu/uploadedFiles/UMC.edu/Content/Administration/Centers_and_Institutes(1)/Cancer_Institute/CI_Community_report_2014_15_FINAL_WEB.pdf

Peer-reviewed publications:

- Levenson AS*, Kumar A, Zhang X. MTA1 family proteins in prostate cancer: biology, significance and therapeutic opportunities. *Cancer Metastasis Rev*, 33: 929-942, 2014
- Dhar S, Kumar A, Li K, Tzivion G, Levenson AS*. Resveratrol regulates PTEN/Akt pathway through inhibition of MTA1/HDAC unit of the NuRD complex in prostate cancer. *BBA Molecular Cell Research*, 1853:265-275, 2015

- Kumar A, Dhar S, Rimando AM, Lage JM, Lewin JR, Zhang X, Levenson AS. Epigenetic potential of resveratrol and analogs in preclinical models of prostate cancer. *Annals of New York Academy of Sciences* 1348:1-9, 2015
- Dhar S, Kumar A, Rimando AM, Zhang X, Levenson AS. Resveratrol and pterostilbene epigenetically restore PTEN expression by targeting oncomiRs of the miR-17 family in prostate cancer. *Oncotarget* 6: 27214-27226, 2015
- Dhar S, Kumar A, Zhang L, Rimando AM, Lage JM, Lewin JR, Atfi A, Zhang X, Levenson AS. Pterostilbene impedes *Pten* loss-driven prostate cancer by targeting MTA1.*Cancer Research* Submitted
- Kumar A, Butt NA, and Levenson AS. Natural epigenetic-modifying molecules in medical therapy. In: *Medical Epigenetics*. Tollefsbol T (ed) Elsevier, Inc. 2015. In press

Published Abstracts:

- Levenson AS, Dhar S, Kumar A, Zhang L, Rimando AM, Lage JM, Lewin JR, Zhang X. Chemopreventive and therapeutic effects of pterostilbene in prostate cancer: epigenetic mechanisms of action. 2014RESVERATROL, 3rd International conference of resveratrol and health; 2014 Nov 30-Dec 5, Waikoloa, Hawaii, LO-09, p.19
- Swati Dhar, Avinash Kumar, Kun Li, Guri Tzivion and Anait S. Levenson. Resveratrol rescues PTEN expression and function by downregulating MTA1/NURD complex and oncomir 17-92 cluster in prostate cancer. The 8th Annual School of Graduate Studies in the Health Sciences' Research Day, UMMC, 2014 October 24, Jackson, MS
- Swati Dhar, Avinash Kumar, Liangfen Zhang, Agnes M. Rimando Janice M. Lage, Jack R. Lewin, Xu Zhang and Anait S. Levenson. Pterostilbene blocks prostate cancer progression in prostate-specific PTEN knockout mouse. The 8th Annual School of Graduate Studies in the Health Sciences' Research Day, UMMC, 2014 October 24, Jackson, MS
- Levenson AS, Dhar S, Kumar A, Rimando AM, Lage JM, Lewin JR, Zhang X. Dietary stilbenes and epigenetic regulation for prostate cancer chemoprevention and treatment. 31st Southern Biomedical Engineering Conference, Abstracts, Session IX (cancer), 2015, p.27
- Levenson AS, Dhar S, Kumar A, Lage JM, Lewin JR, Rimando AM, Zhang X. Epigenetic potential of dietary stilbenes in prostate cancer. American Council for Medicinally Active Plants (ACMAP) 6th
  Annual Conference; 2015 June 9-12, Spokane, WA; JMAP; 2015, 4 (vol 4, Supplement), p.4

Accepted Abstracts:

- Avinash Kumar, Swati Dhar, Nasir A. Butt, Xu Zhang, Luis Martinez, Anait S. Levenson. THE ROLE AND REGULATION OF MTA1- ETS2 AXIS IN PROSTATE CANCER. School of Graduate Studies in the Health Sciences' Research Day, UMMC, 2015 September 18, 2015, Jackson, MS
- Swati Dhar, Nasir A Butt, Avinash Kumar, Xu Zhang, Anait S Levenson. MTA1 DRIVES PROSTATE CANCER PROGRESSION AND METASTASIS THROUGH REGULATION OF ONCO-EPIMICRORNAS. School of Graduate Studies in the Health Sciences' Research Day, UMMC, 2015 September 18, 2015, Jackson, MS
- Nasir A Butt, Swati Dhar, Avinash Kumar, Agnes M. Rimando, Xu Zhang, Anait S. Levenson. NOVEL TARGETED COMBINATION THERAPEUTIC STRATEGY BASED ON NATURAL PRODUCT DRUG SYNERGY WITH CONVENTIONAL EPIGENETIC AGENT. School of Graduate Studies in the Health Sciences' Research Day, UMMC, 2015 September 18, 2015, Jackson, MS

- Benjamin A. Bates, Diva Whalen, Avinash Kumar, Jian-Quan Weng, Agnes M. Rimando, Anait S. Levenson. STILBENE DERIVATIVES INHIBIT PROSTATE CANCER CELL PROLIFERATION AND EXPRESSION OF METASTASIS-ASSOCIATED PROTEIN 1 (MTA1). School of Medicine Research Day, UMMC, 2015 September 30, 2015, Jackson, MS

Presentations:

- 3rd International Conference of Resveratrol and Health, Waikoloa, Hawaii, Nov 30-Dec 5, 2014 "Chemopreventive and therapeutic effects of pterostilbene, a natural analogue of resveratrol, on prostate cancer". Invited plenary speaker (Levenson)

- 31st Southern Biomedical Engineering Conference, New Orleans, LA, Apr 30-May 2, 2015 "Dietary stilbenes and epigenetic regulation for prostate cancer chemoprevention and treatment" Invited plenary speaker (Levenson)

- 6th Annual Conference American Council for Medicinally Active Plants. Spokane, WI, June 9-12, 2015 "Epigenetic potential of dietary stilbenes in prostate cancer management" Invited plenary speaker (Levenson)

- Pterostilbene blocks prostate cancer progression in prostate-specific PTEN knockout mouse. The 8th Annual School of Graduate Studies in the Health Sciences' Research Day, UMMC, 2014 October 24, Jackson, MS; Poster presentation (Kumar, a postdoc)

- Resveratrol rescues PTEN expression and function by downregulating MTA1/NURD complex and oncomir 17-92 cluster in prostate cancer. The 8th Annual School of Graduate Studies in the Health Sciences' Research Day, UMMC, 2014 October 24, Jackson, MS; Poster presentation (Dhar, a postdoc)

7. INVENTIONS, PATENTS and LICENSES: Nothing to report

8. REPORTABLE OUTCOMES: four peer-reviewed articles were published and one manuscript was submitted during the period of Sept 30, 2014 -Sept 29, 2015. Specifically,

Kumar A, Lin S-Y, Rimando AM, Levenson AS*. Plant-derived stilbenes inhibit androgen receptor expression in 22RV1 castrate-resistant prostate cancer cell line. Journal of Medicinally Active Plants (JMAP), Journal of Medicinally Active Plants (JMAP), 3(1):1-8, 2014

Dhar S, Kumar A, Li K, Tzivion G, Levenson AS*. Resveratrol regulates PTEN/Akt pathway through inhibition of MTA1/HDAC unit of the NuRD complex in prostate cancer. *BBA Molecular Cell Research*, 1853:265-275, 2015

Kumar A, Dhar S, Rimando AM, Lage JM, Lewin JR, Zhang X, Levenson AS. Epigenetic potential of resveratrol and analogs in preclinical models of prostate cancer. *Annals of New York Academy of Sciences* 1348:1-9, 2015

Dhar S, Kumar A, Rimando AM, Zhang X, Levenson AS. Resveratrol and pterostilbene epigenetically restore PTEN expression by targeting oncomiRs of the miR-17 family in prostate cancer. *Oncotarget* 6:27214-27226, 2015

Dhar S, Kumar A, Zhang L, Rimando AM, Lage JM, Lewin JR, Atfi A, Zhang X, Levenson AS. Pterostilbene impedes Pten loss-driven prostate cancer by targeting MTA1. *Oncotarget* Submitted

Acknowledgements are made to the DoD PCRP under Award # W81XWH-13-1-0370 in the Acknowledgements section of the papers.

Please also see **section 6** of this document for Abstracts and Presentation information.

9. OTHER ACHIEVEMENTS:

Several projects in the lab are based on the results from this study;1) the role of MTA1 in the inflammation- and epithelial-to-mesenchymal transition in prostate cancer (R01 application); 2) the role of MTA1 in prostate cancer disparity (DoD Health Disparity Award); 3) targeting MTA1 by pterostilbene to sensitize the cells for radiation response; 4) MicroRNA-mediated effects of pterostilbene in prostate cancer; 5) MTA1-regulated miRNA in prostate cancer; 6) Pterostilbene derivatives as potential anticancer agents in prostate cancer.

As a result of these studies, two summer students and one medical student were able to rotate in the lab and learn pathophysiology and molecular biology of prostate cancer along with hands-on experience of tissue culture, molecular biology and biochemical methods.

10. REFERENCES

1. Dias SJ, Li K, Rimando AM, Dhar S, Mizuno CS, Penman AD, Levenson AS. Trimethoxy-resveratrol and piceatannol administered orally suppress and inhibit tumor formation and growth in prostate cancer xenografts. The Prostate, 73:1135-1146, 2013
2. Kai L, Samuel SK and Levenson AS*. Resveratrol enhances p53 acetylation and apoptosis in prostate cancer by inhibiting MTA1/NuRD complex. International Journal of Cancer. 126:1538-48, 2010 (Cover story and art, April 1; *, corresponding author)
3. Dhar S, Kumar A, Li K, Tzivion G, Levenson AS*. Resveratrol regulates PTEN/Akt pathway through inhibition of MTA1/HDAC unit of the NuRD complex in prostate cancer. BBA Molecular Cell Research, 1853:265-275, 2015
4. Dhar S, Kumar A, Rimando AM, Zhang X, Levenson AS. Resveratrol and pterostilbene epigenetically restore PTEN expression by targeting oncomiRs of the miR-17 family in prostate cancer. Oncotarget 6:27214-27226, 2015
5. Kai L, Wang J, Ivanovic M, Chung Y-T, Laskin WB, Schulze-Hoepfner F, Mirochnik Y, Satcher RL and Levenson AS. Targeting prostate cancer angiogenesis through metastasis-associated protein 1 (MTA1). The Prostate 71: 268-280, 2011
6. Li K, Dias SJ, Rimando AM, Dhar S, Mizuno C, Penman AD, Lewin JR, Levenson AS. Pterostilbene acts through metastasis-associated protein 1 to inhibit tumor progression and metastasis in prostate cancer. PLoS ONE, 8: e57542, 2013

11. APPENDICES: please see attached PDF files of published papers and abstracts (09/2014 -09/2015)

Journal of Medicinally Active Plants

Volume 3
Issue 1 *Issues 1-4*

Stilbenes Inhibit Androgen Receptor Expression in 22Rv1 Castrate-resistant Prostate Cancer Cells

Avinash Kumar
University of Mississippi Medical Center, akumar@umc.edu

Shih-Yun Lin
University of Mississippi Medical Center

Swati Dhar
University of Mississippi Medical Center, sdhar@umc.edu

Agnes M. Rimando
USDA,Agriculture Research Service, Natural Products Utilization Research Unit, arimando@olemiss.edu

Anait S. Levenson
University of Mississippi Medical Center, alevenson@umc.edu

Follow this and additional works at: http://scholarworks.umass.edu/jmap

Recommended Citation
Kumar, Avinash, Shih-Yun Lin, Swati Dhar, Agnes M. Rimando, Anait S. Levenson. . "Stilbenes Inhibit Androgen Receptor Expression in 22Rv1 Castrate-resistant Prostate Cancer Cells," *Journal of Medicinally Active Plants* 3(1):1-8.
Available at: http://scholarworks.umass.edu/jmap/vol3/iss1/2

This Article is brought to you for free and open access by ScholarWorks@UMass Amherst. It has been accepted for inclusion in Journal of Medicinally Active Plants by an authorized administrator of ScholarWorks@UMass Amherst. For more information, please contact scholarworks@library.umass.edu.

Stilbenes Inhibit Androgen Receptor Expression in 22Rv1 Castrate-Resistant Prostate Cancer Cells

Avinash Kumar[1], Shih-Yun Lin[1], Swati Dhar[1], Agnes M. Rimando[2] and Anait S. Levenson[*1, 3]

[1]Cancer Institute and [3]Department of Pathology, University of Mississippi Medical Center, Jackson, MS 39216, USA

[2]Unites States Department of Agriculture, Agriculture Research Service, Natural Products Utilization Research Unit, University, MS, USA

[*]**Corresponding author:** alevenson@umc.edu

Manuscript received: September 22, 2014

Keywords: Androgen receptor, piceatannol, pterostilbene; resveratrol, trimethoxy-resveratrol.

ABSTRACT

Androgen receptor (AR) signaling plays an important role in the development and progression of prostate cancer (PCa). Importantly, AR continues to be expressed in advanced castrate-resistant PCa (CRPC), where the AR can have ligand-independent activity. Identification of naturally occurring substances that can inhibit AR expression holds promise for PCa chemoprevention and therapy. Earlier research demonstrated that resveratrol (Res) inhibited androgen-promoted growth, AR expression, and transactivation in androgen-responsive non-metastatic LNCaP PCa cells. In the current study, the effects of Res and three natural analogs [trimethoxy-resveratrol (3M-Res), pterostilbene (Pter), and piceatannol (Pic)] were investigated for effects on the growth of 22Rv1 castrate-resistant cells that express full-length (AR114/110) and truncated form (AR80) of AR. Although all the stilbenes tested inhibited the proliferation of 22Rv1 cells in a dose-dependent manner, 3M-Res was the most potent inhibitor. While AR114/110 responded to the syn-thetic androgen agonist methyltrienolone (R1881) as well as to antiandrogen flutamide, AR80, which lacks a ligand-binding domain, did not respond to R1881, but was inhibited by flutamide. Interestingly, Res, Pter, and Pic, but not 3M-Res, similar to flutamide, inhibited both AR114/110 and AR80 with the effect on AR80 being more prominent with the use of high concentrations of stilbenes. Collectively, the data indicate that both AR-independent (3M-Res) and possibly AR-dependent (Res, Pter, and Pic) mechanisms of cell growth inhibition occurs via these stilbenes. These findings provide evidence for plant-derived stilbenes as attractive and promising pharmacologically safe compounds to be used for diminishing progression and curb worsening of CRPC.

INTRODUCTION

Plant-derived polyphenols are attractive clinical candidates for cancer prevention and treatment. Resveratrol (Res) (*trans*-3,5,4'-trihydroxystilbene) is a polyphenol, a stilbene phytoalexin that is synthesized by a wide variety of plants in response to environmental stress and other stressors (Bhat and Pezzuto, 2002). *Polygonum cuspidatum* (common name Kojokon) is one such plant that produces Res (Burns et al., 2002). Res is also produced by grape

vines (*Vitis vinifera*), primarily in the grape berry skin (Fremont, 2000).

Pterostilbene (Pter) (*trans*-3,5-dimethoxy-4'-hydroxystilbene), a natural analog of Res, is a constituent in blueberries and grapes (Rimando et al., 2004), and trimethoxy-resveratrol (3M-Res) (*trans*-3,5,4'-trimethoxystilbene) is a constituent in *Pterobolium hexapatallum* (common name Indian Redwing) (Wang et al., 2010). Another naturally occurring analog, piceatannol (Pic) (*trans*-3,4,3',5'-tetrahydroxystilbene), which is a constituent in grapes and red wine, contains one extra hydroxy group (Kang et al., 2011). Resveratrol has been widely studied because of various health benefits associated with the compound, such as cardiovascular, neuroprotective, anti-inflammatory, antioxidant, and anticancer effects (Athar et al., 2007; Harikumar and Aggarwal, 2008; Markus and Morris, 2008; Pirola and Frojdo, 2008). In recent years natural analogs of Res have attracted increasing attention as a number of studies have suggested that modifications to the chemical structure, such as methoxylation-hydroxylation (Fig. 1) could enhance bioactivity (Huang et al., 2007; Kondratyuk et al., 2011; Wilson et al., 2008; Gosslau et al., 2008).

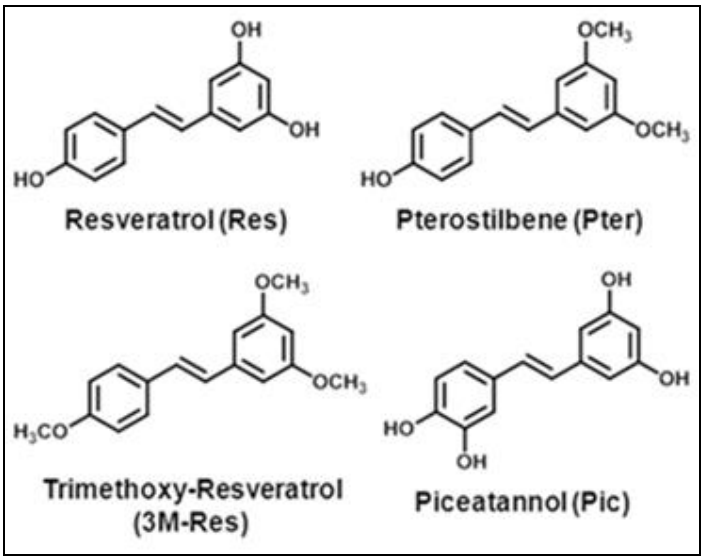

Figure 1. Chemical structures of natural stilbenes used in this study.

Resveratrol (Res), *trans*-3,4,5'-trihydroxystilbene; Pterostilbene (Pter), *trans*-3,5-dimethoxystilbene; Trimethoxy-Resveratrol (3M-Res), *trans*—3,5,4"-trimethoxystilbene; Piceatannol (Pic), *trans*-3,5,3'4'-tetrahydroxystilbene.

Prostate carcinoma, the most commonly diagnosed cancer in men in the Western countries, represents a public health problem with unmet therapy. Signaling through the androgen receptor (AR) plays an essential role in the initiation and progression of prostate cancer. Androgen-deprivation therapy (ADT) is used as a first-line treatment for metastatic prostate cancer, in which AR continues to be expressed and active. After significant clinical response, however, patients with advanced prostate cancer consistently relapse with a more aggressive form of PCa known as castration-resistant PCa (CRPC).

Several mechanisms have been suggested to mediate AR reactivation during CRPC progression, including AR gene amplification or overexpression, expression of splice variants, AR mutations – all of these conferring ligand promiscuity and/or ligand-independent activity that lead to cancer cell proliferation. Since the available anti-androgens have low affinity for AR and cannot completely block androgen action, especially in the presence of increased AR levels and AR variants, the discovery of novel potent and antagonistic blockers of AR is very important.

Kai and Levenson (2011) have previously demonstrated that Res inhibits the activity and decreases levels of AR in the androgen-dependent cell line LNCaP. The AR in these cells bear a mutation T877A in the ligand binding domain that affects the response to androgens and anti-androgens (Mahmoud et al., 2013; Otsuka et al., 2011). Although initially isolated from lymph node metastasis, LNCaP cells in tissue culture represent a relatively "non-aggressive" stage of PCa as these cells form tumors with much difficulty and do not form metastasis in xenografts.

In contrast, 22Rv1 cells are castrate-resistant cells derived from a xenograft that was serially propagated in mice after castration-induced regression and relapse of the parental, androgen-dependent CWR22 xenograft (Sramkoski et al., 1999). In pathophysiology, this represents a late, aggressive stage of PCa expressing 114/110 kDa full-length and truncated 80 kDa AR variants (Guo et al., 2009).

The goal of the current study was to examine the effects of Res and the natural analogs of Res (3M-Res, Pic, and Pter) as potential new AR blockers in 22Rv1 cells. In this study, Res and Res analogs inhibited cell proliferation and full-length as well as truncated AR expression in 22Rv1 cells. The inhibitory effect on truncated AR levels was most prominent at the higher concentrations of the tested compounds. The study results provide substantial evidence for plant-derived stilbenes as promising compounds for use, probably in combination with other anti-androgens, as inhibitors of AR signaling and thereby diminishing progression and worsening of CRPC.

MATERIALS AND METHODS

Chemicals. Resveratrol (Res) and piceatannol (Pic) were purchased from Sigma-Aldrich (St. Louis, MO) and Calbiochem-Novabiochem (San Diego, CA), respectively. Trimethoxy-resveratrol (3M-Res) and pterostilbene (Pter) were chemically synthesized at the USDA, ARS, National Products Utilization Research Unit in Oxford, MS, as previously described (Paul et al., 2010; Rimando et al., 2002). Structures of the synthesized compounds were confirmed by nuclear magnetic resonance spectroscopy and mass spectrometry. All compounds had ≥ 99% purity and were dissolved in high purity DMSO and stored in the dark at -20^{0}C.

Cell culture. The 22Rv1 cells were grown in RPMI 1640 media (GIBCO, Grand Island, NY) containing 10% Fetal Bovine Serum (GIBCO, Grand Island, NY) and 1% antibiotic-antimycotic (GIBCO, Grand Island, NY) at 37°C and 5% CO_2 as previously described for other prostate cancer cells (Dias et al., 2013). For experiments involving treatment with Res and analogs, media was replaced with phenol red-free RPMI-1640 (GIBCO, Grand Island, NY) containing 5% charcoal-stripped serum (GIBCO, Grand Island, NY) at least 8-10 h prior to treatment to eliminate hormonal background.

Cell proliferation assay. Cell viability was measured by the 3-(4,5-dimethylthazol-2-yl)-2,5-diphenyltetrazolium bromide (MTT) assay. Briefly, 22Rv1 cells were seeded at 3x10^3 cells/well density in 96-well plates using usual media. The media was changed to phenol red-free with 5% charcoal-stripped serum 8-10 h prior to treatment. Fresh media (100 µL), containing serial concentrations of Res, 3M-Res, Pter, and Pic, was added each day for 72 h, after which 20 µL of 5 mg/mL MTT (Sigma-Aldrich, St. Louis, MO) was added to the treatment media in the cells. After a 4 h incubation at 37^0 C, the media containing MTT was removed and the formazan crystals were dissolved in 100 µLof solvent (4 mM HCl and 0.1% TritonX-100 in isopropanol). The absorbance of the formazan at 590 nm was measured using Synergy-4 plate reader (BioTek Instruments Inc., Winooski, VT). IC_{50} values were calculated by the linear interpolation method, using MS Excel software (Microsoft, Redmond, WA).

Western blot analysis. Western blot analysis was done as described previously (Dias et al., 2013; Li et al., 2013). Briefly, 22Rv1 cells at 50-60% confluency were treated with selected concentrations of Res and Res analogs for 24 h. The cells were subsequently lysed in RIPA buffer (ThermoFisher, Waltham, MA) containing protease and phosphatase inhibitor cocktail (ThermoFisher, Waltham, MA). The protein concentration in the lysates was measured using the Bio-Rad protein assay reagent (Bio-Rad Laboratories, Hercules, CA). Equal amounts of protein (50 µg) were resolved in 10% SDS-PAGE gel and transferred to a PVDF membrane by Mini-Trans-Blot Electrophoresis Transfer System. The membranes were subsequently probed with AR (N20) antibody (Santa Cruz Biotechnology, Dallas, TX). β-actin (Santa Cruz Biotechnology, Dallas, TX) was used as a loading control. Signals were visualized using the chemiluminescent substrate Super-signal West Dura (ThermoFisher, Waltham, MA). Densitometry was done using Image J software.

Statistical analysis. The differences between the values of experimental and control treatments were analyzed for statistical significance by two-tail Student *t* test. The p values ≤0.05 were considered to be significant.

RESULTS

Prostate cancer inhibition. An examination on the growth of 22Rv1 castrate resistant prostate cancer cells treated with Res and the three natural analogs of Res (3M-Res, Pter, and Pic) was performed. The cells were treated with various

concentrations of the analogs (1-100 µM) in phenol red-free RPMI 1640 media supplemented with 5% charcoal-stripped FBS for 3 days. After treatment, a cell proliferation assay was done to assess the growth inhibitory activity of Res and analogs on 22Rv1 cells. All the tested compounds inhibited the growth of 22Rv1 cells in a dose dependent manner, but with different potencies (Fig. 2).

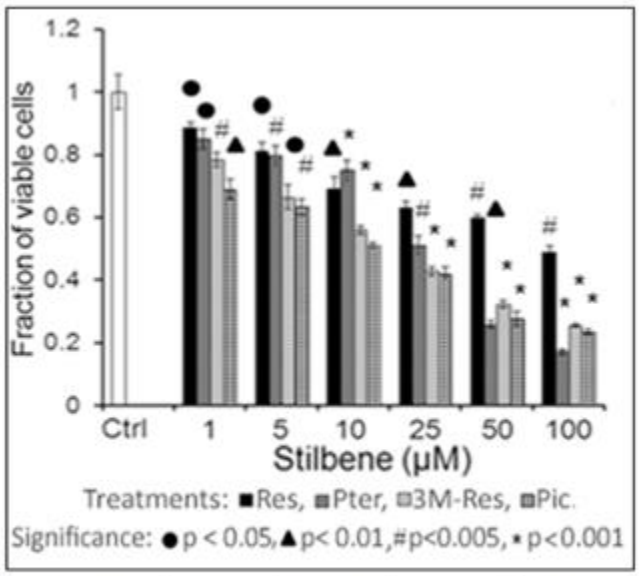

Stilbene	Res	Pter	Pic	3M-Res
IC_{50} (µM)	149.92	19.42	13.88	9.45

Figure 2. The effect of resveratrol and analogs on inhibition of cell growth.

Supplemental: Resveratrol and analogs inhibited growth of 22Rv1 castrate-resistant prostate cancer cells. Cells were grown in media containing selected doses of resveratrol (Res), trimethoxy-resveratrol (3M-Res), pterostilbene (Pter), and piceatannol (Pic). MTT assay was done with formazan measurements at 72 h. Viable cells were plotted as a fraction of untreated cells (Ctrl) (which was set to 1). Data represent the mean ± SE of three independent experiments in which each treatment (data point) was done in triplicates. Statistical significance was determined by two-tail Student *t* test. The p value ≤ 0.05 was considered significant. The IC_{50} values were calculated using the linear interpolation method with MS Excel software.

The cell growth inhibitory effect of Res and analog was determined by the IC_{50} values [50% inhibitory effect cell proliferation], using the liner interpolation method in MS Excel software. IC_{50} of Res 149.92 µM, whereas the other three analogs exhibited a stronger effect on cell proliferation as indicated by lower IC_{50} values of 19.42, 13.88, and 9.45 µM for Pter, Pic, and 3M-Res, respectively. The 3M-Res was the most potent among the Res analogs in inhibiting the growth of 22Rv1 cells, supporting the fact that replacement of all three hydroxy (OH) substituents with methoxy (OCH_3) groups results in a greater growth inhibitory activity (Dias et al., 2013, Gosslau et al., 2008).

Resveratrol and analog inhibition of AR.

Since the growth inhibition of the castrate-resistant prostate cancer cells (22Rv1) by resveratrol and analogs may be related to modulation of AR, the AR protein levels were assessed by Western blot analysis (Fig. 3). The 22Rv1 cells are known to express full-length 114/110 kDa and truncated (80 kDa) AR variants (Guo et al., 2009). The 80 kDa AR variant, which is truncated at the C-terminal, contains N-terminal domain (NTD) and a DNA-binding domain (DBD), but lacks the ligand-binding domain (LBD) (Fig. 4A) (Dehm et al., 2011).

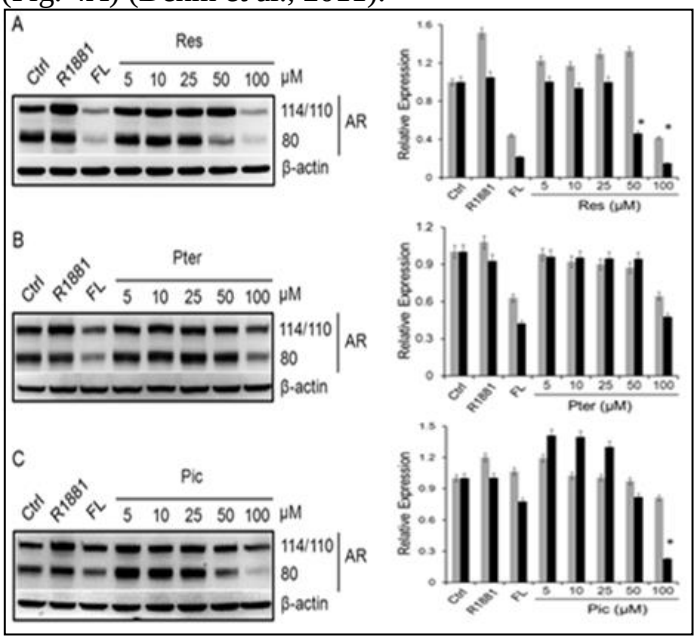

Figure 3. Inhibition of AR expression in 22Rv1 castrate resistant prostate cancer cells.

Supplemental: Western blots (left) indicate the effect of (A) Res, (B) Pter, and (C) Pic on AR protein levels at selected concentrations along with 10 nM R1881 (synthetic androgen); and 100 µM FL (flutamide - anti-androgen) for 24 h. β-actin was used as a loading agent. Graphical representation (right) is from quantitative analysis by Image J software. Control (Ctrl) was set as 1 and AR (AR 114/110, AR 80) levels are expressed relative to the control. Data represent the mean ± SE of three independent trials. *Significant at p < 0.05.

The 114/110 kDa AR variant was recognized as a single band at 110 kDa (AR114/110) while the 80

kDa AR variant (AR80) was recognized separately. The AR114/110, which has ligand-binding domain, responded to the ligand, synthetic androgen (R1881), and the nonsteroidal anti-androgen flutamide (FL), as indicated by the increase and decrease in AR levels upon treatment with R1881 and FL, respectively. AR80, however, did not respond to R1881, but responded to FL, suggesting different mechanisms of FL action than binding to the ligand-binding domain of AR.

Resveratrol treatment decreased AR114/110 levels in these cells, but at a high concentration of 100 µM, whereas AR80 levels were decreased in a dose dependent manner. Pterostilbene treatment initiated reduction of both AR114/110 and AR80 levels, but only at the 100 µM concentration. In contrast, treatment with Pic showed dose dependent lowering of both AR114/110 and AR80 levels with the effect being more prominent in the AR80 levels.

The 3M-Res did not produce a reliable dose-dependent inhibition of either AR114/110 or AR80 (data not shown). The differential effects of Res and analogs on AR114/110 and AR80 may be due to difference in the interaction of these compounds with specific domains of the AR variants (Fig. 4). Cumulative analysis of changes in AR levels by R1881, FL and stilbenes at 50 and 100 µM concentrations is shown in Fig. 4B.

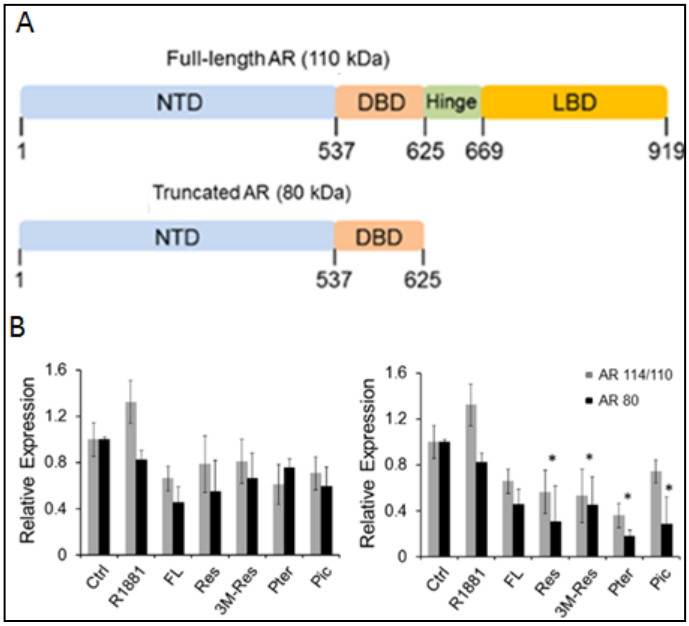

Figure 4. Regulation of full- length and truncated AR levels in 22Rv1 cells by resveratrol and analogs.

Supplemental: **A**. Domain structure of full-length AR (110 kDa) and truncated AR (80 kDa) protein in 22Rv1 cells. **B**. Graphical representa-tion of western blots quantitated by Image J software. Res, 3M-Res, Pter, and Pic reduced the full-length AR (AR114/110) and truncated AR (AR80) levels at 50 µM (left) and 100 µM (right) concentrations. R1881 is a synthetic androgen agonist, and Fl (flutamide is an anti-androgen. Data represent the mean ± SE of three independent replicate trials, *P<0.05.

DISCUSSION

A mainstay therapy of prostate cancer depends on androgen deprivation to which most patients do respond, but relapse with a castrate-resistant clinical outcome. The AR remains constitutively active in several cases of CRPC, however, several cellular and molecular alterations are related to this post-castration activation of the AR, including in-complete blockade of AR-ligand signaling, AR ampli-fications, AR mutations, aberrant AR co-regulator activities and AR splice-variant expression (Karantanos et al., 2013). Accumulating data suggests that both AR-dependent and AR-independent mechanisms are active and contribute to castrate-resistance (Kobayashi et al., 2013).

In the present study, the effect of Res and natural Res analogs on full-length and truncated AR in 22Rv1 cells were investigated. The 22Rv1 cells are unique in harboring splice variants of AR lacking the ligand-binding domain (Tepper et al., 2002) that is frequently expressed (Libertini et al., 2007). This AR is up-regulated in prostate cancer progression and promotes androgen-independent growth resistance (Guo et al., 2009). In earlier studies, Res was shown to induce down-regulation of AR in LNCaP cells (harboring a point mutation in AR protein) by inducing protein degradation through the caspase-3 proteolytic pathway (Kai and Levenson, 2011). From our earlier observations that Res can inhibit AR expression in LNCaP cells led to consideration whether Res and Res natural analogs would have a similar effect on the AR expression in castrate-resistant 22Rv1 cells.

Our data revealed that 3M-Res was

approximately 16-fold the efficiency of Res in inhibiting proliferation of 22Rv1 cells as indicated by their IC_{50} values (Fig. 2). It has been reported that the truncated isoform of AR (AR80) mediates the ligand-independent AR activity responsible for cell proliferation (Marcias et al., 2010). Interestingly, all three analogs were almost equally effective in inducing growth-inhibitory activity at the higher concentrations, and were much more potent than Res. The current data support our earlier observation that replacement of all three hydroxy (OH) substituents of Res with methoxy (OCH_3) groups results in greater growth inhibitory activity (Dias et al., 2013).

Thinking that the growth inhibition by Res and analogs in these cells may be related to modulation of AR, and to understand the effect of Res and Res analogs on the dynamics of the AR protein in 22Rv1 cells, the cells were treated with the test compounds in increasing doses from 5-100 µM and subjected to a western blot analysis to determine the AR protein levels. For controls, the cells were also treated with the synthetic androgen agonist R1881 and the anti-androgen, FL. R1881 enhanced and FL reduced the expression of AR114/110, while AR80 responded only to FL. This action could be expected due to the lack of LBD in AR80. Only Pic demonstrated a dose-dependent down-regulation in AR levels, whereas Res and Pter were effective only at the higher concentrations. Interestingly, 3M-Res did not produce any down-regulation of AR (data not shown) although the 3M-Res was more efficient than the other stilbenes in inhibiting the proliferation of 22Rv1 cells.

An AR-independent inhibition mechanism mediated by 3M-Res may be active in these cells. Of note, the truncated isoform of AR (AR80) was down-regulated more efficiently, as compared to the full-length counterpart, by FL or the stilbenes, suggesting involvement of mechanisms other than AR binding. These observations were corroborated by a test comparison of the relative expression of the full-length vis-à-vis the truncated AR with all the stilbenes at 50 and 100 µM concentrations.

Since the truncated AR can be down-regulated more effectively by the stilbenes than the full-length AR, this may possibly provide a target for therapeutic intervention using combinations of Res and Res analogs in patients that relapse after androgen ablation and present a castration-resistant phenotype.

ACKNOWLEDGEMENTS

The authors thank Dr. Liangfen Zhang for her contribution. The study was partially supported by the Department of Defense Prostate Cancer Research Program under award # W81XWH-13-1-0370 to Anait S. Levenson. Views and opinions of, and endorsements by the author(s) do not reflect those of the US Army of the Department of Defense. We are also grateful to Drs. Richard L. Summers and Janice M. Lage (UMMC) for their continuous support.

REFERENCES

Athar, M., J.H. Back, X. Tang, K.H. Kim, L. Kopelovich, D.R. Bickers, and A.L. Kim. 2007. Resveratrol: a review of preclinical studies for human cancer prevention. Toxicol. Appl. Pharmacol. 224:274–283.

Bhat, K.P. and J.M. Pezzuto. 2002. Cancer chemo-preventive activity of resveratrol. Ann. N.Y. Acad. Sci. 957: 210-229.

Burns, J., T. Yokota, H. Ashihara, M.E. Lean, and A. Crozier. 2002. Plant foods and herbal sources of resveratrol. J. Agric. Food Chem. 50:3337–3340.

Dehm, S.M., L.J. Schmidt, H.V. Heemers, R.L. Vessella, and D.J. Tindall. 2008. Splicing of a novel androgen receptor exon generates a constitutively active androgen receptor that mediates prostate cancer therapy resistance. Cancer Res. 68:5469-5477.

Dias, S.J., K. Li, A.M. Rimando, S. Dhar, C.S. Mizuno, A.D. Penman, and A.S. Levenson. 2013. Trimethoxy-resveratrol and piceatannol administered orally suppress and inhibit tumor formation and growth in prostate cancer xenografts. Prostate. 73:1135-1146.

Dias, S.J., X. Zhou, M. Ivanovic, M.P. Gailey, S. Dhar, L. Zhang, Z. He, A.D. Penman, S. Vijayakumar, and A.S. Levenson. 2013. Nuclear MTA1 overexpression is associated with aggressive prostate cancer, recurrence and metastasis in African Americans. Sci Rep. 3:2331.

Frémont L. 2000. Biological effects of resveratrol. Life Sci. 66:663-673.

Gosslau, A., S. Pabbaraja, S. Knapp, and K.Y. Chen. 2008. Trans- and cis-stilbene polyphenols induced rapid perinuclear mitochondrial clustering and p53-independent apoptosis in cancer cells but not normal cells. Eur. J. Pharmacol. 587: 25-34.

Guo, Z., X. Yang, F. Sun, R. Jiang, D.E. Linn, H. Chen, X. Kong, J. Melamed, C.G. Tepper, H.J. Kung, A.M. Brodie, J. Edwards, and Y. Qiu. 2009. A novel androgen receptor splice variant is up-regulated during prostate cancer progression and promotes androgen depletion-resistant growth. Cancer Res. 69:2305–2313.

Harikumar, K.B. and B.B. Aggarwal. 2008. Resveratrol: a multitargeted agent for age-associated chronic diseases. Cell Cycle. 7:1020–1035.

Huang, X.F., B.F. Ruan, X.T. Wang, C. Xu, H.M. Ge, H.L. Zhu, and R.X. Tan. 2007. Synthesis and cytotoxic evaluation of a series of resveratrol derivatives modified in C2 position. Eur. J. Med. Chem. 42:263-267.

Kai, L. and A.S. Levenson. 2011. Combination of resveratrol and antiandrogen flutamide has synergistic effect on androgen receptor inhibition in prostate cancer cells. Anticancer Res. 31:3323–3330.

Kang, C.H., D.O. Moon, Y.H. Choi, I.W. Choi, S.K. Moon, W.J. Kim, and G.Y. Kim. 2011. Piceatannol enhances TRAIL-induced apoptosis in human leukemia THP-1 cells through Sp1- and ERK-dependent DR5 up-regulation. Toxicol. In Vitro. 25:605–612.

Karantanos, T., P.G. Corn, and T.C. Thompson. 2013. Prostate cancer progression after androgen deprivation therapy: mechanisms of castrate resistance and novel therapeutic approaches. Oncogene. 32:5501-5511.

Kobayashi, T., T. Inoue, T. Kamba, and O. Ogawa. 2013. Experimental evidence of persistent androgen-receptor-dependency in castration-resistant prostate cancer. Int. J. Mol. Sci. 14:15615-15635.

Kondratyuk, T.P., E.J. Park, L.E. Marler, S. Ahn, Y. Yuan, Y. Choi, R. Yu, R.B. van Breemen, B. Sun, J. Hoshino, M. Cushman, K.C. Jermihov, A.D. Mesecar, C.J. Grubbs, and J.M. Pezzuto . 2011. Resveratrol derivatives as promising chemopreventive agents with improved potency and selectivity. Mol. Nutr. Food Res. 55:1249-1265.

Li, K., S.J. Dias, A.M. Rimando, S. Dhar, C.S. Mizuno, A.D. Penman, J.R. Lewin, and A.S. Levenson. 2013. Pterostilbene acts through metastasis-associated protein 1 to inhibit tumor growth, progression and metastasis in prostate cancer. PLoS One. 8:e57542.

Libertini, S.J., C.G. Tepper, V. Rodriguez, D.M. Asmuth, H.J. Kung, and M. Mudryj. 2007. Evidence for calpain-mediated androgen receptor cleavage as a mechanism for androgen independence. Cancer Res. 67:9001-9005.

Mahmoud, A.M., T. Zhu, A Parray, H.R.Siddique, W. Yang, M. Saleem, and M.C Bosland. 2013. Differential Effects of Genistein on Prostate Cancer Cells Depend on Mutational Status of the Androgen Receptor. PLos One. 8: e78479.

Marcias, G., E. Erdmann, G. Lapouge, C. Siebert, P. Barthélémy, B. Duclos, J.P. Bergerat, J. Céraline, and J.E. Kurtz. 2010. Identification of novel truncated androgen receptor (AR) mutants including unreported pre-mRNA splicing variants in the 22Rv1 hormone-refractory prostate cancer (PCa) cell line. Hum Mutat. 31:74-80.

Markus, M.A. and B.J. Morris. 2008. Resveratrol in prevention and treatment of common clinical conditions of aging. Clin. Interv. Aging. 3:331–339.

Otsuka, T., K. Iguchi, K. Fukami, K. Ishii, S. Usui, Y. Sugimura, and K. Hirano. 2011. Androgen receptor W741C and T877A mutations in AIDL cells, an androgen-independent subline of prostate cancer LNCaP cells. Tumour Biol. 32: 1097-1102.

Paul, S., A.J. DeCastro, H.J. Lee, A.K. Smolarek, J.Y. So, B. Simi, C.X. Wang, R. Zhou, A.M. Rimando, and N. Suh. 2010. Dietary intake of pterostilbene, a constituent of blueberries, inhibits the beta-catenin/ p65 downstream signaling pathway and colon carcinogenesis in rats. Carcinogenesis. 31:1272–1278.

Pirola, L. and S. Frojdo. 2008. Resveratrol: One Molecule, Many Targets. IUBMB Life. 60:323–332.

Rimando, A.M., M. Cuendet, C. Desmarchelier, R.G. Mehta, J.M. Pezzuto, and S.O. Duke. 2002. Cancer chemopreventive and antioxidant activities of pterostilbene, a naturally occurring analogue of resveratrol. J. Agric. Food Chem. 50:3453–3457.

Rimando, A.M., W. Kalt, J.B. Magee, J. Dewey, and J.R. Ballington. 2004. Resveratrol, pterostilbene, and piceatannol in vaccinium berries. J. Agric. Food Chem. 52:4713–4719.

Sramkoski, R.M., T.G. Pretlow 2nd, J.M. Giaconia, T.P. Pretlow, S. Schwartz, M.S. Sy, S.R. Marengo, J.S. Rhim, D. Zhang, and J.W. Jacobberger. 1999. A new human prostate carcinoma cell line, 22Rv1. In Vitro Cell. Dev. Biol. Anim. 35:403-409.

Tepper, C.G., D.L. Boucher, P.E. Ryan, A.H. Ma, L. Xia, L.F. Lee, T.G. Pretlow, and H.J..Kung.2002. Characterization of a novel androgen receptor mutation in a relapsed CWR22 prostate cancer xenograft and cell line. Cancer Res. 62:6606-6614.

Wang, T.T., N.W. Schoene, Y.S. Kim, C.S. Mizuno, A.M. Rimando. 2010. Differential effects of resveratrol and its naturally occurring methylether analogs on cell cycle and apoptosis in human androgen-responsive LNCaP cancer cells. Mol. Nutr. Food Res. 54:335–344.

Wilson, M.A., A.M. Rimando, and C.A. Wolkow. 2008. Methoxylation enhances stilbene bioactivity in *Caenorhabditis elegans*. BMC Pharmacol. 8:15.

Biochimica et Biophysica Acta 1853 (2015) 265–275

Contents lists available at ScienceDirect

Biochimica et Biophysica Acta

journal homepage: www.elsevier.com/locate/bbamcr

Resveratrol regulates PTEN/Akt pathway through inhibition of MTA1/HDAC unit of the NuRD complex in prostate cancer

Swati Dhar [a], Avinash Kumar [a], Kun Li [a], Guri Tzivion [a], Anait S. Levenson [a,b,*]

[a] Cancer Institute, University of Mississippi Medical Center, Jackson, MS, USA
[b] Department of Pathology, University of Mississippi Medical Center, Jackson, MS, USA

ARTICLE INFO

Article history:
Received 9 September 2014
Received in revised form 22 October 2014
Accepted 4 November 2014
Available online 13 November 2014

Keywords:
Resveratrol
Prostate cancer
MTA1
PTEN
Acetylation

ABSTRACT

Metastasis associated protein 1 (MTA1) is a component of the nucleosome remodeling and deacetylating (NuRD) complex which mediates gene silencing and is overexpressed in several cancers. We reported earlier that resveratrol, a dietary stilbene found in grapes, can down-regulate MTA1. In the present study, we show that PTEN is inactivated by MTA1 in prostate cancer cells. Further, we show that resveratrol promotes acetylation and reactivation of PTEN via inhibition of the MTA1/HDAC complex, resulting in inhibition of the Akt pathway. In addition, we show that MTA1 knockdown is sufficient to augment acetylation of PTEN indicating a crucial role of MTA1 itself in the regulation of PTEN acetylation contributing to its lipid phosphatase activity. Acetylated PTEN preferentially accumulates in the nucleus where it binds to MTA1. We also show that MTA1 interacts exclusively with PTEN acetylated on Lys^{125} and Lys^{128}, resulting in diminished p-Akt levels. Finally, using orthotopic prostate cancer xenografts, we demonstrate that both resveratrol treatment and MTA1 knockdown enhance PTEN levels leading to a decreased p-Akt expression and proliferation index. Taken together, our results indicate that MTA1/HDAC unit is a negative regulator of PTEN which facilitates survival pathways and progression of prostate cancer and that resveratrol can reverse this process through its MTA1 inhibitory function.

© 2014 Elsevier B.V. All rights reserved.

1. Introduction

"All men are at risk for prostate cancer. Changing the risk factors that can be controlled, such as diet, is one way to reduce prostate cancer risk". Since prostate cancer is age-related and relatively slow growing cancer, chemoprevention becomes the most promising strategy for the future management of this disease. Consequently, bio-reactive dietary compounds with anticancer properties, such as resveratrol, are of particular interest.

Resveratrol, a dietary compound found in berries, peanuts and mostly in grapes and wine, is known for its cardioprotective, anti-inflammatory, antioxidant and anticancer activities [1]. The anticancer action of resveratrol involves modulation of multiple molecular targets and pathways resulting in cell cycle arrest and apoptosis and inhibition of angiogenesis [2–7]. However, there are serious knowledge gaps regarding resveratrol's epigenetic mechanisms of action.

We reported earlier on a new epigenetic target of resveratrol, the metastasis-associated protein 1 (MTA1), which is a part of nucleosome remodeling and deacetylation (NuRD) co-repressor complex that mediates gene silencing [8,9]. We showed that resveratrol causes apoptosis in prostate cancer cells by inhibiting MTA1 and reversing MTA1-mediated deacetylation of p53 [10]. In prostate cancer xenografts, resveratrol treatment reduced mitotic activity and angiogenesis, and in co-operation with MTA1-knockdown, showed improved response with noticeable delay in tumor growth. Importantly, there was significantly increased levels of acetylated p53 (Ac-p53) and significant increase in apoptotic index upon resveratrol treatment [11]. These results clearly indicated that resveratrol alters post-translational modification of tumor suppressor p53 through targeting negative epigenetic modifier MTA1. We observed an inverse relationship between MTA1 and PTEN (phosphatase and tensin homolog deleted on chromosome 10) tumor suppressor protein levels and subsequently hypothesized that MTA1, which is abundantly accumulated in aggressive prostate cancer and metastasis [12–14], may participate in the deacetylation and inactivation of PTEN thereby activating downstream Akt cell survival and migration pathways [15–18]. We further hypothesized that resveratrol by down-regulating MTA1 may reactivate PTEN and rescue apoptotic pathways.

The tumor suppressor PTEN controls a variety of biological processes by negatively regulating the PI3K/Akt cell survival pathway [15,19]. The *Pten* gene is frequently mutated in prostate cancer [20]. At the same time, hypermethylation of the *Pten* promoter, and reduction of PTEN

Abbreviations: MTA1, metastasis-associated protein 1; PTEN, phosphatase and tensin homolog deleted on chromosome 10; Res, resveratrol

* Corresponding author at: Cancer Institute, University of Mississippi Medical Center, 2500 North State Street, Jackson, MS 39216, USA. Tel.: +1 601 815 6072.
E-mail address: alevenson@umc.edu (A.S. Levenson).

http://dx.doi.org/10.1016/j.bbamcr.2014.11.004
0167-4889/© 2014 Elsevier B.V. All rights reserved.

protein levels without mutations in the gene were observed in several cancers, indicating possible epigenetic mechanisms of PTEN regulation [21]. Therefore, it is possible that in addition to a direct mutation of the *Pten* gene, deregulation of PTEN protein on post-translational level plays role in cancer initiation and progression opening therapeutically attractive approaches for PTEN reactivation. Indeed, it has been reported that PTEN can be modified by phosphorylation, oxidation, nitrosylation and ubiquitination [15], and that all these modifications exert negative regulatory effects on PTEN function. However, there is limited literature on acetylation/deacetylation of PTEN and how this modification regulates its function.

In the current study, we provide evidence that there is an inverse relationship between MTA1 and PTEN and that in aggressive prostate cancer, nuclear MTA1 interacts with acetylated PTEN and inhibits its tumor-suppressive functions. Importantly, resveratrol can reactivate PTEN by reversing the negative effect of MTA1/HDAC mediated deacetylation. Our finding offers novel chemopreventive and therapeutic potential of dietary agents for management of prostate cancer.

2. Materials and methods

2.1. Reagents

Resveratrol (Res) (3,5,4′-trihyrdoxy-trans-stilbene) and Trichostatin A (TSA) were purchased from Sigma-Aldrich, IN, USA. SAHA (SuberoylAnilide Hydroxamic acid) was purchased from Cayman Chemicals, MI, USA. Resveratrol was used at 50 μM, SAHA at 10 μM and TSA at 300 nM concentrations for all experiments unless otherwise mentioned.

2.2. Cell culture

Human prostate cancer cells, DU145 and PC3M (ATCC, VA, USA and a gift from Dr. Bergan, Northwestern University, Chicago, respectively), were cultured in RPMI 1640 containing 10% fetal bovine serum (FBS) and 1% antibiotics (Life Technologies, NY, USA) at 37 °C and 5% CO_2. *Pten*$^{+/+}$ and *Pten*$^{-/-}$ mouse prostate epithelial cell lines were a gift from Dr. Tzivion, UMMC and were maintained in DMEM supplemented with 10% FBS with 1% antibiotics at 37 °C and 5% CO_2. 293T cells (ATCC, VA, USA) were maintained in DMEM supplemented with 10% FBS with 1% antibiotics at 37 °C and 5% CO_2. For experiments involving treatments with resveratrol, phenol red-free media containing 10% charcoal-stripped serum (Life Technologies, NY, USA) was used to provide steroid-free background. Cells were transferred to phenol red-free medium one day prior to treatments. Subsequently, cells were either treated with control (Ctrl, Ethanol/DMSO) or resveratrol (Res, 50 μM, unless otherwise mentioned) or SAHA (10 μM) or TSA (300 nM) for 18–24 h.

2.3. Plasmids, transfections and mutagenesis

The 800 pSG5L HA-PTEN (plasmid 10750), [22] and HDAC1-Flag (plasmid 13820) [23] plasmids were received from Addgene, MA, USA. Myc-MTA1 construct was a kind gift from Dr. Rakesh Kumar (George Washington University) and myc-p300 plasmid was a kind gift from Dr. Tzivion, Cancer Institute, UMMC. For transient transfections, 293T and/or PC3M cells were plated in 10 cm dishes (BD Falcon, Corning Life Sciences, MA, USA) to reach 80–90% confluence and were transfected with myc-MTA1, HA-PTEN, HDAC1-Flag, myc-p300 and PTEN mutant constructs or their respective empty vectors (10 μg) in OptiMEM (LifeTechnologies, NY, USA) using Fugene HD (Promega, WI, USA). After 36 h, cells were harvested and immunoprecipitation (IP) and western blot procedures were followed as described in the following sections.

Mutant PTEN constructs were created using the Infusion HD cloning kit (Clontech, CA, USA) following the mutagenesis protocol as per manufacturer's instructions. The following primer sequences were used in inverse PCR reactions for amplifying the designated clones; K125128Q Fwd 5′-tgt**caa**gctgga**caa**ggacgaactggtgtaatgatatgtgcata-3′ and Rev 5′-c**ttg**tccagc**ttg**acagtgaattgctgcaacatgattgtcatctt-3′, K125128R Fwd 5′-ttcactgt**aga**gctgga**aga**ggacgaac-3′ and Rev 5′-gttcgtcc**tct**tccagc**tct**acagtgaaaacg-3′, K402Q Fwd 5′-tacacaaatt aca**caa**gtctgagaattccccgatatcgcctcga-3′ and Rev 5′-tcagac**ttg**tgt aatttgtgtatgctgatcttcatcaaaagg-3′, K402R Fwd 5′-acaaattaca**aga** gtctgagaattccccgatatcgccagctca-3′ and Rev 5′-tcagac**tct**ttgtaatt tgtgtatgctgtctctcaaaaggttcatt-3′. The sequences in bold indicate the mutant amino acid(s) which were verified by sequencing (Davis Sequencing, CA, USA).

2.4. MTA1 silencing

Establishment of stable prostate cancer cell lines with MTA1 knockdown (MTA1shRNA) was described and characterized previously [10–12]. Briefly, the expression ArrestTMGIPZ lentiviral shRNAmir vectors expressing MTA1shRNA and non-silencing empty vector (EV) were purchased from Open Biosystems (GE Dharmacon, CO, USA) and virus particles were generated using 293T cells and packaging plasmid mixture (psPAX2 and pMD2.G, Addgene, MA, USA). Stable positive clones were selected using 1 μg/ml puromycin. The cell lines were stably transfected with luciferase (luc) and selected on G418 (neomycin, Sigma-Aldrich, IN, USA) for high luciferase expression to be used *in vivo* [11].

2.5. Western blot

Western blot analysis was performed as previously described [10–12]. Briefly, cells were harvested in chilled RIPA buffer with protease and phosphatase inhibitors (ThermoScientific, IL, USA). In the experiments with TSA/SAHA treatments we also used deacetylase inhibitors in the buffer. Protein estimation was performed using the Bradford reagent on a SmartSpec 3000 spectrophotometer (BioRad, CA, USA). 70 μg protein was loaded on 10% TGX gel, transferred to PVDF membrane, and probed with the following primary antibodies: Acetylated lysine (#9441), PTEN (#9188), p-Akt (Ser473, #9271), Akt (#4691) and Erk1/2 (#4695) (1:1000, Cell Signaling, MA, USA); MTA1 (A-11), HDAC1 (10E2) and anti-HDAC2 (B-2) (1:200, Santa Cruz Biotechnologies, CA, USA), β-actin (AC-15) and Lamin A (H-102) (1:1000, Santa Cruz Biotechnologies, CA,USA), myc (hybridoma supernatant, 1:250) and Flag (Clone M2, 1:1000, Sigma-Aldrich, IN, USA). Goat anti-mouse or goat anti-rabbit secondary antibodies (1:2500, Sigma-Aldrich, IN, USA) and goat anti-mouse light chain specific antibody (1:1000, Jackson Immunoresearch, PA, USA) were used for detection. Signals were visualized using Supersignal West Dura enhanced chemiluminescent substrate (ThermoScientific, IL, USA) on a Chemidoc Imager (BioRad, CA, USA). Images were quantified using ImageJ software (NIH).

2.6. Immunoprecipitation

Immunoprecipitation assays were performed using the Pierce Classic IP kit (ThermoScientific, IL, USA) as per manufacturer's instructions. Briefly, DU145 cells were plated in 150 mm dishes and cultured till 70–80% confluence. 293T or PC3M cells were transfected as described in Section 2.3. The cells were washed in DPBS (Life Technologies, NY, USA) and harvested in 0.5 ml of IP lysis buffer (Pierce Classic IP kit) with protease and phosphatase inhibitors (ThermoScientific, IL, USA). Lysates were prepared with 20 strokes on a Dounce homogenizer (Sartorius, Goettingen, Germany) and supernatants collected after centrifugation at 14,000 rpm for 10 min at 4 °C (Eppendorf 5430R, NY, USA). The lysates were incubated with 6 μg of primary antibodies or as per manufacturer's instructions: MTA1 (H-166), HDAC1 (10E2), HDAC2

(B-2), PTEN (A2B1), myc (hybridoma supernatant), Flag (Clone M2), acetyl-lysine (#9441,) on a rotating chamber overnight at 4 °C. 20 μl of Protein A/G beads (Pierce Classic IP kit, ThermoScientific, IL, USA) was added to the lysates after washing in spin columns and incubated for 2 h at 4 °C. The IP products were eluted in 2× sample reducing buffer with 20 mM dithiothreitol (DTT). IP elutes were loaded on 10% TGX gels (BioRad, CA, USA) and western blot was performed with indicated antibodies.

2.7. Subcellular fractionation

Fractionations were performed using the NE-PER Nuclear and Cytoplasmic extraction reagent kit (Thermo Scientific, IL, USA) according to the manufacturer's instructions. Briefly, cells were harvested with 0.25% trypsin-EDTA (Life Technologies, NY, USA), washed in DPBS and pelleted by centrifugation at 12,000 rpm for 10 min at 4 °C. 200 μl of buffer CER I was added with protease and phosphatase inhibitors to the cell pellet and vigorously vortexed for 15 s and incubated on ice for 10 min. Thereafter, buffer CER II (11 μl) was added and additionally vortexed and incubated on ice for 5 min. Cytoplasmic extracts were collected as supernatants by centrifuging at 16,000 *g* for 10 min. The cell pellet was washed thrice with 1 ml DPBS to remove cytoplasmic contamination. To the nuclear pellet, 100 μl buffer NER was added and vortexed for 15 s every 10 min for 40 min and supernatants were collected by centrifuging at 16,000 *g* for 10 min. Protein estimations and IP reactions were performed immediately or the extracts were stored at −80 °C for later analysis.

2.8. Immunoflourescence

DU145 cells were plated on sterile cover slips in 35 mm petri dishes (BD Falcon, Corning Life Sciences, MA, USA) so that they were at a confluence of 60–70% on the day of experiment. Cells were fixed in freshly prepared 2% chilled paraformaldehyde (ThermoScientific, IL, USA) for 15 min at room temperature on a rocker, washed with cold PBS and permeabilized in 0.5% TritonX-100/PBS (Fisher Scientific, PA, USA) for 15 min and washed with cold PBS. Non-specific binding was blocked by incubating cells with 10% normal mouse serum, 30 min at room temperature. For dual staining, cells were incubated first with MTA1 antibody (1:50, A-11, Santa Cruz Biotechnologies, CA, USA) followed by secondary antibody Alexa 488 (1:200, Life Technologies, NY, USA) in staining-wash buffer (5% FBS/0.5% TritonX-100/PBS) in dark for 1 h on a rocker. This was followed by washing and incubation with PTEN antibody (FL-403, 1:50, Santa Cruz Biotechnologies, CA, USA) followed by secondary antibody Alexa 633 (1:200, Life Technologies, NY, USA) for 1 h at room temperature. Finally cells were stained with Propidium Iodide (PI, 10 μg/ml, Sigma-Aldrich, IN, USA) and washed and mounted in Vectashield with DAPI (Vector Laboratories, CA, USA). Unstained cells and cells incubated with secondary antibody alone were used as negative controls. Images were acquired with a 63× objective on a Leica Brightfield Fluorescent microscope and Leica TCS SP2 confocal microscope and analyzed using the LAS AF Lite software version 2.6.0 (Leica Microsystems, IL, USA). For quantitation of co-localization, NIS elements Imaging software version 3.10, SP3, Hotfix (Build 644, LO) was used.

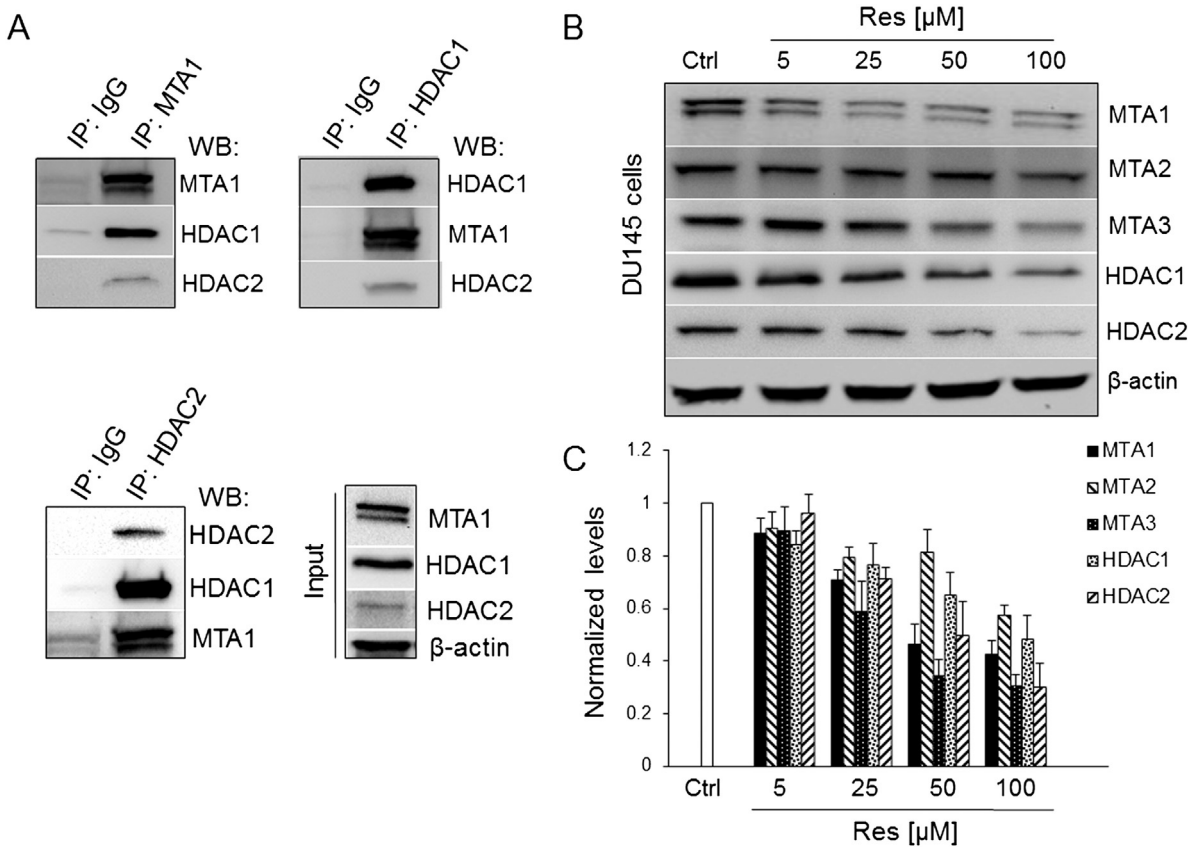

Fig. 1. A) MTA1 and HDAC1 and 2 are in complex. Reciprocal co-immunoprecipitations (co-IP) were performed with lysates from DU145 cells using anti-MTA1, anti-HDAC1 and anti-HDAC2 antibodies and western blot analysis was performed to detect MTA1, HDAC1 and HDAC2 respectively in IP elutes and in whole cell lysates (input). B) Resveratrol inhibits MTA1, MTA2, MTA3, HDAC1 and HDAC2 protein levels in DU145 cells in a dose-dependent manner. Western blot analysis of lysates from DU145 cells treated with Ethanol (Ctrl) or indicated concentrations of resveratrol (Res) for 24 h. C) Graphical representation of results. The vehicle-treated control (Ctrl) is normalized to 1 and protein level changes are expressed relative to Ctrl. The means ± SE of three independent experiments are shown.

2.9. Establishment of orthotopic prostate cancer xenografts in nude mice

Tumor tissues from the orthotopic prostate cancer xenografts described previously [11], were used for immunohistochemistry. Briefly, male nude mice were fed with phytoestrogen-free diet, injected orthotopically (intraprostatic) with DU145-luciferase-tagged MTA1-expressing (Ctrl) and MTA1-knockdown (MTA1shRNA) cells. Control group was treated with vehicle 10% DMSO and treatment group was injected 50 mg/kg bw/day of resveratrol through intraperitoneal (i.p.) administration. Bioluminescence signals were detected every week. The mice were sacrificed at week 8 after cell inoculation. At necropsy, prostates were excised and fixed in 10% neutral-buffered formalin for histopathological and immunohistochemical analysis.

2.10. Immunohistochemistry

Immunochemistry was performed with 4 μm formalin-fixed paraffin embedded tumor sections to evaluate Ki67, PTEN, MTA1 and p-Akt levels as described previously [11–13]. The VECTASTAIN ABC Elite Kit and the ImmPACT DAB kit (Vector Laboratories, CA, USA) were used to visualize staining. The following antibodies were used: anti-Ki67 (1:100, Abcam, MA, USA) and anti-PTEN (1:200, Santa Cruz Biotechnologies, CA, USA), anti-MTA1 and anti-pAkt (1:50, Cell Signaling Technologies, MA, USA). Images were recorded on a Nikon Eclipse 80i microscope and analyzed using the NIS elements BR 3.22.11 software.

2.11. Statistical analysis

Statistical significance (p values) in mean values of two-sample comparison was determined with paired two-tailed Student's *t*-test. A p-value < 0.05 was considered to be statistically significant.

3. Results

3.1. Resveratrol down-regulates components of the nucleosome remodeling and deacetylase (NuRD) complex

We have previously shown that MTA1 physically associates with HDAC1 in prostate cancer cells [10]. Others also demonstrated that MTA1 interacts with both HDAC1 and HDAC2 in breast cancer cells [24,25]. We too found that MTA1 interacts with both HDAC1 and HDAC2, which also interact with each other in DU145 cells (Fig. 1A). These results demonstrate that, in a physiological setting, MTA1/HDAC1/2 occurs as a complex in prostate cancer cells. We reported earlier that resveratrol down-regulates MTA1 and dissociates MTA1/HDAC1 complex [10]. This prompted us to investigate whether resveratrol has any effects on HDAC1 and HDAC2 protein levels directly. Interestingly, we found that resveratrol along with MTA1 inhibition decreases MTA2, MTA3, HDAC1 and HDAC2 levels in DU145 (Fig. 1B and C) and LNCaP cells in a dose-dependent manner (Supplementary Fig. 1).

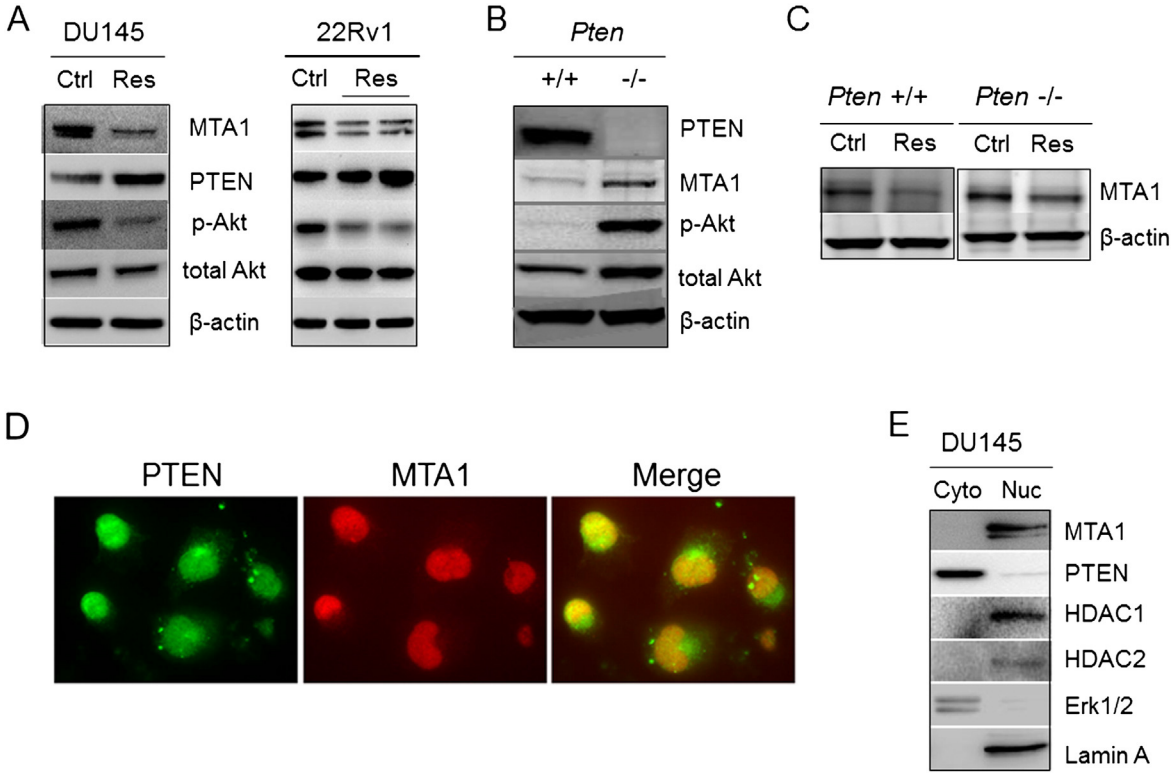

Fig. 2. MTA1 and PTEN are inversely related. A). Resveratrol inhibits MTA1 concomitantly with up-regulation of PTEN and down-regulation of pAkt (Ser 473). Western blot analysis of lysates from DU145 and 22Rv1 cells treated with Ethanol (Ctrl) or resveratrol (Res, 50 μM for Du145 and 50 μM and 100 μM for 22Rv1 cells) for 24 h. B). MTA1 is up regulated in prostate epithelial cells from *Pten* null mice. Western blot analysis of lysates from $Pten^{+/+}$ and $Pten^{-/-}$ cells for MTA1, PTEN, p-Akt (Ser 473), Akt and β-actin as loading control is shown. C) Resveratrol inhibits MTA1 in $Pten^{-/-}$ cell line. $Pten^{+/+}$ and $Pten^{-/-}$ cells were either treated with Ethanol (Ctrl) or resveratrol (Res, 50 μM) and lysates were probed for MTA1. D) Fluorescence microscopy showing co-localization of MTA1 and PTEN in DU145 cells. Cells were fixed, permeabilized and stained with anti-PTEN and anti-MTA1 primary antibody followed by visualization with secondary anti-rabbit Alexa 488 and anti-mouse Alexa 633 antibodies, respectively. Images were acquired using 63× objective on a Leica fluorescent microscope. Images were pseudo-colored in red to represent MTA1 and in green to represent PTEN. Images show PTEN (green) both in nucleus and cytoplasm, and co-localization with MTA1 in nucleus (merge, yellow). E) Subcellular localization and differential expression of MTA1 and PTEN in DU145 cells. Western blot analysis of cytoplasmic (Cyto) and nuclear (Nuc) lysates from DU145 cells is shown. Lamin A and Erk1/2 levels were used as loading controls for nuclear and cytoplasmic fractions, respectively. Subcellular localization shows exclusive nuclear distribution for MTA1, HDAC1 and HDAC2 proteins while PTEN is mostly cytoplasmic and partially nuclear.

3.2. Resveratrol inhibits MTA1 and up-regulates PTEN protein levels in prostate cancer cells: inverse correlation between MTA1 and PTEN

In conjunction with reports on transcriptional regulation of PTEN by HDAC inhibitors [26] and by the MTA1/HDAC4 complex [27], coupled with our own observation of resveratrol behaving as an HDAC inhibitor (Fig. 1B), we found a significant up-regulation of PTEN mRNA upon resveratrol treatment in DU145 and 22Rv1 cells (Supplementary Fig. 2). Importantly, resveratrol mediated down-regulation of MTA1 protein levels was concomitant with up-regulation of PTEN protein and accompanied by a decrease in phosphorylated Akt (p-Akt, S473) levels in DU145 and 22Rv1 cells suggesting an inverse relationship between MTA1 and PTEN (Fig. 2A). To confirm the inverse relationship between these two molecules, we examined MTA1 expression in murine prostate epithelial cells from conditional *Pten* knockout mice and found that *Pten*$^{-/-}$ cells express significantly higher levels of MTA1 compared to *Pten*$^{+/+}$ cells (Fig. 2B) and that resveratrol inhibits MTA1 expression in these cells (Fig. 2C) suggesting a possible negative co-relation between MTA1 expression and PTEN signaling.

In an earlier report by Salot and Gude, MTA1 and PTEN have been shown to co-localize in the nuclei of breast cancer cells [28]. Our immunofluorescence experiments revealed co-localization of MTA1 and PTEN in the nuclei of DU145 cells (Fig. 2D, Mander's overlap coefficient = 0.73, Pearson's coefficient = 0.84). Further experiments using confocal microscopy also confirmed nuclear co-localization of these two proteins in addition to evident cytoplasmic localization of PTEN (Supplementary Fig. 3). On the other hand, subcellular fractionation showed exclusive nuclear localization for MTA1, HDAC1 and HDAC2 while PTEN was mostly cytoplasmic with some amount in the nucleus (Fig. 2E). The fact that MTA1 and PTEN can be detected in the nucleus suggested that MTA1/HDACs co-repressor complex might be involved in post-translational regulation/deactivation of PTEN, which in turn, can lead to the activation of PI3K/Akt survival pathway. This finding substantiated the rationale to explore the crosstalk between MTA1 and PTEN and the role of resveratrol in regulating this signaling.

3.3. PTEN activity is regulated by resveratrol-induced reversible acetylation

To further confirm the inverse relationship between PTEN and MTA1 and to understand the role of the MTA1/HDAC deacetylase complex, we treated DU145 MTA1-expressing (EV) and MTA1 shRNA cells with HDAC inhibitor Trichostatin A (TSA) and performed western blot analysis. MTA1 knockdown enhanced PTEN expression, which was further augmented upon TSA treatment (Fig. 3A). Concomitantly, with increase in total PTEN levels upon MTA1 knockdown, substantiated by TSA treatment, there was a decrease in p-Akt (Ser 473). Interestingly, in addition to expected inhibition of HDAC 1/2 activity, TSA treatment alone reduced MTA1 levels as well (Fig. 3A).

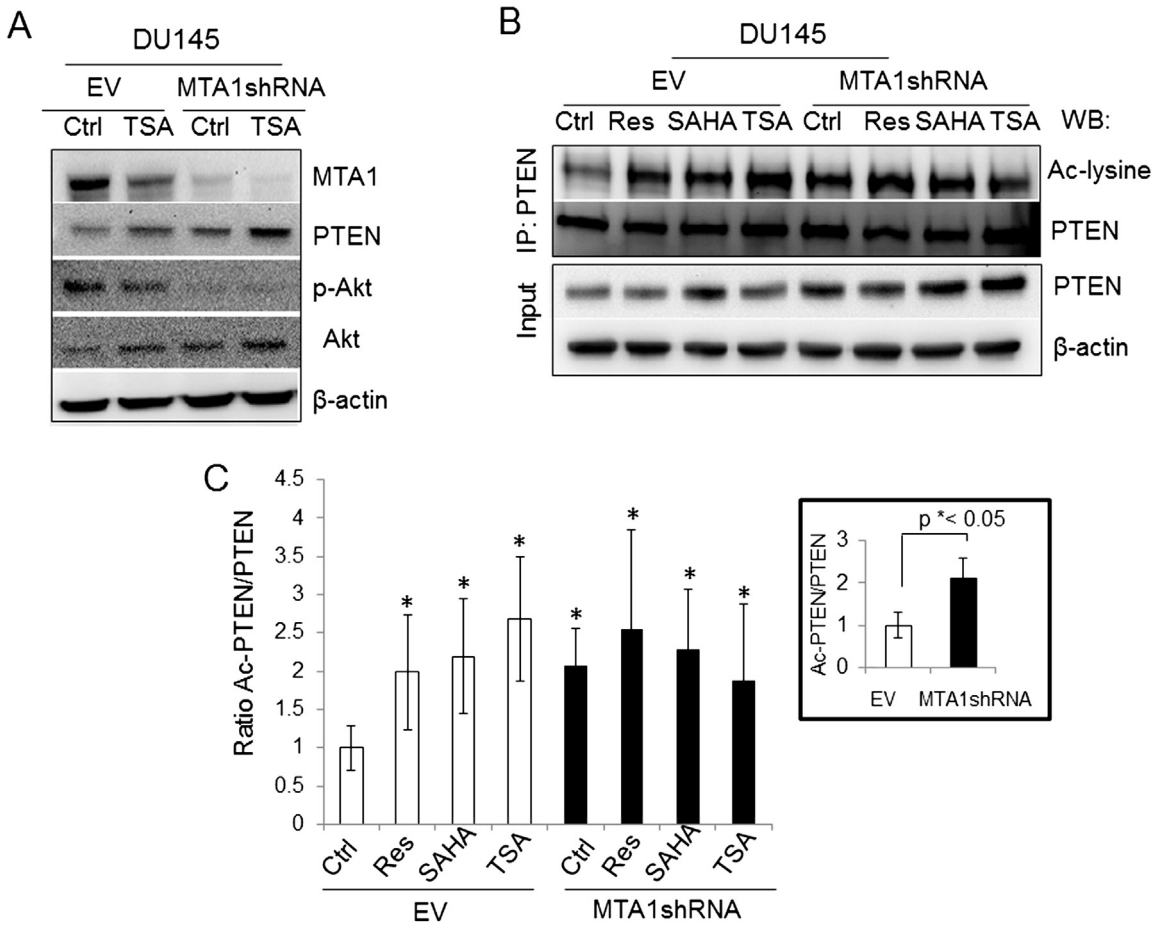

Fig. 3. MTA1 knockdown enhances PTEN while decreasing p-Akt which is augmented by HDAC inhibitor, TSA. A) Western blot analysis of lysates from DU145 empty vector (EV) or MTA1 knockdown (MTA1 shRNA) cells either treated with Ethanol (Ctrl) or Trichostatin A (TSA, 300 nM) for 18 h is shown. B) Resveratrol enhances acetylation of PTEN which is augmented upon MTA1 knockdown. DU145 EV or MTA1 shRNA cells were treated with DMSO (Ctrl), resveratrol (50 μM), Suberoylanilidehydroxamic acid (SAHA, 10 μM) and Trichostatin A (TSA, 300 nM) for 20 h. Cell lysates were immunoprecipitated with anti-PTEN antibody and western blot analysis performed with anti-acetyl-lysine and anti-PTEN antibodies. C) Quantitation for ratio of Ac-PTEN/PTEN was done using Image J software (NIH). EV (Ctrl) was normalized to 1 and all values were calculated relative to Ctrl, *$p < 0.05$. (Inset) Quantitation for ratio of Ac-PTEN/PTEN in DU145 EV versus MTA1 shRNA cells is shown, *$p < 0.05$. Error bars indicate means ± SEM. Representative data from three independent experiments is depicted.

To assess the mechanism of how resveratrol counteracts the negative regulatory effect of MTA1/HDACs on PTEN, we treated DU145 EV and MTA1shRNA cells with resveratrol and HDAC inhibitors, SAHA and TSA and performed IP PTEN and western blot for acetyl lysine (Ac-lysine). Resveratrol significantly increased acetylated PTEN (Ac-PTEN), almost to the same extent as SAHA and TSA (Fig. 3B and C). Interestingly, MTA1 knockdown alone was sufficient to significantly increase Ac-PTEN (Fig. 3C, inset, $p < 0.05$, Ctrl vs MTA1shRNA) suggesting that resveratrol's effect on PTEN acetylation occurs mainly through MTA1 inhibition. Since TSA and SAHA in addition to inhibiting HDACs functions also can directly inhibit MTA1 expression (Fig. 3A and data not shown), it is possible that the observed effects with SAHA and TSA are also mediated through MTA1 and not only through HDACs. Collectively, these results demonstrate that, all three agents resveratrol, SAHA and TSA, may suppress deacetylation and increase acetylation of PTEN by inhibiting each of the three proteins in the complex, although MTA1 knockdown experiments showed dominant role of MTA1 in PTEN deacetylation. These data demonstrate the negative association of MTA1/HDAC1/2 complex with acetylation-dependent activation of PTEN. Further, resveratrol and HDAC inhibitors which target the MTA1/HDACs complex, enhance acetylation of PTEN that, in turn may inhibit Akt phosphorylation.

We noticed that in all our experiments treatment of MTA1 knockdown cells with SAHA and TSA did not induce an additive effect on PTEN acetylation (Fig. 3C) although they did induce PTEN expression (Fig. 3B input). We then asked whether HDAC1 or HDAC2 or both are needed to mediate the effect on PTEN deacetylation. As shown in Fig. 3B, HDAC class I inhibitors, which can inhibit both HDAC1 and 2, increased PTEN acetylation. We then used HDAC1-specific inhibitor (4-(dimethylamino)N-[6-(hydroxyamino)-6-oxohexyl]-benzamide) and found that PTEN acetylation was increased but to a lesser extent than when treated with TSA and SAHA suggesting involvement of HDAC2 in addition to HDAC1 in PTEN deacetylation (data not shown).

3.4. MTA1 knockdown induces accumulation of acetylated PTEN in the nucleus of prostate cancer cells

Since we already observed co-localization of MTA1 and PTEN in the nucleus of DU145 cells (Fig. 2D and E), we further hypothesized that for MTA1 a nuclear protein, to deacetylate PTEN which is predominantly cytoplasmic, would require an event most likely occurring in the nucleus. To answer this possibility, we fractionated cytoplasmic and nuclear extracts from DU145 EV and MTA1shRNA cells treated with TSA and subsequently performed IP PTEN and western blot for Ac-lysine. We found that Ac-PTEN expression was increased in both cytoplasm and nuclear compartments; however, the increase in the nuclear compartment was more dramatic (Fig. 4A and B, *Nuc* vs *Cyto*, $p < 0.05$). Importantly, this effect was prominent in MTA1 knockdown cells, which was further augmented upon TSA treatment (Fig. 4A and B). This data clearly indicated that MTA1 knockdown favorably enhances acetylation of PTEN largely in the nuclear compartment. Further, it indicated that for such a mechanism to be functional a physical interaction between MTA1 and PTEN itself maybe important. Therefore, we next raised the question: does MTA1 interact with PTEN?

3.5. MTA1 does not interact with PTEN in prostate cancer cells

We and others have shown that MTA1 can be localized in both nucleus and cytoplasm with predominance in nuclei in cultured cancer cells and tissues [13,29–33]. In our studies with tissue microarrays of 291 human prostate cancer specimens, MTA1 nuclear localization was directly correlated with aggressiveness of prostate cancer and metastasis [13]. HDAC1 and HDAC2 are mostly nuclear proteins and in prostate cancer, nuclear HDAC1 overexpression has been reported to be correlated with poor prognosis [34] and HDAC2 expression

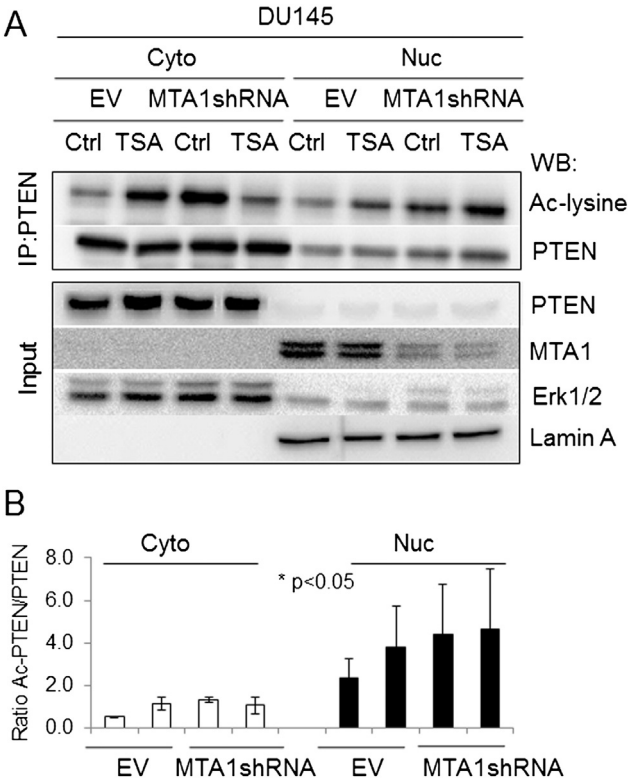

Fig. 4. MTA1 knockdown-induced acetylation of PTEN predominantly occurs in the nucleus of prostate cancer cells. A) DU145 EV and MTA1 shRNA cells were treated with Ethanol (Ctrl) or Trichostatin A (TSA, 300 nM) for 20 h. Cell lysates were fractionated to obtain cytoplasmic and nuclear fractions as detailed in *materials and methods*. Cytoplasmic and nuclear extracts were immunoprecipitated using anti-PTEN antibody and analyzed by western blotting using antibodies to acetyl lysine and PTEN. Erk1/2 and Lamin A were used as loading controls for cytoplasmic and nuclear fractions respectively, *Cyto* Cytoplasm, *Nuc* Nuclear. Representative data from four independent experiments is shown. B) Quantitation for ratio of Ac-PTEN/PTEN, $^*p < 0.05$ indicates significance of nuclear ratio of Ac-PTEN/PTEN versus cytoplasmic determined by paired Student's *T* test. Histogram prepared by calculating raw values obtained using Image J software (NIH). Error bars indicate means ± SEM.

had highly significant prognostic value [35]. This means that deacetylation of PTEN by MTA1/HDACs complex most likely occurs in the nucleus. Since by immunofluorescence and subcellular fractionation experiments we found that MTA1 and PTEN can co-localize in the nucleus, we hypothesized that they could physically interact with each other. However, reciprocal co-immunoprecipitation (Co-IP) analysis for interaction between endogenous MTA1 and PTEN revealed association between MTA1 and HDAC1 and HDAC2 but not PTEN (Fig. 5A). Ectopic overexpression of MTA1, PTEN and HDAC1 by co-transfections of myc-MTA1, HDAC1-Flag and HA-PTEN in 293T cells revealed no interaction between MTA1 and PTEN, consistent with our results in DU145 cells (Fig. 5B). In addition, co-IP experiments with ectopic overexpression of PTEN in PC3M cells that express very high endogenous MTA1 revealed no detectable interaction between MTA1 and PTEN (not even under stringent conditions when MG132, a proteasome inhibitor, was applied to block degradation of MTA1 and increase the probability of interaction, data not shown).

3.6. MTA1 interacts with acetylated PTEN in the nucleus

Since we could not detect an interaction between MTA1 and PTEN, we surmised over the possibility that MTA1/HDACs complex could have more affinity to interact with the acetylated form of PTEN and in turn deacetylate it. To prove this hypothesis, we devised two experiments. First, we boosted acetylation by co expressing HA-PTEN

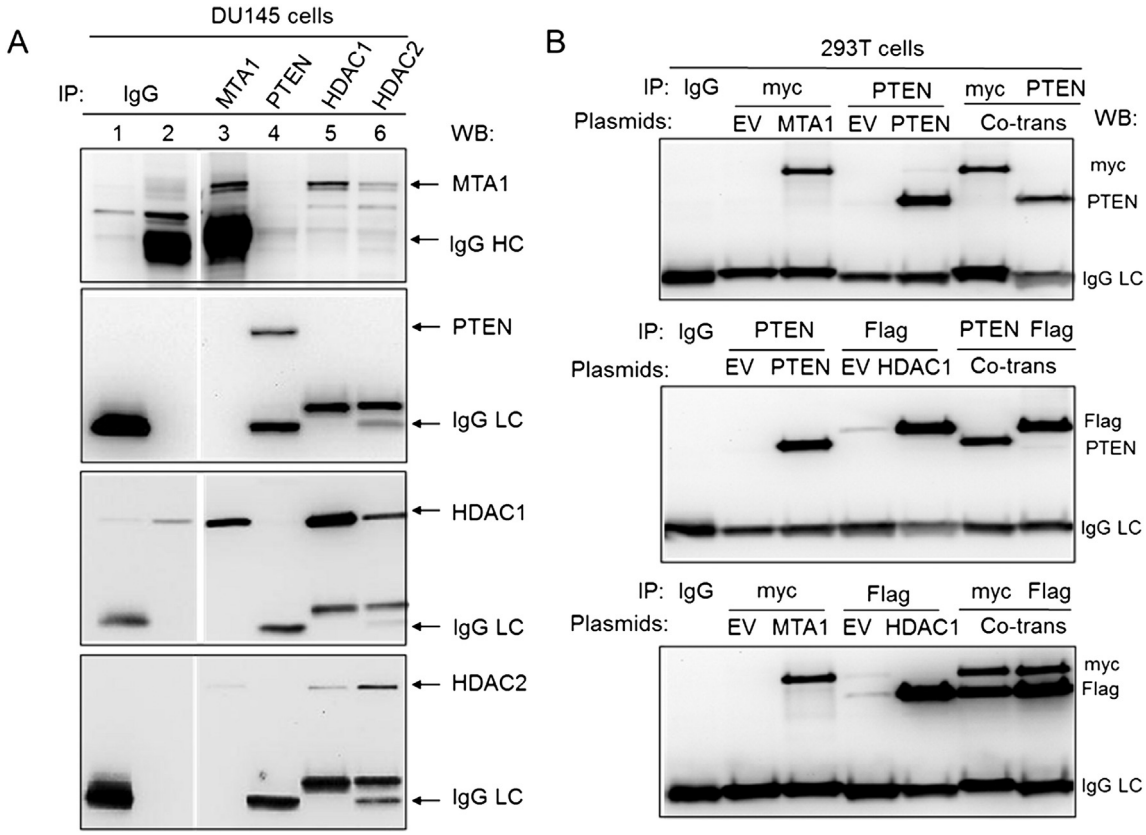

Fig. 5. MTA1 does not interact with PTEN. A) Cell lysates from DU145 cells were immunoprecipitated with antibodies to MTA1, PTEN, HDAC1 and HDAC2 or IgG controls and analyzed by western blotting with corresponding antibodies. B) 293T cells were co-transfected with myc-MTA1, HA-PTEN and HDAC1-Flag and cell lysates were immunoprecipitated with antibodies to myc, PTEN and Flag followed by western blotting. Myc and Flag antibodies were used for detection of MTA1 and HDAC1, respectively. PTEN was detected using anti-PTEN antibody.

plasmid with myc-p300 or with Flag-PCAF constructs, two known acetyltransferases reported for PTEN acetylation [36,37], in PC3M cells and performed IP-western blot to detect MTA1 and PTEN in the IP elutes. We were able to detect an interaction of PTEN with MTA1 and vice versa in cells where acetylation of PTEN was enhanced exclusively using myc-p300 construct (Fig. 6A). The acetylated status of PTEN in these cells was concomitantly confirmed in IP reactions with Ac-lysine antibody and immunoblotting for PTEN (Fig. 6A). Interestingly, co-expression of PCAF did not induce acetylation of PTEN and subsequently did not show an interaction between PTEN and MTA1. These results indicated that MTA1 interacts with the acetylated form of PTEN. Moreover, co-expression of myc-p300 and HA-PTEN leads to a further inhibition of p-Akt levels as compared to expression of HA-PTEN alone, suggesting that acetylation of PTEN leads to an increase in its lipid phosphatase activity (Fig. 6A, input).

In our second strategy, we sought to determine the acetylation site (s) in PTEN that can be involved in the interaction between PTEN and MTA1/HDAC complex. Lysine residues that have been reported to be involved in PTEN acetylation (K125/128 and K402) [36,37] were replaced by either arginine (R) or glutamine (Q) to create acetylation resistant and acetylation mimetic mutants, respectively. PC3M cells were transfected with either wild type PTEN or mutant constructs and IP-western blots were performed to detect PTEN in the lysates. Our data showed that the K125/128Q acetylation mimetic PTEN mutant construct exclusively interacted with MTA1 (Fig. 6B). There was no interaction of MTA1 either with the acetylation resistant K125/128R and K402R mutants or with the acetylation mimetic K402Q mutant. In addition, the K125/128Q acetylation mimetic showed decreased p-Akt (Ser 473) expression, confirming that acetylation of PTEN on these residues enhances its lipid phosphatase activity (Fig. 6B, input). We conclude from the above data that MTA1 interacts exclusively with PTEN which is acetylated at lysines 125 and 128 and that acetylation on these lysines renders PTEN active, as reflected by a reduction in p-Akt.

3.7. Resveratrol-induced tumor regression in orthotopic prostate cancer xenografts is mediated through MTA1 inhibition and PTEN activation

In our previous study, in which we examined MTA1-dependent tumor development and progression in PCa using orthotopic mouse model, we found that resveratrol treatment and MTA1 knockdown significantly inhibited tumor growth, progression, local invasion and spontaneous metastasis [11]. Xenografts expressing MTA1shRNA exhibited significantly reduced tumor growth at week 5 post-transplantation of cancer cells [11]. Moreover, MTA1 knockdown sensitized cells to resveratrol resulting in additional reduction of tumor progression. Using prostate tissues from the same experiment, we stained tumors for MTA1, PTEN and p-Akt and found that treatment with resveratrol simultaneously with decreasing MTA1 levels increased levels of PTEN in control tumors (Fig. 7). Further, MTA1-knockdown xenografts express much higher levels of PTEN compared to MTA1-expressing tumors, and that combination of MTA1-knockdown with resveratrol treatment keeps PTEN levels high. Unfortunately, since acetyl PTEN antibody is not commercially available we were unable to examine levels of acetylated PTEN in these tissues. However, as a readout of PTEN activity we examined p-Akt levels and found that MTA1-knockdown and resveratrol-treated tumors express lower levels of p-Akt compared to untreated controls (Fig. 7). Consistent with the potent antitumor effects, resveratrol-treated and MTA1-knockdown tumors showed reduced

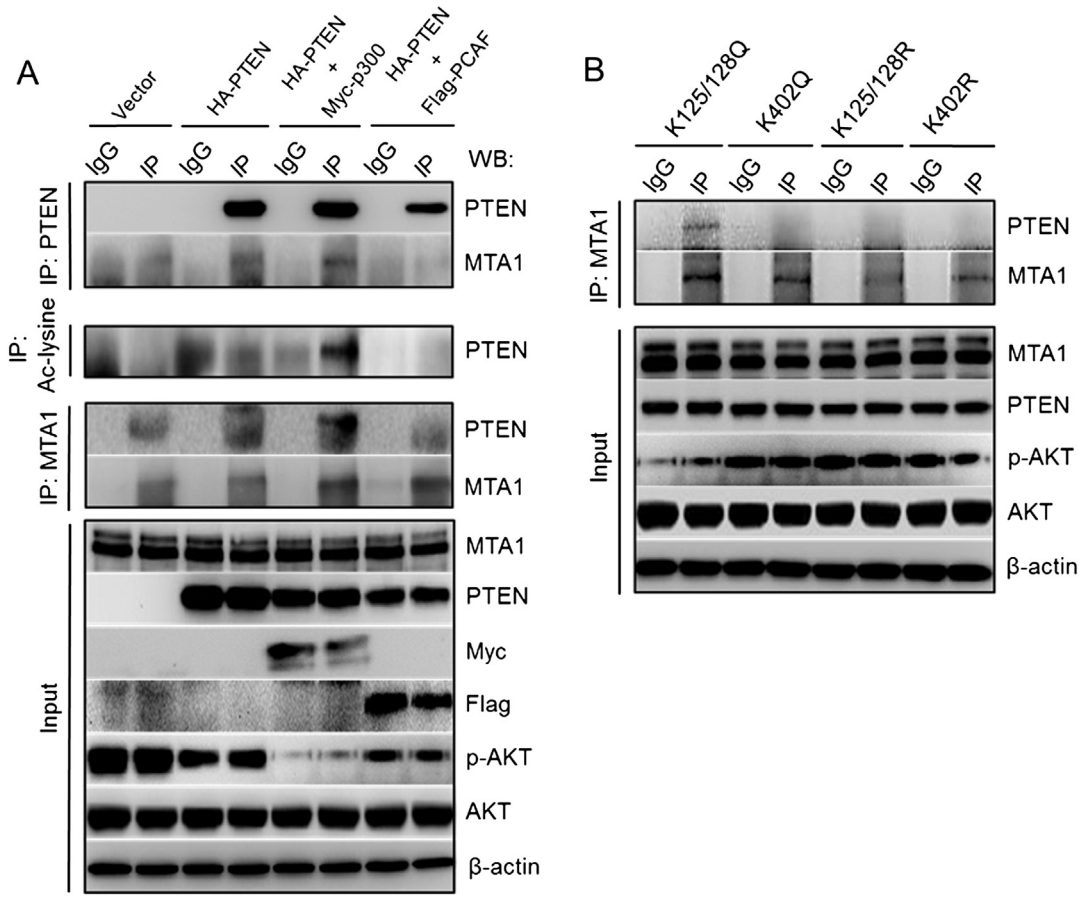

Fig. 6. MTA1 interacts with acetylated PTEN. A) PC3M cells were transfected with empty vector (HA-pSG5L), HA-PTEN, HA-PTEN and myc-p300 or HA-PTEN and Flag-PCAF plasmids. Lysates were immunoprecipitated with anti-PTEN, anti-acetyl lysine and anti-MTA1 antibodies followed by western blot. B) MTA1 interacts with PTEN when it is exclusively acetylated at lysines 125 and 128. PTEN mutant constructs K125/128R, K125/128Q, K402R and K402Q were prepared by site directed mutagenesis using the InFusion HD Cloning kit (Clontech) and confirmed by sequencing as detailed in *materials and methods* section. PC3M cells were transfected with mutant constructs, lysates were immunoprecipitated with anti-MTA1 antibody and analyzed by western blot using anti-PTEN antibody.

mitotic activity (Ki67, Fig. 7) and increased apoptosis compared to control mice as described earlier [11].

4. Discussion

Pharmacologically safe dietary compounds with epigenetic mechanisms of action are of great interest for cancer chemoprevention and therapy [38–40]. We identified resveratrol as a potent inhibitor of MTA1/HDAC1 and re-activator of p53 acetylation in prostate cancer cells [10]. Moreover, combined treatment of LNCaP prostate cancer cells with resveratrol and HDAC inhibitor SAHA resulted in a profound decrease of MTA1 and synergistic increase in acetylated p53 and apoptosis [10]. Since resveratrol had little effect on MTA1 mRNA, we sought the posttranslational regulation of MTA1. Our unpublished results imply that resveratrol causes MTA1 degradation by ubiquitin–proteasome system.

The aim of the present study was to further investigate resveratrol's epigenetic properties, particularly, the MTA1-mediated reversal of acetylation/activation of another tumor suppressor, PTEN, the loss of expression of which or inactivation is frequently found in prostate cancer [41]. We report here on resveratrol regulated rescue of PTEN expression, acetylation, and activity through MTA1 inhibition, which corresponds to its increased ability to inhibit Akt phosphorylation and cancer cell survival.

It has been shown that 30% primary and 60% metastatic tumors contain some kind of PTEN alteration [42,43]. Low PTEN expression is associated with an increased risk of lethal prostate cancer [44]. Consistently increased Akt activation (p-Akt) is associated with high Gleason grade, advanced disease and poor prognosis of prostate cancer [45,46]. Accordingly, mice with prostate-specific loss of *Pten* develop stage-defined prostate cancer with high levels of p-Akt, which progresses to invasive adenocarcinoma and occasionally lymph node metastasis [47]. However, homozygous *Pten* deletion is not common in human prostate cancer, suggesting that additional attenuation of the remaining allele caused by its posttranslational regulation could be a significant contributor for cancer development and progression. Therefore, activation of the remaining allele by reversible epigenetic therapy can restore PTEN activation.

Our original observation of inverse relationship between MTA1 and PTEN in addition to resveratrol's ability to regulate both proteins posed two major questions: First, since MTA1 is part of the deacetylating NuRD complex, does it negatively regulate PTEN by deacetylating it? Second, what role does resveratrol play in MTA1-PTEN signaling?

We and others reported an up-regulation of PTEN protein levels by resveratrol in prostate cancer [48,49]. In this study we have presented evidence that not only up-regulation but activation of PTEN occurs, at least in part, through resveratrol inhibition of components of NuRD deacetylation complex. It has already been reported that TSA promotes PTEN transcriptional activation by increasing acetylation of histones at the PTEN promoter [26] and TSA treatment induced PTEN-mediated apoptosis in oral squamous cell carcinoma [50]. In our experiments, resveratrol increased acetylation of PTEN in MTA1 knockdown cells similar to the effects of HDAC inhibitors, SAHA and TSA, indicating the involvement of MTA1/HDAC complex in PTEN deacetylation.

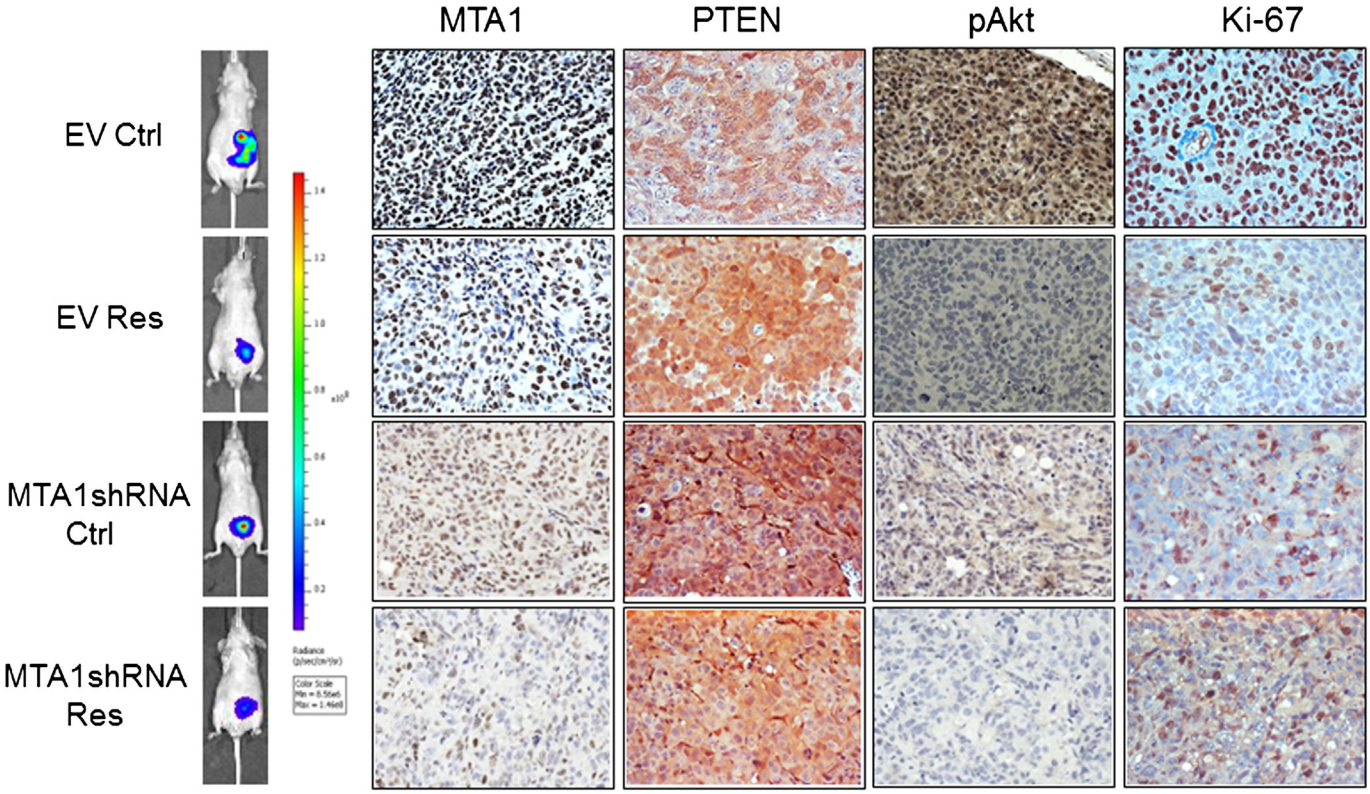

Fig. 7. Resveratrol induces tumor regression in orthotopic xenografts accompanied by decreased MTA1 and pAkt expression which is enhanced upon MTA1 knockdown and mediated via PTEN activation. Male nude mice were injected orthotopically with DU145-luciferase-tagged EV (Ctrl) or MTA1 knockdown (MTA1shRNA) cells and treated with 10% DMSO (Ctrl) or 50 mg/kg bw/day resveratrol (Res). Upon sacrifice, 4 μm sections were prepared from formalin-fixed paraffin embedded prostate tumors and stained using antibodies for MTA1, PTEN, pAkt and Ki-67. *Left*, bioluminescent images of prostate tumors at week 5 are shown. *Right*, representative immunohistochemistry images of MTA1, PTEN, pAkt and Ki67 in Ctrl EV, Res-treated EV, Ctrl MTA1shRNA and Res-treated MTA1shRNA tumors are shown, magnification (×200).

Based on the known preferential nuclear localization of MTA1 and HDACs 1 and 2 and our findings on MTA1 accumulation as a characteristic of aggressive prostate cancer [13], MTA1-mediated deacetylation of PTEN most likely occurs in the nucleus. On the other hand, "classic" lipid phosphatase activity of cytoplasmic PTEN is attributed to its regulation of Akt signaling and apoptosis, while nuclear PTEN plays other important non-canonical roles such as chromosomal stability, DNA repair, and cell cycle arrest [51–54]. Nuclear PTEN positively regulates DNA repair through up-regulation of RAD51, independent of its phosphatase activity [55]. Importantly, nuclear PTEN plays an important role in regulating p53 acetylation and activity [56] as well as p53-mediated G1 growth arrest, cell death, and reduction of reactive oxygen species production [57].

Interestingly, Salot & Gude, reported a physical association of MTA1 with PTEN in breast cancer cells and a possible post-translational regulation of PTEN by MTA1 [28]. However, our vigorous attempts to detect physical interaction between MTA1 and PTEN in prostate cancer, breast cancer and other cells did not yield any positive results.

Therefore, we envisioned a scenario in which MTA1 interacts with acetylated subpopulation of PTEN in prostate cancer cells. Indeed, we visualized an interaction of PTEN with MTA1 and vice versa only upon enhancing acetylation of PTEN, induced specifically by overexpression of p300 acetyltransferase (Fig. 6A). To our knowledge, this is the first report on PTEN acetylation by p300 acetyltransferase while an indirect transcriptional regulation of PTEN by p300 was demonstrated through acetylation of histone H4 by Pan et al. [26]. However, we did not see this effect with PCAF overexpression which counteracts the work by Okumura et al., where they showed that PCAF is responsible for PTEN acetylation at Lys^{125} and Lys^{128}, leading to inhibition of its lipid phosphatase activity [36].

There are only two reports on PTEN acetylation which have identified three acetylation sites (Lys 125 and 128 and Lys 402) but there is a disagreement on the potential role of acetylation in regulating PTEN function. Okumura *et al.* reported that the lipid phosphatase function of PTEN is inhibited when Lys^{125} and Lys^{128} are acetylated by histone acetyltransferase PCAF [36], whereas Ikenoue *et al.* showed that Lys 402 acetylation modulates PTEN interaction with PDZ domain-containing proteins [42]. In our experiments, acetylation mimetic PTEN mutant K125/128Q revealed an exclusive interaction with endogenous MTA1 in PC3M cells (Fig. 6B).

We repeatedly observed an inhibition in p-Akt levels (Ser 473) linked to an increase in PTEN acetylation upon MTA1-knockdown, treatment with TSA and resveratrol, and overexpression of p300 acetyltransferase.

In retrospect, in the study by Okumura et al., acetylation mimetic mutants K125Q and K128Q showed increased p-Akt thus suggesting that acetylation on these lysine residues renders PTEN inactive. However, intriguingly, the double acetylation resistant mutant K125/128R and the double acetylation mimetic mutant K125/128Q, both showed similar enhanced levels of p-Akt which is difficult to comprehend. We, on the other hand, believe that since Lys^{125} and Lys^{128} residues are located in the phosphatase domain of PTEN protein, acetylation of these residues in turn activates lipid phosphatase activity of PTEN protein as indicated by decreased p-Akt levels (Fig. 6B, input). We further believe that in addition to induction of lipid phosphatase activity, acetylation of PTEN on these two residues is a prerequisite for its non-canonical nuclear functions. Moreover, it is conceivable that MTA1/HDAC deacetylating complex will have more affinity towards an acetylated pool of PTEN that is active and present in the nucleus as shown by our data, which following an interaction with MTA1 gets deacetylated and subsequently loses

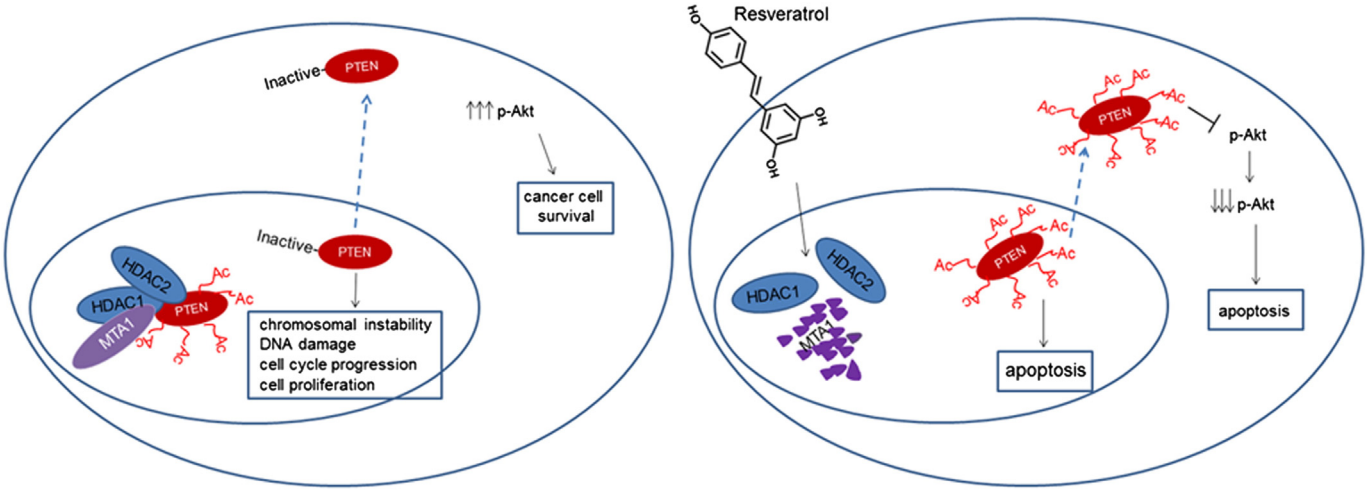

Fig. 8. Our results suggest a model of MTA1-mediated resveratrol regulation of PTEN/Akt pathway. In the absence of resveratrol, MTA1/HDAC complex is intact and localized in the nucleus where it can bind to acetylated PTEN. As a result, PTEN becomes de-acetylated, inactive and either stays in the nucleus, however without tumor suppressive functions, or diffuses to the cytoplasm without any negative consequence to Akt allowing amplification in p-Akt activity which leads to cancer cell survival. In contrast, when treated with resveratrol, owing to down-regulation of MTA1 and HDAC1/2 and as a result of MTA1/HDAC non-functionality, the acetylation of PTEN increases, which leads to enhanced lipid phosphatase activity of PTEN and its nuclear function culminating in apoptosis and inhibition of Akt survival pathway.

its activity. Taken together, we describe a novel association of MTA1 with acetylated PTEN and demonstrate acetylated PTEN as the active form that inhibits p-Akt-associated survival pathways.

Finally we substantiated the functional relevance of enhanced PTEN expression upon resveratrol treatment in orthotopic xenografts with DU145 MTA1 knockdown cells in nude mice. Immunohistochemistry analysis clearly revealed that both resveratrol treatment and MTA1 knockdown enhanced PTEN expression while concomitantly enhancing Ki-67 proliferative index (Fig. 7) and apoptosis as reported earlier [36] and simultaneously lowering p-Akt expression (Fig. 7). Unfortunately, specific acetylated PTEN antibodies are not commercially available restricting our ability to examine acetylation/deacetylation status of PTEN in prostate tissues.

Our results provide a plausible mechanism by which natural compound resveratrol acts on reversing pathological epigenetic changes mediated by co-repressor MTA1/HDAC complex in prostate cancer (Fig. 8). In aggressive prostate cancer, when MTA1 and HDAC1 and 2 are overexpressed and co-localized in the nucleus forming active suppressor unit and causing deacetylation of PTEN protein, tumor-suppressive functions of nuclear PTEN are inhibited. Deacetylated enzymatically inactive PTEN can also translocate to the cytoplasm however without negative consequences on Akt signaling, allowing accumulation of p-Akt and ultimately cancer cell survival. In the presence of resveratrol, which inhibits MTA1 and HDACs and dissociates the complex, interaction between MTA1/HDAC and acetylated PTEN is interrupted leading to accumulation of "free" acetylated PTEN with tumor-suppressive functions such as chromosomal stability, DNA repair and cell cycle arrest. Acetylated PTEN also can translocate to the cytoplasm, resulting in repression of its downstream Akt signaling pathway. In less aggressive prostate tissues, the proportion of acetylated PTEN is higher in cytoplasm and p-Akt signaling is inhibited, partly, due to low and inactive presence of MTA1/HDACs which does not interfere or sequester PTEN by deacetylation. Therefore, we believe that in aggressive prostate cancer, MTA1/HDAC complex associates with nuclear acetylated subpopulation of PTEN reducing its tumor-suppressive functions, although the mechanisms that regulate accumulation of acetylated PTEN in the nucleus and its interaction with MTA1/HDACs are not yet understood. Thus, we conclude that there is an inverse relationship between MTA1 and PTEN levels and propose that under resveratrol treatment which deactivates MTA1/HDACs complex, PTEN regains its activity, possibly by reversed acetylation, which leads to apoptosis & activation of p53 in the nucleus and inhibition of PI3K/Akt survival pathway.

5. Conclusions

We report herein that resveratrol, a dietary compound found in grapes and wine, exerts its anticancer activity in prostate cancer, at least in part, through epigenetic mechanisms, including posttranslational modification and reactivation of PTEN tumor suppressor. Our data indicate that PTEN is inactivated in prostate cancer by a novel negative regulator, MTA1/HDACs: the co-repressor complex deacetylates and inactivates PTEN resulting in inhibition of its nuclear tumor suppressive functions, such as apoptosis, cell cycle arrest, and p53 activation and its cytoplasmic lipid phosphatase function such as down-regulation of p-Akt. We discovered that resveratrol by targeting the MTA1/HDAC complex is able to reverse this negative epigenetic effect and reactivate tumor suppressor PTEN. Together, these findings underscore the importance of dietary compounds with epigenetic capacity and provide valuable awareness for future development of a combinatorial strategy for prostate cancer chemoprevention and treatment involving resveratrol and other MTA1/HDAC inhibitors.

Supplementary data to this article can be found online at http://dx.doi.org/10.1016/j.bbamcr.2014.11.004.

Acknowledgements

The authors thank Dr. Rakesh Kumar, George Washington University, for his generous gift of the myc-MTA1 plasmid, Dr. Zhi He (UMMC, histology core) for technical support in preparing tissue sections and Mr. Steven J Dias for help in preparing data with *Pten*$^{+/+}$ and *Pten*$^{-/-}$ cells. This research was supported by the Department of Defense Prostate Cancer Research Program under award # W81XWH-13-1-0370 to Anait S. Levenson. Views and opinions of, and endorsements by the author(s) do not reflect those of the US Army of the Department of Defense. The authors would also like to thank Dr. Richard L. Summers (UMMC) for his continued support.

References

[1] B.B. Aggarwal, A. Bhardwaj, R.S. Aggarwal, N.P. Seeram, S. Shishodia, Y. Takada, Role of resveratrol in prevention and therapy of cancer: preclinical and clinical studies, Anticancer Res. 24 (2004) 2783–2840.

[2] M. Jang, L. Cai, G.O. Udeani, K.V. Slowing, C.F. Thomas, C.W. Beecher, H.H. Fong, N.R. Farnsworth, A.D. Kinghorn, R.G. Mehta, R.C. Moon, J.M. Pezzuto, Cancer chemopreventive activity of resveratrol, a natural product derived from grapes, Science 275 (1997) 218–220.
[3] N. Kuwajerwala, E. Cifuentes, S. Gautam, M. Menon, E.R. Barrack, G.P. Reddy, Resveratrol induces prostate cancer cell entry into s phase and inhibits DNA synthesis, Cancer Res. 62 (2002) 2488–2492.
[4] E. Pozo-Guisado, M.J. Lorenzo-Benayas, P.M. Fernandez-Salguero, Resveratrol modulates the phosphoinositide 3-kinase pathway through an estrogen receptor alpha-dependent mechanism: relevance in cell proliferation, Int. J. Cancer 109 (2004) 167–173.
[5] E. Brakenhielm, R. Cao, Y. Cao, Suppression of angiogenesis, tumor growth, and wound healing by resveratrol, a natural compound in red wine and grapes, FASEB J. 15 (2001) 1798–1800.
[6] S.H. Tseng, S.M. Lin, J.C. Chen, Y.H. Su, H.Y. Huang, C.K. Chen, P.Y. Lin, Y. Chen, Resveratrol suppresses the angiogenesis and tumor growth of gliomas in rats, Clin. Cancer Res. 10 (2004) 2190–2202.
[7] Y. Kimura, H. Okuda, Resveratrol isolated from *Polygonum cuspidatum* root prevents tumor growth and metastasis to lung and tumor-induced neovascularization in Lewis lung carcinoma-bearing mice, J. Nutr. 131 (2001) 1844–1849.
[8] Y. Toh, S.D. Pencil, G.L. Nicolson, A novel candidate metastasis-associated gene, mta1, differentially expressed in highly metastatic mammary adenocarcinoma cell lines. cDNA cloning, expression, and protein analyses, J. Biol. Chem. 269 (1994) 22958–22963.
[9] Y. Xue, J. Wong, G.T. Moreno, M.K. Young, J. Cote, W. Wang, NURD, a novel complex with both ATP-dependent chromatin-remodeling and histone deacetylase activities, Mol. Cell 2 (1998) 851–861.
[10] L. Kai, S.K. Samuel, A.S. Levenson, Resveratrol enhances p53 acetylation and apoptosis in prostate cancer by inhibiting MTA1/NuRD complex, Int. J. Cancer 126 (2010) 1538–1548.
[11] K. Li, S.J. Dias, A.M. Rimando, S. Dhar, C.S. Mizuno, A.D. Penman, J.R. Lewin, A.S. Levenson, Pterostilbene acts through metastasis-associated protein 1 to inhibit tumor growth, progression and metastasis in prostate cancer, PLoS One 8 (2013) e57542.
[12] L. Kai, J. Wang, M. Ivanovic, Y.T. Chung, W.B. Laskin, F. Schulze-Hoepfner, Y. Mirochnik, R.L. Satcher Jr., A.S. Levenson, Targeting prostate cancer angiogenesis through metastasis-associated protein 1 (MTA1), Prostate 71 (2011) 268–280.
[13] S.J. Dias, X. Zhou, M. Ivanovic, M.P. Gailey, S. Dhar, L. Zhang, Z. He, A.D. Penman, S. Vijayakumar, A.S. Levenson, Nuclear MTA1 overexpression is associated with aggressive prostate cancer, recurrence and metastasis in African Americans, Sci. Rep. 3 (2013) 2331.
[14] M.D. Hofer, R. Kuefer, S. Varambally, H. Li, J. Ma, G.I. Shapiro, J.E. Gschwend, R.E. Hautmann, M.G. Sanda, K. Giehl, A. Menke, A.M. Chinnaiyan, M.A. Rubin, The role of metastasis-associated protein 1 in prostate cancer progression, Cancer Res. 64 (2004) 825–829.
[15] M.S. Song, L. Salmena, P.P. Pandolfi, The functions and regulation of the PTEN tumour suppressor, Nat. Rev. Mol. Cell Biol. 13 (2012) 283–296.
[16] V. Stambolic, A. Suzuki, J.L. de la Pompa, G.M. Brothers, C. Mirtsos, T. Sasaki, J. Ruland, J.M. Penninger, D.P. Siderovski, T.W. Mak, Negative regulation of PKB/Akt-dependent cell survival by the tumor suppressor PTEN, Cell 95 (1998) 29–39.
[17] M.A. Lim, L. Yang, Y. Zheng, H. Wu, L.Q. Dong, F. Liu, Roles of PDK-1 and PKN in regulating cell migration and cortical actin formation of PTEN-knockout cells, Oncogene 23 (2004) 9348–9358.
[18] N. Dey, H.E. Crosswell, P. De, R. Parsons, Q. Peng, J.D. Su, D.L. Durden, The protein phosphatase activity of PTEN regulates SRC family kinases and controls glioma migration, Cancer Res. 68 (2008) 1862–1871.
[19] M.P. Myers, I. Pass, I.H. Batty, J. Van der Kaay, J.P. Stolarov, B.A. Hemmings, M.H. Wigler, C.P. Downes, N.K. Tonks, The lipid phosphatase activity of PTEN is critical for its tumor supressor function, Proc. Natl. Acad. Sci. U. S. A. 95 (1998) 13513–13518.
[20] J. Li, C. Yen, D. Liaw, K. Podsypanina, S. Bose, S.I. Wang, J. Puc, C. Miliaresis, L. Rodgers, R. McCombie, S.H. Bigner, B.C. Giovanella, M. Ittmann, B. Tycko, H. Hibshoosh, M.H. Wigler, R. Parsons, PTEN, a putative protein tyrosine phosphatase gene mutated in human brain, breast, and prostate cancer, Science 275 (1997) 1943–1947.
[21] A. Carracedo, A. Alimonti, P.P. Pandolfi, PTEN level in tumor suppression: how much is too little? Cancer Res. 71 (2011) 629–633.
[22] S. Ramaswamy, N. Nakamura, F. Vazquez, D.B. Batt, S. Perera, T.M. Roberts, W.R. Sellers, Regulation of G1 progression by the PTEN tumor suppressor protein is linked to inhibition of the phosphatidylinositol 3-kinase/Akt pathway, Proc. Natl. Acad. Sci. U. S. A. 96 (1999) 2110–2115.
[23] S. Emiliani, W. Fischle, C. Van Lint, Y. Al-Abed, E. Verdin, Characterization of a human RPD3 ortholog, HDAC3, Proc. Natl. Acad. Sci. U. S. A. 95 (1998) 2795–2800.
[24] P.R. Molli, R.R. Singh, S.W. Lee, R. Kumar, MTA1-mediated transcriptional repression of BRCA1 tumor suppressor gene, Oncogene 27 (2008) 1971–1980.
[25] A. Mazumdar, R.A. Wang, S.K. Mishra, L. Adam, R. Bagheri-Yarmand, M. Mandal, R.K. Vadlamudi, R. Kumar, Transcriptional repression of oestrogen receptor by metastasis-associated protein 1 corepressor, Nat. Cell Biol. 3 (2001) 30–37.
[26] L. Pan, J. Lu, X. Wang, L. Han, Y. Zhang, S. Han, B. Huang, Histone deacetylase inhibitor trichostatin a potentiates doxorubicin-induced apoptosis by up-regulating PTEN expression, Cancer 109 (2007) 1676–1688.
[27] S.D. Reddy, S.B. Pakala, P.R. Molli, N. Sahni, N.K. Karanam, P. Mudvari, R. Kumar, Metastasis-associated protein 1/histone deacetylase 4-nucleosome remodeling and deacetylase complex regulates phosphatase and tensin homolog gene expression and function, J. Biol. Chem. 287 (2012) 27843–27850.
[28] S. Salot, R.P. Gude, MTA1 aids the Akt pathway by inhibiting expression of a key regulator, PTEN, J. Cancer Sci. Ther. 2 (2010) 114–119.
[29] G.L. Nicolson, A. Nawa, Y. Toh, S. Taniguchi, K. Nishimori, A. Moustafa, Tumor metastasis-associated human MTA1 gene and its MTA1 protein product: role in epithelial cancer cell invasion, proliferation and nuclear regulation, Clin. Exp. Metastasis 20 (2003) 19–24.
[30] W.S. Moon, K. Chang, A.S. Tarnawski, Overexpression of metastatic tumor antigen 1 in hepatocellular carcinoma: Relationship to vascular invasion and estrogen receptor-alpha, Hum. Pathol. 35 (2004) 424–429.
[31] M.D. Martin, S.G. Hilsenbeck, S.K. Mohsin, T.A. Hopp, G.M. Clark, C.K. Osborne, D.C. Allred, P. O'Connell, Breast tumors that overexpress nuclear metastasis-associated 1 (MTA1) protein have high recurrence risks but enhanced responses to systemic therapies, Breast Cancer Res. Treat. 95 (2006) 7–12.
[32] X. Zhu, Y. Guo, X. Li, Y. Ding, L. Chen, Metastasis-associated protein 1 nuclear expression is associated with tumor progression and clinical outcome in patients with non-small cell lung cancer, J. Thoracic Oncol. 5 (2010) 1159–1166.
[33] S.H. Li, H. Tian, W.M. Yue, L. Li, C. Gao, W.J. Li, W.S. Hu, B. Hao, Metastasis-associated protein 1 nuclear expression is closely associated with tumor progression and angiogenesis in patients with esophageal squamous cell cancer, World J. Surg. 36 (2012) 623–631.
[34] K. Halkidou, L. Gaughan, S. Cook, H.Y. Leung, D.E. Neal, C.N. Robson, Upregulation and nuclear recruitment of HDAC1 in hormone refractory prostate cancer, Prostate 59 (2004) 177–189.
[35] W. Weichert, A. Roske, V. Gekeler, T. Beckers, C. Stephan, K. Jung, F.R. Fritzsche, S. Niesporek, C. Denkert, M. Dietel, G. Kristiansen, Histone deacetylases 1, 2 and 3 are highly expressed in prostate cancer and HDAC2 expression is associated with shorter PSA relapse time after radical prostatectomy, Br. J. Cancer 98 (2008) 604–610.
[36] K. Okumura, M. Mendoza, R.M. Bachoo, R.A. DePinho, W.K. Cavenee, F.B. Furnari, PCAF modulates PTEN activity, J. Biol. Chem. 281 (2006) 26562–26568.
[37] T. Ikenoue, K. Inoki, B. Zhao, K.L. Guan, PTEN acetylation modulates its interaction with PDZ domain, Cancer Res. 68 (2008) 6908–6912.
[38] T.M. Hardy, T.O. Tollefsbol, Epigenetic diet: impact on the epigenome and cancer, Epigenomics 3 (2011) 503–518.
[39] J. Chen, X. Xu, Diet, epigenetic, and cancer prevention, Adv. Genet. 71 (2010) 237–255.
[40] A. Link, F. Balaguer, A. Goel, Cancer chemoprevention by dietary polyphenols: promising role for epigenetics, Biochem. Pharmacol. 80 (2010) 1771–1792.
[41] M.M. Shen, C. Abate-Shen, Molecular genetics of prostate cancer: new prospects for old challenges, Genes Dev. 24 (2010) 1967–2000.
[42] Y.E. Whang, X. Wu, H. Suzuki, R.E. Reiter, C. Tran, R.L. Vessella, J.W. Said, W.B. Isaacs, C.L. Sawyers, Inactivation of the tumor suppressor PTEN/MMAC1 in advanced human prostate cancer through loss of expression, Proc. Natl. Acad. Sci. U. S. A. 95 (1998) 5246–5250.
[43] I.C. Gray, L.M. Stewart, S.M. Phillips, J.A. Hamilton, N.E. Gray, G.J. Watson, N.K. Spurr, D. Snary, Mutation and expression analysis of the putative prostate tumour-suppressor gene PTEN, Br. J. Cancer 78 (1998) 1296–1300.
[44] K. Zu, N.E. Martin, M. Fiorentino, R. Flavin, R.T. Lis, J.A. Sinnott, S. Finn, K.L. Penney, J. Ma, L. Fazli, M.E. Gleave, T.A. Bismar, M.J. Stampfer, M.N. Pollak, M. Loda, L.A. Mucci, E. Giovannucci, Protein expression of PTEN, insulin-like growth factor I receptor (IGF-IR), and lethal prostate cancer: a prospective study, Cancer Epidemiol. Biomark. Prev. 22 (2013) 1984–1993.
[45] G.E. Ayala, H. Dai, M. Ittmann, R. Li, M. Powell, A. Frolov, T.M. Wheeler, T.C. Thompson, D. Rowley, Growth and survival mechanisms associated with perineural invasion in prostate cancer, Cancer Res. 64 (2004) 6082–6090.
[46] J.A. Engelman, Targeting PI3K signalling in cancer: opportunities, challenges and limitations, Nat. Rev. Cancer 9 (2009) 550–562.
[47] S. Wang, J. Gao, Q. Lei, N. Rozengurt, C. Pritchard, J. Jiao, G.V. Thomas, G. Li, P. Roy-Burman, P.S. Nelson, X. Liu, H. Wu, Prostate-specific deletion of the murine Pten tumor suppressor gene leads to metastatic prostate cancer, Cancer Cell 4 (2003) 209–221.
[48] Y. Wang, T. Romigh, X. He, M.S. Orloff, R.H. Silverman, W.D. Heston, C. Eng, Resveratrol regulates the PTEN/AKT pathway through androgen receptor-dependent and -independent mechanisms in prostate cancer cell lines, Hum. Mol. Genet. 19 (2010) 4319–4329.
[49] S. Dhar, C. Hicks, A.S. Levenson, Resveratrol and prostate cancer: promising role for microRNAs, Mol. Nutr. Food Res. 55 (2011) 1219–1229.
[50] Y.H. Gan, S. Zhang, PTEN/AKT pathway involved in histone deacetylases inhibitor induced cell growth inhibition and apoptosis of oral squamous cell carcinoma cells, Oral Oncol. 45 (2009) e150–e154.
[51] S.M. Planchon, K.A. Waite, C. Eng, The nuclear affairs of PTEN, J. Cell Sci. 121 (2008) 249–253.
[52] L. Salmena, A. Carracedo, P.P. Pandolfi, Tenets of PTEN tumor suppression, Cell 133 (2008) 403–414.
[53] A. Gericke, M. Munson, A.H. Ross, Regulation of the PTEN phosphatase, Gene 374 (2006) 1–9.
[54] J.H. Chung, C. Eng, Nuclear-cytoplasmic partitioning of phosphatase and tensin homologue deleted on chromosome 10 (PTEN) differentially regulates the cell cycle and apoptosis, Cancer Res. 65 (2005) 8096–8100.
[55] W.H. Shen, A.S. Balajee, J. Wang, H. Wu, C. Eng, P.P. Pandolfi, Y. Yin, Essential role for nuclear PTEN in maintaining chromosomal integrity, Cell 128 (2007) 157–170.
[56] A.G. Li, L.G. Piluso, X. Cai, G. Wei, W.R. Sellers, X. Liu, Mechanistic insights into maintenance of high p53 acetylation by PTEN, Mol. Cell 23 (2006) 575–587.
[57] C.J. Chang, D.J. Mulholland, B. Valamehr, S. Mosessian, W.R. Sellers, H. Wu, PTEN nuclear localization is regulated by oxidative stress and mediates p53-dependent tumor suppression, Mol. Cell. Biol. 28 (2008) 3281–3289.

Ann. N.Y. Acad. Sci. ISSN 0077-8923

ANNALS OF THE NEW YORK ACADEMY OF SCIENCES
Issue: *Resveratrol and Health*

Epigenetic potential of resveratrol and analogs in preclinical models of prostate cancer

Avinash Kumar,[1] Swati Dhar,[1] Agnes M. Rimando,[2] Janice M. Lage,[3] Jack R. Lewin,[3] Xu Zhang,[4] and Anait S. Levenson[1,3]

[1]Cancer Institute, University of Mississippi Medical Center, Jackson, Mississippi. [2]United States Department of Agriculture, Agricultural Research Service, Natural Products Utilization Research Unit, University, Mississippi. [3]Department of Pathology, [4]Center of Biostatistics and Bioinformatics, University of Mississippi Medical Center, Jackson, Mississippi

Address for correspondence: Anait S. Levenson, Cancer Institute, University of Mississippi Medical Center, 2500 North State Street, Jackson, MS 39216. alevenson@umc.edu

Lifestyle, particularly diet, is a risk factor for prostate cancer. Dietary polyphenols such as resveratrol possess anticancer properties and therefore have chemopreventive and therapeutic potential. Resveratrol has pleiotropic effects, exerting its biological activity through multiple pathways and targets, including those associated with cancer. Numerous studies have demonstrated the anticancer effects of resveratrol and, to a lesser extent, its analogs, in tissue culture, while *in vivo* observations are limited. Here, we provide a concise summary of our results on epigenetic mechanisms of resveratrol and analogs mediated through regulation of chromatin modifier metastasis-associated protein 1 (MTA1) and microRNAs (miRNAs), and highlight the anticancer effects of these compounds in preclinical models of prostate cancer. We suggest that the identified stilbene responsive mechanism–based biomarkers, such as MTA1 and oncogenic miRNAs, may become indicative of treatment efficacy in prostate cancer. Resveratrol analogs with better bioavailability, conferring superior pharmacological potencies and greater anticancer effects, may become stronger candidates for clinical development.

Keywords: prostate cancer epigenetics; pterostilbene; resveratrol; MTA1; miRNA; preclinical models

Introduction

Prostate cancer is a major public health issue in the United States. Several risk factors, such as family history, age, race, obesity, diet, and environmental factors, have been associated with prostate cancer. Although the link between diet and cancer is complex, epidemiological data confirm diet as a risk factor for prostate cancer.[1] It is estimated that only 5–10% of all prostate cancer cases are hereditary, indicating that most incidents are acquired during the lifetime through reversible epigenetic changes, and therefore can be prevented. Importantly, dietary factors can modulate epigenetic mechanisms of cancer susceptibility, development, and progression.[2–4] Since prostate cancer is a slow-growing cancer and develops in elderly men, chemoprevention using bioactive dietary compounds capable of reversing altered epigenetics may become a useful strategy for the management of the disease in men at high risk, as well as those who are on active surveillance.[2,5,6]

Numerous studies have indicated that resveratrol is a potential dietary chemopreventive and therapeutic agent.[7,8] Importantly, epidemiological studies indicate a reduced prostate cancer risk associated with red wine consumption, attributable to high resveratrol content.[9] However, owing to resveratrol's low bioavailability and rapid metabolism, natural resveratrol analogs with improved pharmacokinetic properties and pharmacological potency hold greater promise as natural product drugs for clinical development.[10,11]

In recent studies, we have accumulated evidence on the anticancer activity of resveratrol and its analogs in prostate cancer by two distinct epigenetic mechanisms, namely through effects on an epigenetic modifier, the metastasis-associated

doi: 10.1111/nyas.12817

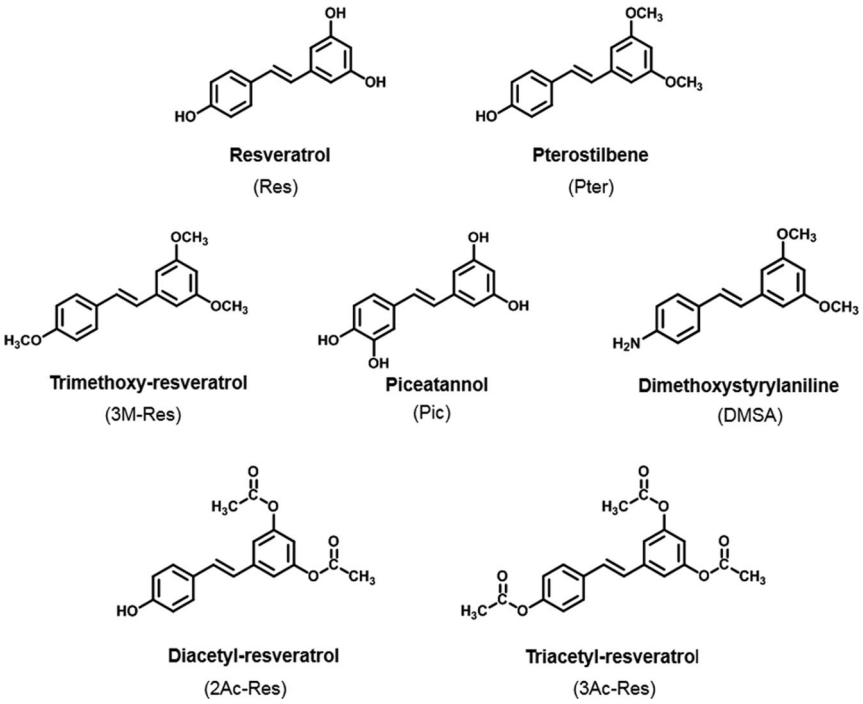

Figure 1. The chemical structures of resveratrol and its analogs used in our studies.

protein 1 (MTA1), and specific microRNAs (miRNAs). We will mostly focus on summarizing our data on the preclinical efficacy of resveratrol and its analogs in prostate cancer.

Resveratrol, its natural analogs, and chemoprevention

Resveratrol (Res, *trans*-3,5,4′-trihydroxystilbene), an active ingredient in red grapes (wine), peanuts, and berries, has been linked to health and disease prevention because of its cardioprotective, antioxidative, anti-inflammatory, and anticancer effects.[12] However, because of limitations including rapid metabolism and low bioavailability, only limited clinical trials of resveratrol have been possible.[13] Studies indicate that the number and position of hydroxyl groups on the benzene ring of resveratrol significantly influence its activity.[11] The most studied resveratrol analogs are natural dietary pterostilbene and piceatannol, both of which have reported anticancer activity. Pterostilbene (Pter, *trans*-3,5-dimethoxystilbene), found in grapes and blueberries, exhibits substantially decreased metabolism[14] and higher bioavailability than resveratrol.[15] The more favorable pharmacokinetic properties of pterostilbene result in better accumulation in tissues.[16,17] Piceatannol (Pic, *trans*-3,5,3′,4′-tetrahydroxystilbene), bearing one more hydroxy group than resveratrol, exhibits a shorter half-life in the plasma and increased metabolism, but nevertheless also has potent anticancer effects.[18–20] Trimethoxy-resveratrol (3M-Res, *trans*-3,5,4′-trimethoxystilbene) is another natural analog, though it is not found in edible sources like the aforementioned other natural analogs but in medicinal plants such as Korean rhubarb.[21] Studies have reported on trimethoxy-resveratrol's enhanced anticancer profile and improved bioavailability compared to resveratrol.[22–25] In particular, trimethoxy-resveratrol demonstrated greater antiproliferative and apoptotic effects in different cancers.[26–28]

We synthesized three natural and three synthetic analogs of resveratrol and characterized their anticancer effects in prostate cancer. Pterostilbene, trimethoxy-resveratrol, and piceatannol are natural analogs, whereas diacetyl-resveratrol (2Ac-Res, *trans*-3,5-diacetylstilbene), triacetyl-resveratrol (3Ac-Res, *trans*-3,5,4′-triacetylstilbene), and dimethoxystyrylaniline (DMSA, *trans*-4-(3,5-dimethoxystyryl)aniline) are synthetic analogs (Fig. 1). In a recent study, we reported the antiproliferative

Table 1. ***In vitro*** **effects of resveratrol and its analogs on the growth of prostate cancer cells**

Stilbene	LNCaP IC_{50} (μM)	DU145 IC_{50} (μM)	PC3M IC_{50} (μM)	22Rv1 IC_{50} (μM)
Res	12.7	42.3	31.5	149.92
Pter	22.8	20.8	17.0	19.42
3M-Res	2.5	9.7	23.3	9.45
Pic	31.7	23.2	34.6	13.88
DMSA	21.3	14.6	22.4	–
2Ac-Res	18.4	34.9	47.8	–
3Ac-Res	10.5	14.2	26.8	–

Note: LNCaP, DU145, and PC3M (Ref. 29); 22Rv1 (Ref. 30). The IC_{50} values were calculated by the Chou–Martin method using CompuSyn software[29] and by the linear interpolation method using MS Excel software.[30]
Res, resveratrol; Pter, pterostilbene; 3M-Res, trimethoxy-resveratrol; Pic, piceatannol; DMSA, dimethoxystyrylaniline; 2Ac-Res, diacetyl-resveratrol; 3Ac-Res, triacetyl-resveratrol.

effects of resveratrol and its analogs in three prostate cancer cell lines representing different stages of prostate cancer progression: androgen-responsive LNCaP, androgen-independent DU145, and highly metastatic PC3M cells. We found that all compounds demonstrated cell-specific growth-inhibitory effects, with trimethoxy-resveratrol being the most potent in LNCaP and DU145 cells, and comparable to pterostilbene in very aggressive PC3M cells[29] (Table 1). Interestingly, synthetic analogs that have replacement of all three hydroxyl substituents, either with acetyl (3Ac-Res) or methoxyl/amino groups (DMSA), also showed considerable growth-inhibitory activity. In the same study evaluating the chemopreventive and therapeutic efficacy of resveratrol and its natural analogs, we demonstrated that pretreatment with resveratrol, trimethoxy-resveratrol, or piceatannol reduced colony formation *in vitro* and tumor formation and growth in xenografts when administered orally, with the analogs exhibiting better tumor-reduction effects. In addition, we found a reduction of proinflammatory IL-6 cytokine by all three stilbenes in murine serum, indicating an anti-inflammatory property, which is known for these agents. Importantly, we found higher accumulation of trimethoxy-resveratrol than resveratrol in both serum and tumor tissues.[29] In a separate study, we found that trimethoxy-resveratrol was again the most potent antiproliferative agent among resveratrol and its natural analogs in 22Rv1 castrate-resistant prostate cancer cells[30] (Table 1).

Resveratrol and its analogs are known to have multiple targets belonging to different signaling pathways, including androgen receptor (AR) signaling in prostate cancer. While we have investigated the regulation of AR by dietary stilbenes,[30] the focus of other studies has been the regulation of epigenetic factors, particularly the chromatin modifier MTA1 and its signaling network and miRNAs (Fig. 2).

Role of MTA1 and miRNAs in prostate cancer

MTA1 is part of the nucleosome remodeling and deacetylase (NuRD) corepressor complex,[31] where it functions as an epigenetic reader to decipher the nucleosome codes.[32] Our initial study identified MTA1 as a part of the prostate cancer "bone metastatic signature," participating in the so-called "vicious cycle" of bone metastasis.[33] We further validated that MTA1 specifically accumulated in lymph nodes and bone metastatic lesions from African American prostate cancer patients.[34] We also found that nuclear MTA1 overexpression progressively increased with the severity of disease progression from prostate intraepithelial neoplasia (PIN) to localized prostate cancer to metastatic disease, and correlated with preoperative prostate-specific antigen levels and disease recurrence.[33,34] *In silico* analysis of available microarray expression data sets also revealed that MTA1 is highly expressed in malignant tumors compared to benign tumors.[35]

Evidence from our studies on various prostate cancer cell lines identified MTA1 as a progression-related protein.[33,36] We observed a significant elevation in acetylation of p53 and induction of apoptosis in LNCaP and DU145 cells deficient in MTA1 (MTA1 knockdown), suggesting antiapoptotic functions for MTA1.[37] Furthermore, we reported decreased invasiveness and angiogenesis in PC3 cells deficient in MTA1 (MTA1 knockdown), suggesting the involvement of MTA1 in proinvasive and proangiogenic functions.[33] Our findings were further reinforced by *in vivo* data on (1) LNCaP and DU145 subcutaneous xenografts, where MTA1 knockdown led to decreased tumor growth, proliferation, and angiogenesis[33] and (2) DU145 orthotopic xenografts, where MTA1 knockdown led to reduced prostate tumor growth, lesser metastasis, and metastasis in fewer

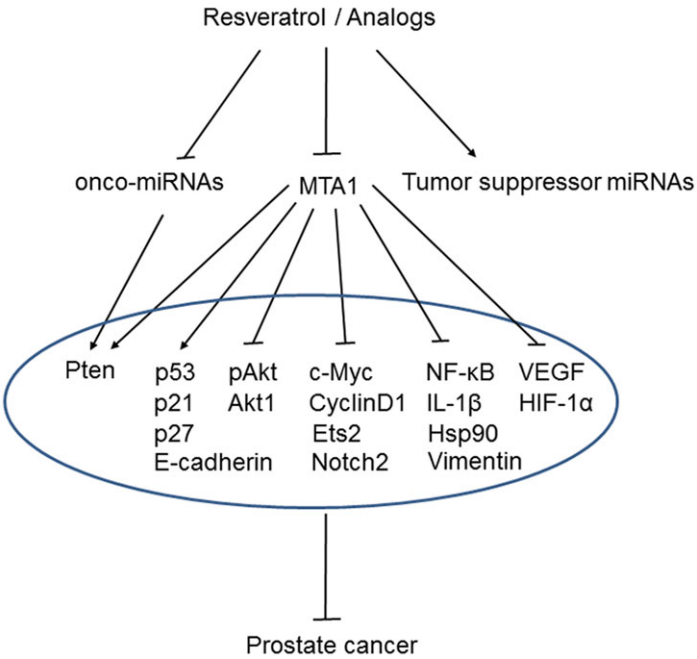

Figure 2. Resveratrol and analogs' epigenetic signaling pathways, summarizing MTA1- and miR-regulated molecular targets and inhibitory effects on prostate cancer.

organs.[36] MTA1's promotion of the malignant phenotype in PC3M cells has also been reported.[38] Recently, we reported positive cross talk between MTA1 and the Akt pathway. Our data showed that prostate cancer cells silenced for MTA1, either genetically or chemically, exhibited increased acetylation of phosphatase and tensin homolog (PTEN), which corresponds with its increased lipid phosphatase activity leading to lower pAkt levels and inhibition of the Akt survival signaling pathway.[39]

MicroRNAs are small noncoding regulatory RNAs that posttranscriptionally repress gene expression through interaction with the complementary target sites in the 3′ untranslated region (3′UTR) of target genes. The critical role of miRNAs in cancer has been well established.[40,41] Specific miRNAs have been reported to be aberrantly expressed in prostate cancer; they are implicated as oncogenes or as tumor suppressors and found to be upregulated or downregulated.[42–44] In addition, the utility of circulating miRNAs as diagnostic, prognostic, and predictive biomarkers in cancer is being closely considered.[45]

We believe that MTA1 and miRNAs have considerable prospects as epigenetic regulators that can influence prostate cancer progression, and therefore targeting MTA1 and/or miRNAs may be a chemopreventive and interventional strategy to abrogate prostate cancer.

Epigenetic actions of resveratrol and analogs in prostate cancer

In recent years, our laboratory discovered that resveratrol and its analogs, apart from the many other mechanisms responsible for their anticancer activity, also exhibit epigenetic actions through targeting of the chromatin modifier MTA1, histone deacetylases (HDACs), and several miRNAs.[36,37,39,46] We showed that resveratrol, by downregulating MTA1, disrupted the MTA1/HDAC unit of the NuRD complex and reversed p53 acetylation, leading to apoptosis in prostate cancer cells through activation of proapoptotic Bax and p21.[37] In a recent report we showed that resveratrol has the ability to not only target MTA1 but also HDAC1 and HDAC2 in prostate cancer cells.[39] Importantly, we showed that the resveratrol-mediated downregulation of MTA1 protein levels was concomitant with upregulation of PTEN mRNA and protein, suggesting an inverse relationship between MTA1 and PTEN.[39] We also

examined natural and synthetic analogs of resveratrol for better epigenetic action through more potent targeting of MTA1, and found that natural resveratrol analogs were more potent than synthetic analogs in downregulating MTA1. Importantly, pterostilbene exhibited sevenfold greater potency in downregulating MTA1 and increasing p53 acetylation than resveratrol in DU145 prostate cancer cells.[36] In the same study, we demonstrated an MTA1-dependent increase in p53 acetylation upon pterostilbene treatment *in vivo* that was superior to that induced by resveratrol.[36] Furthermore, MTA1 ChIP-Seq analysis of prostate tissues from pterostilbene-treated mice revealed a decrease in MTA1-identified peaks, and indicated regulation of MTA1-mediated transcriptional control of genes implicated in prostate tumorigenesis, inflammation, angiogenesis, and survival pathways by pterostilbene. Apart from targeting MTA1 and HDACs, resveratrol and its analogs exhibit epigenetic action through targeting of oncogenic miRNAs (oncomiRs) and induction of tumor-suppressive miRNAs. Using miRNA profiling in LNCaP cells, we reported significant expression of oncogenic miR-17∼92, miR-106a∼363, and miR-106b∼25 clusters, some members of which target the tumor suppressor gene PTEN.[46] We also found that resveratrol significantly altered miRNA profiles in prostate cancer, including members of the oncogenic miR-17 family and miR-7, among others, and tumor-suppressive miRNAs such as miR-296 and miR-654.[46] Our current work in progress using 3′UTR–luciferase reporter and other functional assays suggests that resveratrol and pterostilbene reversal of PTEN expression may be mediated through repression of oncomiRs-17, -20a, -106a, and -106b (unpublished results). The results with pterostilbene having epigenetic targets in prostate cancer provide a rationale for studying pterostilbene's synthetic analogs as candidate epigenetic drugs for future applications in prostate cancer.

Preclinical mouse models of prostate cancer

In order to translate any findings from tissue culture to the clinic, preclinical tumor models are necessary to study and predict *in vivo* drug response. Mouse cancer models have greatly contributed to the basic understanding of cancer mechanisms and anticancer drug discovery.[47–49]

We have developed several prostate cancer mouse models that have specific benefits and limitations for testing new interventions, which could potentially translate to treatments in human prostate cancer patients. These models include prostate cancer xenografts, where cancer is induced experimentally in immunocompromised mice using human cancer cells, and genetically engineered mice (GEM), where cancer is induced by prostate-specific genetic manipulation(s) in immunocompetent animals (Table 2).

Subcutaneous xenograft models

There are several practical advantages of developing subcutaneous tumors: they are the easiest to grow practically with any prostate cancer cell line (LNCaP, DU145, PC3M), and tumor growth can be visualized by gross examination and monitored by caliper measurements and/or bioluminescent imaging. Understandably, for bioluminescent imaging, cancer cells have to be tagged with luciferase and checked for luciferase expression *in vitro* before injection into mice. Subcutaneous tumors from prostate cancer cell lines representing different stages of prostate cancer and carrying certain genetic manipulations such as overexpression or knockdown of a given gene can answer some important mechanistic questions. The main disadvantage of this model is the absence of an adequate tumor environment (i.e., tissue origin that is known to be essential for natural histopathological features of prostate cancer). Also, in some cases when a tumor is large, bioluminescent images of subcutaneous tumors do not correspond to their live images or caliper measurements. Because luciferase detection is possible only in living, metabolically active cells and tumors consist of not only living but also necrotic areas, cell debris, and infiltrating host cells, interference can occur with bioluminescent imaging of large tumors. In addition, substrate availability for subcutaneous tumors is much less than for organs in the peritoneal cavity because of their remote location from the site of luciferin injection necessary for imaging. This latter observation may support an advantage of bioluminescent imaging for orthotopic models.

Orthotopic xenograft models

Although labor intensive and time consuming, xenografts offer improvements over subcutaneous models, since the physiological *in vivo* environment

Table 2. ***In vivo*** **effects of resveratrol and its analogs in mouse models of prostate cancer**

	Cell line	Type of xenograft	Dose; route	Findings
Xenograft models				
	LNCaP-Luc	s.c.	Res, 3M-Res, Pic: 50 mg/kg bw; oral gavage	Pretreatment of mice with Res, 3M-Res, or Pic administered orally reduced tumor formation and growth. 3M-Res was more potent than Pic and Res.[29]
	LNCaP-Luc	Orthotopic	Res: 1.6 g/kg diet; diet supplementation	Work in progress.
	DU145-Luc-EV DU145-Luc-shMTA1	Orthotopic	Res, Pter: 50 mg/kg bw; i.p.	Res, but more so Pter, showed tumor and metastasis inhibitory effects, which was further potentiated upon MTA1 knockdown.[36]
	DU145-Luc-EV DU145-Luc-miR-17/106a	s.c.	Pter: 50 mg/kg bw; i.p.	Work in progress.
	PC3M-Luc	Orthotopic	Pter: 50 mg/kg bw SAHA: 25 mg/kg bw; i.p.	Work in progress.
	Genotype	Description		
Knockout models				
	Pten$^{+/-}$; *Pb-Cre4*	Prostate-specific deletion of one *Pten* allele	Pter: 100 mg/kg diet; diet supplementation	Work in progress.
	Pten$^{-/-}$; *Pb-Cre4*	Prostate-specific deletion of both *Pten* alleles	Pter: 10 mg/kg bw; i.p.	Work in progress.

Res, resveratrol; Pic, piceatannol; Pter, pterostilbene; 3M-Res, trimethoxy-resveratrol; SAHA, suberoylanilide hydroxamic acid; s.c., subcutaneous; i.p., intraperitoneal; bw, body weight.

(i.e., mouse prostate tissue) mimics the original human tumor conditions much better than the subcutaneous tumor. We developed several prostate cancer orthotopic models in which different prostate cancer cells tagged with the luciferase gene were directly injected into the mouse prostate (Fig. 3). Following tumor intake, LNCaP cells, which are nonmetastatic AR-dependent cells, grow progressively and form middle-sized tumors by day 45 (Fig. 3A). In contrast, highly metastatic PC3M tumors develop highly aggressive large tumors in half the period of time, with micrometastasis that can be detected by bioluminescent imaging (Fig. 3B). Moreover, DU145 AR-independent orthotopic xenografts also developed spontaneous site metastasis in kidneys, lung/heart, and liver[36] (Fig. 3C).

Prostate-specific GEM models

The major benefits of these models are preservation of tumor immunity and conservation of the natural history of neoplastic progression and histopathologic features of prostate cancer.[50] We have generated prostate-specific *Pten* heterozygous (*Pten*$^{+/-}$; *Pb-Cre4*) and *Pten* knockout (*Pten*$^{-/-}$; *Pb-Cre4*) mouse models, with chemoprevention and intervention modalities, respectively, that have established MTA1 as a central key regulator in processes

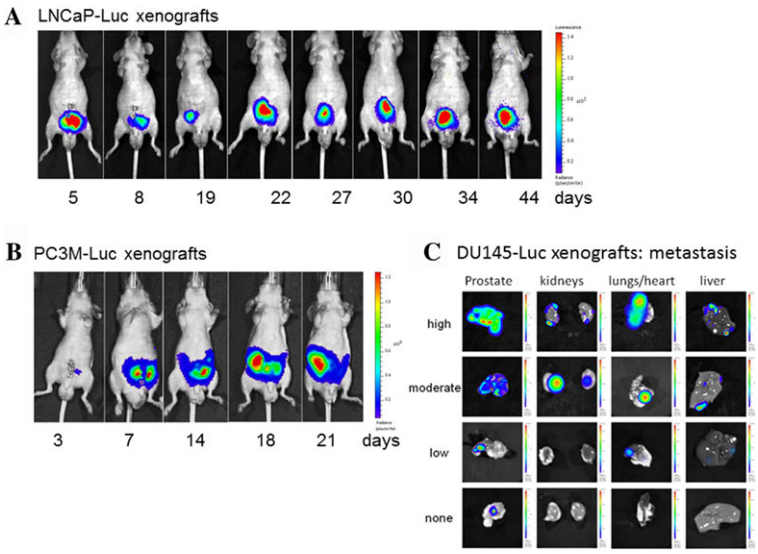

Figure 3. Images of orthotopic prostate cancer xenografts. (A) Bioluminescence images of orthotopic LNCaP-Luc prostate tumor model. (B) Orthotopic PC3M-Luc prostate tumor model. (C) *Ex vivo* images of prostate and metastatic organs removed from mice that developed different degrees of metastasis in DU145-Luc xenografts. For histopathological validation of metastatic lesions, see Ref. 36.

involved not only in prostate cancer progression but also in oncogenic transformation of cells leading to prostate tumorigenesis.

In vivo anticancer and epigenetic effects of resveratrol and analogs in mouse models of prostate cancer

Results of our ongoing studies on the effects of resveratrol and its analogs in preclinical models of prostate cancer are summarized in Table 2. We used the subcutaneous LNCaP model to compare the preventive and anticancer effects of orally administered resveratrol and its natural analogs trimethoxyresveratrol and piceatannol.[29] We found significantly delayed and decreased tumor development and progression in mice treated with these compounds compared to sham-treated mice. Moreover, both piceatannol and, even more so, trimethoxyresveratrol demonstrated greater potency in reducing susceptibility to develop tumor and anticancer activities than the parent compound resveratrol.[29] Further, utilizing the DU145 orthotropic model, we compared the targeted therapeutic efficacy of resveratrol and pterostilbene and found that both compounds inhibited tumor growth and spontaneous metastasis, which was further potentiated upon MTA1 knockdown.[36] Although the differences in efficacy were not statistically significant, pterostilbene demonstrated more favorable pharmacokinetics, accompanied by stronger antiproliferative, antiangiogenic, and proapoptotic effects than resveratrol.[36] In a different DU145 xenograft model, we are currently evaluating the onco-miR–targeted efficacy of pterostilbene upon prolonged intraperitoneal administration.

Finally, toward clinical development of combinatorial treatment strategies, we suggest that the potential of resveratrol and its analogs for anticancer therapy may mostly reside in their ability to sensitize tumor cells for better response to conventional chemotherapeutics or hormonal therapy. To this end, using orthotopic PC3M xenografts, comparison between epigenetic efficacy of pterostilbene and the HDAC inhibitor SAHA (suberoylanilide hydroxamic acid), alone or in combination, is being performed. The data on combination of dietary compounds with agents already in the clinic are limited and merit further study. The insights into the molecular mechanisms of resveratrol/analogs' action may facilitate the development of these compounds as part of successful monotherapy as well as combination therapeutic modalities in reducing advanced metastatic prostate cancer.

It is still unknown whether natural compounds are most effective when consumed daily (chemoprevention) or when taken at higher doses intended

for therapy. We will address these questions using physiologically relevant GEM models, which closely mimic human prostate cancer stage–defined development and histopathology. We are currently evaluating the effects of pterostilbene in prostate-specific *Pten* heterozygous and *Pten* knockout mouse models. We currently believe that pterostilbene, the only known natural product MTA1 inhibitor, blocks prostate tumor development and progression in immunocompetent mice.

Conclusions

Resveratrol and its potent analogs are a novel class of dietary compounds and promising candidates for prostate cancer management. The potential for using resveratrol and analogs for cancer treatment requires further investigation using adequate preclinical models and, vitally, comprehensive clinical trials. The major challenge facing the field is the bioavailability of these compounds. On the basis of our research, dietary pterostilbene may have potential chemopreventive benefits for men at risk or who are diagnosed with early-stage prostate cancer. We suggest that resveratrol analogs with improved potency may be considered as epigenetic chemopreventive and therapeutic agents to be used either alone or in combination with other anticancer drugs for prostate cancer management.

Acknowledgments

Studies described in this paper were supported in part by the Department of Defense Prostate Cancer Research Program under Award W81XWH-13-1-0370 to A.S. Levenson. Views and opinions of and endorsements by the author(s) do not reflect those of the U.S. Army or the Department of Defense. We thank Dr. Richard L. Summers (UMMC) for his continued support.

Conflicts of interest

The authors declare no conflicts of interest.

References

1. Powell, I.J. & F.L. Meyskens, Jr. 2001. African American men and hereditary/familial prostate cancer: intermediate-risk populations for chemoprevention trials. *Urology* **57:** 178–181.
2. Pan, M.H., Y.S. Chiou, L.H. Chen, *et al.* 2015. Breast cancer chemoprevention by dietary natural phenolic compounds: specific epigenetic related molecular targets. *Mol. Nutr. Food Res.* **59:** 21–35.
3. Chiam, K., C. Ricciardelli & T. Bianco-Miotto. 2014. Epigenetic biomarkers in prostate cancer: current and future uses. *Cancer Lett.* **342:** 248–256.
4. Hardy, T.M. & T.O. Tollefsbol. 2011. Epigenetic diet: impact on the epigenome and cancer. *Epigenomics* **3:** 503–518.
5. Abbas, A., W. Patterson 3rd & P.T. Georgel. 2013. The epigenetic potentials of dietary polyphenols in prostate cancer management. *Biochem. Cell Biol.* **91:** 361–368.
6. Jeronimo, C. & R. Henrique. 2014. Epigenetic biomarkers in urological tumors: a systematic review. *Cancer Lett.* **342:** 264–274.
7. Stewart, J.R., M.C. Artime & C.A. O'Brian. 2003. Resveratrol: a candidate nutritional substance for prostate cancer prevention. *J. Nutr.* **133:** 2440S–2443S.
8. Patel, K.R., V.A. Brown, D.J. Jones, *et al.* 2010. Clinical pharmacology of resveratrol and its metabolites in colorectal cancer patients. *Cancer Res.* **70:** 7392–7399.
9. Schoonen, W.M., C.A. Salinas, L.A. Kiemeney, *et al.* 2005. Alcohol consumption and risk of prostate cancer in middle-aged men. *Int. J. Cancer* **113:** 133–140.
10. Kondratyuk, T.P., E.J. Park, L.E. Marler, *et al.* 2011. Resveratrol derivatives as promising chemopreventive agents with improved potency and selectivity. *Mol. Nutr. Food Res.* **55:** 1249–1265.
11. Szekeres, T., P. Saiko, M. Fritzer-Szekeres, *et al.* 2011. Chemopreventive effects of resveratrol and resveratrol derivatives. *Ann. N.Y. Acad. Sci.* **1215:** 89–95.
12. Pirola, L. & S. Frojdo. 2008. Resveratrol: one molecule, many targets. *IUBMB Life* **60:** 323–332.
13. Patel, K.R., E. Scott, V.A. Brown, *et al.* 2011. Clinical trials of resveratrol. *Ann. N.Y. Acad. Sci.* **1215:** 161–169.
14. Dellinger, R.W., A.M. Garcia & F.L. Meyskens Jr., 2014. Differences in the glucuronidation of resveratrol and pterostilbene: altered enzyme specificity and potential gender differences. *Drug Metab. Pharmacokinet.* **29:** 112–119.
15. Yeo, S.C., P.C. Ho & H.S. Lin. 2013. Pharmacokinetics of pterostilbene in Sprague-Dawley rats: the impacts of aqueous solubility, fasting, dose escalation, and dosing route on bioavailability. *Mol. Nutr. Food Res.* **57:** 1015–1025.
16. Kapetanovic, I.M., M. Muzzio, Z. Huang, *et al.* 2011. Pharmacokinetics, oral bioavailability, and metabolic profile of resveratrol and its dimethylether analog, pterostilbene, in rats. *Cancer Chemother. Pharmacol.* **68:** 593–601.
17. Azzolini, M., M. LaSpina, A. Mattarei, *et al.* 2014. Pharmacokinetics and tissue distribution of pterostilbene in the rat. *Mol. Nutr. Food Res.* **58:** 2122–2132.
18. Roupe, K.A., J.A. Yanez, X.W. Teng, *et al.* 2006. Pharmacokinetics of selected stilbenes: rhapontigenin, piceatannol and pinosylvin in rats. *J. Pharm. Pharmacol.* **58:** 1443–1450.
19. Boutegrabet, L., A. Fekete, N. Hertkorn, *et al.* 2011. Determination of stilbene derivatives in Burgundy red wines by ultra-high-pressure liquid chromatography. *Anal. Bioanal. Chem.* **401:** 1513–1521.
20. Lin, L.L., C.Y. Lien, Y.C. Cheng, *et al.* 2007. An effective sample preparation approach for screening the anticancer compound piceatannol using HPLC coupled with UV and fluorescence detection. *J. Chromatogr. B Analyt. Technol. Biomed. Life Sci.* **853:** 175–182.
21. Matsuda, H., T. Kageura, T. Morikawa, *et al.* 2000. Effects of stilbene constituents from rhubarb on nitric oxide

production in lipopolysaccharide-activated macrophages. *Bioorg. Med. Chem. Lett.* **10:** 323–327.
22. Pan, M.H., J.H. Gao, C.S. Lai, *et al.* 2008. Antitumor activity of 3,5,4'-trimethoxystilbene in COLO 205 cells and xenografts in SCID mice. *Mol. Carcinog.* **47:** 184–196.
23. Paul, S., C.S. Mizuno, H.J. Lee, *et al.* 2010. In vitro and in vivo studies on stilbene analogs as potential treatment agents for colon cancer. *Eur. J. Med. Chem.* **45:** 3702–3708.
24. Lin, H.S. & P.C. Ho. 2009. A rapid HPLC method for the quantification of 3,5,4′-trimethoxy-trans-stilbene (TMS) in rat plasma and its application in pharmacokinetic study. *J. Pharm. Biomed. Anal.* **49:** 387–392.
25. Ma, N., W.Y. Liu, H.D. Li, *et al.* 2007. RP-HPLC study of resveratrol derivative (BTM-0512) in rat plasma and tissue distribution. *Yao Xue Xue Bao.* **42:** 1183–1188.
26. Hsieh, T.C., Y.C. Huang & J.M. Wu. 2011. Control of prostate cell growth, DNA damage and repair and gene expression by resveratrol analogues, in vitro. *Carcinogenesis* **32:** 93–101.
27. Hsieh, T.C., C. Wong, D. John Bennett, *et al.* 2011. Regulation of p53 and cell proliferation by resveratrol and its derivatives in breast cancer cells: an in silico and biochemical approach targeting integrin alphavbeta3. *Int. J. Cancer* **129:** 2732–2743.
28. Narayanan, N.K., D. Nargi, C. Randolph, *et al.* 2009. Liposome encapsulation of curcumin and resveratrol in combination reduces prostate cancer incidence in PTEN knockout mice. *Int. J. Cancer* **125:** 1–8.
29. Dias, S.J., K. Li, A.M. Rimando, *et al.* 2013. Trimethoxyresveratrol and piceatannol administered orally suppress and inhibit tumor formation and growth in prostate cancer xenografts. *Prostate* **73:** 1135–1146.
30. Kumar, A., S.Y. Lin, S. Dhar, *et al.* 2014. Stilbenes inhibit androgen receptor expression in 22Rv1 castrate-resistant prostate cancer cells. *J. Medicin. Active Plant.* **3:** 1–8.
31. Xue, Y., J. Wong, G.T. Moreno, *et al.* 1998. NURD, a novel complex with both ATP-dependent chromatin-remodeling and histone deacetylase activities. *Mol. Cell* **2:** 851–861.
32. Nair, S.S., D.Q. Li & R. Kumar. 2013. A core chromatin remodeling factor instructs global chromatin signaling through multivalent reading of nucleosome codes. *Mol. Cell* **49:** 704–718.
33. Kai, L., J. Wang, M. Ivanovic, *et al.* 2011. Targeting prostate cancer angiogenesis through metastasis-associated protein 1 (MTA1). *Prostate* **71:** 268–280.
34. Dias, S.J., X. Zhou, M. Ivanovic, *et al.* 2013. Nuclear MTA1 overexpression is associated with aggressive prostate cancer, recurrence and metastasis in African Americans. *Sci. Rep.* **3:** 2331.
35. Levenson, A.S., A. Kumar & X. Zhang. 2014. MTA family of proteins in prostate cancer: biology, significance, and therapeutic opportunities. *Cancer Metastasis Rev.* **33:** 929–942.
36. Li, K., S.J. Dias, A.M. Rimando, *et al.* 2013. Pterostilbene acts through metastasis-associated protein 1 to inhibit tumor growth, progression and metastasis in prostate cancer. *PLoS One* **8:** e57542.
37. Kai, L., S.K. Samuel & A.S. Levenson. 2010. Resveratrol enhances p53 acetylation and apoptosis in prostate cancer by inhibiting MTA1/NuRD complex. *Int. J. Cancer* **126:** 1538–1548.
38. Wang, H., L. Fan, J. Wei, *et al.* 2012. Akt mediates metastasis-associated gene 1 (MTA1) regulating the expression of E-cadherin and promoting the invasiveness of prostate cancer cells. *PLoS One* **7:** e46888.
39. Dhar, S., A. Kumar, K. Li, *et al.* 2015. Resveratrol regulates PTEN/Akt pathway through inhibition of MTA1/HDAC unit of the NuRD complex in prostate cancer. *Biochim. Biophys. Acta* **1853:** 265–275.
40. Lu, J., G. Getz, E.A. Miska, *et al.* 2005. MicroRNA expression profiles classify human cancers. *Nature* **435:** 834–838.
41. Volinia, S., G.A. Calin, C.G. Liu, *et al.* 2006. A microRNA expression signature of human solid tumors defines cancer gene targets. *Proc. Natl. Acad. Sci. U. S. A.* **103:** 2257–2261.
42. Zhang, B., X. Pan, G.P. Cobb, *et al.* 2007. microRNAs as oncogenes and tumor suppressors. *Dev. Biol.* **302:** 1–12.
43. Leite, K.R., J.M. Sousa-Canavez, S.T. Reis, *et al.* 2011. Change in expression of miR-let7c, miR-100, and miR-218 from high grade localized prostate cancer to metastasis. *Urol. Oncol.* **29:** 265–269.
44. Spahn, M., S. Kneitz, C.J. Scholz, *et al.* 2010. Expression of microRNA-221 is progressively reduced in aggressive prostate cancer and metastasis and predicts clinical recurrence. *Int. J. Cancer* **127:** 394–403.
45. Sapre, N. & L.A. Selth. 2013. Circulating microRNAs as biomarkers of prostate cancer: the state of play. *Prostate Cancer* **2013:** 539680.
46. Dhar, S., C. Hicks & A.S. Levenson. 2011. Resveratrol and prostate cancer: promising role for microRNAs. *Mol. Nutr. Food Res.* **55:** 1219–1229.
47. Cheon, D.J. & S. Orsulic. 2011. Mouse models of cancer. *Annu. Rev. Pathol.* **6:** 95–119.
48. Frese, K.K. & D.A. Tuveson. 2007. Maximizing mouse cancer models. *Nat. Rev. Cancer* **7:** 645–658.
49. Sachs, N. & H. Clevers. 2014. Organoid cultures for the analysis of cancer phenotypes. *Curr. Opin. Genet. Dev.* **24:** 68–73.
50. Shappell, S.B., G.V. Thomas, R.L. Roberts, *et al.* 2004. Prostate pathology of genetically engineered mice: definitions and classification. The consensus report from the Bar Harbor meeting of the Mouse Models of Human Cancer Consortium Prostate Pathology Committee. *Cancer Res.* **64:** 2270–2305.

Resveratrol and pterostilbene epigenetically restore PTEN expression by targeting oncomiRs of the miR-17 family in prostate cancer

Swati Dhar[1], Avinash Kumar[1], Agnes M. Rimando[2], Xu Zhang[3], Anait S. Levenson[1,4]

[1]Cancer Institute, University of Mississippi Medical Center, Jackson, Mississippi, USA

[2]United States Department of Agriculture, Agricultural Research Service, Natural Products Utilization Research Unit, University, Mississippi, USA

[3]Center of Biostatistics and Bioinformatics, University of Mississippi Medical Center, Jackson, Mississippi, USA

[4]Department of Pathology, University of Mississippi Medical Center, Jackson, Mississippi, USA

Correspondence to:
Anait S. Levenson, e-mail: alevenson@umc.edu

Keywords: *oncomiRs, prostate cancer epigenetics, PTEN, pterostilbene, resveratrol*

Received: *July 07, 2015* ***Accepted:*** *July 24, 2015* ***Published:*** *August 06, 2015*

ABSTRACT

In recent years, not only has the role of miRNAs in cancer become increasingly clear but also their utilization as potential biomarkers and therapeutic targets has gained ground. Although the importance of dietary stilbenes such as resveratrol and pterostilbene as anti-cancer agents is well recognized, our understanding of their miRNA-targeting capabilities is still limited. In our previous study, we reported that resveratrol downregulates PTEN-targeting members of the oncogenic miR-17 family, which are overexpressed in prostate cancer. This study investigates the resveratrol and pterostilbene induced miRNA-mediated regulation of PTEN in prostate cancer. Here, we show that both compounds decrease the levels of endogenous as well as exogenously expressed miR-17, miR-20a and miR-106b thereby upregulating their target PTEN. Using functional luciferase reporter assays, we demonstrate that ectopically expressed miR-17, miR-20a and miR-106b directly target PTEN 3'UTR to reduce its expression, an effect rescued upon treatment with resveratrol and pterostilbene. Moreover, while stable lentiviral expression of miR-17/106a significantly decreased PTEN mRNA and protein levels and conferred survival advantage to the cells, resveratrol and more so pterostilbene was able to dramatically suppress these effects. Further, pterostilbene through downregulation of miR-17-5p and miR-106a-5p expression both in tumors and systemic circulation, rescued PTEN mRNA and protein levels leading to reduced tumor growth *in vivo*. Our findings implicate dietary stilbenes as an attractive miRNA-mediated chemopreventive and therapeutic strategy, and circulating miRNAs as potential chemopreventive and predictive biomarkers for clinical development in prostate cancer.

INTRODUCTION

A growing body of experimental evidence suggest an aberrant expression of microRNAs (miRNAs, miRs) in cancer, which can act as oncogenes or tumor suppressors defining the fate of tumor formation [1–3]. Since their discovery as short, single-stranded, noncoding RNA molecules that act as posttranscriptional regulators of gene expression [4, 5], our understanding of the mechanisms of miRNA action has considerably increased. In general, miRNAs bind to sequences in the 3′UTR (3′ untranslated region) of target genes and decrease the stability of nascent mRNA or /and protein translation, which results in decreased production of the target protein [6].

Most importantly, miRNAs have a number of desirable characteristics for clinical application: disease specificity, exceptional stability in various types of clinical

samples, and ability to respond to therapy [7]. These features together with presence of circulating miRNAs in cell-free fraction of blood, i.e. serum and plasma, make miRNAs incomparable potential biomarkers for cancer diagnosis, prediction, and prognosis, which in turn, mark them as valuable targets for the clinical development of anticancer agents [7–9].

In prostate cancer, changes in expression of miRNAs are associated with clinicopathological parameters such as Gleason score and recurrence [8, 10–12]. In particular, there is an overexpression and amplification of oncogenic miR-17~92 and miR-106b~25 clusters in prostate cancer [10, 13, 14]. We too, using miRNA profiling in LNCaP cells, reported significant expression of oncogenic miR-17~92, miR-106a~363, and miR-106b~25 clusters, some members of which target the tumor suppressor gene PTEN (Phosphatase and Tensin homolog) [15]. PTEN is frequently defective in prostate cancer as its deletions/mutations are found in primary and metastatic disease [16]. It was speculated that *PTEN* heterozygosity, when accompanied by miRNA-mediated down-regulation, might be more effective at promoting tumorigenesis than complete homozygous loss of *PTEN* [17]. Since homozygous *PTEN* deletion is not common in human prostate cancer, the role of epigenetic regulators, such as miRNAs, becomes more important in contributing to PTEN expression and activity. This, in turn, opens the door for potential epigenetic therapies, including dietary compounds with the ability to modulate PTEN abundance by suppressing oncogenic miRNAs.

Our knowledge of anticancer therapies, especially dietary compounds that can control aberrant miRNA expression is relatively limited [18, 19]. Dietary stilbenes, such as resveratrol (Res) (*trans*-3, 5, 4′-trihydroxystilbene) and its potent natural analog pterostilbene (Pter) (*trans*-3, 5-dimethoxy-4′-hydroxystilbene), are known for their antioxidant, anti-inflammatory, cardioprotective and anticancer activities [20–22]. Both compounds have pleiotropic anticancer activities that include induction of apoptosis and inhibition of angiogenesis and metastasis [23–31]. Since miRNAs regulate all aspects of cancer biology, one mechanism of anticancer effects of dietary stilbenes may as well be through modulation of miRNAs.

We previously showed that resveratrol significantly altered miRNA profiles in prostate cancer, including members of the oncogenic miR-17 family, predicted to target PTEN [15]. Upregulation of PTEN protein levels by resveratrol in prostate cancer have been reported earlier [15, 32]. One mechanism of PTEN upregulation by resveratrol, reported by us recently, is inhibition of metastasis-associated protein 1 (MTA1)-mediated deacetylation and inactivation of PTEN [27]. However, the role of dietary stilbenes such as resveratrol and pterostilbene in modulating miRNA-mediated regulation of PTEN in prostate cancer has not been investigated.

In the current study, we hypothesized an oncomiR-mediated inhibition of PTEN and provided experimental validation on the ability of resveratrol and pterostilbene to rescue this effect. Our results indicate that both resveratrol and pterostilbene exert their anticancer effects, at least in part, via repression of several members of the oncogenic miR-17 family. We show that by inhibiting these oncomiRs, resveratrol and pterostilbene rescue the expression of PTEN tumor suppressor. This is the first report on dietary stilbenes' miRNA-mediated regulation of PTEN in prostate cancer.

RESULTS

Resveratrol rescues miR-mediated downregulation of PTEN in prostate cancer cells

Previous report from our laboratory showed that the expression levels of miRs from oncogenic miR-17~92, miR-106a~363 and miR-106b~25 clusters were downregulated in LNCaP and DU145 PCa cells treated with 50 μM resveratrol [15]. Based on their seed sequences, the miRNAs of these clusters are grouped into four families, one of which is the miR-17 family that consists of miR-17, miR-20a and b, miR-106a and b and miR-93 [33]. According to miRanda/MicroCosm [34], TargetScan [35] and Diana-microT-CDS [36] prediction algorithms, miRs-17, -20a and -106a and b target tumor suppressor PTEN gene. Independently, we observed an upregulation of PTEN protein levels in DU145 and 22Rv1 cells [15, 27] leading to downregulation of PI3K-Akt signaling by resveratrol [27] and hypothesized that this effect could be regulated, at least in part, by resveratrol-modulation of PTEN-targeting miRNAs. Quantitative RT-PCR analysis confirmed that both resveratrol and its natural analog pterostilbene significantly downregulated miRs-17, -20a, -106a and -106b in DU145 and 22Rv1 prostate cancer cells that express wild type PTEN (Figure 1A).

To establish a direct effect of resveratrol on miRNAs, we examined whether resveratrol regulates ectopically expressed miRs in prostate cancer cells. Resveratrol treatment decreased ectopic miRNA expression similar to its effect on endogenous miRNA (Figure 1B). Further, ectopic overexpression of miRs -17 or -20a or -106b alone resulted in downregulation of their target PTEN mRNA and protein in DU145 cells, which was rescued by treatment with 50 μM of resveratrol (Figure 1C and 1D). Cumulatively, these results suggest that resveratrol's rescue of PTEN mRNA and protein is mediated, at least in part, through its ability to downregulate oncomiRs of the miR-17 family involved in targeting PTEN.

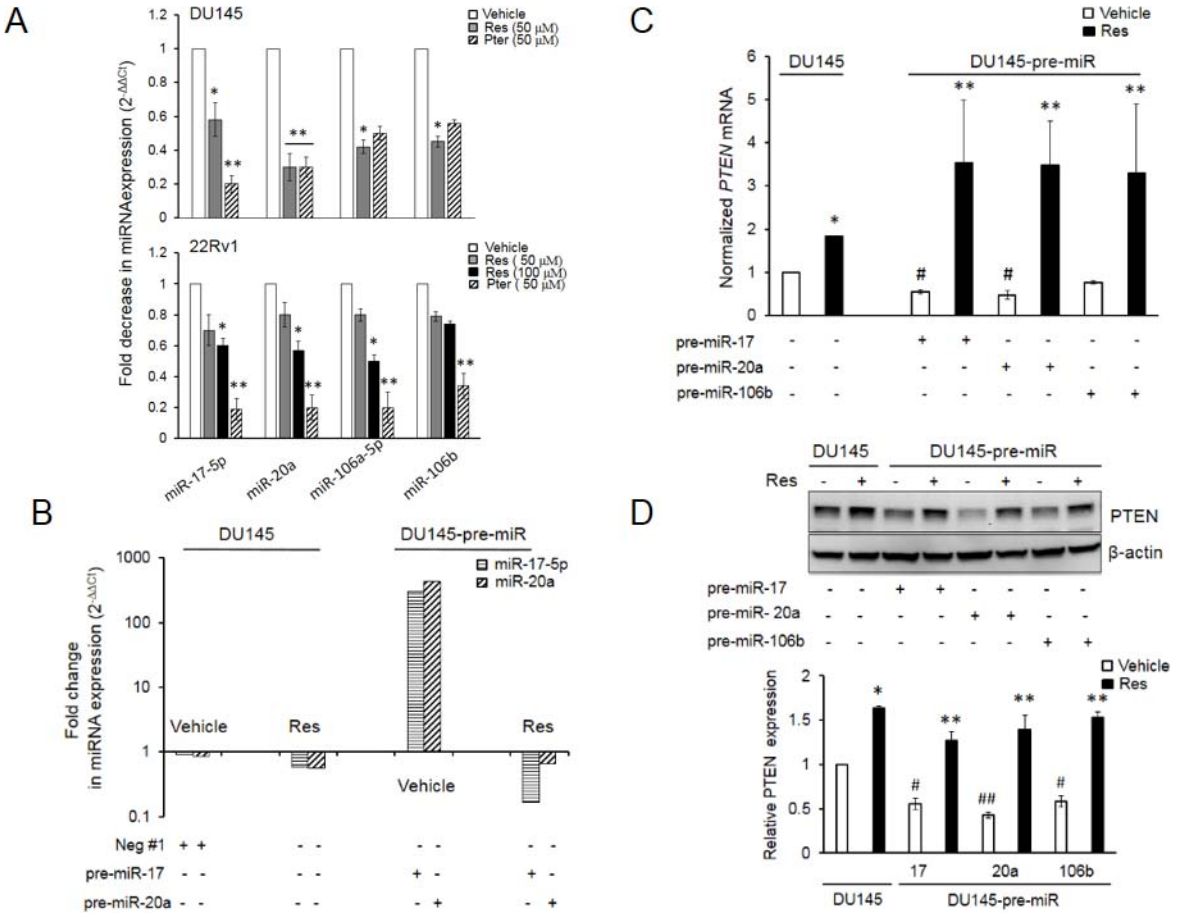

Figure 1: Resveratrol and pterostilbene reversal of miR-mediated downregulation of PTEN mRNA and protein. A. Resveratrol and pterostilbene induced downregulation of miR-17 family oncomiRs in DU145 and 22Rv1 PCa cells. Cells were treated with resveratrol and pterostilbene at indicated concentrations, miRNA was isolated and real time PCR was performed as detailed in Materials and Methods. All samples were within threshold cycle (C_t < 35). **B.** Resveratrol directly targets ectopically expressed miRs in DU145 cells. Relative abundance of miR-17-5p and miR-20a was measured by real time PCR. **C, D.** Resveratrol significantly restored and enhanced PTEN mRNA (C) and protein (D) expression in the presence of ectopically overexpressed miRs, which diminished PTEN expression in vehicle-treated cells. Fold changes in expression of miRNAs and mRNA was calculated by the $2^{-\Delta\Delta Ct}$ method. Data represent the mean ± SEM from three independent experiments. Quantitation of blots was performed using Image J software. Comparisons between non- transfected and miR-transfected samples (#) and vehicle-treated and compound-treated samples (*) are depicted. $^{\#}p < 0.05$; $^{\#\#}p < 0.01$; $^{*}p < 0.05$; $^{**}p < 0.01$. Res, resveratrol; Pter, pterostilbene.

Resveratrol and pterostilbene reverse targeting of PTEN 3′UTR by oncomiRs

To validate whether PTEN is a direct target gene of miRs-17, -20a and -106b, we employed the dual-luciferase reporter assay. For this, PTEN 3′UTR sequence (535 bp) (Supplementary Figure S1) containing either the wild type seed match for all three miRs (GCACTTT) or its mutant (mut) form (GGAGTAT) was amplified and cloned into the pMIRGLO vector, downstream of the luciferase reporter gene. The overall target specificity for miR-17, miR-20a and miR-106b defined by miRanda (http://www.microrna.org) was comparable for these three miRs (Figure 2A). The data showed that the co-expression of miR-17 or miR-20a or miR-106b with wild type 3′UTR (Figure 2B and 2C) but not with mutant 3′UTR (Figure 2D) significantly suppressed the luciferase activity, indicating that these miRs directly target the 3′UTR of PTEN. When cells were treated with either resveratrol or pterostilbene, there was a reversal of miRs' inhibitory effects with wild type 3′UTR (Figure 2B and 2C) and no changes with mutant 3′UTR (Figure 2D). These results indicated that stilbenes can reverse the targeting of PTEN 3′UTR by these miRNAs.

Resveratrol and pterostilbene restore PTEN mRNA and protein expression in DU145 cells stably overexpressing miR-17/106a

In order to further explore the functional relevance of PTEN-targeting miRNAs, we established DU145-Luc cells stably overexpressing miR-17/106a

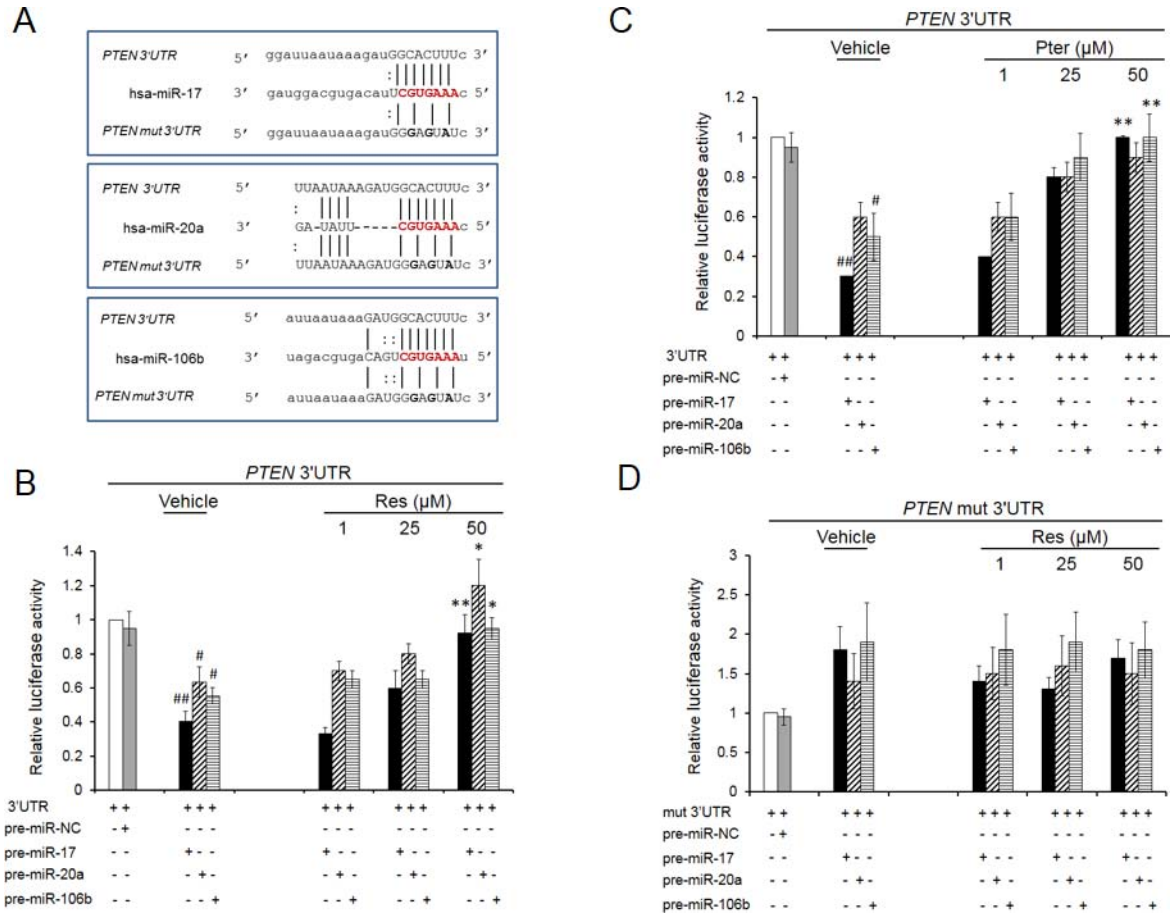

Figure 2: Resveratrol and pterostilbene rescue PTEN inhibition by oncomiRs -17, -20a and -106b. A. Schematic representation of the predicted target sites of miRs-17, -20a and -106b in the 3′UTR of PTEN mRNA. The miRNA seed sequence is shared by all three miRs and shown in red. Mutated nucleotides in the 3′UTR are shown in bold. **B, C.** Resveratrol and pterostilbene oppose *PTEN* 3′UTR targeting. Relative luciferase activity in DU145 cells co-transfected with wt *PTEN* 3′UTR along with either pre-miR-17, -20a or 106b and treated with resveratrol (B) or pterostrilbene (C) **D.** Co-transfections with mutated 3′UTR did not show any inhibitory effect on luciferase activity. MiR-negative#1 was used as a negative control (miR-NC). Values are normalized to Renilla luciferase activity and relative to 3′UTR / EV (Empty Vector) ratio which is set at 1. Data represent the mean ± SEM from four independent experiments. Comparisons between non-transfected and miR transfected samples (#) and vehicle and compound-treated samples (*) are shown. $^{\#}p < 0.05$; $^{\#\#}p < 0.01$; $^{*}p < 0.05$; $^{**}p < 0.01$. Res, resveratrol; Pter, pterostilbene.

referred here after as miR-17/106a MIMIC (Supplementary Figure S2A and S2B). Stable overexpression of miR-17/106a caused a significant downregulation of PTEN mRNA and protein levels (Figure 3A). Moreover, resveratrol efficiently downregulated the levels of ectopically expressed miRs (Figure 3B) resulting in rescue of PTEN mRNA (Figure 3C) and protein (Figure 3D). As seen in Figures 3C and 3D, pterostilbene demonstrated marginally stronger effect in restoring both PTEN mRNA and protein levels. In addition, we observed that overexpression of miRs confers survival advantage to these cells, and the inhibitory effects of both agents on cell growth were more pronounced in miR-17/106a MIMIC cells compared to empty vector (EV) control (Supplementary Figure S2C).These results suggested that the stilbenes rescue PTEN expression by downregulation of miR-17-5p and miR-106a-5p.

Pterostilbene effectively diminishes tumor growth in miR-17/106a overexpressing xenografts

Meta-analysis for correlation of miR-17 and -106a expression in prostate cancer samples [37] clearly indicated a significant overexpression of these miRs in prostate cancer patients compared to normal cohort (Supplementary Figure S3) indicating their clinical significance in PCa and therefore the therapeutic value of targeting these miRNAs. In preclinical studies, to examine the miR-mediated anticancer efficacy of pterostilbene *in vivo*, we implanted DU145-Luc EV and miR-17/106a overexpressing cells on the right flank of male nude mice and treated them with vehicle (10% DMSO) or pterostilbene (50 mg/kg bw). We chose pterostilbene based on its better effects on miR downregulation

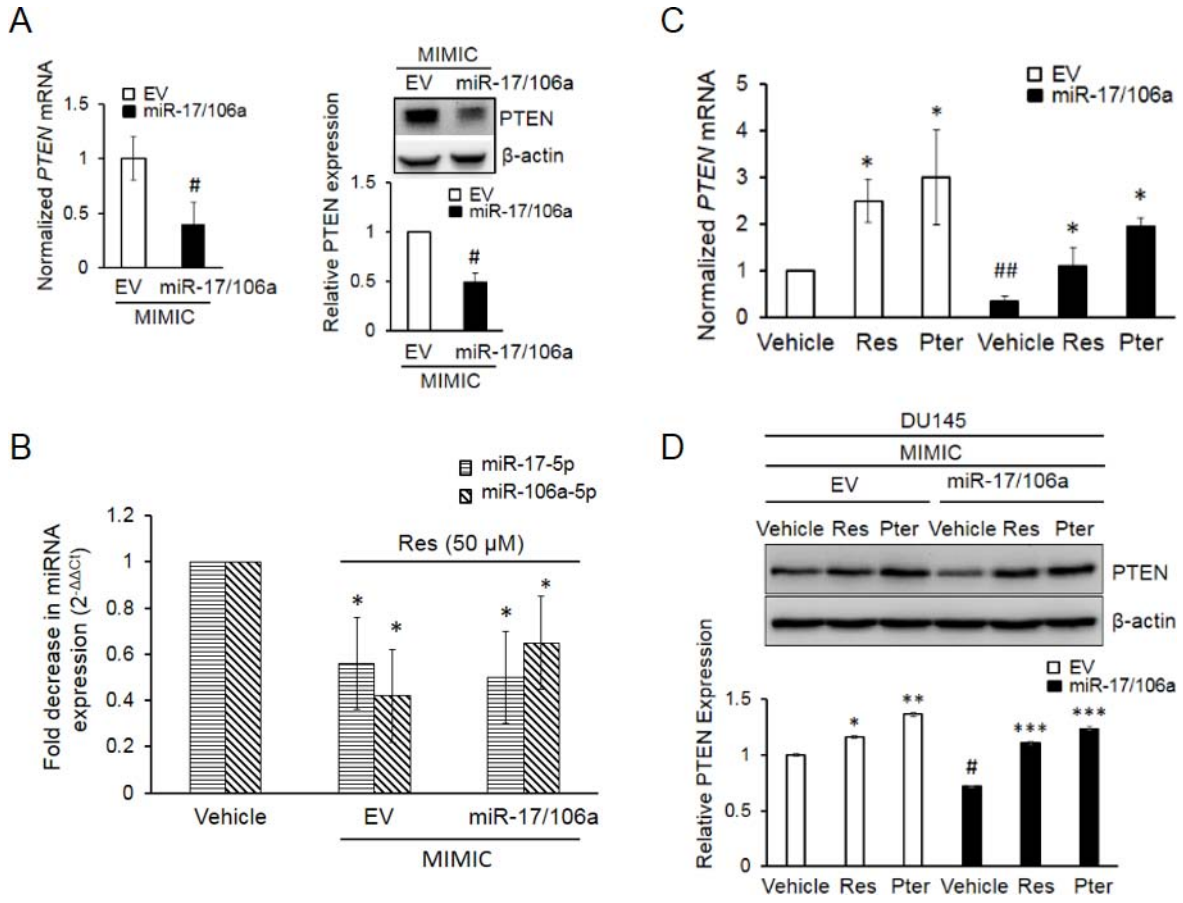

Figure 3: Establishment and characterization of DU145 cells stably overexpressing miR-17/106a. A. PTEN mRNA (left) and protein (right) were significantly decreased in miR-17/106a MIMIC compared to EV MIMIC cells. PTEN mRNA expression was detected by real time PCR and protein was detected by western blot. **B.** Resveratrol inhibits relative abundance of miRs-17 and -106a in EV and miR-17/106a MIMIC cells as detected by real time PCR. **C, D.** Resveratrol and pterostilbene enhanced expression of PTEN mRNA (C) and protein (D) in EV MIMIC and miR-17/106a MIMIC cells. Fold change in expression of miRNAs and mRNA was calculated by the $2^{-\Delta\Delta Ct}$ method. Data represent the mean ± SEM from at least three independent experiments. Quantitation of blots was performed using Image J software. Comparisons between non-transfected and miR transfected samples (#) and vehicle and compound-treated samples (*) are shown. $^{\#}p < 0.05$; $^{\#\#}p < 0.01$; $^{*}p < 0.05$; $^{**}p < 0.01$; $^{***}p < 0.001$. EV, Empty vector, Ctrl, Control, Res, resveratrol; Pter, pterostilbene.

leading to PTEN rescue (Figure 1A, Figure 3C, 3D) and its known potent pharmacokinetics including superior bioavailability and more effective tissue distribution over resveratrol [22, 30, 38–42]. Tumor growth was monitored weekly by both bioluminescent imaging and caliper measurements, which complemented each other, until day 39 when mice were sacrificed and tumors and sera collected for analysis (Figure 4A). Tumor measurements by bioluminescent imaging in the first 18 days clearly revealed that ectopic expression of miR-17/106a promotes tumorigenic properties of cells as evident by accelerated tumor progression and larger tumor volumes in miR-17/106a overexpressing xenografts as compared to the EV group (Figure 4B). Although still not reaching statistical significance at that time, miR-17/106a vehicle-treated tumors exhibited steady growth but revealed non-consistent measurements due to limitations of photon emission detection of large s.c. tumors that consist of necrotic areas and infiltrating host cells [31, 43–45]. On the other hand, caliper-based measurements were feasible only after day 18, after which they were more reliable than bioluminescent measurements and demonstrated statistically significant differences between miR-overexpressing tumors and EV by day 39 (Figure 4C). Importantly, pterostilbene treatment significantly decelerated tumor growth in miR-17/106a overexpressing xenografts without any obvious adverse effects on mice (Supplementary Figure S4A). Pterostilbene treatment downregulated miRs-17 and 106a more efficiently in miR-17/106a overexpressing tumors (Figure 4D) while simultaneously enhancing PTEN mRNA (Figure 4E) and protein expression by approximately three fold (Figure 4F). Immunohistochemical analysis revealed a decrease in PTEN expression along with a five-fold increase in Ki-67 and a three-fold decrease in cleaved Caspase-3 staining in miR-overexpressed tumors compared to that in controls (Figure 5A and 5B). Pterostilbene treatment in both groups, on the other hand,

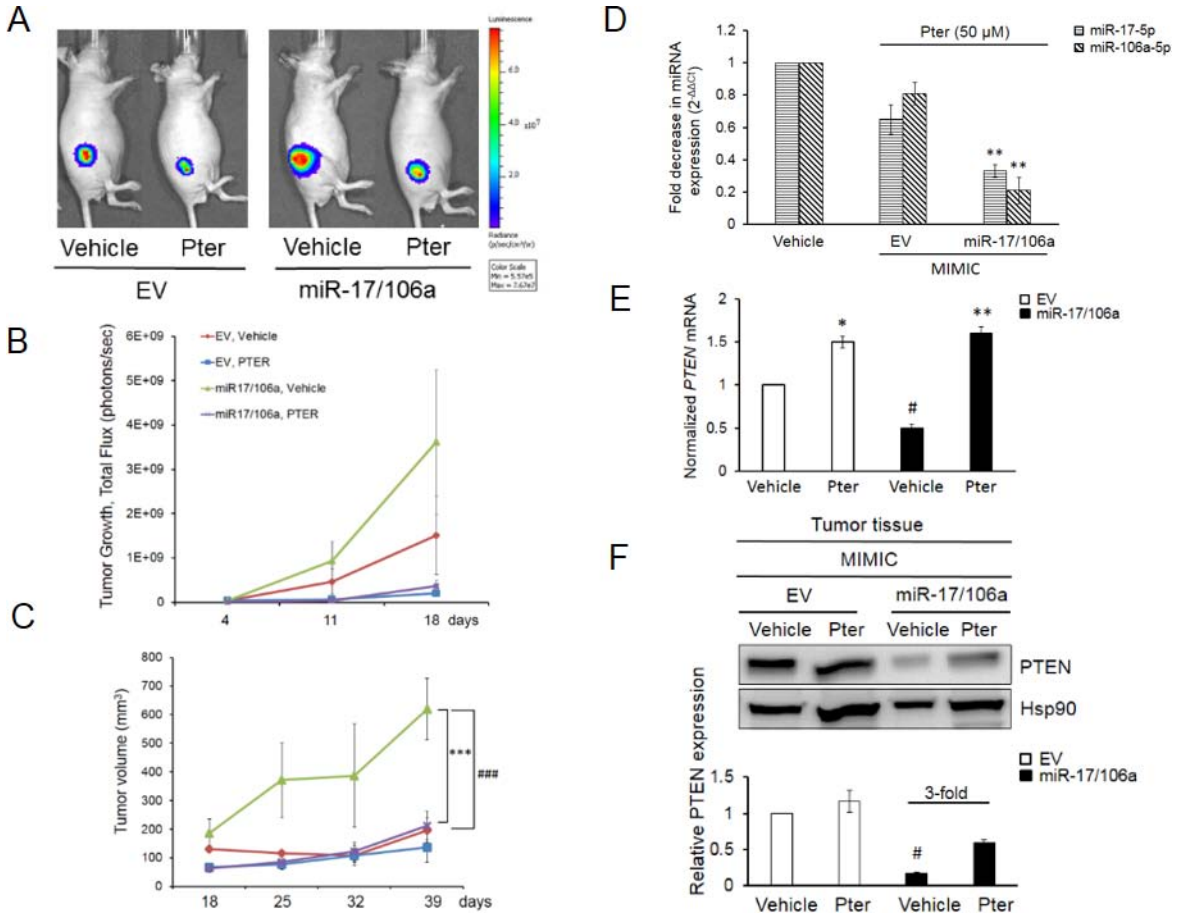

Figure 4: Pterostilbene diminishes the miR-17/106a-promoted tumor growth in prostate cancer xenografts. **A.** Bioluminescent images of representative mice from each group (n = 8 mice per group) at day 39 are shown. **B.** Quantitative analysis of BL signals from day 4 after cancer cell injections until day 18 is shown. Light emission data in Total Flux (photons/sec) are plotted. **C.** Pterostilbene treatment considerably reduced tumor volumes in miR-overexpressing xenografts, which exhibited significantly accelerated tumor growth compared to EV control. Tumor growth was monitored using a digital caliper once a week starting at day 18. **D.** Pterostilbene down-regulated miR expression in 17/106a MIMIC tumors, measured by real time PCR. **E, F.** Pterostilbene rescued PTEN mRNA (E) and protein (F) expression in miR-17/106a MIMIC tumor tissues. Hsp90 was used as loading control and quantitation was performed using Image J software. Comparisons between EV and miR-overexpressing tumors (#) and vehicle and Pter-treated samples (*) are shown. $^{\#}p < 0.05$; $^{\#\#\#}p < 0.001$; $^{*}p < 0.05$; $^{**}p < 0.01$; $^{***}p < 0.001$. Pter, pterostilbene.

reversed these effects and demonstrated more potent effects in miR-overexpressing tumors (Figure 5A and 5B). Collectively, these data demonstrate that pterostilbene could target overexpressed miR levels and still restore PTEN expression leading to a decrease in tumor growth.

A number of studies have assessed the potential of circulating miRNAs to diagnose early-stage prostate cancer [7–9]. The ability of circulating miRNAs as predictors to treatment response or as chemopreventive markers is understudied. We questioned whether pterostilbene can diminish the abundance of secreted miRNAs and whether detection of changes in circulating miRs in response to treatment may be useful in the future clinical applications. To this end, we analyzed the relative abundance of circulating miR-17 and -106a in the sera from both groups of xenografts treated with pterostilbene. First of all, miR-17-5p and miR-106a-5p were highly expressed in sera collected from mice that were injected with miR-17/106a MIMIC cells compared to those that were carrying EV MIMIC cells (Supplementary Figure S4B). The results shown in Figure 5C indicated that in response to pterostilbene treatment reduction in circulating miR-17-5p and miR-106a-5p were more prominent in sera from ectopic miR-expressing xenografts compared to their control counterparts. This implied that beneficial anticancer effects of pterostilbene may be reflected through changes in levels of circulating miRs detected in serum.

DISCUSSION

From a therapeutic perspective, dietary agents are being intensively studied for their anticancer properties. Nutriepigenomic studies, which are in their infancy,

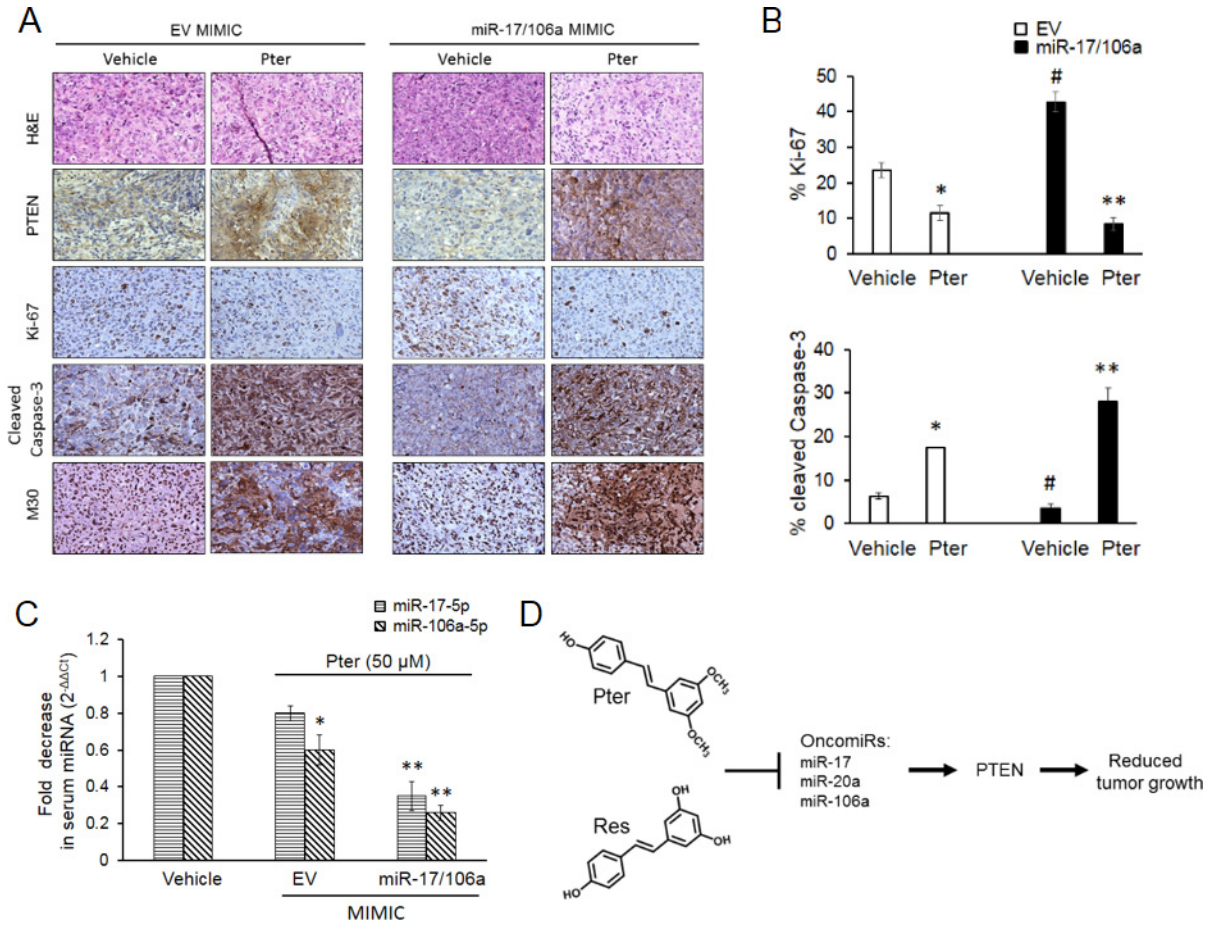

Figure 5: Pterostilbene induces PTEN expression and apoptosis, inhibits tumor cell proliferation and downregulates circulating tumor-derived oncomiRs *in vivo*. A. Representative H&E and IHC images of PTEN, Ki-67 (proliferation); cleaved caspase-3 and M30 (apoptosis) staining in EV and miR-17/106a MIMIC xenografts upon pterostilbene treatment (magnification x100). **B.** Percent quantitation of Ki-67 and cleaved Caspase-3 staining is shown ($n = 3$ per group). **C.** Pterostilbene downregulated oncomiRs in serum of xenograft mice. Quantitative RT-PCR analysis of circulating levels of miRs-17-5p and -106a-5p in sera ($n = 3$ per group) from EV MIMIC and miR-17/106a MIMIC xenograft mice. Data represents the mean ± SEM of three independent experiments. Comparisons between EV and miR-overexpressing tumors (#) and vehicle and Pter-treated samples (*) is depicted. $^{\#}p < 0.05$; $^{*}p < 0.05$; $^{**}p < 0.01$. **D.** Proposed model of miR-regulated anticancer activity of dietary stilbenes. Pterostilbene and resveratrol inhibit expression of PTEN targeting miR-17 family oncomiRs, which leads to rescue of tumor suppressor PTEN expression resulting in inhibition of tumor growth. Pter, pterostilbene.

are focusing on bioactive dietary factors-induced beneficial changes in gene expression through epigenetic modifications [46]. Several studies have recently highlighted the anti-cancer role of dietary compounds via their effect on microRNAs aberrantly expressed in malignant cells [18, 19, 47]. An initial large scale miRnome analysis of lung, breast, stomach, prostate, colon and pancreatic tumors revealed high expression of miR-17 and miR -20a among others [2]. Among these oncomiRs, miR-17~92 cluster, described as oncomiR 1 has been shown to be overexpressed in several cancers [48]. We detected significantly increased expression of miRs-17, -20a, -106a and -106b and the ability of dietary resveratrol to downregulate these oncomiRs in miRNA profiling studies of prostate cancer cells [15].

Our current work expands on these initial findings by demonstrating direct association between oncomiRs and their target, functional involvement of miRNAs in tumor manifestation, and, importantly, the ability of resveratrol and its potent analog pterostilbene to reverse silencing effects of miRNAs on tumor suppressor PTEN.

Although oncogenic potential of miR-17~92 and miR-106b~25 clusters in targeting 3′UTR of PTEN mRNA has been recently reported [13, 48], we investigated the ability of resveratrol and pterostilbene to counteract oncomiRs. Indeed, while ectopic overexpression of miRs -17, -20a and -106a induced a significant loss in PTEN 3′UTR luciferase activity with miR-17 revealing most striking down-regulation, both resveratrol and pterostilbene rescued this loss of luciferase signal in a dose-dependent

manner, indicating that there is a direct effect of treatment on ectopically overexpressed miRNAs. As expected, the inhibitory effect of resveratrol and pterostilbene treatment on these oncomiRs was reflected in the elevated PTEN mRNA and protein expression levels.

Of note, resveratrol diminished the abundance of ectopically overexpressed oncomiRs in transiently transfected DU145 cells almost with the same potency as it did the endogenous expression of miRs-17 and -20a, indicating that there could be a possible affinity of resveratrol for a pool of oncomiRs, which are overexpressed in a system such as in transformed cells. This hypothesis is attested by our findings of relatively higher abundance of these oncomiRs and their better targeting by resveratrol in DU145 prostate cancer cells compared to "normal" RWPE-1 cells (data not shown). Since commercially available synthetic miRNAs are described as pre-miRs, which after introduction in the cellular system undergo processing by Dicer to generate mature miRNAs, it is plausible that resveratrol acts either directly on mature miRNAs and/or on the molecular substrates responsible for generating the mature miRNAs. There are evidence in literature for both possibilities. Hagiwara *et al*., have shown that resveratrol and more so pterostilbene enhances the transcriptional activation of certain tumor suppressive miRNAs and Argonaute-2 (Ago-2), a key regulator of miRNA homeostasis and biogenesis [49]. On the other hand, direct interaction of resveratrol with mature miRNAs, which could potentially alter their interaction with the target mRNA, was reported recently by Baselga-Escudero and colleagues [50]. No data is available on regulation of Dicer, Drosha or other miRNA machinery-related genes by dietary compounds in prostate cancer. We believe that there is a possibility for stilbenes to regulate other microRNA processing components including Dicer, which have been shown to be upregulated in prostate cancer [10, 51], subsequently diminishing cellular pools of oncomiRs. However, based on the differential effect of resveratrol on the expression of oncomiRs (downregulation) and tumor suppressor miRNAs (upregulation), it would be safe to assume that the specificity of the resveratrol-mediated downregulation of miR-17 family could come from resveratrol's regulation of some transcription factor(s) that regulate the transcription of these miRNA genes (unpublished data).

The more potent anticancer properties of pterostilbene can be explained by its chemical structure differences from resveratrol where two hydroxyl groups of resveratrol are replaced by two methoxy groups, which makes pterostilbene more stable, lipophilic and membrane-permeable [52]. We and others have reported earlier a more effective inhibition of prostate tumor cell growth *in vitro* and *in vivo* by pterostilbene, and essentially, greater accumulation of pterostilbene in serum and tissues compared to resveratrol [30, 38–41].

Proof-of concept *in vivo* studies using miR-17/106a overexpressing tumor cells clearly showed accelerated tumor development in immunocompromised mice that was efficiently counteracted upon pterostilbene treatment, which resulted in enhanced PTEN expression and apoptosis. This provides substantial preclinical evidence for the therapeutic ability of dietary stilbenes in regulating tumor development and progression via miR-mediated mechanisms.

Finally, to further potentiate the importance of our finding for relevance to clinical application, we determined the changes in circulating levels of miRs-17 and -106a from sera of tumor bearing mice. We found a three-fold higher expression of these tumor-derived oncomiRs in the sera of miR-overexpressing mice compared to their empty vector counterparts, which was efficiently downregulated by pterostilbene. Detection of serum circulating miRNAs in prostate cancer animal models and clinical cohorts of prostate cancer patients has been reported [7–9, 53], however, the regulation of circulating miRs in serum by dietary compounds has not been investigated. In this report, we demonstrated that pterostilbene treatment not only leads to reduction of tumor growth but also affects the levels of circulating miRs, which can be utilized as chemopreventive and predictive markers in prostate cancer.

In conclusion, we show here that high miRs-17, -20a, -106a and -106b expression is strongly correlated with prostate cancer progression, and confirm PTEN tumor suppressor as a key target of these oncomiRs in prostate cancer cells. Importantly, we demonstrate oncomiR-mediated anticancer effects of resveratrol and pterostilbene, which suggest that restoring PTEN expression may be a feasible approach for prostate cancer chemoprevention and therapy (Figure 5D). To the best of our knowledge, our study is the first to address the functional consequences of onco-miRNA downregulation by dietary pterostilbene *in vivo*. Also, for the first time, we demonstrate the modulation of circulating oncomiRs in murine serum in response to treatment by natural agent, which opens possibilities for miRNA utilization as chemopreventive biomarkers in prostate cancer. These findings provide a novel perspective on how dietary stilbenes may function as chemopreventive and anticancer agents by modulating miRNAs, alterations of which can be responsible for prostate cancer predisposition and progression.

MATERIALS AND METHODS

Reagents

Resveratrol was purchased from Sigma-Aldrich, Indianapolis, USA. Pterostilbene was synthesized following previously published procedures [54]. The purity of pterostilbene was determined to be >99%. Stock

solutions of resveratrol and pterostilbene were made using high purity DMSO (MP Biomedicals, Solon, USA) and kept at 4°C, in the dark.

Cell culture

Prostate cancer cell lines DU145 and 22Rv1 were purchased from ATCC, Manassas, USA and maintained in RPMI-1640 (Life Technologies, NY, USA) containing 10% FBS as described previously [28, 29]. Cells were maintained in an incubator at 37°C with 5% CO_2. Both cell lines were last authenticated using short tandem repeat profiling at Research Technology Support Facility, Michigan State University in July 2014. Resveratrol and pterostilbene treatment were carried out as previously described [28–31].

Cloning and dual- luciferase reporter assay

We amplified a 535 bp region of the *PTEN* 3′UTR encompassing the miR-17, -20a and -106b seed sequence and cloned into the Sac I (New England Biolabs, Ipswich, USA) site of pMIRGLO vector (Promega, Madison, USA) downstream of the Firefly luciferase gene using the InFusion HD cloning kit (Clontech, Mountain View, USA). The orientation of the insert was verified by sequencing (Davis Sequencing). To introduce three-point mutations into the seed sequence of the miRs binding site, we used the InFusion mutagenesis method (Clontech, Mountain View, USA) as per manufacturer's instructions. The wild type primers used were as follows: forward, 5′- CTA GTT GTT TAA ACG AGC TCT CTG ACA CCA CTG ACT CTG ATC CA- 3′; reverse, 5′- GAC TCG AGG CTA GCG AGC TCA GTA GGC TTT GAA GGA CAG CAG GA- 3′ (bold letters represent Sac I cloning site). The mutated primers used were as follows: forward, 5′ -GGA TTA ATA AAG ATG GGA GTA TCC CG- 3′; reverse, 5′ -TTT CTG AGC ATT CCC TCC ATT CCC- 3′ (underlined indicates mutated nucleotides). Luciferase reporter assay was performed using the Dual-Luciferase Reporter Assay System (Promega, Madison, USA). After cells were co-transfected with either wild type or mutant 3′UTR *PTEN* (800 ng) and 50 nM synthetic Pre-miRs -17 or -20a or -106b or with non-targeting miR Negative #1 (miR-NC, negative control, Life Technologies, NY, USA) treated with resveratrol/pterostilbene, luciferase activity was measured on a Synergy 4 plate reader (Biotek Instruments). Firefly luciferase activity was normalized for transfection efficiency to Renilla luciferase activity. The ratio of *PTEN* 3′UTR alone to Empty Vector (EV) alone (3′UTR/EV) was set as control (Ctrl = 1) and all changes in luciferase activity were calculated relative to Ctrl.

Generation of DU145 luciferase expressing cells

DU145 luciferase (DU145-Luc) cells were established, expanded and tested for their Luc activities using an IVIS Spectrum (Perkin Elmer, Waltham, USA) as described previously [30].

Stable overexpression of miR-17/106a in DU145-Luc cells

DU145-Luc cells were stably transduced with commercially available miRIDIAN shMIMIC lentiviral microRNA particles expressing miR-17/106a (hsa-miR-106a miRIDIAN shMIMIC), termed as miR-17/106a MIMIC and Empty shMIMIC lentiviral particles, termed as EV MIMIC (Thermo Fisher Scientific, Waltham, USA). MiR-17 and miR-106a share the same seed sequence except for a cytosine residue in miR-17replaced by an adenine in miR-106a at the 5′ end. The plasmid is based on the pSMART vector with a puromycin selection and GFP cassette. Cells were transduced using OptiMEM medium (Life Technologies, NY, USA) which contained 6 μg/ml polybrene (Sigma-Aldrich, Indianapolis, USA) with lentiviral particles at multiplicity of infection (MOI) = 8. On day 4 post-transduction, puromycin (Sigma-Aldrich, Indianapolis, USA) selection was initiated and GFP-positive clones were selected using cloning cylinders. Cells were plated in 24-well plates for expansion and propagated at a final concentration of 200 μg/ml puromycin.

Quantitative real-time RT-PCR

RNA was isolated from DU145 and 22Rv1 cells using miRNeasy Mini Kit (Qiagen) as previously described [15]. Real-time PCR was performed using custom primers specific for hsa-miR-17-5p, hsa-miR-20a, hsa-miR106a-5p, hsa-miR-106b and miRCURY LNA™ Universal RT microRNA PCR kit (Exiqon, Vedbaek, Denmark). SNORD44 was used an internal reference. Specific PrimeTime™ human PTEN primers were used: forward 5′-GAACTTGTCTTCCCGTCGT-3′ and reverse 5′-AATGTTCAGTGGCGGAACT-3′ (Integrated DNA Technologies, Coralville, USA). For estimation of tumor-derived circulating miRNAs in murine serum, miRNA isolation was performed with 50 μl of sera. Each sample was spiked with 5 nM of Cel-miR-39 (Integrated DNA Technologies, Coralville, USA) from *Caenorhabditis elegans* as an internal reference control (Exiqon, Vedbaek, Denmark). Fold changes in miRNA/mRNA expression was estimated by the $2^{-\Delta\Delta Ct}$ method [55].

Western blot

Whole-cell lysis was performed as previously described [15, 27]. The membranes were probed with anti-PTEN (1:1000, Cell Signaling, Danvers, USA) and anti-β-actin antibodies (1:2500, Santa Cruz Biotechnologies, Dallas, USA). Signals were visualized using the SuperSignal West Dura chemiluminescence kit

(Thermo Fisher Scientific, Waltham, USA) and imaged on a Chemidoc gel imager (Bio-Rad, Hercules, USA). Images were quantified using the Image J software (NIH).

Cell viability assay

Proliferation of cells treated with resveratrol and pterostilbene was determined by MTT (Sigma-Aldrich, Indianapolis, USA) assay as described [56]. Absorbance of the formazan was measured using Synergy-4 plate reader after 72 h of treatment. IC_{50} values were calculated by the linear interpolation method using MS Excel.

Prostate cancer xenografts

Fox $n1^{nu/nu}$ male mice were purchased from Harlan Laboratory at seven weeks of age. Housing and care of all animals were in accordance with the guidelines established by the University's Institutional Animal Care and Use Committee. Upon arrival, all animals were given a phytoestrogen-free AIN-76A diet (Research Diets, New Brunswick, USA) *ad libitum*. Mice were randomly divided into two groups of 16 mice each for both cells lines. 2 x 10^6 DU145-Luc EV MIMIC or miR-17/106a MIMIC cells in combination with 50% matrigel (BD Biosciences, San Jose, USA, total volume 200 µl) were inoculated subcutaneously (s.c.) on the dorsal right flank of mice. On day 4, bioluminescence was measured in all animals and based on the total flux signal intensities, mice in each group were randomized into two subgroups each ($n = 8$): vehicle (10% DMSO) and treated with pterostilbene (50 mg/kg bw). Intraperitoneal injections (i.p.) were performed daily, 5 days a week, for 39 days. Bioluminescent and caliper measurements were taken weekly as previously described [29–31]. Calculation of tumor volume by digital Vernier caliper measurements were done by using formula as before [29, 31]. The mice were sacrificed at day 39 and tumors were excised. Total RNA and protein were isolated and the remaining tissue was placed in 10% formalin for histological and immunohistochemical (IHC) analysis. Blood was also collected at sacrifice, and serum samples were stored at -80°C until further analysis.

Immunohistochemistry

Four µm thick formalin-fixed paraffin embedded tumor sections were stained as per the protocol described previously [30] to evaluate PTEN (1:250, Cell Signaling, Danvers, USA), Ki-67 (1:100, Abcam, Cambridge, USA), cleaved-Caspase 3 (1:500, Cell Signaling, Danvers, USA) and M30 (1:100, Roche, Indianapolis, USA). The VECTASTAIN ABC Elite kit and the ImmPACT DAB kit (Vector Laboratories, Burlingame, USA) were used to visualize staining. Images were recorded on a Nikon Eclipse 80i microscope. Ki-67 and cleaved-Caspase-3 stained nuclei were quantitated using ImageTool software.

GEO database analysis

The data related to GSE21036 were acquired from Gene Expression Omnibus (GEO) website. We used the Bioconductor and GEO query package to access the expression data, platform and clinical data of the study. The expression data were log2-transformed and processed by the between-array variance stabilization normalization. The expression levels of given microRNA were summarized by boxplot in the tumor and normal sample subgroups separately.

Statistical analysis

The differences between groups were analyzed by the two-sample two-tailed Student's *t* test. For animal studies, one-way ANOVA was used to assess the difference in mean among given groups. Levene's test was performed to test equal-variance assumption. The Welch's one-way ANOVA method was used when unequal variances were present. The pairwise comparison was conducted when significant differences in mean were verified. Bonferroni adjusted *p* values were reported in pairwise comparisons. Statistical significance was set as $p \leq 0.05$. All data are cumulative of at least three independent experiments.

ACKNOWLEDGMENTS

We are extremely grateful to Dr. Zhi He (Histology Core, UMMC) for preparing tissue sections, to Dr. Kun Li for establishing DU145-Luc cell line and to Dr. Liangfen Zhang (Department of Pathology, UMMC) for her excellent technical assistance with animal experiments. We also thank Drs. Richard L. Summers and Janice M. Lage (UMMC) for their continued support.

CONFLICTS OF INTEREST

The authors declare no conflicts of interest

FINANCIAL SUPPORT

This study was supported in part by the Department of Defense Prostate Cancer Research Program under Award W81XWH-13-1-0370 to AS Levenson. Views and opinions of, and endorsements by the author(s) do not reflect those of the US Army of the Department of Defense.

Editorial note

This paper has been accepted based in part on peer-review conducted by another journal and the authors' response and revisions as well as expedited peer-review in Oncotarget.

REFERENCES

1. Lu J, Getz G, Miska EA, Alvarez-Saavedra E, Lamb J, Peck D, Sweet-Cordero A, Ebert BL, Mak RH, Ferrando AA, Downing JR, Jacks T, Horvitz HR, Golub TR. MicroRNA expression profiles classify human cancers. Nature. 2005; 435:834–838.
2. Volinia S, Calin GA, Liu CG, Ambs S, Cimmino A, Petrocca F, Visone R, Iorio M, Roldo C, Ferracin M, Prueitt RL, Yanaihara N, Lanza G, et al. A microRNA expression signature of human solid tumors defines cancer gene targets. Proc Natl Acad Sci U S A. 2006; 103:2257–2261.
3. Zhang B, Pan X, Cobb GP, Anderson TA. microRNAs as oncogenes and tumor suppressors. Dev Biol. 2007; 302:1–12.
4. Ambros V. microRNAs: tiny regulators with great potential. Cell. 2001; 107:823–826.
5. He L, Hannon GJ. MicroRNAs: small RNAs with a big role in gene regulation. Nat Rev Genet. 2004; 5:522–531.
6. Filipowicz W, Bhattacharyya SN, Sonenberg N. Mechanisms of post-transcriptional regulation by microRNAs: are the answers in sight?. Nat Rev Genet. 2008; 9:102–114.
7. Sapre N, Selth LA. Circulating MicroRNAs as Biomarkers of Prostate Cancer: The State of Play. Prostate Cancer. 2013; 2013:539680.
8. Brase JC, Johannes M, Schlomm T, Falth M, Haese A, Steuber T, Beissbarth T, Kuner R, Sultmann H. Circulating miRNAs are correlated with tumor progression in prostate cancer. Int J Cancer. 2011; 128:608–616.
9. Selth LA, Townley S, Gillis JL, Ochnik AM, Murti K, Macfarlane RJ, Chi KN, Marshall VR, Tilley WD, Butler LM. Discovery of circulating microRNAs associated with human prostate cancer using a mouse model of disease. Int J Cancer. 2012; 131:652–661.
10. Ambs S, Prueitt RL, Yi M, Hudson RS, Howe TM, Petrocca F, Wallace TA, Liu CG, Volinia S, Calin GA, Yfantis HG, Stephens RM, Croce CM. Genomic profiling of microRNA and messenger RNA reveals deregulated microRNA expression in prostate cancer. Cancer Res. 2008; 68:6162–6170.
11. Leite KR, Sousa-Canavez JM, Reis ST, Tomiyama AH, Camara-Lopes LH, Sanudo A, Antunes AA, Srougi M. Change in expression of miR-let7c, miR-100, and miR-218 from high grade localized prostate cancer to metastasis. Urol Oncol. 2011; 29:265–269.
12. Spahn M, Kneitz S, Scholz CJ, Stenger N, Rudiger T, Strobel P, Riedmiller H, Kneitz B. Expression of microRNA-221 is progressively reduced in aggressive prostate cancer and metastasis and predicts clinical recurrence. Int J Cancer. 2010; 127:394–403.
13. Poliseno L, Salmena L, Riccardi L, Fornari A, Song MS, Hobbs RM, Sportoletti P, Varmeh S, Egia A, Fedele G, Rameh L, Loda M, Pandolfi PP. Identification of the miR-106b~25 microRNA cluster as a proto-oncogenic PTEN-targeting intron that cooperates with its host gene MCM7 in transformation. Sci Signal. 2010; 3:ra29.
14. Hudson RS, Yi M, Esposito D, Glynn SA, Starks AM, Yang Y, Schetter AJ, Watkins SK, Hurwitz AA, Dorsey TH, Stephens RM, Croce CM, Ambs S. MicroRNA-106b-25 cluster expression is associated with early disease recurrence and targets caspase-7 and focal adhesion in human prostate cancer. Oncogene. 2013; 32:4139–4147.
15. Dhar S, Hicks C, Levenson AS. Resveratrol and prostate cancer: promising role for microRNAs. Mol Nutr Food Res. 2011; 55:1219–1229.
16. Li J, Yen C, Liaw D, Podsypanina K, Bose S, Wang SI, Puc J, Miliaresis C, Rodgers L, McCombie R, Bigner SH, Giovanella BC, Ittmann M, T. PTEN, a putative protein tyrosine phosphatase gene mutated in human brain, breast, and prostate cancer. Science. 1997; 275:1943–1947.
17. Trotman LC, Niki M, Dotan ZA, Koutcher JA, Di Cristofano A, Xiao A, Khoo AS, Roy-Burman P, Greenberg NM, Van Dyke T, Cordon-Cardo C, Pandolfi PP. Pten dose dictates cancer progression in the prostate. PLoS Biol. 2003; 1:E59.
18. Li Y, Kong D, Wang Z, Sarkar FH. Regulation of microRNAs by natural agents: an emerging field in chemoprevention and chemotherapy research. Pharm Res. 2010; 27:1027–1041.
19. Saini S, Majid S, Dahiya R. Diet, microRNAs and prostate cancer. Pharm Res. 2010; 27:1014–1026.
20. Harikumar KB, Aggarwal BB. Resveratrol: a multitargeted agent for age-associated chronic diseases. Cell Cycle. 2008; 7:1020–1035.
21. Pirola L, Frojdo S. Resveratrol: one molecule, many targets. IUBMB Life. 2008; 60:323–332.
22. Kondratyuk TP, Park EJ, Marler LE, Ahn S, Yuan Y, Choi Y, Yu R, van Breemen RB, Sun B, Hoshino J, Cushman M, Jermihov KC, Mesecar AD. Resveratrol derivatives as promising chemopreventive agents with improved potency and selectivity. Mol Nutr Food Res. 2011; 55:1249–1265.
23. Benitez DA, Pozo-Guisado E, Alvarez-Barrientos A, Fernandez-Salguero PM, Castellon EA. Mechanisms involved in resveratrol-induced apoptosis and cell cycle arrest in prostate cancer-derived cell lines. J Androl. 2007; 28:282–293.
24. Brakenhielm E, Cao R, Cao Y. Suppression of angiogenesis, tumor growth, and wound healing by resveratrol, a natural compound in red wine and grapes. FASEB J. 2001; 15:1798–1800.
25. Kozuki Y, Miura Y, Yagasaki K. Resveratrol suppresses hepatoma cell invasion independently of its anti-proliferative action. Cancer Lett. 2001; 167:151–156.
26. Kimura Y, Okuda H. Resveratrol isolated from Polygonum cuspidatum root prevents tumor growth and metastasis to

lung and tumor-induced neovascularization in Lewis lung carcinoma-bearing mice. J Nutr. 2001; 131:1844–1849.

27. Dhar S, Kumar A, Li K, Tzivion G, Levenson AS. Resveratrol regulates PTEN/Akt pathway through inhibition of MTA1/HDAC unit of the NuRD complex in prostate cancer. Biochim Biophys Acta. 2015; 1853:265–275.
28. Kai L, Samuel SK, Levenson AS. Resveratrol enhances p53 acetylation and apoptosis in prostate cancer by inhibiting MTA1/NuRD complex. Int J Cancer. 2010; 126:1538–1548.
29. Kai L, Wang J, Ivanovic M, Chung YT, Laskin WB, Schulze-Hoepfner F, Mirochnik Y, Satcher RL Jr, Levenson AS. Targeting prostate cancer angiogenesis through metastasis-associated protein 1 (MTA1). Prostate. 2011; 71:268–280.
30. Li K, Dias SJ, Rimando AM, Dhar S, Mizuno CS, Penman AD, Lewin JR, Levenson AS. Pterostilbene acts through metastasis-associated protein 1 to inhibit tumor growth, progression and metastasis in prostate cancer. PLoS One. 2013; 8:e57542.
31. Dias SJ, Li K, Rimando AM, Dhar S, Mizuno CS, Penman AD, Levenson AS. Trimethoxy-resveratrol and piceatannol administered orally suppress and inhibit tumor formation and growth in prostate cancer xenografts. Prostate. 2013; 73:1135–1146.
32. Wang Y, Romigh T, He X, Orloff MS, Silverman RH, Heston WD, Eng C. Resveratrol regulates the PTEN/AKT pathway through androgen receptor-dependent and -independent mechanisms in prostate cancer cell lines. Hum Mol Genet. 2010; 19:4319–4329.
33. Mendell JT. miRiad roles for the miR-17-92 cluster in development and disease. Cell. 2008; 133:217–222.
34. John B, Enright AJ, Aravin A, Tuschl T, Sander C, Marks DS. Human MicroRNA targets. PLoS Biol. 2004; 2:e363.
35. Krek A, Grun D, Poy MN, Wolf R, Rosenberg L, Epstein EJ, MacMenamin P, da Piedade I, Gunsalus KC, Stoffel M, Rajewsky N. Combinatorial microRNA target predictions. Nat Genet. 2005; 37:495–500.
36. Paraskevopoulou MD, Georgakilas G, Kostoulas N, Vlachos IS, Vergoulis T, Reczko M, Filippidis C, Dalamagas T, Hatzigeorgiou AG. DIANA-microT web server v5.0: service integration into miRNA functional analysis workflows. Nucleic Acids Res. 2013; 41:W169–173.
37. Taylor BS, Schultz N, Hieronymus H, Gopalan A, Xiao Y, Carver BS, et al. Integrative genomic profiling of human prostate cancer. Cancer Cell. 2010; 18:11–22.
38. Yeo SC, Ho PC, Lin HS. Pharmacokinetics of pterostilbene in Sprague-Dawley rats: the impacts of aqueous solubility, fasting, dose escalation, and dosing route on bioavailability. Mol Nutr Food Res. 2013; 57:1015–1025.
39. Kapetanovic IM, Muzzio M, Huang Z, Thompson TN, McCormick DL. Pharmacokinetics, oral bioavailability, and metabolic profile of resveratrol and its dimethylether analog, pterostilbene, in rats. Cancer Chemother Pharmacol. 2011; 68:593–601.
40. Dellinger RW, Garcia AM, Meyskens FL Jr. Differences in the glucuronidation of resveratrol and pterostilbene: altered enzyme specificity and potential gender differences. Drug Metab Pharmacokinet. 2014; 29:112–119.
41. Azzolini M, La Spina M, Mattarei A, Paradisi C, Zoratti M, Biasutto L. Pharmacokinetics and tissue distribution of pterostilbene in the rat. Mol Nutr Food Res. 2014; 58:2122–2132.
42. McCormack D, McFadden D. Pterostilbene and cancer: current review. J Surg Res. 2012; 173:e53–61.
43. Rehemtulla A, Stegman LD, Cardozo SJ, Gupta S, Hall DE, Contag CH, Ross BD. Rapid and quantitative assessment of cancer treatment response using *in vivo* bioluminescence imaging. Neoplasia. 2000; 2:491–495.
44. Kim JB, Urban K, Cochran E, Lee S, Ang A, Rice B, Bata A, Campbell K, Coffee R, Gorodinsky A, Lu Z, Zhou H, Kishimoto TK, Lassota P. Non-invasive detection of a small number of bioluminescent cancer cells *in vivo*. PLoS One. 2010; 5:e9364.
45. Zhang C, Yan Z, Arango ME, Painter CL, Anderes K. Advancing bioluminescence imaging technology for the evaluation of anticancer agents in the MDA-MB-435-HAL-Luc mammary fat pad and subrenal capsule tumor models. Clin Cancer Res. 2009; 15:238–246.
46. Gallou-Kabani C, Vige A, Gross MS, Junien C. Nutri-epigenomics: lifelong remodelling of our epigenomes by nutritional and metabolic factors and beyond. Clin Chem Lab Med. 2007; 45:321–327.
47. Milenkovic D, Jude B, Morand C. miRNA as molecular target of polyphenols underlying their biological effects. Free Radic Biol Med. 2013; 64:40–51.
48. Olive V, Jiang I, He L. mir-17-92, a cluster of miRNAs in the midst of the cancer network. Int J Biochem Cell Biol. 2010; 42:1348–1354.
49. Hagiwara K, Kosaka N, Yoshioka Y, Takahashi RU, Takeshita F, Ochiya T. Stilbene derivatives promote Ago2-dependent tumour-suppressive microRNA activity. Sci Rep. 2012; 2:314.
50. Baselga-Escudero L, Blade C, Ribas-Latre A, Casanova E, Suarez M, Torres JL, Salvado MJ, Arola L, Arola-Arnal A. Resveratrol and EGCG bind directly and distinctively to miR-33a and miR-122 and modulate divergently their levels in hepatic cells. Nucleic Acids Res. 2014; 42:882–892.
51. Chiosea S, Jelezcova E, Chandran U, Acquafondata M, McHale T, Sobol RW, Dhir R. Up-regulation of dicer, a component of the MicroRNA machinery, in prostate adenocarcinoma. Am J Pathol. 2006; 169:1812–1820.
52. Cichocki M, Paluszczak J, Szaefer H, Piechowiak A, Rimando AM, Baer-Dubowska W. Pterostilbene is equally potent as resveratrol in inhibiting

12-O-tetradecanoylphorbol-13-acetate activated NFkappaB, AP-1, COX-2, and iNOS in mouse epidermis. Mol Nutr Food Res. 2008; 52:S62–70.

53. Yaman Agaoglu F, Kovancilar M, Dizdar Y, Darendeliler E, Holdenrieder S, Dalay N, Gezer U. Investigation of miR-21, miR-141, and miR-221 in blood circulation of patients with prostate cancer. Tumour Biol. 2011; 32:583–588.

54. Paul S, DeCastro AJ, Lee HJ, Smolarek AK, So JY, Simi B, Wang CX, Zhou R, Rimando AM, Suh N. Dietary intake of pterostilbene, a constituent of blueberries, inhibits the beta-catenin/p65 downstream signaling pathway and colon carcinogenesis in rats. Carcinogenesis. 2010; 31:1272–1278.

55. Livak KJ, Schmittgen TD. Analysis of relative gene expression data using real-time quantitative PCR and the 2(-Delta Delta C(T)) Method. Methods. 2001; 25:402–408.

56. Kumar A, Lin SY, Dhar S, Rimando AM, Levenson AS. Stilbenes Inhibit Androgen Receptor Expression in 22Rv1 Castrate-resistant Prostate Cancer Cells. Journal of Medicinally Active Plants. 2014; 3:1–8.

SUPPLEMENTARY FIGURES

"Resveratrol and pterostilbene epigenetically restore PTEN expression by targeting oncomiRs of the miR-17 family in prostate cancer"

3'UTR of human *PTEN* mRNA

...ATTTTTTTTTATCAAGAGGGATAAAACACCA
TGAAAATAAACTTGAATAAACTGAAAATGGAC
CTTTTTTTTTTTAATGGCAATAGGACATTGTG
TCAGATTACCAGTTATAGGAACAATTCTCTTT
TCCTGACCAATCTTGTTTTACCCTATACATCC
ACAGGGTTTTGACACTTGTTGTCCAGTTGAAA
AAAGGTTGTGTAGCTGTGTCATGTATATACCT
TTTTGTGTCAAAAGGACATTTAAAATTCAATT
AGGATTAATAAAGATGGCACTTTCCCGTTTTA
TTCCAGTTTTATAAAAAGTGGAGACAGACTGA
TGTGTATACGTAGGAATTTTTTCCTTTTGTGT
TCTGTCACCAACTGAAGTGGCTAAAGAGCTTT
GTGATATACTGGTTCACATCCTACCCCTTTGC
ACTTGTGGCAACAGATAAGTTTGCAGTTGGCT
AAGAGAGGTTTCCGAAGGGTTTTGCTACATTC
TAATGCATGTATTCGGGTTAGGGGAATGGAGG
GAATGCTCAGAAAGGAAATAATTTTATGCTGG
ACTCTGGACCATATACC...

Supplementary Figure S1: Sequence of human PTEN 3' UTR (535 bp) cloned in pMIRGLO vector. The seed match (GCACTTT, position 272) for miR-17, -20a and -106b is underlined.

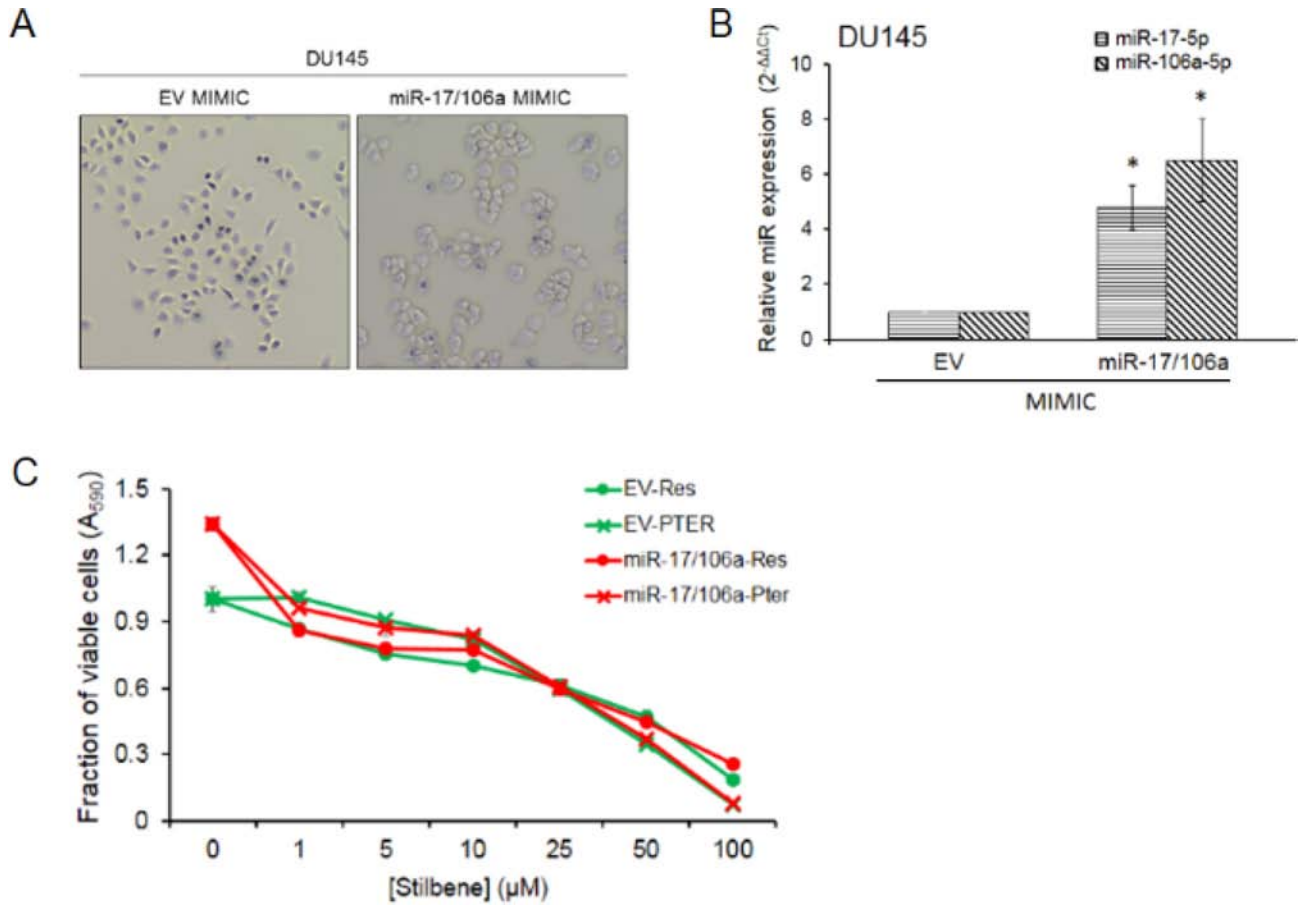

Supplementary Figure S2: Characterization of miR-17/106a overexpressing DU145-luciferase cells. A. Stable transduction of miR-17/106a MIMIC in DU145-luciferase cells showed altered morphology compared to EV MIMIC cells. The cells transduced with miR-17/106a appeared relatively rounded and enlarged compared to cells transduced with EV MIMIC, which assumed regular triangle-shaped appearance of DU145 cells (Magnification x40). **B.** Relative expression of miRs-17-5p and 106a-5p in stably transfected cells. **C.** Comparison of Res and Pter treatment on DU145 EV and DU145- miR-17/106a MIMIC cell viability *in vitro*. Data represent the mean ± SEM from three independent experiments. IC50 was calculated for Res (28.2 vs 33.7) and Pter (11.1 vs 11.3) in EV and miR-17/106a cells, respectively.

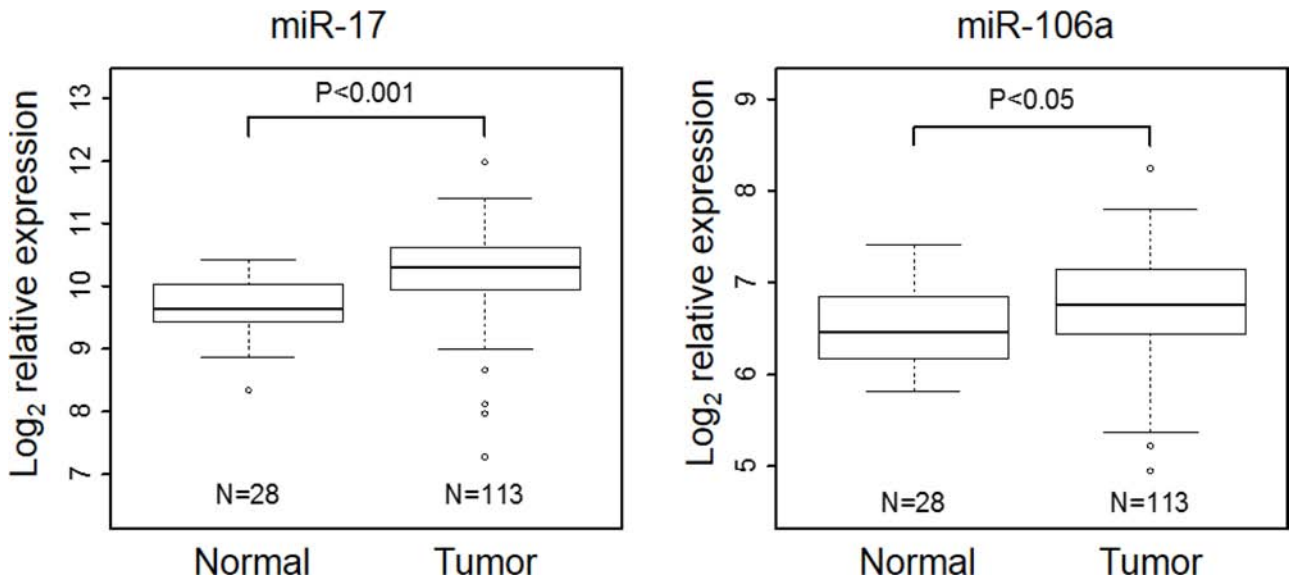

Supplementary Figure S3: Significant overexpression of miR-17 and miR-106a in human prostate cancer samples. The expression data acquired from Gene Expression Omnibus (GEO) related to GSE21036 was log2-transformed and represented. Comparison between normal and tumor samples was evaluated by the two-sample *t* test.

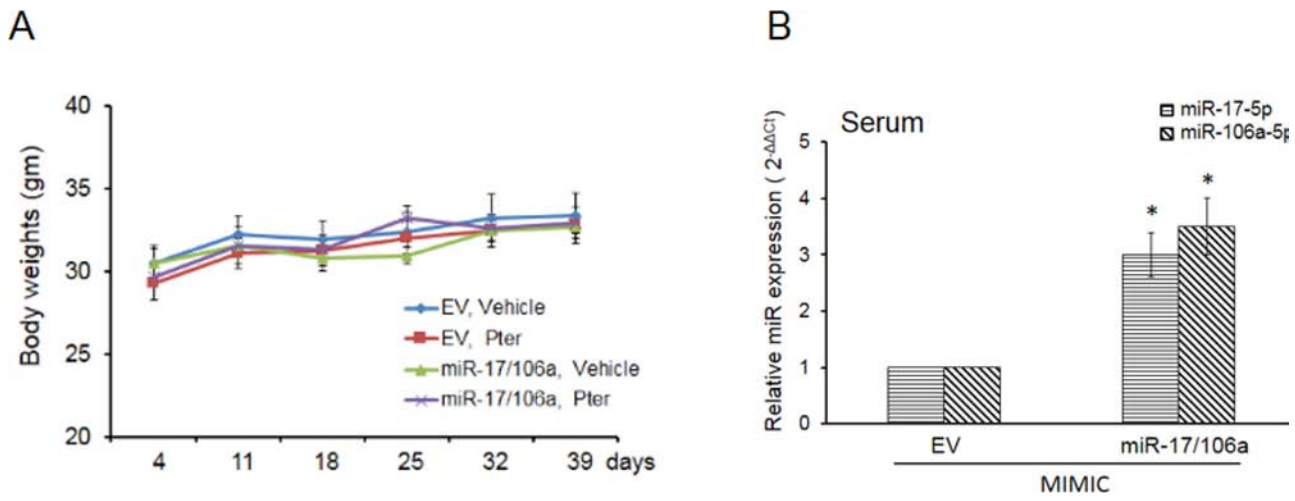

Supplementary Figure S4: A. Body weight analysis of nude mice with EV MIMIC and miR-17/106a MIMIC tumors in vehicle and pterostilbene treated groups (*n* = 8 mice per group). Mice were weighed once per week for 6 weeks. There were no significant differences in the body weights of mice among all groups ($p = 0.61$). **B.** Relative expression of miR-17-5p and miR106a-5p in serum samples from EV and miR-overexpressing xenografts. Data represents the mean ± SEM from two independent experiments ($n = 3$ mice per group), $*p < 0.05$.

2014 RESVERATROL

3rd International conference of resveratrol and health

November 30th to December 3rd, 2014
Hilton Waikoloa Village • Waikoloa, Hawai'i Island

resveratrol2014.hawaii-conference.com

UNIVERSITAS ROSKILDENSIS · IN TRANQUILLO MORS · IN FLUCTU VITA ·

THE DANIEL K. INOUYE COLLEGE OF PHARMACY · UNIVERSITY OF HAWAI'I AT HILO

UNIVERSITY of HAWAI'I · HILO CONFERENCE CENTER

LO-09 Chemopreventive and therapeutic effects of pterostilbene on prostate cancer: epigenetic mechanisms of action

Anait S. Levenson[1,2], Swati Dhar[1], Avinash Kumar[1], Liangfen Zhang[2], Agnes M. Rimando[3], Janice M Lage[2], Jack R. Lewin [2], Xu Zhang[4]

1. Cancer Institute, University of Mississippi Medical Center, Jackson, MS, USA. 2. Department of Pathology, University of Mississippi Medical Center, Jackson, MS, USA. 3. United States Department of Agriculture, Natural Product Utilization Research Unit, University, MS, USA. 4. Center of Statistics and Bioinformatics, University of Mississippi Medical Center, MS, USA

alevenson@umc.edu

A potential strategy for cancer therapy is to discover/develop epigenetic agents that can restore normal dynamics between active and repressive chromatin. Studies in our laboratory have shown that dietary stilbenes such as resveratrol and its potent analogues inhibit epigenetic modifier metastasis-associated protein 1 (MTA1) expression in prostate cancer cell lines and xenografts. Pterostilbene, a natural analogue of resveratrol that is accumulated in blueberries, showed highest MTA1 inhibitory activity in prostate cancer cell lines compared to parent resveratrol and other analogues. Moreover, pterostilbene treatment of orthotopic xenografts demonstrated inhibition of MTA1-mediated p53 deacetylation, higher apoptotic index and less angiogenesis compared to control mice. In the present study, we investigated the efficacy of pterostilbene in the treatment of prostate cancer in prostate-specific Pten-null immunocompetent mice. In this cancer-prone preclinical model, PIN develops at 6 weeks, invasive adenocarcinoma at 10-15 weeks, and possible metastasis at later stages, closely mimicking prostate cancer progression in men. Since MTA1 is a master chromatin remodeler that is overexpressed in human prostate cancer, we addressed two major questions: 1) does MTA1 cooperate with Pten loss in prostate cancer progression?, and if so 2) can pterostilbene arrest prostate cancer progression by inhibiting MTA1 and its regulatory functions such as cell survival and angiogenesis? We report here that pterostilbene reduces progression of prostate cancer in this transgenic mouse model through inhibition of epigenetic modifier MTA1 and its associated inflammation and tumorigenesis as well as Akt, VEGF, and AR survival pathways. Therefore, our present findings of therapeutic efficacy of dietary pterostilbene in preclinical setting may possibly make pterostilbene the first MTA1-inhibitor moved into a clinical trial.

31st SOUTHERN BIOMEDICAL ENGINEERING CONFERENCE

31st SBEC Annual Meeting Program

April 30th-May 2nd, 2015

Crowne Plaza New Orleans Airport, Kenner, LA

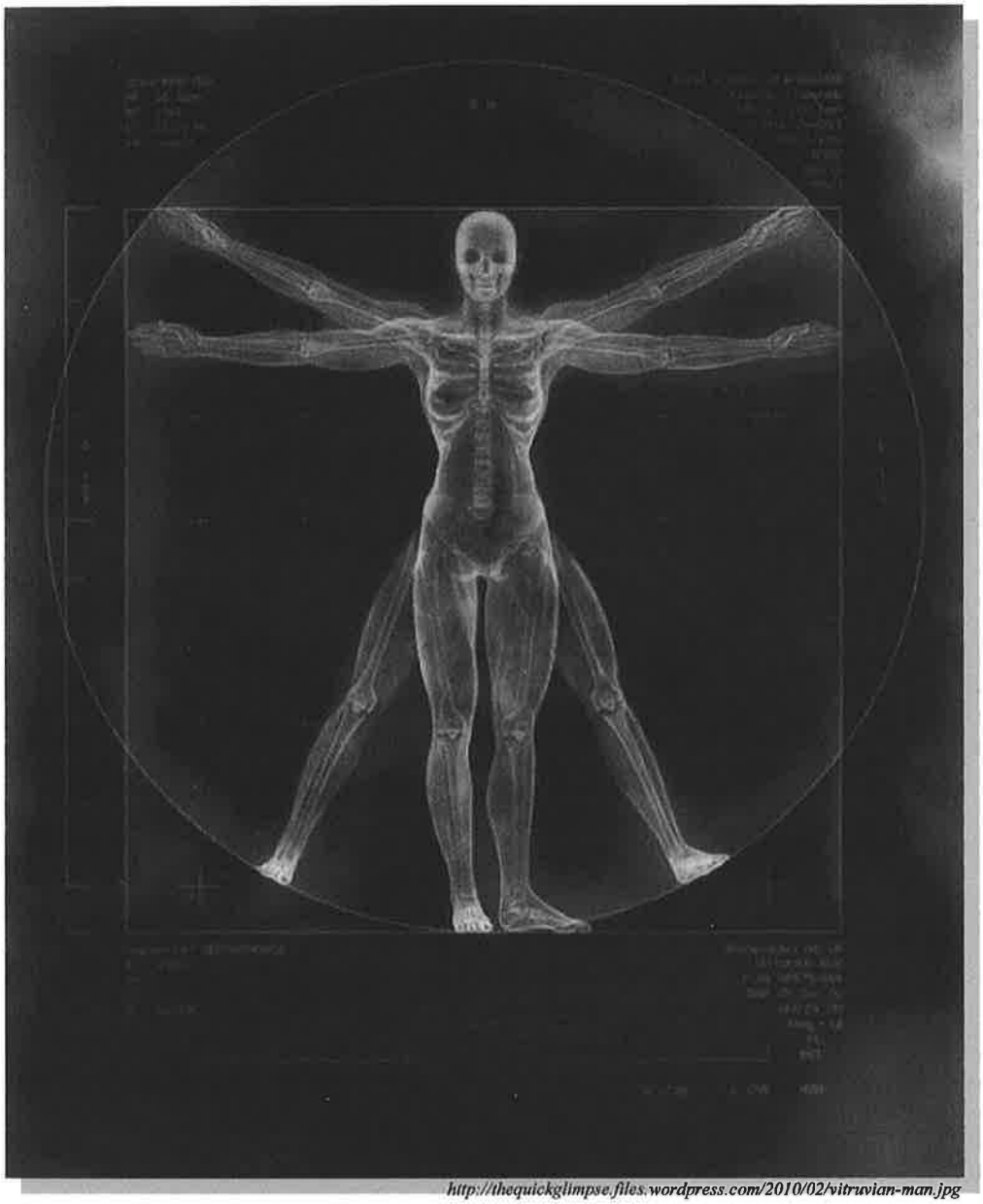

http://thequickglimpse.files.wordpress.com/2010/02/vitruvian-man.jpg

Endorsed by the Society for Biomaterials

Sponsored by Mississippi Academy of Sciences

pulse exchanged with a chirped pulse which allows for the SPEN encoding while in the present of a gradient. SPEN-DWI was obtained at six b-values along the principal axes. Post-processing of the SPEN-DWI datasets was carried out using MATLAB for echo alignment and the application of a super-resolution algorithm. ADC maps were calculated in MATLAB incorporating all background gradient corrections for the SPEN-DWI sequence. ADC data was acquired by 1 and 4 segmented DW-EPI for comparison. Our results show that the quality of the SPEN-DWI and resulting ADC maps make this form of single-shot acquisition a clear choice for comprehensive, high-throughput *in vivo* stroke studies at ultra-high fields and/or heterogeneous signal regions.

Scoliosis Analog Model for the Evaluation of Bracing Technology

Cloe Chung, and Denis DiAngelo,
The University of Tennesse Health Science Center, Memphis, TN

Introduction: Thoracolumbar braces are commonly used to treat Adolescent Idiopathic Scoliosis (AIS). Braces serve to reduce and prevent progression of the spinal curve by applying multidirectional corrective forces. These forces may cause translational (inward, upward) and derotational (twist) responses of the spine. The objective was to develop an assembly capable of quantifying brace structural stiffness properties by measuring the corrective forces components.

Methods: A novel mechanical equivalent analog model of the AIS condition was designed and developed to simulate a 40° spinal deformity. A linkage-based model was used in conjunction with a biorobotic testing platform to quantify scoliosis brace structural stiffness properties. Measurements of the force components applied to the model and displacement of the linkage assembly were used to calculate the brace stiffness. The brace was tested in both a constrained (via Velcro straps) configuration and an unconstrained configuration.

Results: Calculated stiffness was expressed as a resistive force relative to the angular change of the linkage system from 30° to 70°. For the unconstrained and constrained configurations, vertical forces ranged between 10 and 100N and stiffness values were 4.5 N/deg in the Z direction and 0.3 N/deg in the X direction, and 40 and 400N and 51.3 N/deg and 0.1 N/deg respectively.

Discussion: Structural properties provide a means to compare bracing technology and better understand design features. For example, addition of Velcro straps increased stiffness of the native brace 10 fold. This test assembly could be used as a design tool and to develop a standard for classifying braces.

Multiple Path Particle Dosimetry Simulation of Respiratory Deposition of Nanoaerosol in the Mouse Lung

Mohammed Ali[1], Bradford Gutting[2], Victor Morozov[3], and Monique van Hoek[4]
[1]Dept of Industrial Systems and Technology, Jackson State university, Jackson, MS, Naval Surface Warfare Center, Dahlgren VA, [3]Institute of Theoretical and Experimental Biophysics of the Russian Academy of Sciences, Pushchino, Moscow, [4]George Mason University, Manassas, VA

This study computationally predicted how inhaled particles, including nanoaerosol particles get transported, disseminated and deposited inside the mouse lung. Here, Multiple Path Particle Dosimetry (MPPD) program model was used to run simulations of experimental conditions and the deposition results were compared with reported literature. Antibiotic inhalation therapy is currently a topic of interest. Its application to treat lung infections in humans has been shown to be promising in cystic fibrosis. Nanoaerosol (particle approx. 100 nm) delivery of antibiotics has recently been proposed to promote survival of mice. However, the respiratory deposition of an antibiotic nanoaerosol in various regions of the lung is unknown. In this work the physical and mechanical properties of the antibiotic nanoaerosol were used to conduct simulation in MPPD specific to BALB/c mice lung morphology. Substantial widespread comparisons were infeasible since there are only a handful reported studies of inhalation of nanoparticles (NPs) for mice. A satisfactory agreement was found between the simulation results with the experimental data on titanium dioxide (TiO_2) nanoaerosol delivery to the mice. Tracheobronchial (TB) deposition result of this study has also shown good agreement when comparing with reported numerical deposition determined by typical path mathematical model. However, Head, TB and Pulmonary (P) deposition results have differed with those reported previously by another experimental study of radiolabelled aluminosilicate submicron particles.

Choice of Statistical Techniques: Parametric Versus Non Parametric Methods

Elgenaid Hamadain
University of Mississippi Medical Center

The choice of statistical technique for any data has a profound influence on inference, interpretation, and therefore, the conclusion derived from it. Understanding this choice is important for critical evaluation of biomedical literature. A potential source of confusion in analyzing any data is whether to use parametric or non-parametric statistics. The importance of this issue cannot be underestimated. Knowledge of several statistical concepts are needed to understand the difference between parametric and nonparametric methods. If measurement scale is nominal or ordinal then one should use non-parametric statistics. If interval or ratio scales are used, then use parametric statistics. Other consideration is distribution of the data. If data are approximately normal, parametric methods should be used. Nonparametric tests are sometimes called distribution-free tests because they are based on fewer assumptions. Non-paramteric procedures are less powerful because they use less information in their calculation. If a distribution deviates markedly from normality, then you take the risk that the statistic will be inaccurate. The safest thing to do is to use an equivalent non-parametric statistic. If you get it wrong, you risk using an incorrect method or you may use a less statistically powerful procedure. If sample sizes are large, parametric tests are robust to departures from normality. However, because of cost and potential risks to humans and animals, many of the sample sizes in the biomedical literature are far from being large. It can sometimes be difficult to assess whether a continuous outcome follows a normal distribution and, thus, whether a parametric or nonparametric test is appropriate. Several statistical tests exist to assess normality including Kolmogorov-Smirnov test, the Anderson-Darling test, and the Shapiro-Wilk test. Each test is essentially a goodness of fit test. This presentation discusses all aspects of statistical test choice comparing parametric tests with equivalent nonparametric counterpart for t-test, Paired t-test, one-way ANOVA, and regression and correlation techniques with real examples using several statistical software primary, SPSS.

Session IX (Cancer)

Dietary Stilbenes and Epigenetic Regulation for Prostate Cancer Chemoprevention and Treatment

Levenson AS[1,2]*, Swati Dhar[1], Avinash Kumar[1], Agnes M. Rimando[3], Janice M. Lage[2], Jack R. Lewin[2] and Xu Zhang[4]
[1]Cancer Institute and [2]Department of Pathology, [4] Center of Biostatistics and Bioinformatics, University of Mississippi Medical Center, Jackson, MS [3]United States Department of Agriculture, Agricultural Research Service, Natural Products Utilization Research Unit, University, MS

Prostate cancer is the most often diagnosed cancer and the second leading cause of cancer deaths in males in the US. Prostate cancer arises through genetic and epigenetic alterations. Epigenetic mechanisms implicated in prostate cancer include gene silencing via

action of co-repressor complexes (i.e. deacetylation) and changes in microRNA profiles.

Epidemiological studies suggest association between diet and lower risk of prostate cancer. Dietary stilbenes (resveratrol and its potent analogs) are phenolic compounds with anti-inflammatory, anti-oxidant and anti-cancer activity. Importantly, these compounds can modulate epigenetics and influence cancer susceptibility and progression. In this presentation, I will provide compelling evidence on epigenetic mechanisms of resveratrol and its analogs through regulation of the chromatin modifier metastasis-associated protein 1 (MTA1), MTA1-associated network and certain oncomiRs and highlight the anticancer effects of these compounds in vitro and in preclinical models of prostate cancer. It is our hope that resveratrol's analogs with better bioavailability, thereby conferring superior pharmacological potency and greater anticancer effects through epigenetic mechanisms, may become strong candidates for clinical development.

Identifying Hormone Independent Targets & Drug Designing For Breast and Prostate Cancers

Pradip K. Biswas
Laboratory of Computational Biophysics & Bioengineering, Department of Physics, Tougaloo College, Tougaloo MS

Breast and prostate cancers together affect about three million people every year and kills about 30% of them (16% in USA!!). Estrogen Receptor (ER) alpha and Androgen Receptor (AR), are the two main nuclear hormone proteins that are responsible for the progressions of breast and prostate tumors, respectively, and represent the main targets for hormonal therapies. However, about 70% of breast and prostate tumors develop resistances in hormonal therapies and they sustain growth in hormone-independent manners. In order to develop hormone-independent inhibitors, we elucidate protein-protein and protein-DNA interfaces of ER and AR and identify and validate alternate targets for drug designing.

Using the crystal structures of ER and AR DNA and Ligand binding domains, molecular modeling, molecular dynamics simulations, and bioinformatics we identified the hydrogen-bonding contacts and the sequence motifs that are responsible for dimerization and/or DNA recognition. The crucial amino acids of a motif are then grafted on stable helices (alanine or leucine) in order to develop peptidic inhibitors.

In ER ligand binding domain, three sequence motifs are identified to recognize the ER dimerization interface and one of them LQXXHQXXAQ (497-506) has been used to develop inhibitor peptides. When subjected to in-vitro testing in MCF-7 cell lines, these inhibitors are found to inhibit ER expression in the presence of hormones in a competing manner as with 4-hydroxy-tamoxifen. In AR, no suitable target exists in the ligand binding domain but we identified a sequence motif LCAXRXD motif (578-584) in AR DNA binding domain. The key amino acids of this motif are grafted on stable helices and in-silico testing are in progress to design a hormone-independent inhibitor for prostate cancer.

Author acknowledges financial support from MS-INBRE funded by NCRR/NIH-5P20RR016476-11 and NIGMS/NIH-8P20GM103476-11.

Theranostic Hybrid Graphene Materials With Label-Free Biosensing And Combined Therapy Capability

Paresh C. Ray, Christine Tchounwou, Stacy Jones, Yongliang Shi, Aruna Vangara, Rajashekhar Kanchanapally, Bhanu Priya Viraka Nellore, Sudarson Sekhar Sinha, Avijit Pramanik, Suhash Reddy Chavva
Department of Chemistry and Biochemistry, Jackson State University, Jackson, MS

Breast cancer is one of the major public health issue for women in this world, which kills more than half million women every year. It is now well recognized that the detection of breast cancer circulating tumor cells (CTCs) is an invaluable tool for monitoring the progression and finding possible therapies to save life. Since CTCs are extremely rare in blood, even for cancer patient, it is till now highly challenging to capture and identify them. Here I will discuss, our recent report on the development of theranostic hybrid grapehen oxide, graphene quantum dots and hybrid single wall carbon nanotube (SWCNT) for targeted capture of SK-BR-3 breast tumor cells from infected blood sample, followed by accurate multimodal diagnosis and effective photothermal killing of breast cancer. Reported data indicate that theranostic graphene nanomaterials can have enormous potential for real life CTC capture and therapy applications, once it is optimized properly in clinical settings.

Novel Antibody Conjugated Hybrid Gold-Graphene Oxide Nanoparticles for the Treatment of Cytomegalovirus Infection

Madeline A. Aylward[1], Karen Stokes[2], Sudarson S. Sinha[3], Paresh C. Ray[3] and Ritesh Tandon[1*]
[1]Department of Microbiology and Immunology, University of Mississippi Medical Center, 2500 North State Street, Jackson, MS 39216, USA. [2] Department of Molecular and Cellular Physiology, Center for Cardiovascular Disease and Sciences, Center for Molecular and Tumor Virology, Louisiana State University Health Sciences Center, 1501 Kings Highway, Shreveport, LA 71130. [3]Department of Chemistry and Biochemistry, Jackson State University, 1400 J.R Lynch Street, Jackson, MS 39217, USA.

Human cytomegalovirus (HCMV) is a herpesvirus that causes major health problems in neonates as well as in immunocompromised individuals (1). At present, a vaccine is not available for HCMV infection and available antiviral drugs suffer from toxicity, poor efficacy and resistance (1, 2). Earlier, we reported the efficacy of bioconjugated gold nanoparticles (GNP) as antiviral against HCMV (3). Here, we report the synthesis and application of antibody conjugated second-generation hybrid gold-graphene oxide nanoparticles for the inhibition of mouse cytomegalovirus (MCMV) infection, so that this approach can be tested in an animal model. Due to the high yield production, low cost, and interesting electronic and optical properties graphene and its derivative graphene oxide hold great promise for real life applications. By attaching the surface of graphene oxide with plasmonic nanoparticles, one can achieve a nanoplatform with huge surface area, higher sensitivity and selectivity, and better theranostic. These hybrid nanoparticles are superior to pure gold nanoparticles in several ways: (i) high yield and low cost of production. (ii) tremendously increased effective surface area, (iii) significantly improved sensitivity, selectivity and photothermal killing abilities, (iv) they can form a sheet structure for coating on detection devices, and because carbon is their major content, (v) the particles are expected to be inert in vivo. For the purpose of this project, we raised M55 (gB) monoclonal mouse antibody and conjugated it with the newly synthesized popcorn shaped gold graphene oxide hybrid nanoparticles to produce M55-GOPop. These nanoparticles block MCMV replication, virus-induced cytopathogenic effects and virus spread in cell culture without inducing cytotoxicity. When injected in BALB/c mice, these nanoparticles are tolerated well, as indicated by the comparable weight and health status of the M55-GOPop injected mice and the saline injected mice. MCMV-infected mice that are mock treated loose significant weight over a period of 14 days post infection; however, M55-GOPop treated mice continue to gain weight over this period indicating promising viral inhibition properties of M55-GOPop in vivo. Thus, we have not only designed a potential antiviral strategy that specifically blocks HCMV infection in cell culture but we have also characterized the effectiveness of this approach in a mouse model.

References:

1. Krause PR, Bialek SR, Boppana SB, Griffiths PD, Laughlin CA, Ljungman P, Mocarski ES, Pass RF, Read JS, Schleiss MR,

Journal of Medicinally Active Plants

Volume 4
Issue 2 Supplement

ACMAP 6th Annual Conference Spokane-WA

Follow this and additional works at: h3p://scholarworks.umass.edu/jmap

Recommended Citation
. . "ACMAP 6th Annual Conference Spokane-WA," Journal of Medicinally Active Plants 4 (Supplement).
Available at: h3p://scholarworks.umass.edu/jmap/vol4/iss2/4

□ is Abstracts is brought to you for free and open access by ScholarWorks@UMass Amherst. It has been accepted for inclusion in Journal of Medicinally Active Plants by an authorized administrator of ScholarWorks@UMass Amherst. For more information, please contact scholarworks@library.umass.edu.

6th Annual Conference

American Council for Medicinally Active Plants

Washington State University, Spokane, WA USA

June 9-12, 2015

proliferation of androgen-dependent human prostate cancer cells through induction of apoptosis and inhibition of inflammation. Results of the current study suggest that the volatile principles of kumquats have great potential for the prevention of cancer. This project is based upon work supported by USDA-NIFA No. 2010-34402-20875, "Designing Foods for Health," through the Vegetable & Fruit Improvement Center and State funding 2013-121277 VFIC-TX State appropriation.

ORAL SESSION ABSTRACTS

Oral 1. Epigenetic potential of dietary stilbenes in prostate cancer

Anait S. Levenson[1,2*], Swati Dhar[1], Avinash Kumar[1], Janice M. Lage[2], Jack R. Lewin[2], Agnes M. Rimando[3], and Xu Zhang[4]. [1]Cancer Institute, University of Mississippi Medical Center, Jackson, MS 39216, [2]Pathology Department, University of Mississippi Medical Center, Jackson, MS 39216, [3]USDA, Agriculture Research Service, Natural Products Utilization Unit, University, MS 38677, [4]Biostatistics & Bioinformatics, University of Mississippi Medical Center, Jackson, MS 39216. e-mail: alevenson@umc.edu

Abstract: Dietary stilbenes (resveratrol and its potent analogs) are phenolic compounds with anti-inflammatory, anti-oxidant and anti-cancer activity. Importantly, these compounds can modulate epigenetics and influence cancer susceptibility and progression. Prostate cancer is the most often diagnosed cancer and the second leading cause of cancer deaths in males in the US. Epidemiological studies suggest association between diet and lower risk of prostate cancer. Epigenetic mechanisms implicated in prostate cancer include gene silencing via action of co-repressor complexes (i.e. deacetylation) and changes in microRNA profiles. In this presentation, I will provide compelling evidence on epigenetic mechanisms of resveratrol and its analogs through regulation of the chromatin modifier metastasis-associated protein 1 (MTA1), MTA1-associated network and certain oncomiRs and highlight the anticancer effects of these compounds in vitro and in preclinical models of prostate cancer. It is our hope that resveratrol's analogs with better bioavailability, thereby conferring superior pharmacological potency and greater anticancer effects through epigenetic mechanisms, may become strong candidates for clinical development.

Oral 2. Further studies on pterostilbene as PPARα ligand

Agnes M. Rimando[1*], Shabana I. Khan[2], Cassia S. Mizuno[3], Guang Ren[4], Suresh T. Mathews[5], Hyunsook Kim[6], Wallace Yokoyama[7]. [1]USDA ARS P.O. Box 1848, University, MS 38677, [2]National Center of Natural Products Research, University of Mississippi, Oxford, MS 38655, [3]College of Pharmacy, University of New England, Portland, ME, 04103, [4]University of Alabama at Birmingham School of Medicine, Birmingham, AL 35233, [5]Auburn University, Auburn, AL 36849, [6]Kongkuk University, South Korea, [7]USDA ARS WRRC, Albany, CA 94710. e-mail: agnes.rimando@ars.usda.gov

Abstract: We previously demonstrated pterostilbene is an agonist for the nuclear transcription factor peroxisome proliferator activated receptor alpha isoform (PPARα), and showed that PPARα activation by pterostilbene was higher than that of ciprofibrate, a clinically used hypolipidemic drug, at 100 μM. In the present study, we investigated PPARα activation by pterostilbene together with compounds known to occur in blueberries (resveratrol, anthocyanins, catechins) and fibrate drugs (as positive controls) at concentrations ranging from 3.12 to 50.00 μM, in rat hepatoma cell line H4IIEC3. Pterostilbene exhibited a dosedependent activation of PPARα, similar to those of the fibrate drugs ciprofibrate and fenofibrate. In the presence of chenodeoxycholic acid, a specific inhibitor of PPARα, pterostilbene showed dose-dependent decreases in luciferase response paralleling those of Wy-1463, a synthetic PPARα ligand. Docking studies were performed and provided validation of the results obtained in the *in vitro* assays. We further explored whether pterostilbene

Dietary Pterostilbene is a Novel MTA1-targeted Chemopreventive and Therapeutic Agent in Prostate Cancer

Swati Dhar[1,*], Avinash Kumar[1,*], Liangfen Zhang[1,2], Agnes M. Rimando[3], Janice M. Lage[2], Jack R. Lewin[2], Azeddine Atfi[1,4], Xu Zhang[5], and Anait S. Levenson[1,2]

[1]Cancer Institute, University of Mississippi Medical Center, Jackson, MS, USA

[2]Department of Pathology, University of Mississippi Medical Center, Jackson, MS, USA

[3]United States Department of Agriculture, Agriculture Research Service, Natural Product Utilization Research Unit, University, MS, USA

[4]Department of Biochemistry, University of Mississippi Medical Center, Jackson, MS, USA

[5]Center of Biostatistics and Bioinformatics, University of Mississippi Medical Center, Jackson, MS, USA

[*]S.D. and A.K. contributed equally to this work.

Correspondence to: Anait S Levenson, e-mail: alevenson@umc.edu

Keywords: pterostilbene, prostate cancer, chemoprevention, therapy, MTA1, *Pten*-loss

ABSTRACT

Dietary nutrients with ability to reverse adverse epigenetic events have great potential for cancer chemoprevention. Overexpression of the epigenetic modifier metastasis-associated protein 1 (MTA1) is associated with aggressive human prostate cancer. The purpose of this study was to determine MTA1-driven mechanisms in pre-clinical models of prostate cancer and whether pterostilbene, a natural potent analog of resveratrol, may effectively target MTA1 to prevent prostate cancer development and progression.. Here, we show that high levels of MTA1 expression in *Pten*-loss prostate cooperate with key oncogenes, including c-Myc and Akt among others, to promote prostate cancer progression. In addition, loss-of-function studies using human prostate cancer cells indicated direct involvement of MTA1 in inducing inflammation and epithelial-to-mesenchymal transition. Importantly, pharmacological inhibition of MTA1 by pterostilbene resulted in decreased proliferation and angiogenesis and increased apoptosis, thereby restraining prostatic intraepithelial neoplasia (PIN) formation in prostate-specific *Pten* heterozygous mice by 50 % and reducing tumor development and progression in prostate-specific *Pten*-null mice by 52 %. Taken together, our pre-clinical findings highlight MTA1 as a key upstream regulator of prostate tumorigenesis and cancer progression and offer pre-clinical proof for pterostilbene as a promising lead natural agent for MTA1-targeted chemopreventive and therapeutic strategy to curb prostate cancer.

INTRODUCTION

Besides the classic view of cancer etiology, which includes genetic alterations, substantial data support the idea that dietary/lifestyle factors affect cancer incidence and progression through promoting chronic inflammation and oxidative stress along with epigenetic alterations associated with cancer initiation, promotion and progression [1, 2]. Along these lines, anti-inflammatory and anti-oxidant epigenetic dietary agents are of great interest for cancer prevention and treatment, particularly for slow growing and age-related prostate cancer, for which diet is a risk factor [3].

One of the known epigenetic alterations in various cancers, including prostate cancer, is overexpression of the master chromatin remodeler, metastasis-associated protein 1 (MTA1) [4], which correlates with higher grade tumor, recurrence, metastasis and poor prognosis [5-11]. MTA1 acts as a part of the NuRD co-repressor complex that is involved in histone deacetylation and silencing of gene expression [4]. Alterations in the expression or regulation of MTA1 leads to deregulated chromatin, which results in altered gene transcription and/or inappropriate gene silencing [12].

MTA1 is a progression and metastasis-associated protein, whose increased nuclear expression is associated with a more aggressive phenotype and recurrence in human prostate cancer [8-10]. Our studies with prostate cancer cell lines and xenografts have highlighted the functional relevance of MTA1 in promoting tumor growth, invasion, angiogenesis and metastasis [9, 13].While the exact molecular mechanisms that govern MTA1 activity in cancer are poorly understood, our group and others have showed that MTA1 can elicit anti-apoptotic effects through p53 deacetylation [14, 15] or pro-angiogenic actions via positive regulation of VEGF

expression [9, 16]. We also detected significantly higher tumor growth in PTEN-deficient LNCaP-xenografts compared to the PTEN-expressing DU145-xenografts, although both expressed MTA1 [9]. This observation coupled with our recent observation of PTEN's acetylation status regulation by MTA1 [17] prompted speculation that MTA1 might cooperate with PTEN loss for the establishment and progression of prostate cancer.

Although the link between diet, cancer and epigenetics is complex, epigenetic dietary agents are of great interest for cancer prevention and treatment [18]. Previously, we have shown that dietary stilbenes, commonly found in grapes and blueberries, inhibit MTA1 expression and function in prostate cancer [9, 13, 15]. Pterostilbene (PTER), a potent natural *trans*-3,5-dimethylether analog of resveratrol, based on its superior pharmacokinetic and pharmacodynamic properties [13, 19-22] appears the strongest candidate for clinical development.

Our previous studies emphasized the relevance of MTA1 as a viable therapeutic target and pterostilbene as a potent pharmacological inhibitor of MTA1 [9, 11, 13, 17]. In the current study, we evaluated the MTA1-targeted efficacy of pterostilbene in autochthonous prostate cancer pre-clinical models that harbor prostate-specific *Pten* heterozygous (*Pb-Cre4*; *Pten*$^{+/f}$, hereafter referred as *Pten*$^{+/f}$) and *Pten* knockout (*Pb-Cre4*; *Pten*$^{f/f}$, hereafter referred as *Pten*$^{f/f}$), which represent chemoprevention and intervention scenarios, respectively. We found that *Pten* loss resulted in a marked increase in MTA1 expression leading to activation of MTA1-dependent oncogenic and tumor progression-related signaling pathways. Importantly, pterostilbene both as dietary supplementation and interventional daily injections, through targeting MTA1 and its tumor promoting network, inhibits inflammation, proliferation and angiogenesis and induces apoptosis, which results in reduction of prostatic intraepithelial neoplasia (PIN) lesions and

adenocarcinomas in precancerous *Pten*$^{+/f}$ and cancer-prone *Pten*$^{f/f}$ models, respectively. Therefore, we believe that our present findings of chemopreventive and therapeutic efficacy of an epigenetic dietary agent pterostilbene as a novel MTA1-targeted strategy, may have potential clinical applications in prostate cancer management.

RESULTS

Pten loss-induced MTA1 upregulation promotes prostate tumorigenesis and progression

We chose prostate-specific *Pten*-loss mouse models, represented by *Pten* heterozygous (*Pten*$^{+/f}$) and *Pten*-null (*Pten*$^{f/f}$) mice that are most suitable for testing novel chemopreventive and therapeutic options due to close resemblance to the human disease and an intact immune system. Based on our previous studies suggesting a possible inverse relationship between MTA1 and PTEN [9, 17], we hypothesized that targeted therapy to inhibit MTA1 would be effective for blocking *Pten* loss-driven prostate tumor growth and progression.

To assess the possible involvement of MTA1 in *Pten* loss-driven prostate tumorigenesis, we examined MTA1 levels in prostate tissues from *Pten*$^{+/f}$, which exhibit precancerous PIN at 8-10 months of age [23]. We found that loss of only one *Pten* allele was sufficient to substantially increase MTA1 both at protein and mRNA levels (Figure 1 A-C), suggesting that the observed MTA1 upregulation was at the transcriptional level and that MTA1 may be involved in the initiation stage of prostate cancer.

Given that MTA1 has transcriptional co-repressor and co-activator functions [11, 24, 25], we hypothesized that MTA1 upregulation could transcriptionally perturb genes and assist pathways

which promote tumorigenesis. Our MTA1 ChIP-Seq analysis using prostates from 10-month-old *Pten*$^{+/f}$ mice identified 38,000 peaks, including key oncogenes such as c-Myc, Akt1, Ets2, Notch2, CyclinD1 and Hsp90 [26-31] (Supplementary Table S1). Immunoblot analysis showed increased protein expression for these molecules as well as an increase in AR and TGFβ1 levels in the *Pten*$^{+/f}$ prostates compared to normal prostates (Figure 1B). Quantitative real-time PCR (qRT-PCR) showing upregulation of Akt1, c-Myc, Ets2 and Hsp90 mRNA validated these genes as transcriptional targets of MTA1 (Figure 1C).

In the *Pten*$^{f/f}$ (*Pten*-null) mice, which mimic stage-defined progression of human prostate cancer [23], we found an age-dependent increase in MTA1 expression along with expected increased levels of p-Akt as compared to their normal counterparts (Figure 1D and E), suggesting a strong correlation with the progression of prostate cancer. This notion has been supported by our previous studies of human specimens, in which MTA1 overexpression was correlated with prostate cancer progression, aggressiveness and metastasis [9, 10]. Immunohistochemical (IHC) analysis of the *Pten*-null prostates showed high MTA1 expression not only in the multilayers of luminal epithelial cells but also in the reactive stroma (Figure 1D). Since several factors and cytokines, including NF-κB (p65), IL-1β, and Hsp90 have been implicated either in MTA1 regulatory network or induction of reactive stroma or both [32-34], we found that concomitant with MTA1, the expression of these proteins was increased with continued tumor development (Figure 1E), suggesting a pro-inflammatory role for MTA1 in both the tumor and reactive stroma. Moreover, the expression of E-cadherin (an epithelial marker) was downregulated along with upregulation of Vimentin (a mesenchymal marker) (Figure 1E), indicating the involvement of MTA1 in epithelial-to-mesenchymal transition (EMT) of prostate

cancer cells. Importantly, NF-κB (p65), IL-1β, Hsp90, E-cadherin and Vimentin were among the target gene promoters identified in our MTA1 ChIP-Seq analysis (Supplementary Table S1).

To gain insights into the mechanistic basis for the MTA1 upregulation in *Pten* loss-driven prostate tumorigenesis and tumor progression, we studied the effects of MTA1 knockdown in the human prostate cancer cell lines, LNCaP and DU145. We found a reduction in NF-κB (p65), IL-1β, and Vimentin and upregulation of E-cadherin protein levels in MTA1 knockdown (shMTA1) prostate cancer cells (Figure 2A and B), suggesting direct involvement of MTA1 in inflammation and EMT in prostate cancer. Likewise, we detected a reduction in the levels of c-Myc, CyclinD1, Notch2, Ets2, and Hsp90 both at protein and mRNA levels in shMTA1 cells (Figure 2A and B), suggesting a role for MTA1 upstream to the critical oncogenes c-Myc, Notch2 and Ets2. As expected, we found an activation of the Akt survival signaling pathway [23], which was accompanied by changes in AR levels in *Pten*$^{+/f}$ and *Pten*$^{f/f}$ mice (Figure 1A, B and D, E). The upregulation of Akt at both mRNA and protein levels was concomitant with increased MTA1 in the murine prostates (Figure 1B, C and E). Since Akt1 was among the MTA1 target promoters in the MTA1 ChIP-Seq analysis (Supplementary Table S1), we hypothesized possible direct association between MTA1 and Akt. Indeed, MTA1 depletion in *Pten*-deficient LNCaP cells led to partial inactivation of Akt, at least in part, through downregulation of Akt mRNA and protein (Figure 2B, top and C). Besides, inhibition of the Akt pathway by phosphatidylinositol 3-kinase (PI3K) inhibitor LY294002 led to reduced MTA1 protein and mRNA in prostate cancer PC3M cells (Figure 2D and E). Akt pathway is known to promote the stability of c-Myc protein [35], an identified transcriptional activator of MTA1 [36, 37]. We found that inhibition of Akt pathway led to a reduction in c-Myc protein levels (Figure 2D) but not mRNA (data not shown). On the other hand, the downregulaton of MTA1 by LY294002 was both at protein and mRNA levels

(Figure 2D and E), suggesting that the Akt pathway positively regulates MTA1, at least in part, at the transcriptional level by promoting the stability of c-Myc protein **(**Figure 2F). Together, these results suggest a direct positive crosstalk between MTA1 and Akt pathway independent of PTEN.

To ascertain the clinical significance of our findings, we investigated the correlation between MTA1 and PTEN in human prostate cancer by analyzing the expression of MTA1 and PTEN mRNA in the GSE41967 dataset [38] from the Gene Expression Omnibus (GEO) database. We observed a significant inverse correlation between MTA1 and PTEN and that this correlation became stronger with severity of the disease as evidenced by the increased Gleason scores (Figure 3A). Moreover, as expected, we found a significant positive correlation between MTA1 and AKT1 (Figure 3B, top**)** and no correlation between MTA1 and AR (Figure 3B**,** bottom) in the same dataset.

Collectively, these data support a central role of MTA1 and MTA1-dependent signaling, including novel MTA1-Akt and MTA1-c-Myc feed-forward loops (Figure 2F), as significant drivers of *Pten*-loss induced prostate tumorigenesis and cancer progression suggesting that targeting MTA1 can abrogate both tumor initiation and progression in prostate cancer.

Pterostilbene diminishes prostate cancer initiation, growth and progression in prostate-specific *Pten* loss mouse models

In chemoprevention modality, $Pten^{+/f}$ mice were fed phytoestrogen-free AIN 76A diet supplemented with pterostilbene (100 mg/kg diet) for 8-10 months while in intervention

modality *Pten* $^{f/f}$ mice were treated with daily pterostilbene (10 mg/kg bw) i.p. injections and monitored for prostate lesions at 6, 10, 15, 20, 25 and 33 weeks of age.

Gross anatomy (Figure 4A, top) and *ex vivo* images (Figure 4A, middle) of urogenital system (UGS) as well as dissected prostatic lobes (Figure 4A, bottom) from mice on PTER-Diet clearly indicated smaller prostates relative to controls, although differences in food intake were not significant and the pterostilbene supplemented diet did not have any adverse effects on the mice (Supplementary Figure S1). All mice by 8-10 months of age developed high grade PIN, however mice on PTER-diet showed 50% reduction in the number of glands involved in PIN (Figure 4B and Supplementary Table S2) and more favorable histopathology with restored normal ductal structures accompanied by higher PTEN protein expression, as evident by H&E and PTEN staining (Figure 4C).

In the *Pten*-null model, by 10 weeks of age, 67% of the *Pten*$^{f/f}$ mice contained regions of pre-invasive adenocarcinoma with enlarged, hardened prostates, which progressed to invasive adenocarcinoma by 25-33 weeks of age in all the mice examined but shrank upon pterostilbene treatment as evident by gross anatomy (Figure 4D, top and middle) and *ex vivo* images of dissected prostatic lobes (Figure 4D, bottom) and UGS weights (Figure 4E). Overall, 64% of the vehicle-treated mice exhibited pre-invasive or invasive adenocarcinoma whereas daily 10 mg/kg pterostilbene treatment reduced the incidence of adenocarcinomas to 12% and halted the progression at PIN stage (Figure 4F and G and Supplementary Table S3). As seen in Figure 4G and Supplementary Figure S2, vehicle-treated mice developed enlarged prostates characterized by disorganized glandular structures, which contained regions of cribriform carcinoma with signs of microinvasion, *i.e.*, loss of the basal membrane (SMA) and CK8-positive luminal cells that escaped into reactive stroma. In contrast, PTER-treated mice mostly showed characteristics of

PIN, which retained a basal layer of SMA-positive cells and CK8-positive luminal cells along with residual hypercellularity. We did not find any lymph node metastasis even in mice aged over one year, by examining in total 34 renal and iliac lymph nodes of control or treated mice (Supplementary Figure S3).

To determine whether pterostilbene reaches the target tissue, we analyzed pterostilbene concentrations in prostate tissues, as well as in the serum, from *Pten*$^{+/f}$ and *Pten*$^{f/f}$ mice. We found accumulation of pterostilbene in the prostates from both mouse models, with apparent greater accumulation when administered i.p. (Supplementary Table S4), suggesting that high lipophilicity, membrane permeability and metabolic stability of pterostilbene [19-21] secure its potent biological activity *in vivo.*

Pterostilbene targets *Pten* loss-induced MTA1 upregulation and its associated signaling

To elucidate the molecular mechanisms responsible for pterostilbene efficacy, we examined its effects on MTA1 expression in prostate tissues from *Pten*$^{+/f}$ and *Pten*$^{f/f}$ mice. We found downregulation of MTA1 protein levels in *Pten*$^{+/f}$ prostates as detected by immunoblotting and IHC (Figure 5A and B). Remarkably, these prostate tissues showed elevated levels of PTEN protein (Figure 5A and Supplementary Figure S4C), highlighting the potential of dietary epigenetic therapy to restore the expression as well as the activity of the remaining PTEN allele, which can be further gauged by decreased p-Akt levels (Figure 5A and B). Additionally, PTEN and MTA1 gene expression analysis by qRT-PCR demonstrated elevated PTEN and decreased MTA1 mRNA levels in the prostate tissues from mice on PTER-diet, suggesting targeting of MTA1 by pterostilbene at transcriptional level with consequent decreased recruitment of MTA1

onto PTEN promoter (Figure 5D and Supplementary Table S1). This is consistent with known MTA1-PTEN relationship [17, 39].

Since there is a direct relationship between MTA1 and Akt (Figure 1B and C and Figure 2A and B), pterostilbene prevents the activation of Akt pathway, at least in part, by targeting MTA1 and thereby decreasing MTA1 recruitment onto Akt1 promoter (Figure 5D). Moreover, pterostilbene also reverses the MTA1-associated perturbation of key oncogenes as demonstrated by the decreased levels of c-Myc, CyclinD1, Notch2, Ets2 and Hsp90 proteins in the prostate tissues (Figure 4A) presumably at the transcriptional level through decreased recruitment of MTA1 onto these target promoters (Figure 5D and Supplementary Table S1). Prostates from mice on PTER-Diet also exhibited downregulation of TGFβ1, a well-known upstream activator of MTA1 [40] (Figure 4A)**.** Interestingly, although independent from MTA1, pterostilbene also reduces the AR levels (Figure 5A and B)**,** further strengthening it's potential as a suitable chemopreventive agent to reduce the risk of prostate cancer.

To further investigate the lobe-specific differential impact of pterostilbene treatment, we performed immunoblot analysis using right anterior (AP_R), left anterior (AP_L) and dorso-latero-ventral (DLV) prostatic lobes from *Pten*$^{+/f}$, Cre-negative (NP) mice and mice on control and PTER diet (Figure 5E and F). In normal prostates, MTA1 was detected at very low levels in the lobes. In contrast, MTA1 was highly expressed in all lobes with various intensities, the highest being detected in AP_L. Importantly, the increase in MTA1 levels in all lobes in *Pten* heterozygous mice was profoundly inhibited by pterostilbene (Figure 5E and F). Pterostilbene treatment also inhibited p-Akt and AR levels, with the effects most evident in AP.

In the intervention strategy with cancer-prone *Pten*-null mice, in which progressive increase in MTA1 levels were associated with age-related aggressiveness of prostate cancer (Figure 1E),

we found a substantial decrease in MTA1 levels in response to pterostilbene treatment at any ages examined by immunoblotting or IHC (Figure 6A and C and Supplementary Figure S4). Moreover, this downregulation of MTA1 by pterostilbene significantly altered the expression of MTA1-dependent decrease in expression of pro-inflammatory IL-1β and Hsp90 as well as with E-cadherin (Figure 6A), possibly through decreased recruitment of MTA1 onto these gene promoters (Figure 6B). Importantly, pterostilbene intervention inhibited MTA1-associated maintenance of already highly activated Akt pathway. Here again, pterostilbene treatment showed downregulation of AR levels (Figure 6A and C). In the context of prostate lobes, once again, MTA1 was highly expressed in all lobes of *Pten*$^{f/f}$ prostates with various intensities, and the highest fold increase, compared to normal prostates, was observed in the anterior lobes (Figure 6D and Supplementary Figure S5). Age and progression related increases in MTA1 were inhibited on an average by 50% in all prostatic lobes of mice treated with pterostilbene (Figure 6D and Supplementary Figure S5). Pterostilbene had less consistent p-Akt-inhibitory effects in different lobes; yet, remarkably the effect was mostly evident in the AP_L prostatic lobe, in which MTA1 inhibition by pterostilbene was most significant. It is quite possible that one of the mechanisms of pterostilbene inhibition of the Akt pathway in these mice is through MTA1. Finally, AR levels were also markedly reduced in the prostates from the pterostilbene-treated group compared to control mice (Figure 6D and Supplementary Figure S5).

Altogether, diet with pterostilbene supplementation or daily pterostilbene injections in *Pten*$^{+/f}$ and *Pten*$^{f/f}$ immunocompetent pre-clinical mouse models, respectively, reduced the profound increase in MTA1 and the coordinate expression of multiple components of MTA1 tumor-promoting signaling, demonstrating the *in vivo* efficacy of pterostilbene as a targeted chemopreventive and intervention strategy.

Pterostilbene reduces MTA1-induced cellular proliferation and angiogenesis, and promotes MTA1-dependent apoptosis in *Pten* loss-driven prostate cancer

The restoration of a more favorable histopathology by pterostilbene in both *Pten*$^{+/f}$ and *Pten*$^{f/f}$ mice through targeting of MTA1 and its associated signaling may functionally involve inhibition of proliferation and induction of apoptosis. The number of Ki-67 positive tumor cells was decreased by about three fold in mice on pterostilbene diet (Figure 7A, top and B, left) and about three to five fold in mice of different age injected with pterostilbene (Figure 8A and B, top and Supplementary Figure S6). Moreover, immunostaining and immunoblot analyses for cleaved Caspase-3 showed that apoptosis in prostate tissues from mice on pterostilbene diet was substantially increased (four to five-fold) **(**Figure 7A, bottom and B, right and C). Notably, pterostilbene treatment in the *Pten* $^{f/f}$ mice also exhibited a marked and an age-dependent increase in cleaved Caspase-3 immunostaining (Figure 8C and D), indicative of prolonged treatment benefits.

Since we found p21 and p27, known key regulators of proliferation and apoptosis [41-43] among the targets identified from MTA1 ChIP-Seq analysis (Supplementary Table S1), we demonstrated low levels of p21 and p27 in *Pten*$^{+/f}$ prostate tissues (Figure 7D, left), which was rescued by pterostilbene diet (Figure 7D, right) due to a decreased recruitment of MTA1 onto p21 and p27 promoter (Figure 7E). Further, we validated the upregulation of these molecules at protein and mRNA levels in MTA1 knockdown human prostate cancer cells (Figure 7F and G).

We previously reported that resveratrol/pterostilbene suppressed the MTA1-dependent decrease in acetylation of p53, which led to decreased apoptosis in prostate cancer [13, 15]. In

Pten$^{f/f}$ prostates, we found age-dependent increased acetylation of p53 upon treatment with pterostilbene together with induction of pro-apoptotic Bak (Figure 8E and F), which is likely due to MTA1 inhibition by pterostilbene.

Finally, consistent with our previous reports on the link between MTA1 and angiogenesis [9, 13] and our current finding of VEGF-C as a MTA1 target (Supplementary Table S1), pterostilbene treatment led to decreased angiogenesis, as evident by CD31 and VEGF-C immunostaining (Figure 8A, middle and bottom and B, bottom and Supplementary Figure 6). In addition to the already observed direct link between MTA1 and the pro-angiogenic factor IL-1β [44] (Figure 1E and Figure 2A) and its reversal by pterostilbene treatment (Figure 6A), ChIP-Seq analysis showed decreased recruitment of MTA1 onto VEGF-C promoter upon pterostilbene treatment (Figure 8G). Taken together, these results demonstrate that pterostilbene treatment inhibits tumor cell proliferation and angiogenesis and induces apoptosis in *Pten*-loss prostate tumors, at least in part, due to inhibition of MTA1.

DISCUSSION

Here, we report on a previously unknown mechanism-based importance of the chromatin modifier MTA1 in *Pten* loss-driven prostate tumors. Mechanistically, we demonstrated that aberrant overexpression of MTA1 resulted in activation of MTA1-dependent transcriptional signatures that promote proliferation, inflammation, invasion and survival of cancer cells. Importantly, we demonstrated that pharmacological inhibition of MTA1 and its associated network by a natural dietary compound pterostilbene, exhibited chemopreventive and therapeutic

efficacy as evident by the decreased severity of PIN and complete prevention of progression to carcinoma in preclinical mouse models of prostate cancer (Figure 9).

In our previous studies regarding the clinical significance of MTA1 in prostate cancer, we found that nuclear overexpression of MTA1 was correlated with high Gleason score, aggressive disease, recurrence, and bone metastasis [9, 10]. Moreover, MTA1 overexpression was a prognostic factor for more aggressive disease and worse outcome in African American men [10]. Based on our previous *in vitro* and *in vivo* findings on MTA1-mediated molecular mechanisms underlying prostate cancer progression [9, 17], we had hypothesized cooperation of MTA1 with *Pten* loss in prostate tumor growth, survival and angiogenesis. We now demonstrate that inhibition of MTA1 and its associated network act together to inhibit precancerous PIN development and tumor growth in pre-clinical *Pten*-loss mouse models. This data appear highly clinically relevant because in addition to well established critical role of PTEN tumor suppressor in prostate cancer [45, 46], analyses of human prostate tumor specimens revealed an inverse correlation between MTA1 and PTEN, which became stronger with severity of the disease (Figure 3A). Therefore, our data support the concept that patients with deregulated PTEN/Akt pathway, which comprise 21-42% of patients with prostate cancer [47], most likely have overexpression of MTA1 and may benefit from MTA1-targeted therapy. Moreover, since increased levels of MTA1 is associated with increased Akt activity and PI3-kinase inhibitors also target MTA1 (Figure 2D), combinatorial therapy using pterostilbene and PI3-kinase inhibitors may be considerably more effective with additive or synergistic anticancer effects along with lower toxicity.

Although the exact function of MTA1 chromatin modifier as an epigenetic reader and transcription factor is unclear, MTA1 is a master dual co-regulator that associates with both the

repressed and active chromatin depending on its own methylation status [12]. Results from our ChIP-Seq analysis identified oncogenic c-Myc, Cyclin D1, Ets2, Akt1 and Notch2, pro-inflammatory Hsp90, pro-angiogenic VEGF-C, and pro-apoptotic p27 as novel transcriptional targets of MTA1. We demonstrated that MTA1 acts as a coactivator for c-Myc, CyclinD1, Ets2, Notch2, and VEGF-C and as a co-repressor for pro-apoptotic p27 in addition to the already reported regulation of Vimentin, E-cadherin and p21 by MTA1[40, 48, 49]. Ongoing analysis of our RNA Pol II ChIP-Seq data aims to further validate biological significance of MTA1 binding to the promoters of all these genes. Notably, pterostilbene reduced recruitment of MTA1 onto all target promoters as evident by resulting lower binding peaks (Supplementary Table S1).

We previously reported on an inverse relationship of MTA1 with PTEN and the ability of MTA1 to regulate activation of the PTEN/Akt pathway through deacetylation of PTEN [17]. Others have reported MTA1 transcriptional repression of PTEN [39]. Here, we confirmed the inverse relationship between MTA1 and PTEN on the transcriptional level, and also identified MTA1 binding to PTEN promoter by ChIP-Seq analysis. The fact that we detected upregulation of PTEN mRNA and protein in *Pten*$^{+/f}$ mice upon pterostilbene-mediated downregulation of MTA1 conveys the feasibility of therapeutically attractive approaches for PTEN re-activation by epigenetic-targeted agents. In addition, we identified novel MTA1-Akt and MTA1-c-Myc feed-forward loops in prostate cancer. This ability to simultaneously activate multiple tumor-promoting pathways defines MTA1 as a key upstream epigenetic driver in prostate cancer initiation and progression.

One of the most striking observations in our models was that MTA1 levels were dramatically increased not only in prostate epithelial cells but also in reactive stroma. While there is a well-established association between inflammation, reactive stroma and prostate cancer [50], the

underlying mechanisms remain elusive. Our study demonstrate the possible role of MTA1 in epithelial-stromal interaction. Importantly, since the oncogenic potential of MTA1 might also be linked to other cell types in the reactive stroma, the anti-inflammatory effects of pterostilbene mediated through MTA1-associated NF-κB, IL-1β, Hsp90 may play an important additive beneficiary role in its antitumor activity.

We found increased AR levels in *Pten*$^{+/f}$ and *Pten*$^{f/f}$ mouse models. Immunohistochemical experiments showed expression of AR by secretory luminal cells and its overexpression in high grade PIN and specifically in adenocarcinoma, when reactive stroma is present [51]. Although both MTA1 and AR had similar patterns of behavior in our pre-clinical models, we did not find any direct evidence on whether overexpression of MTA1 could contribute to the activation of AR signaling. On the other hand, several studies have suggested a cross-talk between the PI3K/Akt and AR signaling pathways albeit with contradictory data on either positive or negative effect on AR [52-54]. We observed a positive association between Akt and AR, but we did not find any direct relationship between MTA1 and AR. Importantly, the inhibitory effects of pterostilbene on AR levels not only in epithelial cells but also in the stroma, represent another additional beneficiary factor, which potentially defines favorable histopathology of the lesions upon pterostilbene exposure. Our studies in human prostate cancer cells also demonstrated inhibitory effects of pterostilbene on AR levels [55]. Our data reason that combined inhibition of MTA1 and AR by pterostilbene provides for its maximal efficacy in *Pten* deficient tumors.

Despite the observed master epigenetic regulatory properties of MTA1 and the fact that increased MTA1 is a poor prognostic marker in prostate cancer [10], MTA1 has not yet been used as a therapeutic target. The concept of "epigenetic therapy" for cancer has developed during the last two decades [56, 57], and efforts were largely driven towards the development of

inhibitors of druggable epigenetic enzymes such as inhibitors of DNA methylation or histone deacetylation [56]. Limited studies are available on targeting other epigenetic regulators, such as epigenetic readers and transcription factors [58]. Our serendipitous finding of MTA1 as a new molecular target of resveratrol and its analogs [13, 15] opened opportunities for further pre-clinical validation of the efficacy of dietary stilbenes as natural epigenetic therapy in prostate cancer. Particularly, pterostilbene, a potent natural analog of resveratrol, showed the strongest MTA1 inhibition in different prostate cancer cells in culture and marginally better efficacy than the parent resveratrol in xenografts [13]. Others have also demonstrated anticancer effects of pterostilbene in prostate cancer through multiple mechanisms, which include reduction of prostate-specific antigen, promotion of apoptosis, alteration of cell cycle and inhibition of cell growth [59-61]. However, this is the only study on chemopreventive and therapeutic efficacy of pterostilbene in preclinical models of prostate cancer. While the improved bioavailability of pterostilbene and its distribution in various tissues has been reported [19-22], we detected accumulation of pterostilbene in the prostate tissues, with higher concentrations when administered i.p., providing evidence that pterostilbene reaches the target organ and thereby exerts its anticancer effects. This finding may be clinically relevant since the dosage we used both in diet and i.p. was roughly equivalent to the reported non-toxic and effective doses in rodents [20, 62, 63] and human [64, 65].

In summary, utilizing clinically relevant disease models of prostate cancer, we demonstrated that pterostilbene inhibits prostate tumorigenesis and cancer progression by regulating MTA1-driven inflammation, EMT and survival responses. Our results clearly showed that pterostilbene by profoundly downregulating MTA1 and its associated tumor-promoting cellular pathways, strongly inhibited cancer cell proliferation and angiogenesis together with inducing apoptosis,

which paralleled the improvement in histological severity of PIN and prevention of its progression to poorly differentiated carcinoma. In addition, we identified panel of MTA1-guided molecules that are responsive to pterostilbene treatment and, therefore, can be utilized not only as prognostic but also as predictive biomarkers, with some of them having the feasibility of being detected in the blood (IL-1β, VEGF). Of particular importance, we have successfully defined the functional significance of highly increased MTA1 expression and activity for prostate cancer tumorigenicity and progression and demonstrated the MTA1-targeted chemopreventive and therapeutic efficacy of pterostilbene. As such, our findings offer a solid foundation to endorse chemopreventive and interventional clinical trials with pterostilbene for personalized targeted prostate cancer management. Thus, it is likely that targeting MTA1 and MTA1-associated molecular and cellular events by dietary pterostilbene in the high-risk population and patients with early stages of prostate cancer, i.e. patients on active surveillance with deregulated MTA1, could be the most needed immediate chemopreventive strategy. Moreover, in the future, as other pharmacological inhibitors of MTA1 such as HDAC inhibitors [15] or PI3-kinase inhibitors (Figure 2D) are validated *in vivo*, combinatorial strategies with pterostilbene can be considered for more effective but less toxic therapeutic approaches in targeted patient population with advanced disease.

MATERIALS AND METHODS

Reagents

Phytoestrogen-free AIN 76A diet was obtained from Research Diets, Inc. Pterostilbene was synthesized according to protocol described previously [66]. The structure was confirmed by spectroscopy. The purity of pterostilbene was determined to be > 99. 9%. Pterostilbene powder was shipped to Research Diets, Inc for formulation of pterostilbene supplemented AIN 76A diet at a concentration of 100 mg/kg diet. Upon receiving pterostilbene supplemented diet, it was aliquoted into separate portions, sealed in aluminum foil and kept at 4^0C until use. For injections, pterostilbene (10 mg/kg bw) was suspended in 10% DMSO, freshly every day and kept in dark until use.

Cell culture

Human prostate cancer cells, LNCaP, DU145 (ATCC) and PC3M (a gift from Dr. Bergman, Northwestern University) were cultured in RPMI1640 (Life Technologies) containing 10% FBS and antibiotics at 37^0C and 5% CO_2. Establishment of prostate cancer cell lines with stable MTA1 knockdown (MTA1shRNA) has been described and characterized previously [13, 15]. All cell lines were last authenticated using short tandem repeat profiling at Research Technology Support Facility, Michigan State University in 2014. Cells were tested for mycoplasma using the Universal Mycoplasma Detection Kit (ATCC).

Generation of prostate-specific *Pten* heterozygous and knockout mice

Animal housing, care and treatments were in accordance with approved protocol #1272A by Institutional Animal Care and Use Committee of UMMC. During the study, animals were

permitted free access to drinking water and food, and were monitored daily for their general health. C57BL/6J mouse homozygous for the "floxed" allele of *Pten* gene (*Pten* $^{f/f}$) was purchased from Jackson Laboratories and bred with *Pb-Cre4* male from the B6.Cg genetic background (NCI mouse repository) that specifically express *Cre* recombinase in the prostate epithelium [23]. Tail-genotyping was performed using the following primers: PTEN geno olMR9554F:5′-CAA GCA CTC TGC GAA CTG AG-3′; PTEN geno olMR9555R:5′-AAG TTT TTG AAG GCA AGA TGC-3′ with wt band of 156 bp and mutant band of 328 bp; and Cre F: 5′-TCG CGA TTA TCT TCT ATA TCT TCA G-3′; Cre R: 5′-GCT CGA CCA GTT TAG TTA CCC-3′ with a band of 393 bp. PCR was performed on an Eppendorf thermocycler. We used male *Pb-Cre4*; *Pten*$^{+/f}$ prostate-specific heterozygous mice (abbreviated as *Pten*$^{+/f}$ in the text and figures) in experiments with dietary supplementation of pterostilbene, and male *Pb-Cre4*; *Pten*$^{f/f}$ prostate-specific knockout mice (abbreviated as *Pten*$^{f/f}$ in the text and figures) in experiments with i.p. injections of pterostilbene. Normal prostates (NP) from *Cre*-negative; *Pten*$^{+/f}$ or *Cre*-negative; *Pten*$^{f/f}$ were processed as normal controls.

Dose calculations

In our previous study with orthotopic prostate cancer xenografts, we extrapolated the dose from resveratrol chemopreventive studies in human colorectal cancer [67] by using Body Surface Are (BSA) formula for dose translation [68] and demonstrated that both resveratrol and pterostilbene had anticancer and antimetastatic effects at 50 mg/kg/day, i.p. administration, with higher accumulation of pterostilbene in serum. Bearing in mind known higher bioavailability of pterostilbene and lower weight of pups used in the current study, we finalized pterostilbene dose

at 10 mg/kg bw per day, i.p. for this study. In addition, we accumulated circumstantial data with higher doses of pterostilbene (25, 50 and 100 mg/kg bw). For the calculation of concentration of pterostilbene in the diet, we used DD = (SD x BW)/FI formula (Research Diets, Inc) where, DD is Diet Dose (mg compound/kg Diet); SD is Single Dose (mg compound/kg bw/day); BW is Body Weight (g bw/animal) and FI is Daily Food Intake (g Diet/day). We finalized pterosilbene dose at 100 mg/kg diet.

Treatment

After series of carefully designed breeding strategies and genotyping, we collected *Pten*$^{+/f}$ male mice, which after simple randomization, were maintained on AIN 76A (n=21) and AIN 76A diet supplemented with pterostilbene (n=30) until sacrifice (chemoprevention design). For an intervention study we procured a total of 64 *Pten*$^{f/f}$ male mice maintained on AIN76A diet and employed by simple randomization with slightly larger allocation probability for treatment group. Mice were treated five days per week i.p with either 10% DMSO (vehicle control, n =31) or 10 mg/kg bw of pterostilbene (n = 33). The animals were started on treatment immediately after weaning for either 3 weeks (6 week-old), 7 weeks (10 week-old), 12 weeks (15 week-old), 17 weeks (20 week-old), 22 weeks (25 week-old) or 30 weeks (33 week-old). As an overall control, an additional group of littermates with *Cre*- negative *Pten*$^{+/f}$ or *Pten*$^{f/f}$ genotype, which possess normal prostates were also put on AIN 76A diet. Necropsy was performed at 8-10 months for *Pten*$^{+/f}$ and respective time points (3-30 weeks of treatment) for *Pten*$^{f/f}$ mice.

Mouse procedures

At the time of sacrifice, an abdominal midline incision was made and lower urogenital tract, including prostate, seminal vesicles and bladder was removed *en bloc* and washed with cold PBS. Dissection of different lobes of each prostate [left anterior prostate (AP_L); right AP (AP_R) and the entire dorso-latero-ventral (DLV) lobe] was done under dissecting microscope. Tissues were homogenized, and protein lysates were made using RIPA buffer. For histological analysis the urogenital system was fixed with 10% neutral-buffered formalin (see below). For visualization and isolation of lymph nodes, 15-week-old mice and older were anesthetized with 2.0% isoflurane, and 5% Evans Blue dye (Sigma-Aldrich) was injected s.c. into the mouse hind footpad [69]. After 30 min, mice were euthanized with CO_2 and dissected to locate lymph nodes of interest. The blue-labeled iliac and renal lymph nodes were removed, washed in PBS and fixed with 10% neutral-buffered formalin. To check for gross metastasis, a laparotomy was performed. Necropsy notes were collected for all animals with descriptions of the prostate, seminal vesicles, bladder and other organs or tissues showing any abnormalities. In addition, photographs were made of gross anatomy of mice urogenital systems. At the end, blood was collected and serum was obtained by centrifugation and stored at -80^{0}C.

Histopathology and immunohistochemistry

Tissue paraffin embedding, sectioning and H&E staining were performed by the Histology Core facility, Department of Pathology, UMMC. Sections (4 µm) were prepared from formalin-fixed paraffin embedded tissues and mounted on slides. Histological sections were prepared by hematoxylin and eosin (H&E) staining and were evaluated independently by two pathologists

(JML and JRL) who were blinded to the treatment. Immunohistochemistry was performed as described previously [9, 13] using antibodies against Ki-67, CK8, SMA, MTA1, pAkt, PTEN, AR, CD31; VEGF-C and cleaved caspase-3 (see "Antibodies" section), the Vectastain ABC Elite Kit and the ImmPACT DAB kit (Vector Laboratories). Images were viewed and recorded on Nikon Eclipse 80i microscope. The ImageTool software was used to count positively-stained cells in five randomly selected fields.

RNA analysis

Mouse prostates and cell pellets were harvested and immediately stored in RNA later (Sigma-Aldrich) at -80^{0}C until analysis. Prostate tissues were homogenized, after which total RNA fraction was isolated using the RNeasy mini kit (Qiagen). The quality of the RNA was determined on a Bio-Rad Experion analyzer. PCR was performed on a CFX96 Real Time PCR Detection System (Bio-Rad) using the primer sequences given in Supplementary Table S5, and fold changes in gene expression was determined using the $2^{-\Delta\Delta Ct}$ method [70].

Immunoblot analysis

Lysates were prepared from homogenized prostate tissues and the cell lines in the RIPA buffer containing protease and phosphatase inhibitor cocktail (ThermoFisher Scientific). 70 μg of protein was loaded in 10-15% SDS-PAGE and transferred onto polyvinylidene difluoride (PVDF) membranes. Membranes were incubated in 5% nonfat dry milk/TBST blocking buffer for 1 h at room temperature, followed by an overnight incubation at 4 ^{0}C in the presence of

corresponding antibodies (see "Antibodies" section). Membranes were washed with TBST and incubated in the presence of HRP-conjugated secondary antibodies. Signal detection was carried out using SuperSignal West Dura chemiluminescent substrate (ThermoFisher Scientific). Signal quantitation was conducted with Image J software (http://rsb.info.nih/gov/nih-image/).

Antibodies

Antibodies to the following markers were used for IHC and Western blots: rabbit MTA1 (D40D1) (Cell Signaling Technologies, #5647, 1:50 for IHC, 1:1000 for western blotting); rabbit p-Akt (D9E) (Cell Signaling Technologies, #4060, 1:50 for IHC, 1:1000 for western blotting); rabbit PTEN (D4.3) (Cell signaling Technologies, #9188, 1: 125 for IHC, 1:1000 for western blotting); rabbit AR (N-20) (Santa Cruz Biotechnologies, sc-816, 1:500 for IHC, 1:500 for western blotting); rabbit cleaved caspase-3 (D175)(5A1E) (Cell Signaling Technologies, #9664, 1:100 for IHC, 1:1000 for western blotting); rabbit Ki-67 (SP6) (Abcam, ab16667, 1:100 for IHC); rabbit SMA (Abcam, ab5694, 1:800 for IHC); rabbit CK8 (EP16284) (Abcam, ab53280, 1:800 for IHC), rabbit CD31 (SP-38) (Novus Biologicals, NBP1-49805, 1:500 for IHC); rabbit VEGF-C (Novus Biologicals, NB110-61022, 1:100 for IHC). The following antibodies were used for western blot analysis: rabbit Akt (C67E7) (Cell Signaling Technologies, #4691, 1:1000); rabbit Hsp70 (W27) (Santa Cruz Biotechnologies, sc-24, 1:1000); rabbit Hsp90 (H-114) (Santa Cruz Biotechnologies, sc-7947, 1:1000); rabbit Ac-p53 (Abcam, ab61241, 1:100); mouse p53 (3H2820) (Santa Cruz Biotechnologies, sc-71821, 1:100); mouse Bak (G-23) (Santa Cruz Biotechnologies, sc-832, 1:100); rabbit Vimentin (D21H3) (Cell Signaling Technologies, #5741, 1:1000), rabbit E-cadherin (24E10) (Cell Signaling Technologies, #3195,

1:1000); goat IL-1β (C-20) (Santa Cruz Biotechnologies, sc-1250, 1:200), rabbit NF-κB p65 (H-286) (Santa Cruz Biotechnologies, sc-7151, 1:200); rabbit p21 (C-19) (Santa Cruz Biotechnologies, sc-397, 1:100); mouse p27 (F-8) (Santa Cruz Biotechnologies, sc-1641, 1:100) , mouse Ets2 (E-5) (Santa Cruz Biotechnologies, sc-365666, 1:200); rabbit TGF-β1 (V) (Santa Cruz Biotechnologies, sc-146, 1:200); rabbit c-Myc (N-262) (Santa Cruz Biotechnologies, sc-764, 1:200), mouse hybridoma Notch2 (Developmental Studies Hybridoma Bank, University of Iowa, C651.6DbHN, 1:1000) and mouse Cyclin D1(BD Bioscience, #554180, 1:500).

Tissue/serum analysis of PTER concentrations by gas chromatography and mass spectrometry (GC-MS)

Prostate tissues and serum samples were collected at sacrifice, and kept at -80 ^{0}C until analysis. Extraction of pterostilbene from prostate tissues was performed following method in Dias *et al*. [10]. Analysis of pterostilbene in the extract was performed by GC-MS according to published procedures [13]. Extraction and analysis of pterostilbene in the serum was performed according to published procedures [13].

ChIP-Seq experiments and analysis

Pten$^{+/f}$ mouse prostates were isolated as described above and 200 mg of tissue was used to perform ChIP-Seq with MTA1 Ab (Bethyl Laboratories, A300-911A, 4 μg) at Active Motif. Reads were aligned to the mouse genome (mm10). Peak calling was performed using the SICER algorithm at a cutoff of FDR1E-10. The numbers of peaks identified was about 38,000 and

33,000 for MTA1 (Ctrl and PTER, respectively). The ChIP- Seq profiles presented were generated using the UCSC Genome browser.

Echo MRI analysis

Pten$^{+/f}$ male mice on Ctrl-Diet (n = 21) and on PTER-Diet (n = 30) were individually housed for weekly determination of body weight and body composition starting at 3 months of age until 12 months of age in order to examine any effect of pterostilbene diet supplementation on body weight regulation. Body composition was assessed weekly using magnetic resonance imaging (EchoMRI-900TM, Echo Medical System) to quantify lean mass, fat mass, free water and total water content in conscious mice.

GEO database analysis

We downloaded the raw expression dataset, GSE41967 [38] from GEO website. The base-2 logarithm transformation was applied to the raw expression data. The transformed expression data were further quantile normalized. Each pair of the selected genes were depicted in the scatter plots. The Spearman rank correlation coefficient was used for correlation assessment to accommodate the skewed distributions. The associated p value was calculated based on the null hypothesis of no correlation. We used the Bioconductor and the "normalize.quantiles" function in the "preprocessCore" package to process the expression data.

Statistical analysis

The histograms were depicted to assess the normality of continuous outcomes. The differences in continuous outcomes between the control and experimental groups were evaluated using the two-sample *t*-test, as well as the Welch's *t*-test when data exhibited unequal variances between the two groups. The Fisher's exact test was used to evaluate the effect of pterostilbene on cancer incidence. In power analysis it was determined that use of 18 mice in each of the vehicle control and pterostilbene injected groups would yield 86% power for confirming a significant association, under the assumption that the vehicle control and pterostilbene injection would be associated with 60% and 10% of adenocarcinoma incidence rates, respectively. Power analysis on mPIN incidence suggested that 7 mice per group and 80 glands per mouse would yield 95% of power for confirming a significant association, under the assumption that glands in the control and pterostilbene groups would be associated with 20% and 12% of mPIN incidence rate, respectively. The experiment of comparing the mRNA levels between the control and experimental groups involved multiple genes. The p values were not adjusted for multiple testing because our study of the gene effects was exploratory in nature. All p values were two-sided and p values less than 0.05 were considered as significant.

ACKNOWLEDGEMENTS

We are thankful to Dr. Z. He (UMMC, Department of Pathology) for preparing paraffin blocks and H&E staining, Dr. J.M. Docarmo (UMMC, Department of Biophysics and Physiology) for help with EchoMRI studies, and Dr. P. Labhart (Active Motif, CA) for his assistance in analyzing ChIP-Seq data. We would also like to thank Dr. K. Xu (UMMC, Cancer

Institute) for insightful suggestions on mice breeding. We are also grateful to Dr. R. Summers (UMMC) for his continued support.

CONFLICTS OF INTEREST

The authors declare no conflicts of interest

GRANT SUPPORT

This work was supported in part by the Department of Defense Prostate Cancer Research Program under Award # W81XWH-13-1-0370 to AS Levenson. Views and opinions of, and endorsements by the author(s) do not reflect those of the US Army of the Department of Defense.

REFERENCES

1. De Marzo AM, Platz EA, Sutcliffe S, Xu J, Gronberg H, Drake CG, Nakai Y, Isaacs WB,Nelson WG. Inflammation in prostate carcinogenesis. Nat Rev Cancer. 2007; 7: 256-269.
2. Nelson WG, Yegnasubramanian S, Agoston AT, Bastian PJ, Lee BH, Nakayama M,De Marzo AM. Abnormal DNA methylation, epigenetics, and prostate cancer. Front Biosci. 2007; 12: 4254-4266.
3. Powell IJ,Meyskens FL, Jr. African American men and hereditary/familial prostate cancer: Intermediate-risk populations for chemoprevention trials. Urology. 2001; 57: 178-181.

4. Xue Y, Wong J, Moreno GT, Young MK, Cote J,Wang W. NURD, a novel complex with both ATP-dependent chromatin-remodeling and histone deacetylase activities. Mol Cell. 1998; 2: 851-861.

5. Jang KS, Paik SS, Chung H, Oh YH,Kong G. MTA1 overexpression correlates significantly with tumor grade and angiogenesis in human breast cancers. Cancer Sci. 2006; 97: 374-379.

6. Toh Y, Kuwano H, Mori M, Nicolson GL,Sugimachi K. Overexpression of metastasis-associated MTA1 mRNA in invasive oesophageal carcinomas. Br J Cancer. 1999; 79: 1723-1726.

7. Sasaki H, Moriyama S, Nakashima Y, Kobayashi Y, Yukiue H, Kaji M, Fukai I, Kiriyama M, Yamakawa Y,Fujii Y. Expression of the MTA1 mRNA in advanced lung cancer. Lung Cancer. 2002; 35: 149-154.

8. Hofer MD, Kuefer R, Varambally S, Li H, Ma J, Shapiro GI, Gschwend JE, Hautmann RE, Sanda MG, Giehl K, Menke A, Chinnaiyan AM,Rubin MA. The role of metastasis-associated protein 1 in prostate cancer progression. Cancer Res. 2004; 64: 825-829.

9. Kai L, Wang J, Ivanovic M, Chung YT, Laskin WB, Schulze-Hoepfner F, Mirochnik Y, Satcher RL, Jr.,Levenson AS. Targeting prostate cancer angiogenesis through metastasis-associated protein 1 (MTA1). Prostate. 2011; 71: 268-280.

10. Dias SJ, Zhou X, Ivanovic M, Gailey MP, Dhar S, Zhang L, He Z, Penman AD, Vijayakumar S,Levenson AS. Nuclear MTA1 overexpression is associated with aggressive prostate cancer, recurrence and metastasis in African Americans. Sci Rep. 2013; 3: 2331.

11. Levenson AS, Kumar A,Zhang X. MTA family of proteins in prostate cancer: biology, significance, and therapeutic opportunities. Cancer Metastasis Rev. 2014; 33: 929-942.

12. Nair SS, Li DQ,Kumar R. A core chromatin remodeling factor instructs global chromatin signaling through multivalent reading of nucleosome codes. Mol Cell. 2013; 49: 704-718.

13. Li K, Dias SJ, Rimando AM, Dhar S, Mizuno CS, Penman AD, Lewin JR,Levenson AS. Pterostilbene acts through metastasis-associated protein 1 to inhibit tumor growth, progression and metastasis in prostate cancer. PLoS One. 2013; 8: e57542.

14. Moon HE, Cheon H,Lee MS. Metastasis-associated protein 1 inhibits p53-induced apoptosis. Oncol Rep. 2007; 18: 1311-1314.

15. Kai L, Samuel SK,Levenson AS. Resveratrol enhances p53 acetylation and apoptosis in prostate cancer by inhibiting MTA1/NuRD complex. Int J Cancer. 2010; 126: 1538-1548.

16. Yoo YG, Kong G,Lee MO. Metastasis-associated protein 1 enhances stability of hypoxia-inducible factor-1alpha protein by recruiting histone deacetylase 1. EMBO J. 2006; 25: 1231-1241.

17. Dhar S, Kumar A, Li K, Tzivion G,Levenson AS. Resveratrol regulates PTEN/Akt pathway through inhibition of MTA1/HDAC unit of the NuRD complex in prostate cancer. Biochim Biophys Acta. 2015; 1853: 265-275.

18. Ho E, Beaver LM, Williams DE,Dashwood RH. Dietary factors and epigenetic regulation for prostate cancer prevention. Adv Nutr. 2011; 2: 497-510.

19. Azzolini M, La Spina M, Mattarei A, Paradisi C, Zoratti M,Biasutto L. Pharmacokinetics and tissue distribution of pterostilbene in the rat. Mol Nutr Food Res. 2014; 58: 2122-2132.

20. Yeo SC, Ho PC,Lin HS. Pharmacokinetics of pterostilbene in Sprague-Dawley rats: the impacts of aqueous solubility, fasting, dose escalation, and dosing route on bioavailability. Mol Nutr Food Res. 2013; 57: 1015-1025.

21. Kapetanovic IM, Muzzio M, Huang Z, Thompson TN,McCormick DL. Pharmacokinetics, oral bioavailability, and metabolic profile of resveratrol and its dimethylether analog, pterostilbene, in rats. Cancer Chemother Pharmacol. 2011; 68: 593-601.

22. Dellinger RW, Garcia AM,Meyskens FL, Jr. Differences in the glucuronidation of resveratrol and pterostilbene: altered enzyme specificity and potential gender differences. Drug Metab Pharmacokinet. 2014; 29: 112-119.

23. Wang S, Gao J, Lei Q, Rozengurt N, Pritchard C, Jiao J, Thomas GV, Li G, Roy-Burman P, Nelson PS, Liu X,Wu H. Prostate-specific deletion of the murine Pten tumor suppressor gene leads to metastatic prostate cancer. Cancer Cell. 2003; 4: 209-221.

24. Manavathi B,Kumar R. Metastasis tumor antigens, an emerging family of multifaceted master coregulators. J Biol Chem. 2007; 282: 1529-1533.

25. Toh Y,Nicolson GL. The role of the MTA family and their encoded proteins in human cancers: molecular functions and clinical implications. Clin Exp Metastasis. 2009; 26: 215-227.

26. Varmus HE. The molecular genetics of cellular oncogenes. Annu Rev Genet. 1984; 18: 553-612.

27. Testa JR,Bellacosa A. AKT plays a central role in tumorigenesis. Proc Natl Acad Sci U S A. 2001; 98: 10983-10985.

28. Radtke F,Raj K. The role of Notch in tumorigenesis: oncogene or tumour suppressor? Nat Rev Cancer. 2003; 3: 756-767.

29. Dhulipal PD. Ets oncogene family. Indian J Exp Biol. 1997; 35: 315-322.

30. Neckers L. Chaperoning oncogenes: Hsp90 as a target of geldanamycin. Handb Exp Pharmacol. 2006; 259-277.

31. Bates S,Peters G. Cyclin D1 as a cellular proto-oncogene. Semin Cancer Biol. 1995; 6: 73-82.

32. Pakala SB, Bui-Nguyen TM, Reddy SD, Li DQ, Peng S, Rayala SK, Behringer RR,Kumar R. Regulation of NF-kappaB circuitry by a component of the nucleosome remodeling and deacetylase complex controls inflammatory response homeostasis. J Biol Chem. 2010; 285: 23590-23597.

33. Bui-Nguyen TM, Pakala SB, Sirigiri RD, Xia W, Hung MC, Sarin SK, Kumar V, Slagle BL,Kumar R. NF-kappaB signaling mediates the induction of MTA1 by hepatitis B virus transactivator protein HBx. Oncogene. 2010; 29: 1179-1189.

34. Bohonowych JE, Hance MW, Nolan KD, Defee M, Parsons CH,Isaacs JS. Extracellular Hsp90 mediates an NF-kappaB dependent inflammatory stromal program: implications for the prostate tumor microenvironment. Prostate. 2014; 74: 395-407.

35. Sears R, Nuckolls F, Haura E, Taya Y, Tamai K,Nevins JR. Multiple Ras-dependent phosphorylation pathways regulate Myc protein stability. Genes Dev. 2000; 14: 2501-2514.

36. Zhang XY, DeSalle LM, Patel JH, Capobianco AJ, Yu D, Thomas-Tikhonenko A,McMahon SB. Metastasis-associated protein 1 (MTA1) is an essential downstream effector of the c-MYC oncoprotein. Proc Natl Acad Sci U S A. 2005; 102: 13968-13973.

37. Zhu W, Cai MY, Tong ZT, Dong SS, Mai SJ, Liao YJ, Bian XW, Lin MC, Kung HF, Zeng YX, Guan XY,Xie D. Overexpression of EIF5A2 promotes colorectal carcinoma cell aggressiveness by upregulating MTA1 through C-myc to induce epithelial-mesenchymaltransition. Gut. 2012; 61: 562-575.

38. Powell IJ, Dyson G, Land S, Ruterbusch J, Bock CH, Lenk S, Herawi M, Everson R, Giroux CN, Schwartz AG,Bollig-Fischer A. Genes associated with prostate cancer are differentially

expressed in African American and European American men. Cancer Epidemiol Biomarkers Prev. 2013; 22: 891-897.

39. Reddy SD, Pakala SB, Molli PR, Sahni N, Karanam NK, Mudvari P,Kumar R. Metastasis-associated protein 1/histone deacetylase 4-nucleosome remodeling and deacetylase complex regulates phosphatase and tensin homolog gene expression and function. J Biol Chem. 2012; 287: 27843-27850.

40. Pakala SB, Singh K, Reddy SD, Ohshiro K, Li DQ, Mishra L,Kumar R. TGF-beta1 signaling targets metastasis-associated protein 1, a new effector in epithelial cells. Oncogene. 2011; 30: 2230-2241.

41. Wong SC, Chan JK, Lee KC,Hsiao WL. Differential expression of p16/p21/p27 and cyclin D1/D3, and their relationships to cell proliferation, apoptosis, and tumour progression in invasive ductal carcinoma of the breast. J Pathol. 2001; 194: 35-42.

42. Xiong Y, Hannon GJ, Zhang H, Casso D, Kobayashi R,Beach D. p21 is a universal inhibitor of cyclin kinases. Nature. 1993; 366: 701-704.

43. Gartel AL,Tyner AL. The role of the cyclin-dependent kinase inhibitor p21 in apoptosis. Mol Cancer Ther. 2002; 1: 639-649.

44. Nicholson B, Schaefer G,Theodorescu D. Angiogenesis in prostate cancer: biology and therapeutic opportunities. Cancer Metastasis Rev. 2001; 20: 297-319.

45. McMenamin ME, Soung P, Perera S, Kaplan I, Loda M,Sellers WR. Loss of PTEN expression in paraffin-embedded primary prostate cancer correlates with high Gleason score and advanced stage. Cancer Res. 1999; 59: 4291-4296.

46. Pourmand G, Ziaee AA, Abedi AR, Mehrsai A, Alavi HA, Ahmadi A,Saadati HR. Role of PTEN gene in progression of prostate cancer. Urol J. 2007; 4: 95-100.

47. Kinkade CW, Castillo-Martin M, Puzio-Kuter A, Yan J, Foster TH, Gao H, Sun Y, Ouyang X, Gerald WL, Cordon-Cardo C,Abate-Shen C. Targeting AKT/mTOR and ERK MAPK signaling inhibits hormone-refractory prostate cancer in a preclinical mouse model. J Clin Invest. 2008; 118: 3051-3064.

48. Tuncay Cagatay S, Cimen I, Savas B,Banerjee S. MTA-1 expression is associated with metastasis and epithelial to mesenchymal transition in colorectal cancer cells. Tumour Biol. 2013; 34: 1189-1204.

49. Li DQ, Pakala SB, Reddy SD, Ohshiro K, Peng SH, Lian Y, Fu SW,Kumar R. Revelation of p53-independent function of MTA1 in DNA damage response via modulation of the p21 WAF1-proliferating cell nuclear antigen pathway. J Biol Chem. 2010; 285: 10044-10052.

50. Sfanos KS,De Marzo AM. Prostate cancer and inflammation: the evidence. Histopathology. 2012; 60: 199-215.

51. Leav I, McNeal JE, Kwan PW, Komminoth P,Merk FB. Androgen receptor expression in prostatic dysplasia (prostatic intraepithelial neoplasia) in the human prostate: an immunohistochemical and in situ hybridization study. Prostate. 1996; 29: 137-145.

52. Manin M, Baron S, Goossens K, Beaudoin C, Jean C, Veyssiere G, Verhoeven G,Morel L. Androgen receptor expression is regulated by the phosphoinositide 3-kinase/Akt pathway in normal and tumoral epithelial cells. Biochem J. 2002; 366: 729-736.

53. Li P, Lee H, Guo S, Unterman TG, Jenster G,Bai W. AKT-independent protection of prostate cancer cells from apoptosis mediated through complex formation between the androgen receptor and FKHR. Mol Cell Biol. 2003; 23: 104-118.

54. Lin HK, Wang L, Hu YC, Altuwaijri S,Chang C. Phosphorylation-dependent ubiquitylation and degradation of androgen receptor by Akt require Mdm2 E3 ligase. EMBO J. 2002; 21: 4037-4048.

55. Kumar A, Lin SY, Dhar S, Rimando AM,Levenson AS. Stilbenes Inhibit Androgen Receptor Expression in 22Rv1 Castrate-resistant Prostate Cancer Cells. Journal of Medicinally Active Plants. 2014; 3: 1-8.

56. Jones PA. At the tipping point for epigenetic therapies in cancer. J Clin Invest. 2014; 124: 14-16.

57. Ahuja N, Easwaran H,Baylin SB. Harnessing the potential of epigenetic therapy to target solid tumors. J Clin Invest. 2014; 124: 56-63.

58. Campbell RM,Tummino PJ. Cancer epigenetics drug discovery and development: the challenge of hitting the mark. J Clin Invest. 2014; 124: 64-69.

59. Lin VC, Tsai YC, Lin JN, Fan LL, Pan MH, Ho CT, Wu JY,Way TD. Activation of AMPK by pterostilbene suppresses lipogenesis and cell-cycle progression in p53 positive and negative human prostate cancer cells. J Agric Food Chem. 2012; 60: 6399-6407.

60. Chakraborty A, Gupta N, Ghosh K,Roy P. In vitro evaluation of the cytotoxic, anti-proliferative and anti-oxidant properties of pterostilbene isolated from Pterocarpus marsupium. Toxicol In Vitro. 2010; 24: 1215-1228.

61. Wang TT, Schoene NW, Kim YS, Mizuno CS,Rimando AM. Differential effects of resveratrol and its naturally occurring methylether analogs on cell cycle and apoptosis in human androgen-responsive LNCaP cancer cells. Mol Nutr Food Res. 2010; 54: 335-344.

62. Chang J, Rimando A, Pallas M, Camins A, Porquet D, Reeves J, Shukitt-Hale B, Smith MA, Joseph JA,Casadesus G. Low-dose pterostilbene, but not resveratrol, is a potent neuromodulator in aging and Alzheimer's disease. Neurobiol Aging. 2012; 33: 2062-2071.

63. Remsberg CM, Yanez JA, Ohgami Y, Vega-Villa KR, Rimando AM,Davies NM. Pharmacometrics of pterostilbene: preclinical pharmacokinetics and metabolism, anticancer, antiinflammatory, antioxidant and analgesic activity. Phytother Res. 2008; 22: 169-179.

64. Riche DM, Riche KD, Blackshear CT, McEwen CL, Sherman JJ, Wofford MR,Griswold ME. Pterostilbene on metabolic parameters: a randomized, double-blind, and placebo-controlled trial. Evid Based Complement Alternat Med. 2014; 2014: 459165.

65. Riche DM, McEwen CL, Riche KD, Sherman JJ, Wofford MR, Deschamp D,Griswold M. Analysis of safety from a human clinical trial with pterostilbene. J Toxicol. 2013; 2013: 463595.

66. Joseph JA, Fisher DR, Cheng V, Rimando AM,Shukitt-Hale B. Cellular and behavioral effects of stilbene resveratrol analogues: implications for reducing the deleterious effects of aging. J Agric Food Chem. 2008; 56: 10544-10551.

67. Patel KR, Brown VA, Jones DJ, Britton RG, Hemingway D, Miller AS, et al. Clinical pharmacology of resveratrol and its metabolites in colorectal cancer patients. Cancer Res. 2010; 70: 7392-7399.

68. Reagan-Shaw S, Nihal M,Ahmad N. Dose translation from animal to human studies revisited. FASEB J. 2008; 22: 659-661.

69. Harrell MI, Iritani BM,Ruddell A. Lymph node mapping in the mouse. J Immunol Methods. 2008; 332: 170-174.

70. Livak KJ,Schmittgen TD. Analysis of relative gene expression data using real-time quantitative PCR and the 2(-Delta Delta C(T)) Method. Methods. 2001; 25: 402-408.

FIGURE LEGENDS

Figure 1: MTA1 promotes the *Pten* loss-driven prostate tumorigenesis and cancer progression. A. Comparison of H&E and IHC of MTA1, p-Akt and PTEN in the prostates from 10-month-old *Pten*$^{+/f}$ mice and Cre-negative normal prostate (NP) controls. Scale bars, 100 μm. **B.** Immunoblots of MTA1, PTEN, p-Akt, Akt, AR, c-Myc, CyclinD1, TGFβ1, Notch2, Ets2, and Hsp90 and **C**. qRT-PCR analysis of MTA1, Akt1, c-Myc, Ets2 and Hsp90 mRNA levels in the prostate tissues from 10-month-old *Pten*$^{+/f}$ mice compared to NP controls. **D**. Comparison of H&E, MTA1, and p-Akt staining in the prostate tissues from 10-week-old *Pten*$^{f/f}$ mice and NP controls. Scale bars, 100 μm. **E.** Immunoblots of MTA1, p-Akt, Akt, AR, NF-κB (p65), IL-1β, Hsp90, E-cadherin (E-cad) and Vimentin in the prostate tissues from *Pten*$^{f/f}$ mice compared to NP controls, isolated at the ages mentioned. Hsp70 was used as a loading control. qRT-PCR data represent the mean ± SEM (n = 3), *$p < 0.05$ (two-tailed, two-sample t-test).

Figure 2: MTA1 directly regulates key molecular drivers of tumor promotion. A. Immunoblots of MTA1, NF-κB (p65), IL-1β, Hsp90, E-cadherin (E-cad), Vimentin, c-Myc, Cyclin D1, Notch2, and Ets2 in LNCaP (left) and DU145 (right) cells expressing (EV) and silenced for MTA1 (shMTA1). **B**. qRT-PCR of MTA1, Ets2, Akt1, Notch2, c-Myc, Cyclin D1

and Hsp90 mRNA levels in LNCaP (top) and DU145 (bottom) EV and shMTA1 cells. **C**. Immunoblot of MTA1, p-Akt and Akt in LNCaP EV and shMTA1 cells. **D**. Immunoblot of p-Akt, Akt, c-Myc and MTA1 and **E**. qRT-PCR of MTA1 mRNA levels in PC3M cells treated with vehicle (DMSO) and LY (LY294002). **F.** Proposed mechanism involved in *Pten* loss-induced upregulation of MTA1, exhibiting the MTA1-Akt and MTA1-c-Myc feed-forward signaling loops (blue arrows), putative Akt-MTA1 link (dotted arrow). β-actin was used as a loading control. qRT-PCR data represent the mean ± SEM (n = 3), *$p < 0.05$; **$p < 0.01$ (two-tailed, two-sample t-test).

Figure 3: GEO analyses for correlation of MTA1 with PTEN, AKT1 and AR. GSE41967 study of human prostate tissues (n=639)[38] was used. Scatter plot depicting **A.** strong negative correlation between MTA1 and PTEN ($r = -0.349$, whole cohort), which becomes stronger with increased Gleason score ($r = -0.299$, Gleason < 7; $r = -0.348$, Gleason = 7; $r = -0.433$, Gleason > 7, $p < 0.001$); **B**. positive MTA1 correlation with AKT1 expression ($r = 0.499$, whole cohort, $p < 0.001$); and no correlation between MTA1 and AR ($r = 0.021$, whole cohort. $p = 0.592$). p values were calculated using two-tailed one-sample z-test for a correlation coefficient.

Figure 4: Pterostilbene reduces PIN formation in *Pten*$^{+/f}$ and blocks progression to adenocarcinoma in *Pten*$^{f/f}$ mice. **A**. Gross anatomy (top) and ex vivo images (middle) of urogenital system (UGS) and dissected prostate lobes (AP_R, right anterior; AP_L, left anterior, and DLV, dorso-latero-ventral) (bottom) of the representative prostates from 10-month-old *Pten*$^{+/f}$ mice on phytoestrogen free AIN76 diet (Ctrl-Diet) and 100 mg/kg diet supplementation with pterostilbene (PTER-Diet). **B**. Percentage of prostate glands from 10-month-old *Pten*$^{+/f}$ mice on

Ctrl- (n = 6) and PTER-Diet (n = 7) involved in high grade mouse PIN (mPIN). $p < 0.001$ (Fisher's exact test). **C.** Comparison of H&E prostate histology and PTEN staining in representative 10-month-old mice with NP and *Pten*$^{+/f}$ mice on Ctrl- and PTER-Diet. Scale bars, 100 μm. **D**. Gross anatomy of the representative UGS from 10-week-old (top) and 33-week-old (middle) *Pten*$^{f/f}$ mice treated with vehicle (DMSO) and 10 mg/kg bw PTER. Representative images of dissected prostate lobes of *Pten*$^{f/f}$ mice (bottom). **E.** Comparison of UGS weights of vehicle or PTER treated *Pten*$^{f/f}$ mice, isolated at the indicated ages (n = 3/group). *$p < 0.05$ (two-tailed, two-sample t-test). **F**. Incidence of mPIN, pre-invasive and invasive adenocarcinoma (AC) in *Pten*$^{f/f}$ mice treated with vehicle (n = 19) and PTER (n = 18). $p < 0.01$ (Fisher's exact test). **G**. Comparison of H&E, smooth muscle actin (SMA) and cytokeratin 8 (CK8) staining from representative 6-, 10- and 25-week-old mice with NP and vehicle or PTER treated *Pten*$^{f/f}$ mice. Arrows indicate loss of SMA staining and CK8 positive luminal cells in the stroma of vehicle treated *Pten*$^{f/f}$ mice as signs of invasiveness. Scale bars, 100 μm.

Figure 5: Inhibition of MTA1 and its associated signaling by pterostilbene (PTER) in *Pten*$^{+/f}$ mice. A. Immunoblots of MTA1, PTEN, p-Akt, Akt, AR, c-Myc, CyclinD1, TGFβ1, Notch2, Ets2, and Hsp90 of prostate tissues from representative 10-month-old *Pten*$^{+/f}$ mice on Ctrl- and PTER-Diet. Hsp70 was a loading control. **B.** Comparison of MTA1, p-Akt and AR IHC staining of the prostate sections from representative 10-month-old *Pten*$^{+/f}$ mice on Ctrl- and PTER-Diet. NP, normal prostate. Scale bars, 100 μm. **C.** qRT-PCR of PTEN and MTA1 mRNA levels in prostate tissues from 10-month-old *Pten*$^{+/f}$ mice on Ctrl- and PTER-Diet. Data are mean ± SEM (n = 3), *$p < 0.05$; **$p < 0.01$ (two-tailed, two-sample t-test). **D.** Comparative analysis of MTA1 binding in the prostate tissues of *Pten*$^{+/f}$ mice on Ctrl- and PTER-Diet. Representative

MTA1 ChIP-Seq tracks for Pten, Akt1, c-Myc, CyclinD1, Notch2, Ets2 and Hsp90 gene loci at 10 kb resolution are shown. **E.** Quantitation of MTA1, p-Akt/Akt and AR expression in prostate lobes of 10 month-old *Pten*$^{+/f}$ mice on Ctrl- and PTER-Diet (see F). Data represent the mean ± SEM (n = 3), *p < 0.05; **p < 0.01 (two-tailed, two-sample t-test). **F.** Immunoblots of MTA1, p-Akt, Akt and AR in the dissected prostatic lobes (AP_R, right anterior; AP_L, left anterior, and DLV, dorso-latero-ventral) from 10-month-old *Pten*$^{+/f}$ mice on Ctrl- and PTER-Diet. Hsp70 was used as a loading control.

Figure 6: Inhibition of MTA1 and its associated signaling by pterostilbene (PTER) in *Pten*$^{f/f}$ mice. **A**. Immunoblots of MTA1, p-Akt, Akt, AR, IL-1β, Hsp90 and E-cadherin (E-cad) in the prostate tissues of vehicle and PTER treated *Pten*$^{f/f}$ mice, isolated at indicated ages. Hsp70 was a loading control. **B**. Comparative analysis of MTA1 binding in the prostate tissues of *Pten*$^{+/f}$ mice on Ctrl- and PTER-Diet. Representative MTA1 ChIP-Seq tracks for IL-1β, E-cadherin and Vimentin gene loci at 10 kb resolution are shown. **C**. Comparison of IHC staining of MTA1, p-Akt and AR in the prostate sections with carcinoma lesions from representative 10-, 25- and 33-week old vehicle or PTER treated *Pten*$^{f/f}$ mice and NP controls. Scale bars, 100 μm. **D**. Immunoblots of MTA1, p-Akt, Akt and AR in the dissected prostate lobes from vehicle or PTER-treated 10- and 25-week-old *Pten*$^{f/f}$ mice. Hsp70 was used as a loading control. For quantitation of MTA1, p-Akt/Akt and AR expression in prostate lobes of *Pten*$^{f/f}$ mice at different ages (n =3/group) see Supplementary Figure 5.

Figure 7: Pterostilbene significantly inhibits MTA1-dependent cell proliferation and induces MTA1-targeted apoptosis in *Pten*$^{+/f}$ mice. A. Representative Ki-67 (top) and cleaved

Caspase-3 (bottom) staining of prostate tissues from 10-month-old *Pten*$^{+/f}$ mice on Ctrl- and PTER-Diet. Scale bars, 100 μm (Ki-67) and 50 μm (cleaved Caspase-3). **B**. Quantitation of Ki-67 (left) and cleaved Caspase-3 (right) positive cells of prostate tissues from 10-month-old *Pten*$^{+/f}$ mice on Ctrl- and PTER-Diet (n = 5/group). **C**. Immunoblots of total and cleaved Caspase-3 in prostate tissues of 10-month-old *Pten*$^{+/f}$ mice on Ctrl- and PTER-Diet. **D**. Immunoblots of p21 and p27 in the prostate tissues of 10-month-old *Pten*$^{+/f}$ mice compared to NP controls (left) and mice on Ctrl- and PTER-Diet (right). **E**. Comparative analysis of MTA1 binding in the prostate tissues of *Pten*$^{+/f}$ mice on Ctrl- and PTER-Diet. Representative ChIP-Seq tracks for p21 and p27 gene loci at 10 kb resolution are shown. **F**. Immunoblots of p21 and p27 in LNCaP (top) and DU145 (bottom) cells expressing (EV) and silenced for MTA1 (shMTA1). **G**. qRT-PCR of p21 and p27 mRNA levels in cells expressing MTA1 and silenced for MTA1 (shMTA1). Data are mean ± SEM (n = 3), *p < 0.05; **p < 0.01 (two-tailed, two-sample t-test).

Figure 8: Pterostilbene significantly inhibits MTA1-dependent cell proliferation and angiogenesis and induces MTA1-targeted apoptosis in *Pten*$^{f/f}$ mice. A. Representative Ki-67 (top, each panel), CD31 (middle, each panel) and VEGF-C (bottom, each panel) staining of the prostate tissues from *Pten*$^{f/f}$ mice treated with vehicle and PTER, at indicated ages. Arrows indicate vessels. Scale bars, 100 μm. **B**. Quantitation of Ki-67 (top) and CD31 (bottom) positive cells of prostate tissues from mice treated with vehicle and PTER (n = 5/group). **C**. Representative images and **D**. Quantitation of cleaved Caspase-3 staining at the indicated ages of vehicle and PTER treated *Pten*$^{f/f}$ mice (n =5/group). Scale bars, 10 μm. Data are mean ± SEM (n = 3), *p < 0.05; **p < 0.01; ***p < 0.001 (two-tailed, two-sample t-test). **E.** Immunoblots of MTA1, Ac-p53, p53 and Bak in the prostate tissues from vehicle and PTER treated *Pten*$^{f/f}$ mice,

isolated at the indicated ages. NP, normal prostate. Hsp70 and β-actin were used as loading controls from prostate tissues and cell lysates, respectively. **F**. Densitometry of the Ac-p53/p53 ratio from the representative blot. **G**. Comparative analysis of MTA1 binding in the prostate tissues of *Pten*$^{+/f}$ mice on Ctrl- and PTER-Diet. Representative MTA1 ChIP-Seq tracks for Vegf-c gene locus at 10 kb resolution are shown.

Figure 9: Schematic representation of MTA1-targeted effects of pterostilbene in prostate cancer. Significantly increased levels of MTA1, a key upstream epigenetic regulator, promote inflammation, tumorigenesis, EMT, angiogenesis, and survival signaling and repress apoptosis. Pterostilbene (PTER) targets MTA1 and MTA1-guided molecular drivers of tumor promotion, thereby blocking the *Pten* loss-driven prostate tumorigenesis and cancer progression.

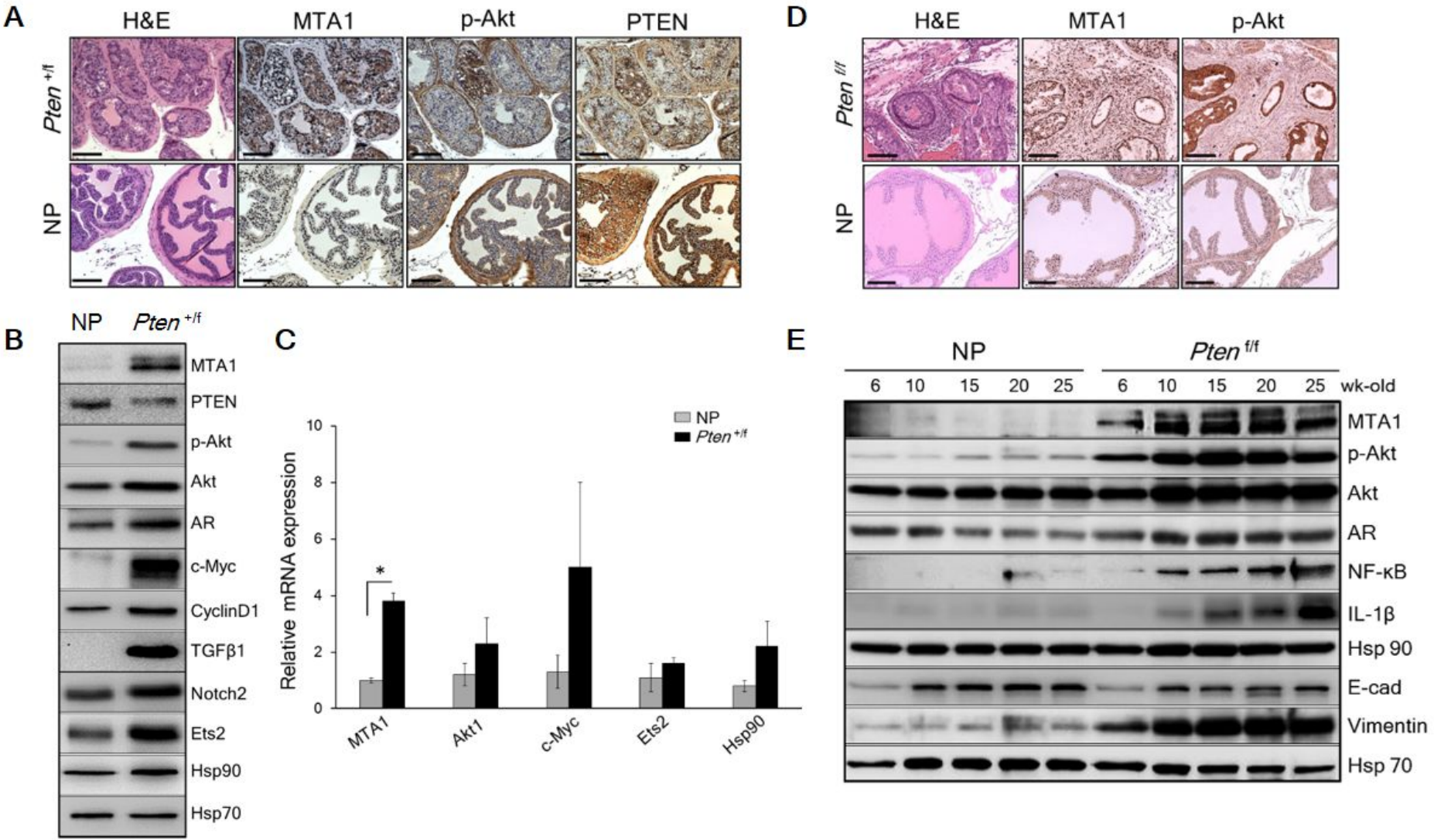
A
H&E
MTA1
p-Akt
PTEN
Pten +/f
NP
D
H&E
MTA1
p-Akt
Pten f/f
NP
B
NP
Pten +/f
MTA1
PTEN
p-Akt
Akt
AR
c-Myc
CyclinD1
TGFβ1
Notch2
Ets2
Hsp90
Hsp70
C
NP
Pten +/f
Relative mRNA expression
10
8
6
4
2
0
*
MTA1
Akt1
c-Myc
Ets2
Hsp90
E
NP
Pten f/f
6 10 15 20 25 6 10 15 20 25 wk-old
MTA1
p-Akt
Akt
AR
NF-κB
IL-1β
Hsp 90
E-cad
Vimentin
Hsp 70

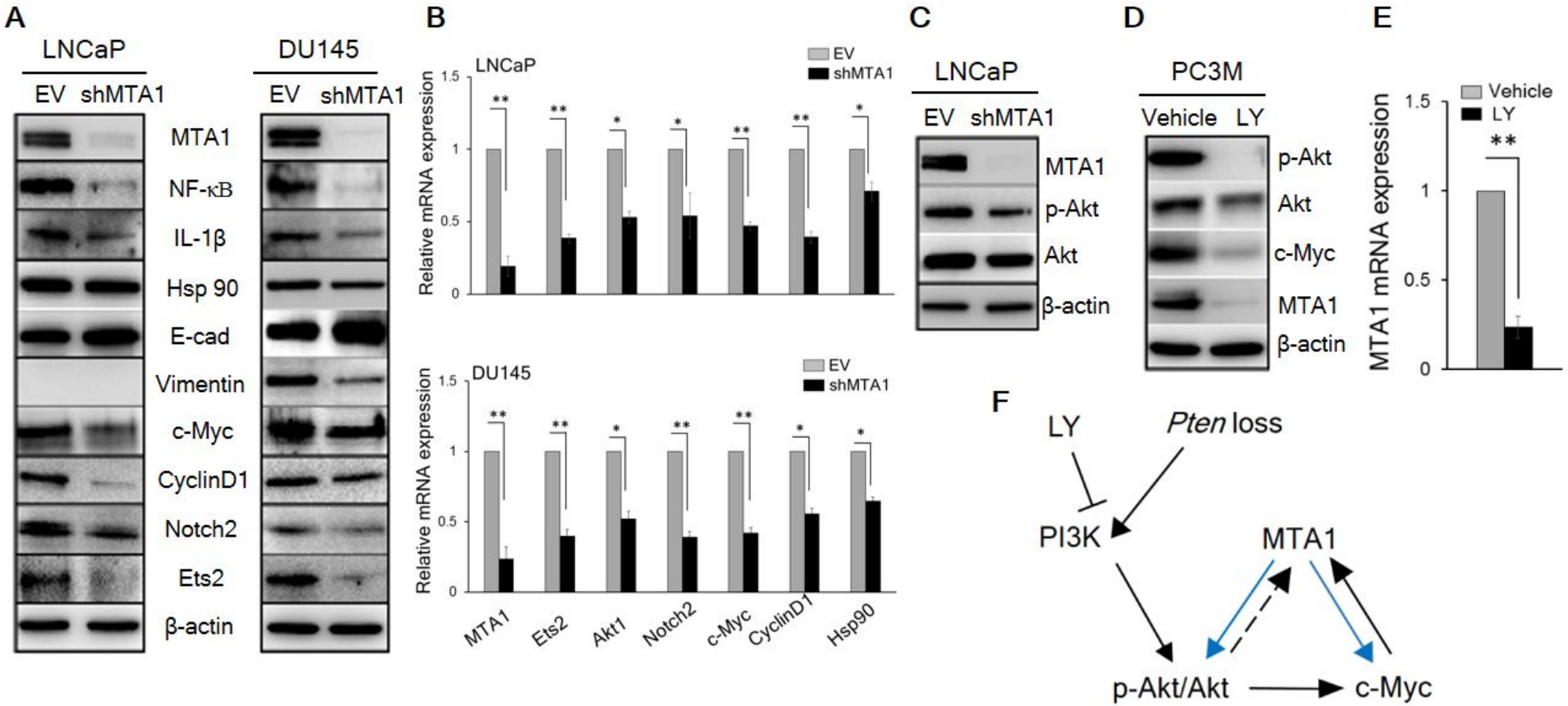
A
LNCaP
DU145
EV shMTA1
EV shMTA1
MTA1
NF-κB
IL-1β
Hsp 90
E-cad
Vimentin
c-Myc
CyclinD1
Notch2
Ets2
β-actin
B
LNCaP
EV
shMTA1
Relative mRNA expression
DU145
MTA1
Ets2
Akt1
Notch2
c-Myc
CyclinD1
Hsp90
C
LNCaP
EV shMTA1
MTA1
p-Akt
Akt
β-actin
D
PC3M
Vehicle LY
p-Akt
Akt
c-Myc
MTA1
β-actin
E
Vehicle
LY
MTA1 mRNA expression
F
LY
Pten loss
PI3K
MTA1
p-Akt/Akt
c-Myc

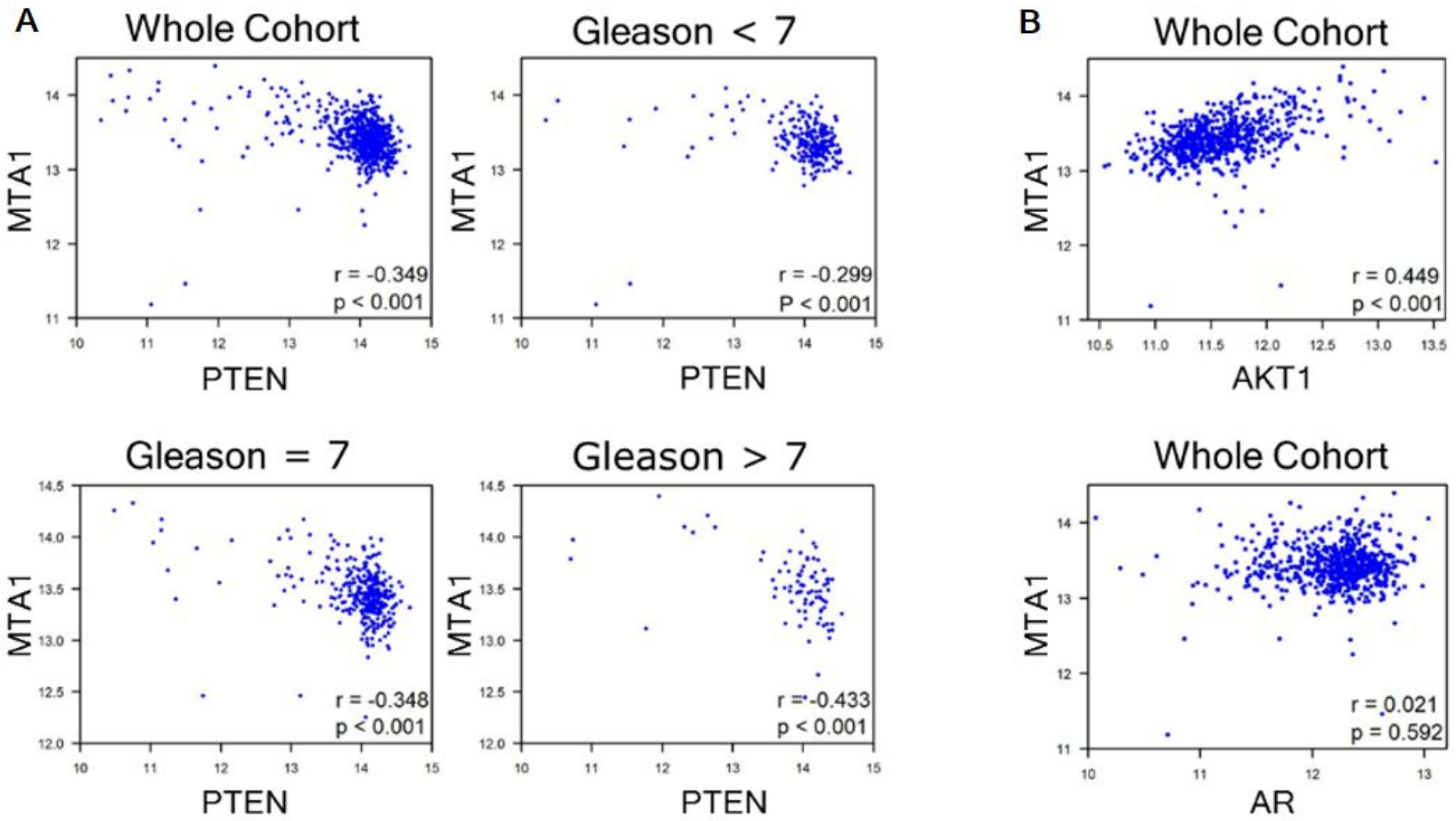
A
Whole Cohort
MTA1
PTEN
r = -0.349
p < 0.001
Gleason < 7
MTA1
PTEN
r = -0.299
P < 0.001
Gleason = 7
MTA1
PTEN
r = -0.348
p < 0.001
Gleason > 7
MTA1
PTEN
r = -0.433
p < 0.001
B
Whole Cohort
MTA1
AKT1
r = 0.449
p < 0.001
Whole Cohort
MTA1
AR
r = 0.021
p = 0.592

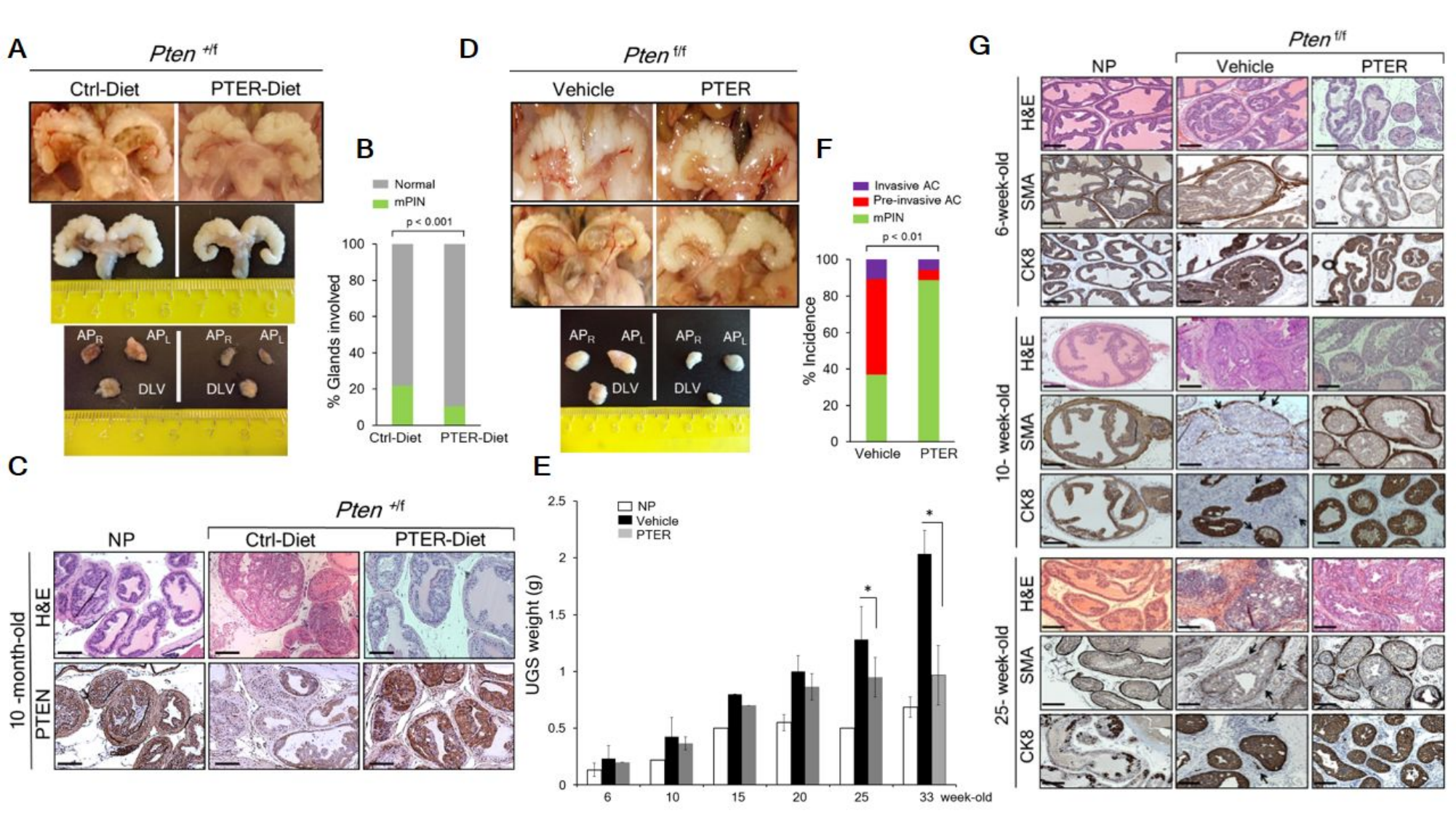
A
Pten +/f
Ctrl-Diet
PTER-Diet
AP_R
AP_L
DLV
B
Normal
mPIN
p < 0.001
% Glands involved
Ctrl-Diet
PTER-Diet
C
Pten +/f
NP
Ctrl-Diet
PTER-Diet
10 -month-old
H&E
PTEN
D
Pten f/f
Vehicle
PTER
E
NP
Vehicle
PTER
UGS weight (g)
week-old
F
Invasive AC
Pre-invasive AC
mPIN
p < 0.01
% Incidence
G
Pten f/f
6-week-old
10- week-old
25- week-old
SMA
CK8

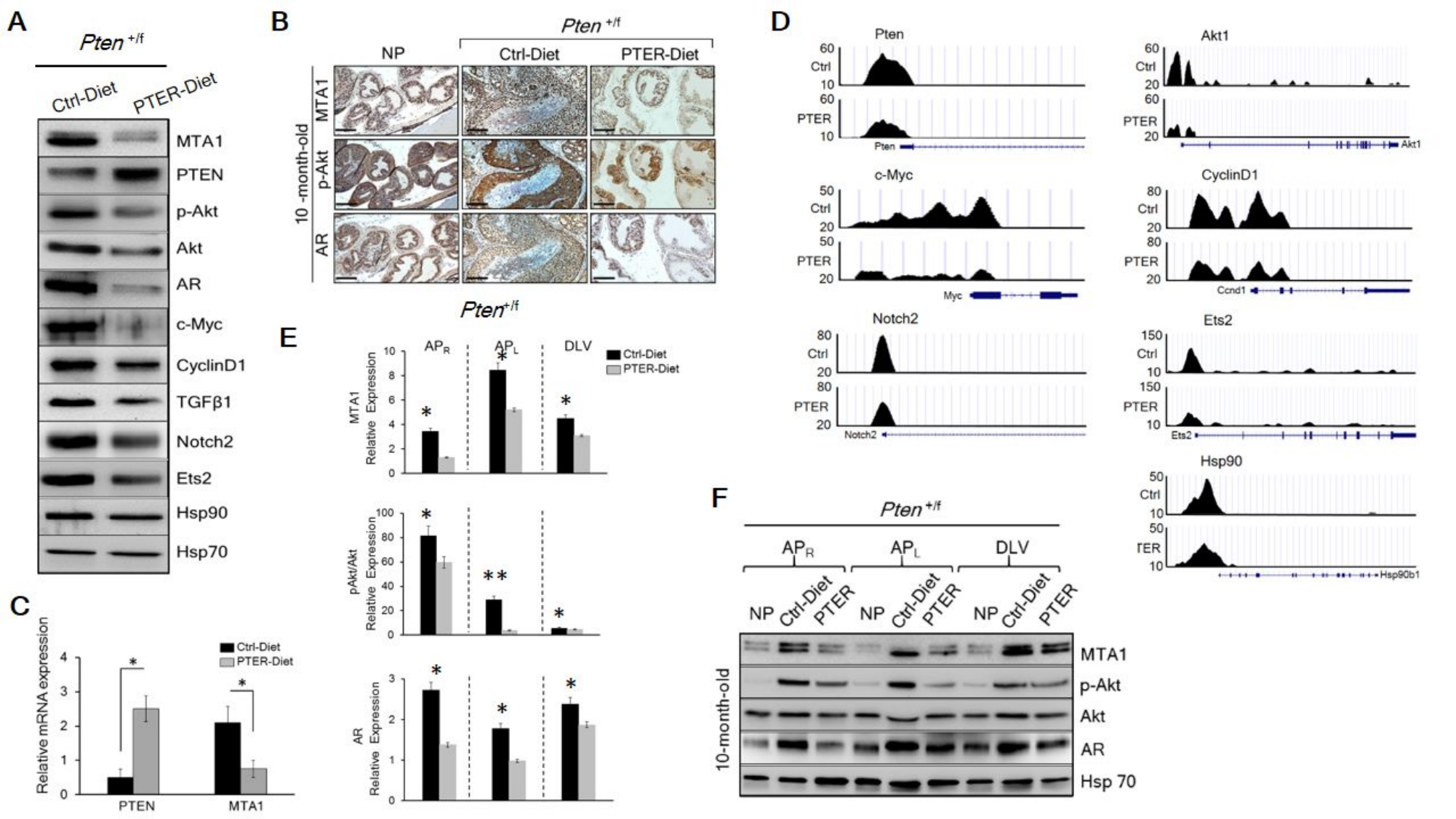
A
Pten +/f
Ctrl-Diet
PTER-Diet
MTA1
PTEN
p-Akt
Akt
AR
c-Myc
CyclinD1
TGFβ1
Notch2
Ets2
Hsp90
Hsp70
B
Pten +/f
NP
Ctrl-Diet
PTER-Diet
10 -month-old
MTA1
p-Akt
AR
C
Relative mRNA expression
Ctrl-Diet
PTER-Diet
PTEN
MTA1
E
Pten+/f
APR
APL
DLV
Ctrl-Diet
PTER-Diet
MTA1 Relative Expression
pAkt/Akt Relative Expression
AR Relative Expression
D
Pten
Ctrl
PTER
Akt1
c-Myc
CyclinD1
Notch2
Ets2
Hsp90
F
Pten +/f
APR
APL
DLV
NP
Ctrl-Diet
PTER
10-month-old
MTA1
p-Akt
Akt
AR
Hsp 70

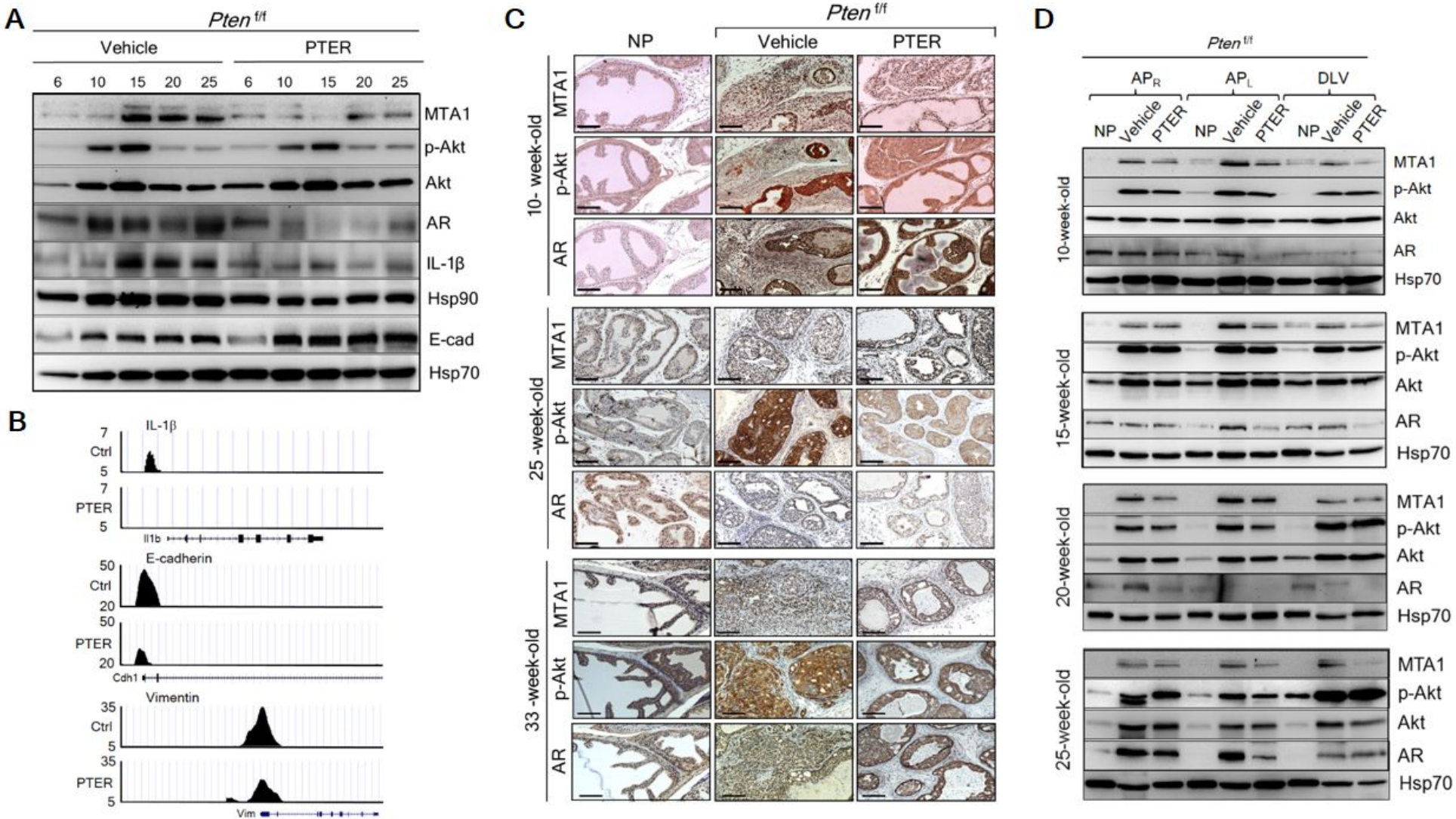
A
Pten f/f
Vehicle
PTER
6 10 15 20 25 6 10 15 20 25
MTA1
p-Akt
Akt
AR
IL-1β
Hsp90
E-cad
Hsp70
B
IL-1β
Ctrl
PTER
Il1b
E-cadherin
Cdh1
Vimentin
Vim
C
Pten f/f
NP
Vehicle
PTER
10- week-old
25 -week-old
33 -week-old
MTA1
p-Akt
AR
D
Pten f/f
AP_R
AP_L
DLV
NP Vehicle PTER NP Vehicle PTER NP Vehicle PTER
10-week-old
15-week-old
20-week-old
25-week-old
MTA1
p-Akt
Akt
AR
Hsp70

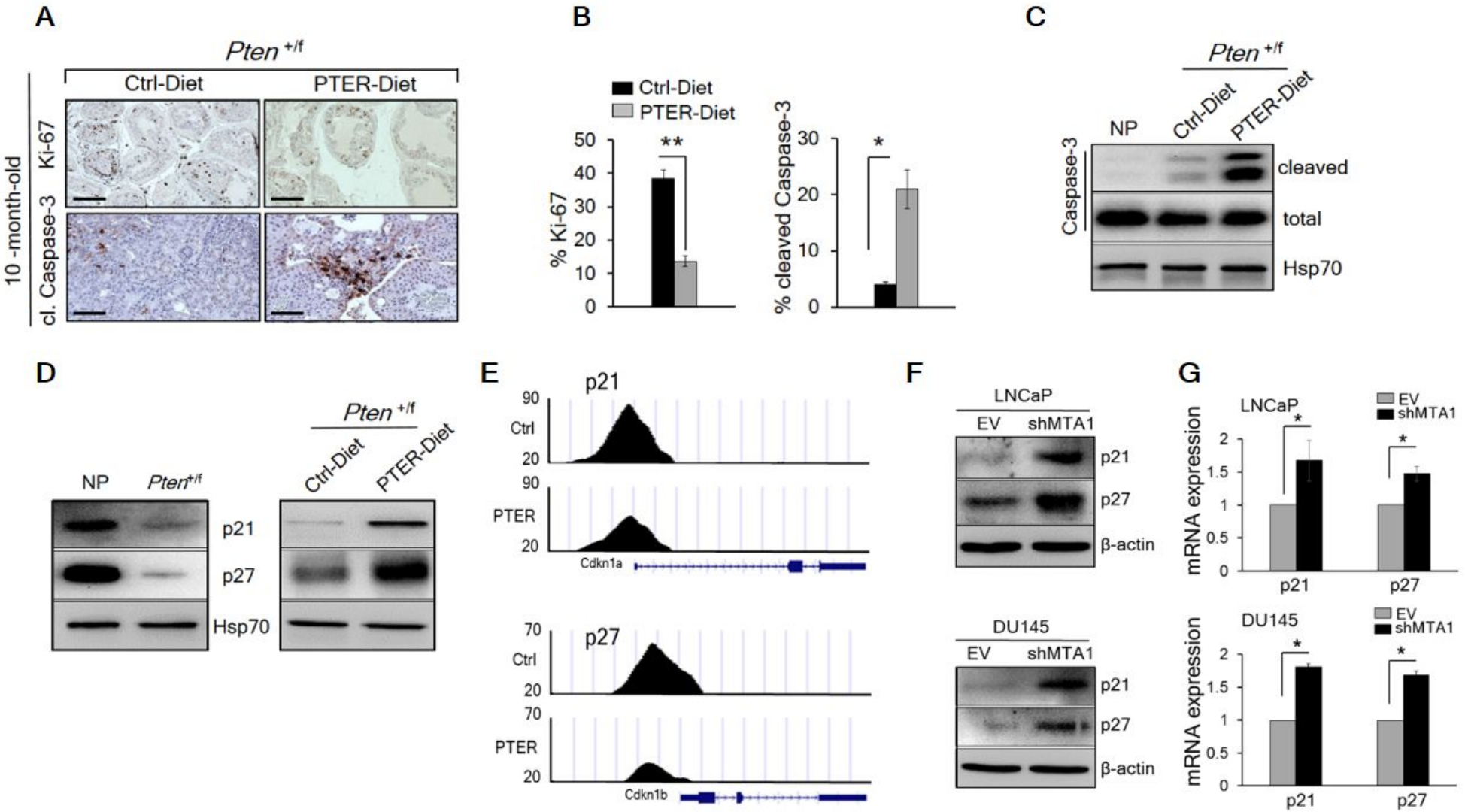
A
Pten +/f
Ctrl-Diet
PTER-Diet
10 -month-old
Ki-67
cl. Caspase-3
B
Ctrl-Diet
PTER-Diet
% Ki-67
% cleaved Caspase-3
C
Pten +/f
NP
Ctrl-Diet
PTER-Diet
Caspase-3
cleaved
total
Hsp70
D
Pten +/f
NP
Pten+/f
Ctrl-Diet
PTER-Diet
p21
p27
Hsp70
E
p21
Ctrl
PTER
Cdkn1a
p27
Cdkn1b
F
LNCaP
EV
shMTA1
p21
p27
β-actin
DU145
G
LNCaP
DU145
EV
shMTA1
mRNA expression
p21
p27

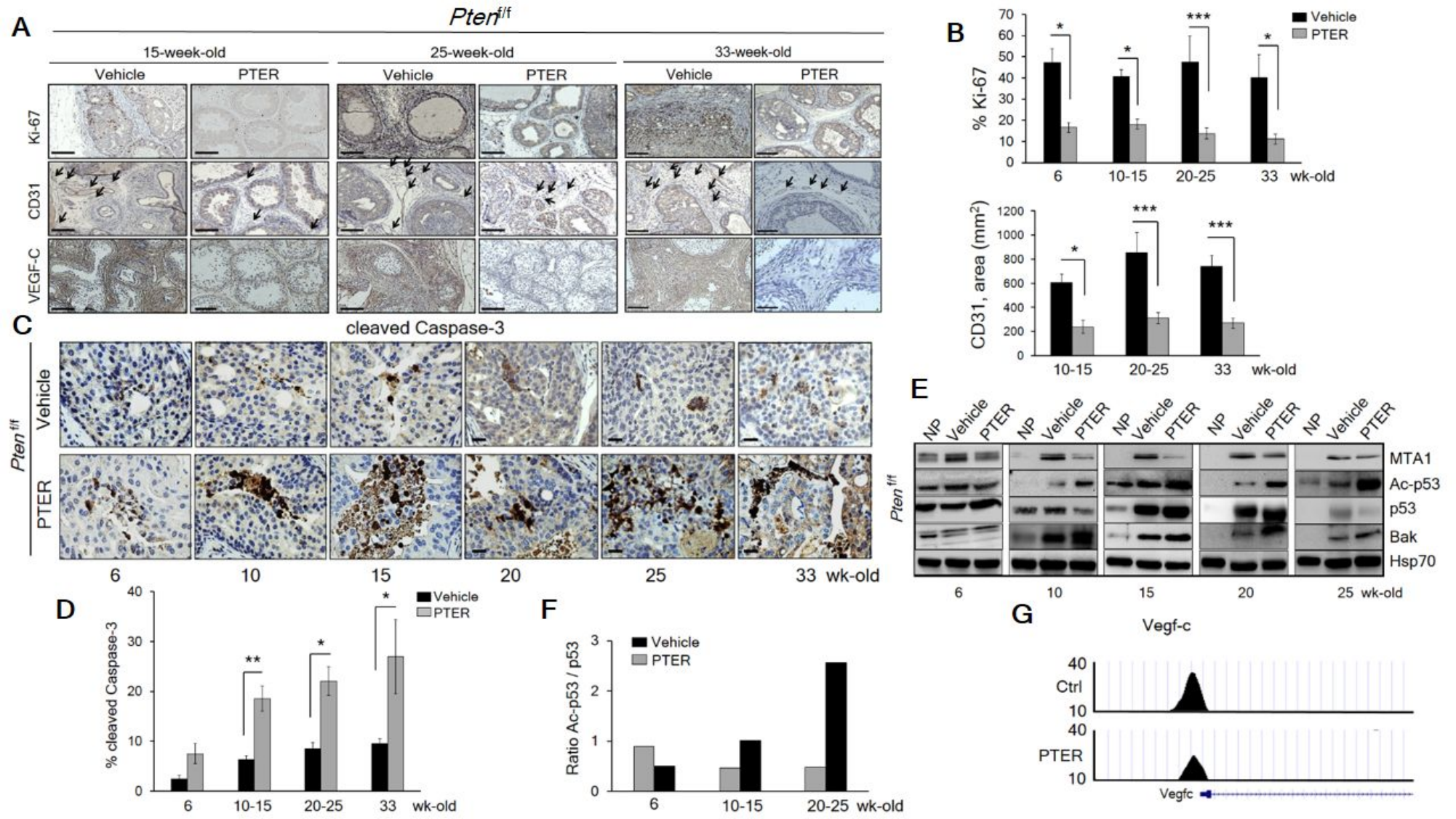
A
Pten f/f
15-week-old
25-week-old
33-week-old
Vehicle
PTER
Ki-67
CD31
VEGF-C
B
% Ki-67
Vehicle
PTER
6
10-15
20-25
33
wk-old
CD31, area (mm²)
C
cleaved Caspase-3
Pten f/f
Vehicle
PTER
6
10
15
20
25
33 wk-old
D
% cleaved Caspase-3
E
NP
Vehicle
PTER
MTA1
Ac-p53
p53
Bak
Hsp70
F
Ratio Ac-p53 / p53
G
Vegf-c
Ctrl
PTER
Vegfc

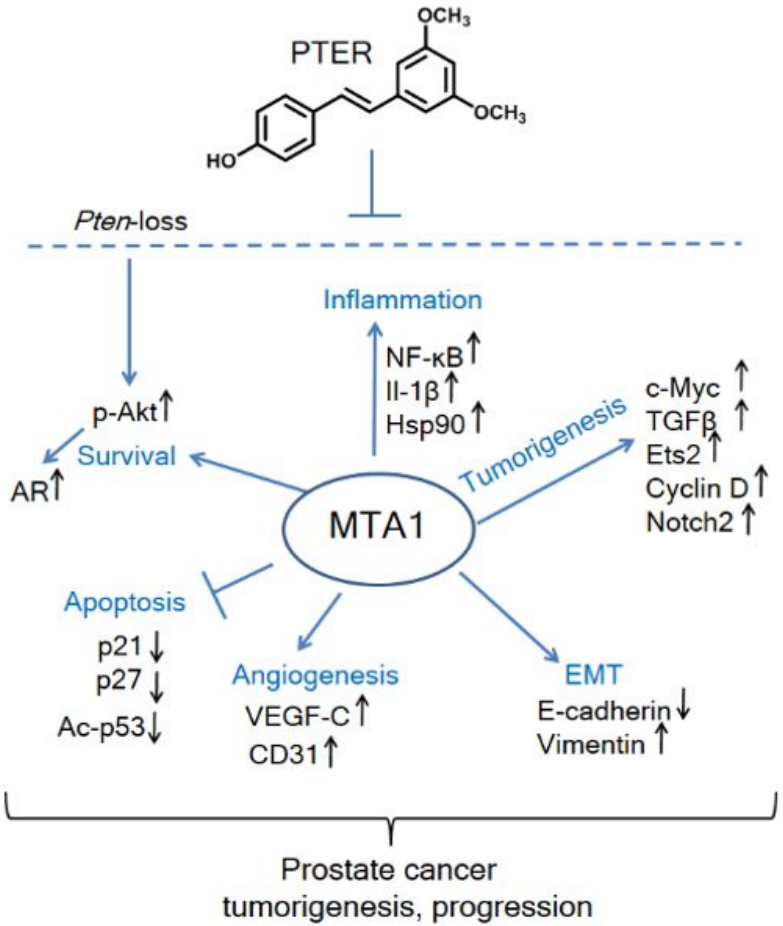
PTER
OCH3
OCH3
HO
Pten-loss
Inflammation
NF-κB↑
Il-1β↑
Hsp90↑
p-Akt↑
Survival
AR↑
MTA1
Tumorigenesis
c-Myc ↑
TGFβ ↑
Ets2↑
Cyclin D↑
Notch2↑
Apoptosis
p21↓
p27↓
Ac-p53↓
Angiogenesis
VEGF-C↑
CD31↑
EMT
E-cadherin↓
Vimentin↑
Prostate cancer
tumorigenesis, progression

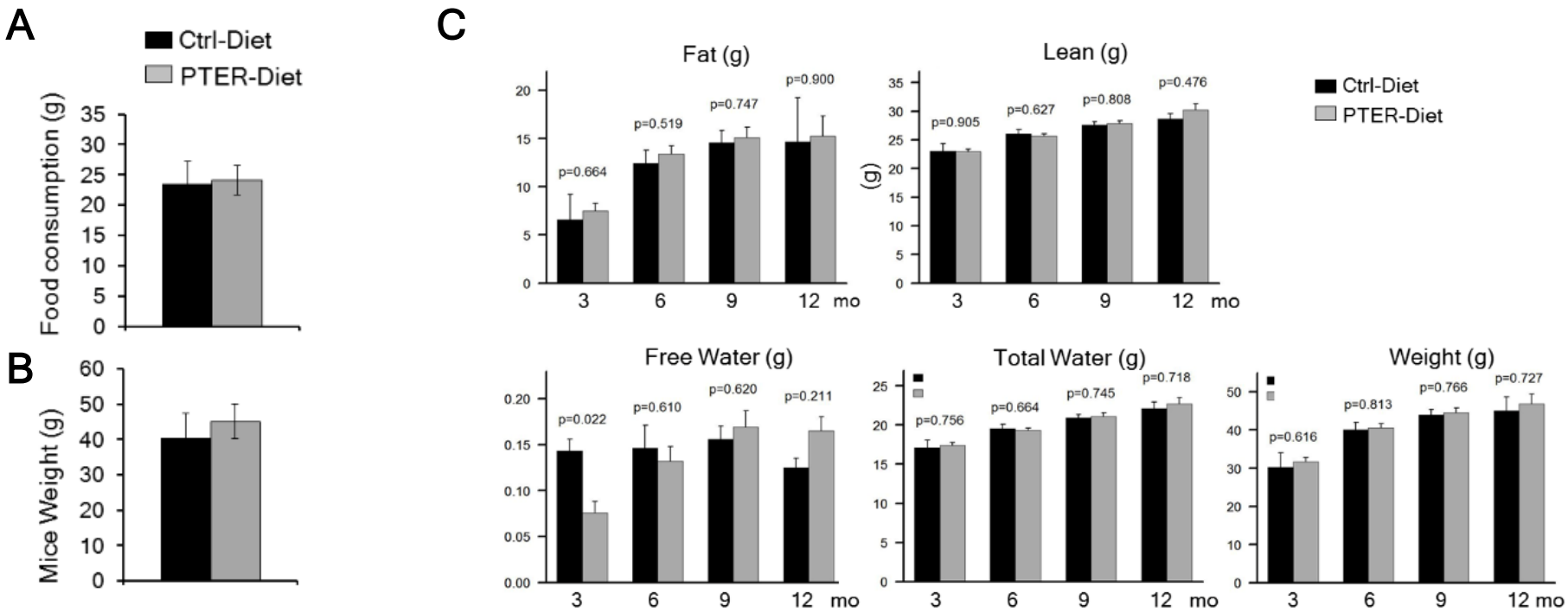

Figure S1. Effect of pterostilbene supplemented diet on *Pten*$^{+/f}$ mice. All mice consumed food and water *ad libitum*. There was no significant differences in **A.** food consumption, ***B.*** mice weights between the control (Ctrl-Diet) and PTER-Diet groups. **C**. EchoMRI measurements for fat, lean, water and weight were comparable for both Ctrl-Diet and PTER-Diet groups at 3-, 6-, 9- and 12- months (mo) of age. Data are mean ± SEM from each age group. 3 mo: Ctrl (n = 2), PTER (n = 6); 6 mo: Ctrl (n =13); PTER (n = 19); 9 mo: Ctrl (n = 18); PTER (n = 26); 12 mo: Ctrl (n = 4); PTER (n = 11). Two accumulations for each mouse. p values were calculated using two-tailed two-sample *t*-test.

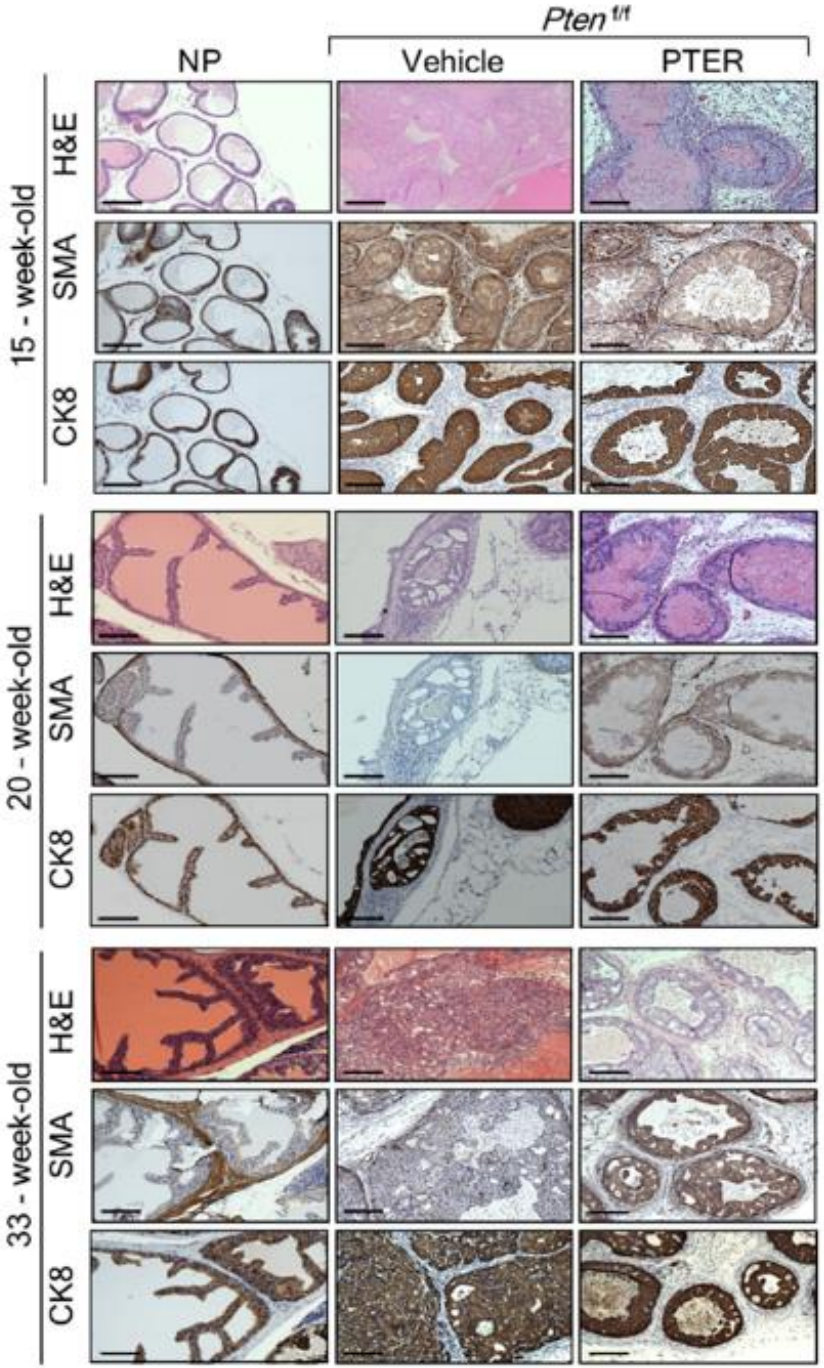

Figure S2. Histopathology of *Pten*$^{f/f}$ mice at 15, 20 and 33-weeks age. Comparison of H&E prostate histology (top, each panel) and IHC for SMA (middle, each panel) and CK8 (bottom, each panel) in prostate tissues from representative 15-, 20- and 33- week old Cre-negative mice with normal prostate (NP) and *Pten*$^{f/f}$ mice treated with vehicle and PTER. Scale bars, 100 µm

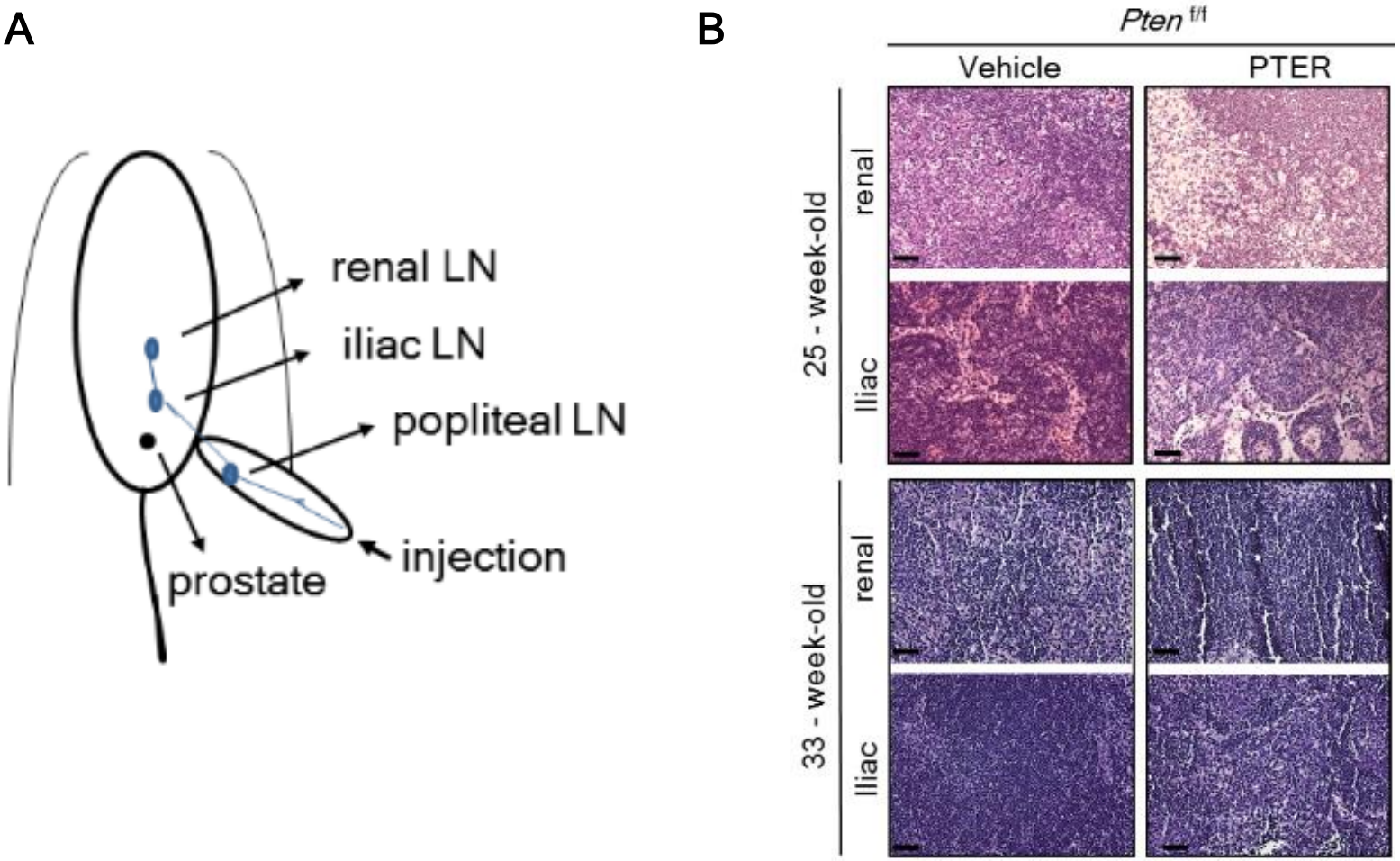

Figure S3. Lymph nodes (LN) analyses of *Pten*$^{f/f}$ mice. **A**. Schematic of the renal and iliac lymph nodes in the mouse. .**B**. Comparison of the H&E LN histology of representative 25-week-old and 33-week-old *Pten*-null vehicle and PTER-treated mice. Lymph nodes were isolated after injecting the mice subcutaneously at the foot pad (25µl/ foot pad) with Evans Blue dye and euthanizing after 30 minutes. The Evans Blue dye labels the popliteal LN, which drains centrally to the iliac and renal LNs along the midline. All lymph nodes were benign. Scale bars, 50 µm

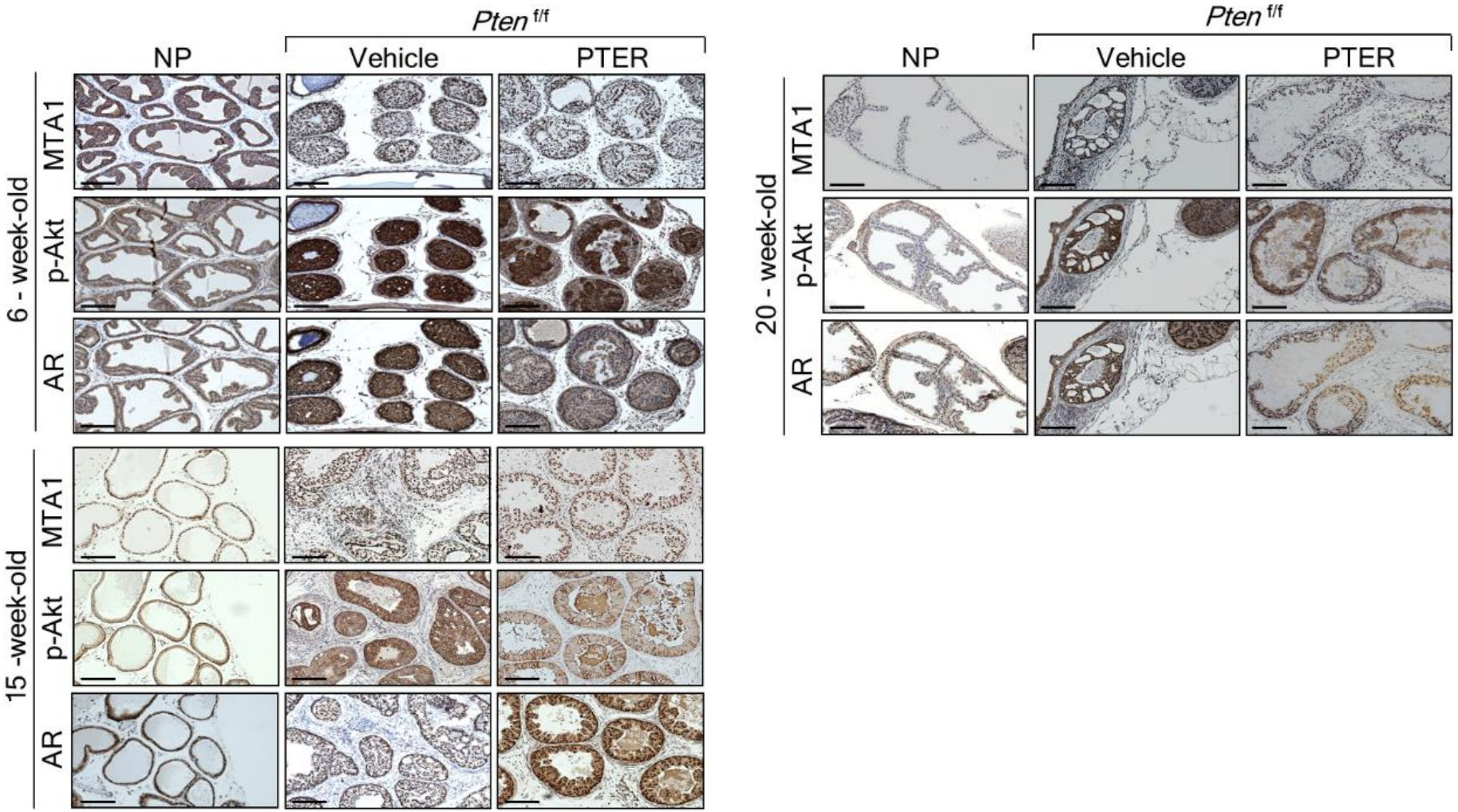

Figure S4. IHC analyses of representative 6-, 15-, and 20- week-old *Pten*$^{f/f}$ mice**.** Comparison of IHC for MTA1 (top, each panel), p-Akt (middle, each panel) and AR (bottom, each panel) from prostate tissues of representative 6-, 15-, and 20- week-old Cre-negative (NP) and *Pten*$^{f/f}$ vehicle and PTER treated mice, respectively. Scale bars, 100 µm

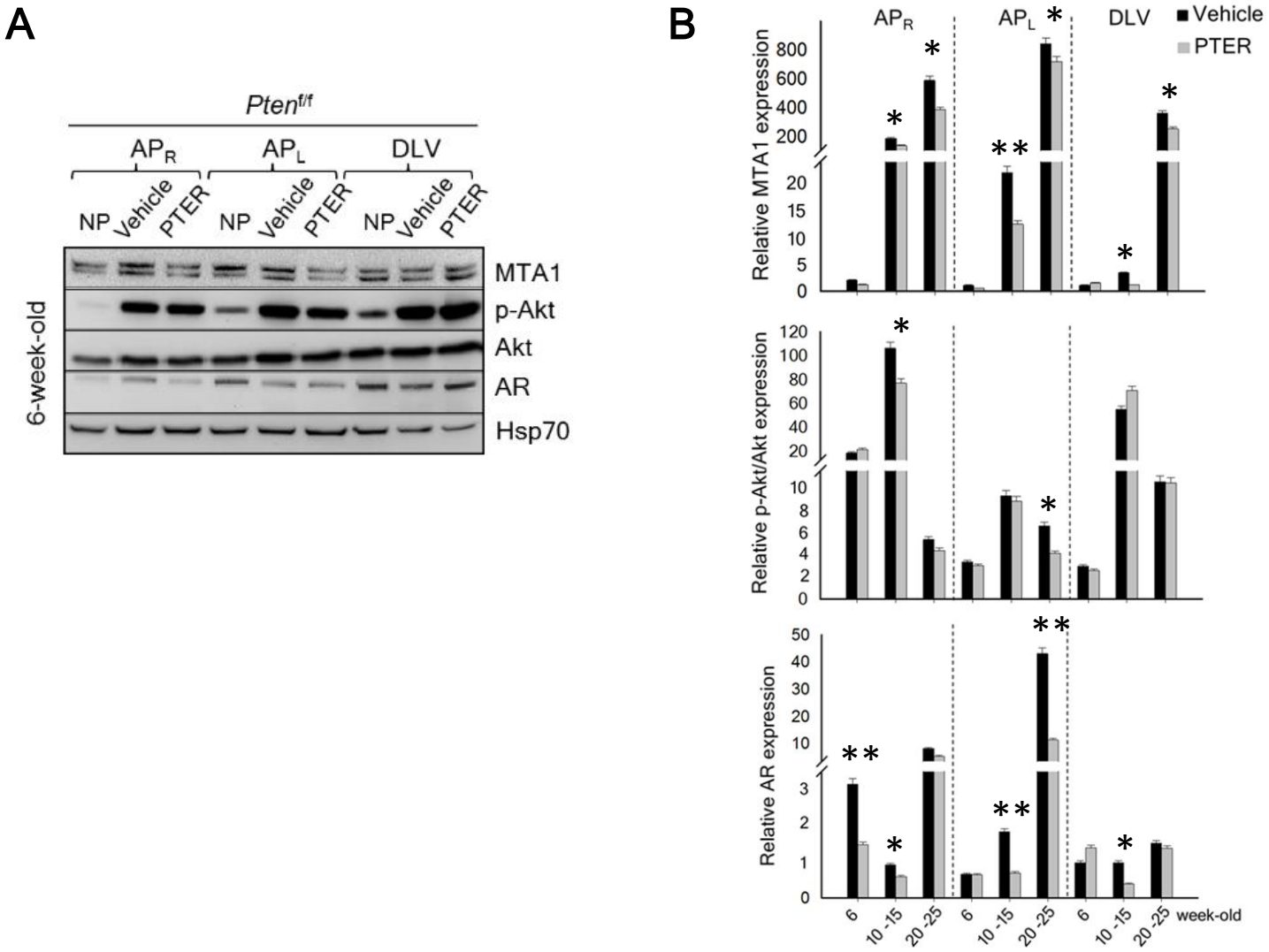

Figure S5. Prostate lobe-specific differential impact of pterostilbene (PTER) treatment. (*A*) Representative immunoblots of MTA1, p-Akt, Akt, AR in lysates from prostate lobes isolated from 6-week-old *Cre*-negative (NP) and *Pten*$^{f/f}$ vehicle and PTER treated mice. Hsp70 was used as a loading control. (*B*) Quantitation of MTA1, p-Akt/Akt and AR expression in prostate lobes of *Pten*$^{f/f}$ mice at different ages (also see Fig. 6**.** Values are mean ± SEM. **p<0.01, *p<0.05 (two-tailed, two-sample *t*-test).

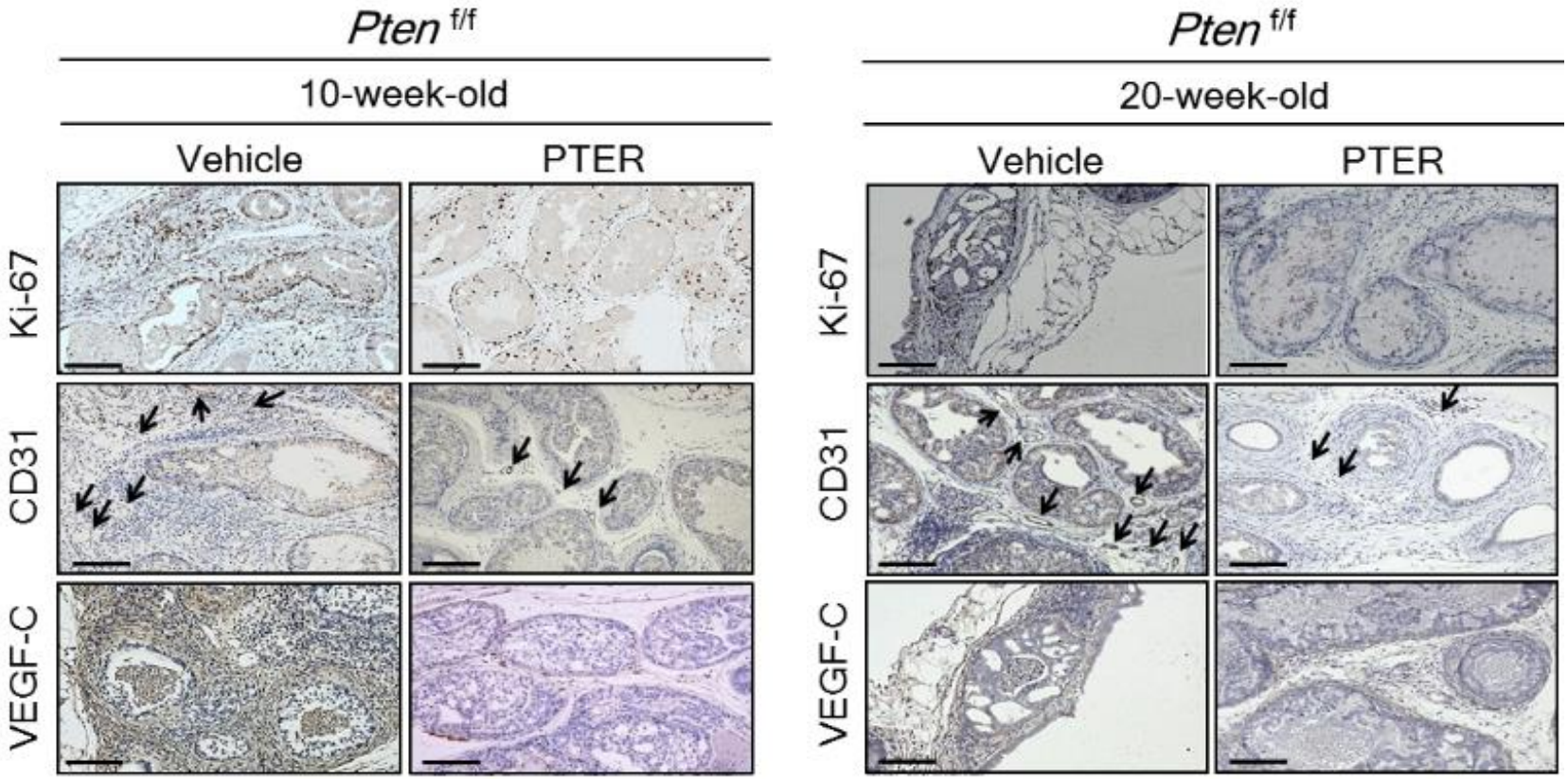

Figure S6. Pterostilbene (PTER) reduces proliferation and angiogenesis in prostate tissues of 10-, and 20- week-old *Pten*$^{f/f}$ mice. Representative IHC images for Ki-67 (top, each panel), CD31 (middle, each panel), VEGF-C (bottom, each panel) from *Pten*$^{f/f}$ mice treated with vehicle and PTER are shown. Scale bars, 100 μm (Ki-67, CD31, VEGF-C). Arrows indicate vessels. Also see **Figure 8**A and B.